SOLUTION STUDIES ON VARIOUS TRINUCLEAR METAL COMPLEXES

A thesis submitted for the degree of

DOCTOR OF PHILOSOPHY

in the Faculty of Science of the

University of St. Andrews

by

Glenmore Powell

December 1991

United College of

St. Salvator and St. Leonard,

St. Andrews

Dedication

To the loving memory of my mother.

DECLARATION

I, Glenmore Powell, hereby certify that this thesis has been composed by myself, that it is a record of my own work and that it has not been accepted in partial or complete fulfilment of any other degree or professional qualification.

I was admitted to the Faculty of Science of the University of St. Andrews under Ordinance General Nº. 12 in October 1988 and as a candidate for the degree of Ph. D. in October 1989.

Signed: December 1991.

CERTIFICATION

I hereby certify that the candidate has fulfilled the conditions of the Resolution and Regulations appropriate to the degree of Ph. D.

Signed: ..... December 1991.

ACKNOWLEDGEMENTS

I wish first of all to sincerely thank my supervisor, Dr. David Richens for his excellent supervision, cooperation and guidance throughout the duration of my course. I would also like to thank the following technical members of staff of the Department: Mr. Jim Bews (computing), Mr. Colin Smith (glassblowing), Mrs. Melanja Smith (NMR) and Mrs. Sylvia Smith (elemental analysis). Special thanks is also extended to Dr. Anne Powell (University of East Anglia) for X-ray crystallographic work.

I also wish to express my gratitude to the Trustees of the Sir James Irvine Postgraduate Fund for granting me a scholarship and for providing funding throughout the course of study. My family and friends, especially Lorraine Webster, are acknowledged for the considerable support and encouragement they have provided, and last, but not least, I owe a debt of gratitude to Miss Mary Glendinning for helping with the typing of the thesis.

CONTENTS

Page

Dedication

Declaration

Certification

Copyright

List of Abbreviations

Acknowledgements

Contents

Abstract

Chapter one 1

1.1 Introduction 2

1.1.1 Trinuclear Mo(IV) and W(IV) ions $M_3X_4(OH_2)_9]^{4+}$ (M = Mo or W; X = O or S. 2

1.1.2 Oxo/sulphido bridged trinuclear Mo(IV) and W(IV) aqua ions. 12

1.1.3 Molybdenum-tungsten mixed-metal trinuclear aqua ions $[M_3X_4(OH_2)_9]^{4+}$ (M_3 = Mo_2W or MoW_2; X = O or S). 15

1.2 Experimental 21

1.2.1 Standardisation of reactants 21

1.2.2 Preparation of complexes 21

1.2.2.1 Preparation of hexachloromolybdate(III) 21

1.2.2.2 Preparation of potassium hexachloromolybdate(III) 22

1.2.2.3 Preparation of solutions of $[Mo_3O_4(OH_2)_9]^{4+}$ 22

1.2.2.4 Preparation of solutions of $[Mo_3S_4(OH_2)_9]^{4+}$ 23

1.2.3 Kinetic study of NCS^- complexation on $Mo_3O_4^{4+}$ 24

1.2.4 Determination of the acid dissociation constant for 25

the $[Mo_3O_4(OH_2)_9]^{4+}$ aqua ion

1.2.5 Determination of the acid dissociation constant for the $[Mo_3S_4(OH_2)_9]^{4+}$ aqua ion 29

1.3 Results 36

1.3.1 Kinetic study of 1:1 NCS^- substitution on $Mo_3O_4^{4+}$ 36

1.3.1.1 Dependence on thiocyanate concentration 36

1.3.1.2 Dependence on hydrogen ion concentration 36

1.4 Discussion 43

1.4.1 Water exchange on the $Mo_3O_4^{4+}$ and $Mo_3S_4^{4+}$ aqua ions 48

1.5 References 55

Chapter two 60

2.1 Introduction 61

2.1.1 Trinuclear carboxylate clusters of tungsten(IV) and molybdenum(IV) 61

2.1.2 Molybdenum-tungsten mixed-metal trinuclear carboxylate clusters: $[M_3O_2(OAc)_6(H_2O)_3]^{2+}$ (M = Mo_2W or MoW_2) 69

2.1.3 The H3O2- bridging ligand in Mo(IV) and W(IV) tri-nuclear carboxylate clusters 74

2.2 Experimental 81

2.2.1 Reagents 81

2.2.2 Standardisation of reactants 81

2.2.3 Measurement of pH 82

2.2.4 Spectrophotometry 82

2.2.5 Oxygen-17 NMR measurements 82

2.2.6 Preparation of complexes 85

2.2.6.1 Preparation of (μ_3-dioxo) hexakis (μ-acetato) tri-aquatrimolybdenum(IV) perchlorate, $[Mo_3O_2(OAc)_6$- 85

$(H_2O)_3](ClO_4)_2$

2.2.6.2 Preparation of (μ_3-dioxo) hexakis(μ-acetato)tri-aquatritungsten(IV) perchlorate, $[W_3O_2(OAc)_6(H_2O)_3](ClO_4)_2$ 89

2.2.6.3 Preparation of (μ_3-oxo)hexakis(μ-acetato)triaqua-tritungsten(IV) perchlorate, $[W_3O(OAc)_6(H_2O)_3](ClO_4)_2$ 89

2.2.7 Kinetic studies 90

2.2.7.1 Anation by NCS^- on $[Mo_3O_2(OAc)_6(H_2O)_3]^{2+}$ 90

2.2.7.2 Anation by oxalate on $[Mo_3O_2(OAc)_6(H_2O)_3]^{2+}$ 91

2.2.7.3 Anation by NCS^- on $[MoW_2O_2(OAc)_6(H_2O)_3]^{2+}$ 92

2.2.7.4 Anation by oxalate on $[W_3O_2(OAc)_6(H_2O)_3]^{2+}$ 92

2.2.7.5 Anation by NCS^- on $[W_3O(OAc)_6(H_2O)_3]^{2+}$ 93

2.3 Results 94

2.3.1 Thiocyanate anation of $[Mo_3O_2(OAc)_6(H_2O)_3]^{2+}$ 94

2.3.1.1 Dependence on thiocyanate concentration 94

2.3.2 Oxalate anation of $[Mo_3O_2(OAc)_6(H_2O)_3]^{2+}$ 105

2.3.2.1 Dependence on total oxalate concentration 105

2.3.2.2 Dependence on hydrogen ion concentration 108

2.3.3 Thiocyanate anation of $[MoW_2O_2(OAc)_6(H_2O)_3]^{2+}$ 121

2.3.3.1 Dependence on $[SCN^-]$ 121

2.3.4 Oxalate anation of $[W_3O_2(OAc)_6(H_2O)_3]^{2+}$ 125

2.3.4.1 Dependence on total oxalate concentration 125

2.3.5 Thiocyanate anation studies on $[W_3O(OAc)_6(H_2O)_3]^{2+}$ 129

2.3.6 Water exchange 132

2.4 Discussion 134

2.4.1 $[Mo_3O_2(OAc)_6(OH_2)_3]^{2+}$ 134

2.4.2 $[MoW_2O_2(OAc)_6(OH_2)_3]^{2+}$ 141

2.4.3 $[W_3O_2(OAc)_6(OH_2)_3]^{2+}$ 143

2.4.4 $[W_3O(OAc)_6(OH_2)_3]^{2+}$ 144
2.5 Studies on the redox chemistry of the $[M_3O_2(OAc)_6(H_2O)_3]^{2+}$ (M = Mo, W, MoW_2) and $[W_3O(OAc)_6(H_2O)_3]^{2+}$ complexes 150
2.5.1 Introduction 150
2.5.2 Experimental 150
2.5.2.1 Electrochemistry 150
2.5.3 Results and discussion 151
2.5.3.1 $[Mo_3O_2(OAc)_6(OH_2)_3]^{2+}$ 151
2.5.4 Chemical reduction of $[Mo_3O_2(OAc)_6(H_2O)_3]^{2+}$ 152
2.5.4.1 Estimation of the formal oxidation state for Mo in the emerald-green solution obtained on the chemical reduction of $[Mo_3O_2(OAc)_6(H_2O)_3]^{2+}$ 153
2.5.4.2 $[W_3O_2(OAc)_6(OH_2)_3]^{2+}$ 158
2.5.4.3 $[W_3O(OAc)_6(OH_2)_3]^{2+}$ 158
2.5.4.4 Attempted controlled potential reduction of $[W_3O(OAc)_6(H_2O)_3]^{2+}$ 159
2.5.4.5 $[MoW_2O_2(OAc)_6(OH_2)_3]^{2+}$ 162
2.6 References 163
Chapter three 168
3.1 General introduction 169
3.1.1 Trinuclear μ_3-oxo carboxylate-bridged complexes 169
3.1.1.1 Electronic spectra 172
3.1.1.2 Vibrational spectra 173
3.1.1.3 Electrochemistry 174
3.1.1.4 Magnetic susceptibility 176
3.1.2 Mixed-metal trinuclear (μ_3-O) carboxylate complexes 178
3.1.2.1 Preparation 178

3.1.2.2 Electronic spectra 179
3.1.2.3 Structural studies 180
3.1.2.4 Vibrational spectra 182
3.1.2.5 Magnetic susceptibility 183
3.1.3 Trinuclear ruthenium μ_3-oxo carboxylate-bridged complexes 184
3.1.3.1 Pyridine and pyrazine derivatives 188
3.1.3.2 Ligand bridged trinuclear ruthenium clusters 194
3.1.3.3 Isonicotinamide derivatives 197
3.1.3.4 Phosphine derivatives 200
3.1.3.5 DMF derivatives 202
3.1.4 Mixed-metal ruthenium μ_3-oxo carboxylate complexes 203
3.1.4.1 Substitution studies on theterminal ligands 205
3.2 Experimental 207
3.2.1 Preparation of reagents 207
3.2.2 Standardisation of reagents 207
3.2.3 Measurement of pH 207
3.2.4 Instrumentation 207
3.2.5 Preparation of complexes 208
3.2.5.1 Preparation of (μ_3-oxo) hexakis(μ-acetato)triaquatriruthenium(III) acetate, $[Ru_3O(OAc)_6(H_2O)_3]OAc$ 208
3.2.5.2 Preparation of (μ_3-oxo) hexakis(μ-acetato)triaquatriruthenium(III) perchlorate, $[Ru_3O(OAc)_6(H_2O)_3]ClO_4$ 209
3.2.5.3 Preparation of (μ_3-oxo) hexakis(μ-acetato)triisonicotinamidetriruthenium(III) hexafluorophosphate, $[Ru_3O(OAc)_6(iso)_3]PF_6$ 210

3.2.6 Crystal data for $[Ru_3O(OAc)_6(H_2O)_3]ClO_4.HClO_4.H_2O$ 210
3.2.6.1 Data collection and processing 211
3.2.6.2 Structure analysis and refinement 211
3.2.7 Oxygen-17 NMR measurements of water exchange on $[Ru_3O(OAc)_6(H_2O)_3]^+$ 212
3.2.7.1 Kinetic analysis 213
3.2.8 Kinetic studies of complexation of isonicotinamide with $[Ru_3O(OAc)_6(H_2O)_3]^+$ 213
3.3 Results and discussion 214
3.3.1 Structure description and discussion of $[Ru_3O(OAc)_6(H_2O)_3]ClO_4.HClO_4.H_2O$ 214
3.3.2 Water exchange 217
3.3.3 Complexation of isonicotinamide with $[Ru_3O(OAc)_6(H_2O)_3]^+$ 219
3.3.3.1 Product analysis 219
3.3.4 Kinetics of isonicotinamide complexation on $[Ru_3O(OAc)_6(H_2O)_3]^+$ 222
3.3.4.1 Dependence on total isonicotinamide concentration 222
3.3.4.2 Dependence on hydrogen ion concentration 222
3.4 References 232
Chapter four 239
4.1 Introduction 240
4.2 Experimental 249
4.2.1 Spectrophotometry 249
4.2.2 Gas chromatograph 249
4.2.3 Preparation of tris(pyridine) hexa μ-acetato-μ_3-oxotriruthenium(III) perchlorate $[Ru_3O(OAc)_6$- 250

$(py)_3]ClO_4$

4.2.4 Preparation of tris(pyridine) hexa -μ-acetato-μ_3 -oxotriruthenium(III, III, II): $[Ru_3O(OAc)_6(py)_3]$ 251

4.2.5 Preparation of bis(pyridine) carbonyl hexa-μ-acetato-μ_3-oxotriruthenium(III): $[Ru_3O(OAc)_6$-$(CO)(py)_2]$ 252

4.2.6 Preparation of μ_3-oxo-triaquahexakis(acetato) iron(II) diiron(III): $[Fe^{II}Fe^{III}_2(OAc)_6(H_2O)_3]$ 253

4.2.7 Preparation of μ_3-oxo-tris(pyridine)hexakis-(acetato)iron(II) diiron(III)hemipyridine: $[Fe^{II}Fe^{III}O(OAc)_6(py)_3](py)_{0.5}$ 253

4.2.8 Preparation of bis(μ-acetato)(μ-oxo)bis(tris(pyridine))ruthenium(III) ion: $[Ru_2O(OAc)_2(py)_6]^{2+}$ 254

4.3 Results and discussion 254

4.4 References 259

Appendices 263

Appendix one 264

Appendix two 265

Appendix three 267

Appendix four 268

Appendix five 270

ABSTRACT

The kinetics (25 °C) of 1:1 complexing of NCS^- for H_2O at Mo on the cluster $[Mo_3O_4(OH_2)_9]^{4+}$ has been reinvestigated in Hpts, I = 2.0 M (Lipts). The results have indicated extensive (H_2O) acid dissociation of the cluster (K_a = 0.51 M) which is in agreement with the spectrophotometric titration value of 0.43 M (25 °C). The substitution proceeds solely by NCS^- replacement of H_2O on the monohydroxy form, with rate constant $k_1 = 5.27\ M^{-1}s^{-1}$. Extensive acid dissociation on the analogous $Mo_3S_4^{4+}$ aqua ion was also verified by spectrophotometric determination in both ClO_4^- (K_a = 0.23 M) and pts^- (K_a = 0.15 M) media. These investigations have revealed that pts^- is involved in an ion-pair outer-sphere association with the cluster species, presumably due to hydrogen bonding. The results are discussed in conjunction with previous water exchange studies conducted on these species.

The kinetics of substitution and / or exchange at the terminal aqua ligands on $[M_3O_2(OAc)_6(OH_2)_3]^{2+}$ (M_3 = Mo_3, MoW_2, W_3) (IV, IV, IV) and $[W_3O(OAc)_6(OH_2)_3]^{2+}$ (III, III, IV) have been studied. A two stage process corresponding to stepwise substitution of NCS^- for H_2O in the Mo_3 complex was observed with a rate constant (per metal ion) of $9.4 \times 10^{-6}\ s^{-1}$ at 25 °C for the first step ($\Delta H^{\neq}$ = 140.7 ± 0.9 kJ mol^{-1}; ΔS = +130.6 ± 2.7 J $K^{-1}mol^{-1}$). The substitution of the aqua ligands by oxalate on the Mo_3 complex was also studied. A mechanism involving both $HC_2O_4^-$ and $C_2O_4^{2-}$ as anating species was proposed; the respective rate constants (25 °C) are as follows: $8.94 \times 10^{-5}\ M^{-1}s^{-1}$ ($\Delta H^{\neq}$ = 76.2 ± 0.3 kJ mol^{-1}; $\Delta S^{\neq}$ = -67.0 ± 0.9 J K^{-1} mol^{-1}) and ~$1.6 \times 10^{-5}\ s^{-1}$ ($\Delta H^{\neq}$ = 120.0 ± 8.6 kJ mol^{-1}; $\Delta S^{\neq}$ = +85.0 ± 26.8 J $K^{-1}mol^{-1}$). The water exchange rate constant at 25 °C is $5.6 \times 10^{-6}\ s^{-1}$ ($\Delta H^{\neq}$ = 125.85 ± 9.62

kJ mol^{-1}; $\Delta S^{\neq}$ = 76.58 ± 30.03 J K^{-1} mol^{-1}). An I_D mechanism is suggested for the terminal ligand substitution of this complex. The water exchange rate constant for the Mo_3 complex is larger than the value (1.02 x 10^{-6} s^{-1} at 25 °C) for the corresponding W_3 complex ($\Delta H^{\neq}$ = 58.30 ± 8.39 kJ mol^{-1}; $\Delta S^{\neq}$ = -164.3 ± 24.9 J K^{-1} mol^{-1}) for which in contrast an associative type of mechanism is indicated. Results for the water exchange on the mixed-metal MoW_2 complex has provided direct evidence for a more inert Mo centre (more d^3 character) when compared to the homonuclear Mo_3 species but exchange at the W atoms is comparable to that on the homonuclear W_3 complex. Of the four species studied the monocapped μ_3-oxo tungsten complex was found to be the most labile; the rate constant for water exchange being 5.3 x 10^{-4} s^{-1} (25 °C) ($\Delta H^{\neq}$ = 51 ± kJ mol^{-1}; $\Delta S^{\neq}$ = -135 ± J K^{-1} mol^{-1}). The difference in the formal oxidation state and / or the presence of one μ_3-capping oxo ligand is believed to be responsible for its more labile nature. An associative type of mechanism is again tentatively assigned. The results on these species have verified the importance of a conjugate-base assigned mechanism for substitution / exchange of water on the $[M_3X_4(OH_2)_9]^{4+}$ (M = Mo, W; X = O, S) cluster ions.

The electrochemical properties of the four species were also studied. Evidence for the electrochemical generation of the hitherto unknown mono-μ_3-oxo capped complex $[Mo_3O(OAc)_6(OH_2)_3]^{2+}$ is presented as well as characterisation of the first $W(III)_3$ trinuclear species.

The $[Ru_3O(OAc)_6(OH_2)_3]^{+}$ complex has been synthesised and characterised by X-ray crystallography, revealing the existence of both $HClO_4$ and H_2O molecules of crystallisation. There is also extensive hydrogen bonding between the terminal H_2O ligands and the ClO_4^-

counter ions. The cation is the first $Ru(III)_3$ μ_3-oxo trinuclear carboxylate to be structurally characterised and its structure is compared with analogous species.

Both the water exchange and isonicotinamide substitution of the $[Ru_3O(OAc)_6(OH_2)_3]^+$ H_2O ligands have been studied at I = 1.0 M ($NaCF_3SO_3$). The acidity dependence (2.4 < pH < 3.5) for the isonicotinamide reaction is consistent with the existence of two parallel pathways involving complexation of the ligand with $[Ru_3O(OAc)_6(OH_2)_3]^+$ and $[Ru_3O(OAc)_6(OH_2)(OH)_2]^-$. Rate constants (25 °C) and activation parameters for the two paths are: $[Ru_3O(OAc)_6(OH_2)_3]^+$, $k_1 = 0.57 \times 10^{-3}$ $M^{-1}s^{-1}$, $\Delta H_1^{\neq} = 116.9 \pm 11.4$ kJ mol^{-1}, $\Delta S_1^{\neq} = +85.1 \pm 36.0$ J K^{-1} mol^{-1}; and $[Ru_3O(OAc)_6(OH_2)(OH)_2]^-$, $k_2 = 0.29 \times 10^{-3}$ $M^{-1}s^{-1}$, $\Delta H_2^{\neq} = 101.2 \pm 7.8$ kJ mol^{-1}, $\Delta S_2^{\neq} = +26.9 \pm 24.6$ J K^{-1} mol^{-1}. The water exchange rate constant (25 °C) is 1.08×10^{-3} s^{-1}. A negligible ion-pair constant has been assumed between the isonicotinamide and the complex species. The results highlight the first successfully monitored complexation reaction of $[Ru_3O(OAc)_6(OH_2)_3]^+$ and a similar mechanism has been proposed for both pathways. A dissociative mechanism seems relevant.

Different trinuclear and dinuclear carboxylate complexes namely $[Ru_3O(OAc)_6(OH_2)_3]^+$, $[Fe_3O(OAc)_6(py)_{3.5}]$, $[Ru_3O(OAc)_6(py)_2(CO)]$ and $[Ru_2(OAc)_2(py)_6]$ have been compared in their ability to catalytically oxygenate cyclohexane under Gif IV conditions *i.e.* using pyridine as solvent, zinc as reductant, acetic acid as proton source and O_2/air as oxidant. The results showed that the iron complex is the best catalyst under these conditions followed by $[Ru_3O(OAc)_6(OH_2)_3]^+$ with the ruthenium dimer as the least active. A tentative mechanism has been proposed involving the formation of a hydrocarbon radical, hydrogen

atom abstraction and reaction of the radical with O_2 to form a hydroperoxide.

CHAPTER ONE

1.1 INTRODUCTION

1.1.1 Trinuclear Mo(IV) and W(IV) Ions $M_3X_4(OH_2)_9]^{4+}$ (M = Mo or W; X = O or S)

Significant contributions have been made over the years toward the understanding of the Chemistry of the Mo(IV) and W(IV) aqua ions. A lot of interest is still being generated in these species as well as other closely related ones.

The red aqua ion of molybdenum (IV), first isolated by Souchay *et al* [1] in 1966, is now well characterised and established as containing the cyclic trinuclear metal cluster unit $[Mo_3O_4(OH_2)_9]^{4+}$ (Fig 1.1).

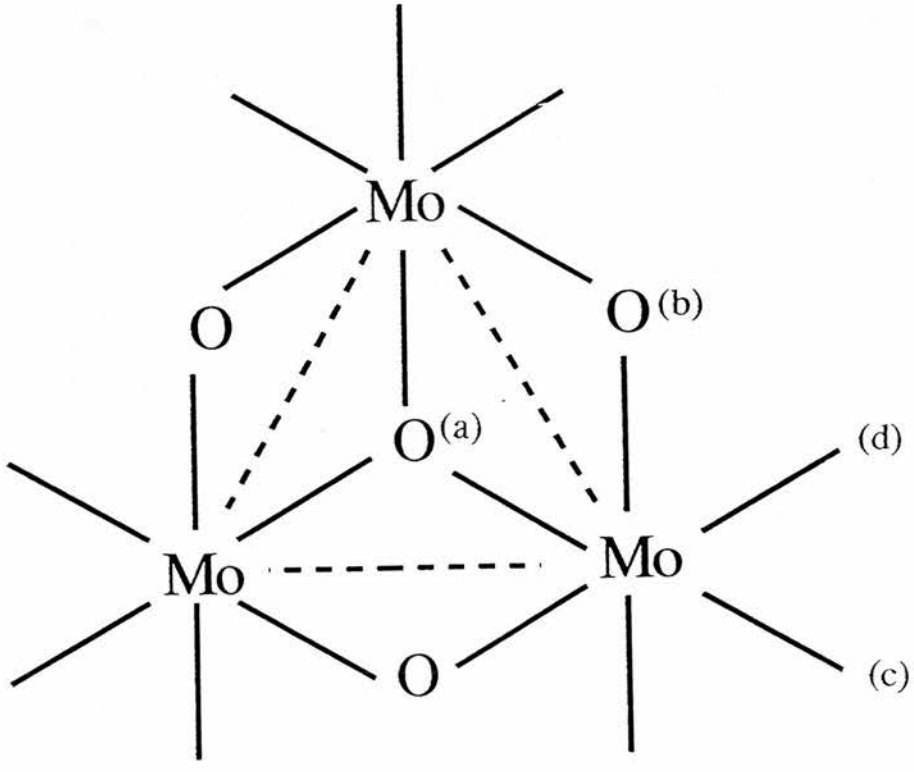

Fig 1.1.: Structure of the $[Mo_3O_4(OH_2)_9]^{4+}$ cluster (water ligands are omitted for the sake of clarity)

The preparation of this complex is generally carried out *via* a comproportionation reaction involving Mo(VI) as $Na_2[MoO_4].2H_2O$, or Mo(V) as the aqua dimer $Mo_2O_4^{2+}$, with $K_3[MoCl_6]$ in 2 M Hpts for 1-2 hours at 80-90 °C.[2]

$$[MoO_4]^{2-} + 2[MoCl_6]^{3-} + 12H^+ \longrightarrow [Mo_3O_4]^{4+} + 12HCl \qquad (1.1)$$

The aqua ion is fairly stable in this form and can be purified by Dowex cation exchange chromatography (50W -X2 resin). Elution is carried out using non-complexing, non-oxidising acids such as *p*-toluene sulphonic acid (Hpts) or trifluoromethenesulphonic acid (triflic acid). Perchloric acid is unsuitable since this results in slow oxidation to yellow Mo(V).[3]

Since its first isolation several structures for the Mo(IV) aqua ion have been proposed.[4-7] X-Ray structural studies of derivative complexes using oxalate,[8,9] EDTA[10], thiocyanate[11] and MIDA[12] have indicated a trimeric oxo-bridged core in the solid state. The confirmation that the trinuclear unit is maintained in aqueous solution was obtained from studies involving ^{18}O labelling[9,13] techniques and ^{17}O NMR.[14] Conclusive support for the trimeric core was finally obtained through a crystal structure of the aqua ion itself, $[Mo_3O_4(OH_2)_9](pts)_4.13H_2O$[15], shown in Figure 1.2. It was found that the three Mo(IV) atoms are practically equivalent in the range of the experimental errors with the average Mo-Mo bond distance being 2.48Å The metal-metal separation is characteristic for a single Mo-Mo bond interaction which agrees well with previous molecular orbital calculations performed by Cotton and coworkers[16] who interpreted the electronic structure of the ion as containing single M-M bonds in the triangular framework.

There are four different types of oxygen atom coordinated to each metal. It has been shown recently by Richens *et al*, [15] using ^{17}O NMR that all of the core oxygen atoms consisting of one capping μ_3-oxo (a) and three bridging μ-oxo ligands (b) , are extremely inert to substitution, which is contrary to an earlier report.[9] The ^{17}O NMR

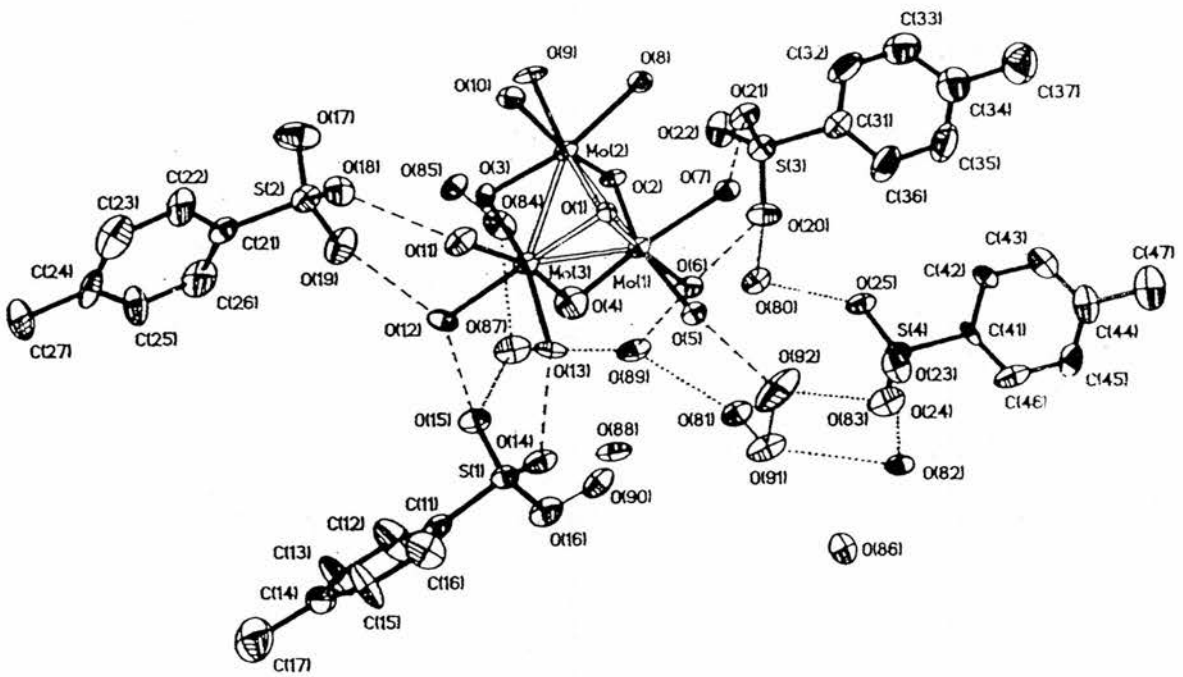

Fig. 1.2: Low temperature (240K) crystal structure of $[Mo_3O_4(OH_2)_9](pts)_4.13H_2O$

studies have also shown that the water ligands *trans* to the bridging μ-oxo groups (d) exchange some 10^5 times faster than those *trans* to the capping μ_3-oxo groups (c).[15]

The corresponding tungsten (IV) aqua ion, $[W_3O_4(OH_2)_9]^{4+}$, is also known.[17-19] The preparation and characterisation of which was first reported by Segawa and Sasaki in 1985.[17] However, separate studies[19] with regard to the published[17] synthetic route, involving acid

aquation of $K_2[WCl_6]$, have given clear evidence that the major product is not the $[W_3O_4(OH_2)_9]^{4+}$ aqua ion but probably the monochloro aqua species $[W_3O_4(OH_2)_8Cl]^{3+}$. Sykes and coworkers[20] have also found that the use of HCl yielded mainly chloroaqua species and a low yield of the aqua ion which was however increased substantially when Hpts was used. Successive columns of Dowex 50W- X8 and 50W -X2 resins were used to separate the aqua ion from the chloroaqua species. An X-ray crystallographic study[17] of the complex $(NH_4)_2\{N(C_2H_5)_4\}_3$-$[W_3O_4(NCS)_9].nH_2O$ has confirmed the presence of the trimeric $W_3O_4^{4+}$ core and provides the basis for assuming that the aqua ion is $[W_3O_4(OH_2)_9]^{4+}$ thus structurally analogous to $[Mo_3O_4(OH_2)_9]^{4+}$.[21,22] Further additional proof was supplied by dynamic multinuclear ($^{17}O/^{183}W$) NMR studies.[19] The existence of the ions $[M_3O_4(OH_2)_9]^{4+}$ (M_3 = Mo_3 or W_3) allowed the first comparative study of the solution chemistry of an aqua ion formed by both elements.

Acid hydrolysis of $[WCl_6]^{2-}$ is the only successful route through to the $W_3O_4^{4+}$ aqua ion. Comproportionation reactions involving W(VI) or W(V) with W(III) are not successful in contrast to molybdenum, probably due to the differing redox properties of the various oxidation states for tungsten. On the other hand hydrolysis of $[MoCl_6]^{2-}$ does provide an alternative route to $Mo_3O_4^{4+}$ in addition to the comproportionation reaction. $W_3O_4^{4+}$ is much more sensitive to air oxidation than $Mo_3O_4^{4+}$and can only survive on the minutes time scale in air. This increase in reducing property characterises many compounds of tungsten in comparison to those of molybdenum.

Studies on the molybdenum (IV) and tungsten (IV) aqua ions have been extended to include redox and substitution reactions. The substitution properties of the $Mo_3O_4^{4+}$ aqua ion were investigated[21] using both NCS^- and oxalate as incoming ligands while the former

ligand has been used in the case of the $W_3O_4^{4+}$ aqua ion.[20] Care was taken to undertake these studies under conditions appropriate for 1:1 complex formation as the major process at any one metal centre. The kinetic studies have highlighted the 3-fold symmetry of these aqua ions and the data were treated with the assumption that statistical kinetics apply.[23] For the conditions in which the ligands were in large (≥ 10-fold) excess the rate constants obtained were three times those with the aqua ion in excess, and to allow for this difference the ligands concentrations were divided by three; the explanation being that three independent and identical metal sites are available to the incoming ligand at any one time. In the molybdenum(IV) aqua ion study[21] substitution was found to proceed solely *via* the monohydroxy form. The rate constants for $HC_2O_4^-$ (3.3 $M^{-1}s^{-1}$) and NCS^- (4.8 $M^{-1}s^{-1}$), I=2.0 M (Lipts) reacting with the monohydroxy form were in close agreement, consistent with an I_d process. Perhaps not surprising similar behaviour in the anation kinetics of the $W_3O_4^{4+}$ aqua ion by NCS^- was subsequently obtained.[20] The rate constant obtained for this process (1.2 $M^{-1}s^{-1}$), however, was an order of magnitude slower than for the corresponding reaction on $Mo_3O_4^{4+}$ (13.5 $M^{-1}s^{-1}$) in perchlorate medium (I=2.0 M, $LiClO_4$). As in the case of the molybdenum (IV) analogue substitution on W(IV) was observed to proceed solely by replacement of H_2O on the monohydroxy form. Recent ^{17}O NMR studies[15] have shown that it is one of the d- H_2O's that is involved in deprotonation occurring presumably on the same molybdenum atom undergoing water replacement; the lability believed to be due to activation *via* a *cis* 'conjugate' base effect. As mentioned a dissociative interchange (I_d) mechanism has been suggested for substitution on these molybdenum (IV) and tungsten (IV) species.[15] This mechanism is widely suggested as being appropriate to conjugate base

forms[24-26] and further support comes from the near identical rates of substitution by NCS^- and oxalate for molybdenum(IV) together with the order of magnitude slower rate observed for tungsten(IV). An intriguing finding in these studies [15,20,21] however was the very high values found for the acid dissociation constant ($pK_a<1$) for these already extensively hydrolysed species. It was thus of interest to conduct further independent investigations with regard to substitution studies on the $Mo_3O_4^{4+}$ aqua ion in order to confirm this surprising behaviour. The results of such an investigation will be reported later in this chapter. Water exchange studies by ^{17}O NMR support the conjugate base mechanism and will also be discussed later in connection with the confirmation of the NCS^- results un order to make final conclusions.

It is now well established that the molybdenum (IV) aqua ion is readily reduced to a green molybdenum (III) species by Zn/Hg under air-free conditions.[27-29] It is presumed that this ion is still trinuclear from both the ready reversibility of the redox process and from the fact it possesses a different electronic spectrum from those of the well defined mononuclear[30] and dinuclear[31] aqua ions of molybdenum (III). Electrochemical [28,29] and ^{18}O[9] studies have also shown that the four oxo groups of $Mo_3O_4^{4+}$ are retained throughout the redox cycle and become protonated up on reduction suggesting a formula $Mo_3(OH)_4^{5+(aq)}$ for the molybdenum (III) product. Extensive protonation consistent with a charge of >4+ is also implied from cation-exchange behaviour.[27]

Studies have also shown that a mixed-valence intermediate,[27,28] molybdenum (III,III,IV), builds up under certain conditions, the build up of which is favoured as both the acidity and the co-ordinating tendency of the anion [29] are increased. A feature of the electronic spectrum of this mixed-valence species is a broad band at 1050 nm

(ε=100 $M^{-1}cm^{-1}$ per Mo atom).[27] This has been assigned to an intervalence transition.[23] Exposure of the molybdenum (III,III,III) ion to oxygen resulted in oxidation to molybdenum (III,III,IV) and then to molybdenum (IV,IV,IV).[28] So far there is evidence only of trace amounts of the other mixed-valence species, molybdenum (III,IV,IV) which appears to rapidly disproportionate.

Despite these detailed studies the precise solution structures of these reduced products were poorly characterised until very recently. Studies by Richens and Guille-Photin[32] have identified two forms of the molybdenum (III,III,III) aqua ion. Following the reduction of ^{17}O-enriched samples of $Mo_3O_4^{4+}$ by Eu^{2+} the solution structures of the Mo(III,III,III) and Mo(III,III,IV) products were obtained using ^{17}O NMR. The analysis of chemical shifts and peak integrations have indicated the structure $[Mo_3(\mu\text{-}OH)_4(OH_2)_{10}]^{6+}$ for the mixed-valence species delocalised on the NMR time scale and two structures $[Mo_3(\mu_3\text{-}OH)(\mu\text{-}OH)_3(OH_2)_9]^{5+}$ (I) and $[Mo_3(\mu\text{-}OH)_4(OH_2)_{10}]^{5+}$ (II) for trinuclear Mo(III,III,III) in an $[H^+]$-dependent equilibrium; structure II being favoured at high acidity.

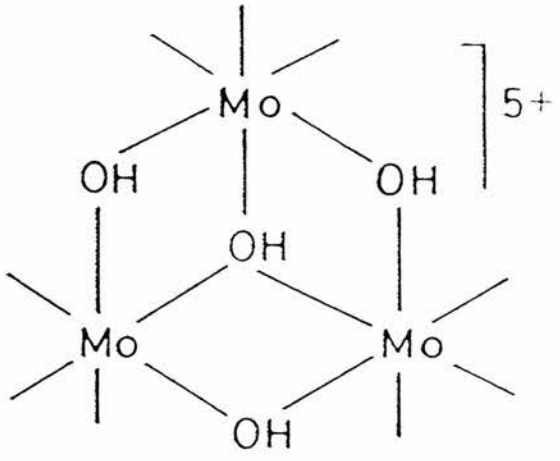

(I)

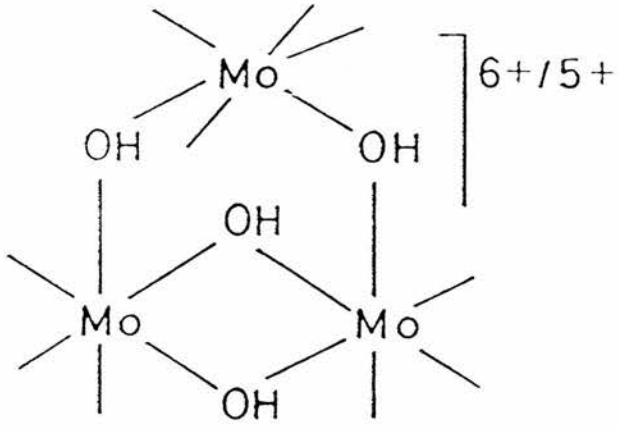

(II)

The reduction of the corresponding $W_3O_4^{4+}$ aqua ion occurs readily with Zn/Hg to an emerald-green mixed valence, W(III,III,IV) species but there is no evidence for the W(III,IV,IV) or the W(III,III,III) aqua ions.[19] The reduced species is rapidly reoxidised to the W(IV,IV,IV) aqua species on exposure to air. In contrast to the ease of chemical reduction of the $W_3O_4^{4+}$ species the electrochemical reduction[19] of $W_3O_4^{4+}$ is rather difficult to achieve and reproduce. Using polarographic techniques an irreversible reduction wave for $W_3O_4^{4+}$ in 2M Hpts at 25 °C was reported by Segawa and Sasaki[17] at -0.25 V (*vs* NHE). More recent independent studies[19] using cyclic voltammetry at a hanging Hg drop electrode under similar conditions, however, have failed to detect such a wave. Finally in one isolated experiment,[19] a reversible $2e^-$ reduction wave centered at -0.79 V(*vs* NHE) was detected, which is believed to be due to formation of the mixed-valence W(III,III,IV) ion. This reduction wave has been difficult to reproduce and appears to depend upon the attainment of a highly negative cathodic limit possible only with the use of very pure, freshly prepared reagents.[19] Furthermore the unsuccessful reduction of $W_3O_4^{4+}$ to W(III,III,IV) using Eu^{2+} (E^o= -0.41 V *vs* NHE) provided further evidence that the potential for reduction is more highly negative and is more consistent with the value of -0.79 V rather than -0.25 V as reported by Segawa and Sasaki.[17] Oxygen-17 NMR studies[19] have confirmed that protonation of the μ-O groups occurs on formation of the W(III,III,IV) ion with evidence of an 'open' structure (II) for $W_3(OH)_4^{6+}$, fluctional on the NMR timescale, similar to that previously found for molybdenum. Further studies are planned on these species using variable temperature ^{95}Mo and ^{183}W NMR in the hope of measuring the energy barriers involved with structural equivalence of the μ-OH groups on the NMR time-scale.

The corresponding μ-sulphido aqua compounds $[M_3S_4(OH_2)_9]^{4+}$ (M=Mo or W) have been prepared and fully characterised. The green $Mo_3S_4^{4+}$ aqua ion can be prepared simply by heating $[Mo_4S_4(OH_2)_{12}]^{5+}$ in 1-2 M HCl at ~ 90 °C. The cuboidal ion $[Mo_4S_4(OH_2)_{12}]^{5+}$ can be obtained by $NaBH_4$ reduction of the cysteinato bis (μ-sulphido) $Mo_2(V)$ complex: $Na_2[Mo_2O_2S_2(cys)_2].4H_2O$.[33] The $Mo_3S_4^{4+}$ aqua ion can also be prepared by refluxing $Mo(CO)_6$ and Na_2S in acetic anhydride under N_2.[34,35] This green aqua ion is stable indefinitely in acid solutions (pH < 1) and unlike the μ-oxo analogue does not react overnight with O_2 and ClO_4^- .The existence of the $Mo_3S_4^{4+}$ core has been confirmed by X-ray structure analyses of several derivative complexes as well as that of the aqua ion itself.[36] It is structurally similar to the $Mo_3O_4^{4+}$ core, having one μ_3- and three μ-sulphido ligands. The average Mo-Mo bond length of 2.735Å in $[Mo_3S_4(OH_2)_9]^{4+}$ [36] is longer than that in $[Mo_3O_4(OH_2)_9]^{4+}$ (2.48Å).[15]

The 1:1 substitution of H_2O on the $Mo_3S_4^{4+}$ aqua ion by NCS^- occurs much more rapidly (~ 10^2 times) than in the μ-oxo analogue and requires study by stopped-flow techniques.[33] In this case the substitution process was found to proceed both by the aqua and monohydroxy forms in contrast to the μ-oxo analogue. As found with the μ-oxo ion, a statistical factor of three is relevant and the kinetic data require consideration of a large acid dissociation constant (>0.1M). This has now been confirmed by independent spectrophotometric measurements (see results and discussion in this chapter) and is an interesting finding given the observed 10^2x labilising effect on the water liqands; this effect not being transmitted by a change in their acidity.

Unlike the $Mo_3O_4^{4+}$ aqua ion[28,29,32] no electrochemical or chemical reduction of $Mo_3S_4^{4+}$ (aq)[33] has yet been observed. It has however been established that in neutral solution $[Mo_3S_4(IDA)_3]^{2-}$ can

be reduced to the Mo(III,III,IV) and Mo(III,IV,IV) states by cyclic voltammetry at a glassy carbon electrode.[37]

The analogous $W_3S_4^{4+}$ aqua ion is also well established.[38-40] This aqua ion can be prepared by the reduction of $(NH_4)_2WS_4$ with $NaBH_4$ and purified by the use of Sephadex G-15 and Dowex 50W-X4 cation exchangers in succession.[38] The aqua ion in 2M Hpts is stable toward air oxidation. The $W_3S_4^{4+}$ aqua ion has been confirmed as having an incomplete cubane type structure[39] similar to that of its molybdenum analogue.[36] The average W-W bond length of the aqua ion is 2.724Å[39] which is very slightly shorter than the averaged Mo-Mo distance of 2.735Å.[36]

The kinetics of the 1:1 complexing of NCS^- for H_2O at tungsten on the $W_3S_4^{4+}$ and $W_3O_3S^{4+}$ (μ_3-S) aqua ions has been investigated.[41] Such a study has allowed a reactivity pattern for the $[W_3O_xS_{4-x}(OH_2)_9]^{4+}$ ions to be made. The formation rate constant (k_f / $M^{-1}s^{-1}$) in 2.0 M $HClO_4$ (I=2.00 M) for $W_3S_4^{4+}$,$W_3O_3S^{4+}$ and $W_3O_4^{4+}$ are 38.4, 0.0080 and 0.11, respectively, giving a similar trend to that of the correspoding Mo^{IV}_3 aqua ions (see page 14), which however react an order of magnitude faster. The $W_3S_4^{4+}$ aqua ion was found to react *via* both the aqua ion and the monohydroxy form in contrast to the $W_3O_4^{4+}$ aqua ion which reacts *via* only the conjugate-base form. This behaviour is very similar to that for the $[Mo_3O_xS_{4-x}(H_2O)_9]^{4+}$ series of complexes in which the substitution of $Mo_3S_4^{4+}$ involves the aqua ion as well as the monohydroxy form, whereas the other $Mo_3O_xS_{4-x}^{4+}$ aqua ions so far studied react only *via* the monohydroxy form. The acid dissociation constant (K_a) of 0.35 M found for $W_3S_4^{4+}$ is in the observed range 0.2-0.5 M, apparently typically of these species.

A cyclic voltammogram (glassy carbon electrode) of the $W_3S_4^{4+}$aqua ion in 2 M Hpts showed no appreciable peak in the range

0.7 to -0.7 V (*vs* SCE).[38] This lack of redox behaviour is similar to that observed for the analogous $Mo_3S_4^{4+}$ aqua ion[33] and may be a reflection of a lower tendency for the μ-sulphido groups to become protonated upon reduction.

1.1.2 Oxo/Sulphido Bridged Trinuclear Mo(IV) and W(IV) Aqua Ions

The synthesis of oxo-sulphido Mo(IV,IV,IV) complexes in the series $Mo_3O_xS_{4-x}^{4+}$ as aqua ions has been reported. The preparation of the grey $Mo_3O_2S_2^{4+}$ species (μ_3-sulphido) for example, can be prepared by essentially the same route as for $Mo_3O_4^{4+}$, by reacting $[MoCl_6]^{3-}$ with the aqua di-μ-sulphido $Mo_2(V)$ complex $[Mo_2O_2S_2(H_2O)_6]^{2+}$.[42] The structure of the product has been characterised crystallographically as $(pyH)_5[Mo_3O_2S_2(NCS)_9].2H_2O$.[42]

Different approaches namely electrochemical and $NaBH_4$ reduction methods have been used to prepare the dark green $Mo_3OS_3^{4+}$ ion (μ_3-oxo) along with the green cubic cluster complex $Mo_4S_4^{5+}$.[37,43-45] By the electrochemical route using pairs of $Mo_2(V)$ complexes, $[Mo_2O_4(cys)_2]^{2-}$ $[Mo_2O_3S(cys)_2]^{2-}$ and $[Mo_2O_2S_2(cys)_2]^{2-}$ in equimolar quantities, followed by cation-exchange purification, a series of eight different aqua ions have been obtained. Their UV-visible spectral characteristics along with those of other closely related species are displayed in Table 1.1. The analogous tungsten species have so far not yet been reported. The synthetic pathways used by Sykes may not be possible since the corresponding tungsten starting materials are

Table 1.1: UV-Visible Spectra of Triangular Oxo/Sulphido Aqua Ions of Mo(IV) and W(IV)

Complex	λ_{max}/ nm	ε^* $M^{-1}cm^{-1}$	Ref
$[Mo_3(\mu_3\text{-}O)(\mu\text{-}O)_3(OH_2)_9]^{4+}$	505 300(sh)	189 1560	13
$[Mo_3(\mu_3\text{-}O)(\mu\text{-}O)_2(\mu\text{-}S)(OH_2)_9]^{4+}$	511 332		44
$[Mo_3(\mu_3\text{-}S)(\mu\text{-}O)_3(OH_2)_9]^{4+}$	512 333	153 930	44
$[Mo_3(\mu_3\text{-}O)(\mu\text{-}S)_2(\mu\text{-}O)(OH_2)_9]^{4+}$	545 327	188 2490	44
$[Mo_3(\mu_3\text{-}S)(\mu\text{-}O)_2(\mu\text{-}S)(OH_2)_9]^{4+}$	568 335	207 2330	44
$[Mo_3(\mu_3\text{-}O)(\mu\text{-}S)_3(OH_2)_9]^{4+}$	580 332	206 2500	44
$[Mo_3(\mu_3\text{-}S)(\mu\text{-}S)_2(\mu\text{-}O)(OH_2)_9]^{4+}$	588 410(sh) 370(sh) 332	263 2980	44
$[Mo_3(\mu_3\text{-}S)(\mu\text{-}S)_3(OH_2)_9]^{4+}$	603 366 248	362 5550 8219	33
$[W_3(\mu_3\text{-}O)(\mu\text{-}O)_3(OH_2)_9]^{4+}$	455	375	17
$[W_3(\mu_3\text{-}S)(\mu\text{-}O)_2(\mu\text{-}S)(OH_2)_9]^{4+}$	506	381	46
$[W_3(\mu_3\text{-}O)(\mu\text{-}S)_3(OH_2)_9]^{4+}$	535	408	47
$[W_3(\mu_3\text{-}S)(\mu\text{-}S)_3(OH_2)_9]^{4+}$	560 315	546 8650	38
$[Mo_2W(\mu_3\text{-}O)(\mu\text{-}O)_3(OH_2)_9]^{4+}$	515 400(sh)	168 227	48
$[Mo_2W(\mu_3\text{-}S)(\mu\text{-}S)_3(OH_2)_9]^{4+}$	595 490(sh)	298 322	49
$[MoW_2(\mu_3\text{-}S)(\mu\text{-}S)_3(OH_2)_9]^{4+}$	568 490	363 320	49

*ε is per trimer

unavailable. However, Cotton *et al* [34,35,50] have devised an alternative route for the synthesis of $Mo_3S_4^{4+}$ and $Mo_4S_4^{5+}$, which may be of synthetic value for the tungsten species in the future. In this procedure $Mo(CO)_6$ is refluxed in acetic anhydride containing dry Na_2S under N_2. The products are purified by ion-exchange following filtration and dilution. The corresponding reaction using $W(CO)_6$ however yielded a complicated mixture of products, one of which being identified as the $W_3S_4^{4+}$. Using this same method some progress has been made with the isolation of the purple tungsten species $[W_3(\mu\text{-}O)_3(\mu_3\text{-}S)(NCS)_9]^{5-}$ [51] This complex together with other mixed oxo/sulphido derivatives have been structurally characterised thus providing the series $W_3O_xS_{4-x}^{4+}$ (x=0-4).[17,38,39,46,50,51]

The mixed oxo/sulphido clusters are rather interesting in terms of their substitution behaviour and Ooi *et al* [52] have shown that whereas introduction of μ_3-S for μ_3-O actually lowers the rate of water substitution by an order of magnitude, replacing μ-O with μ-S causes a labilising effect: 10^3x when all three μ-O are replaced. This strongly implies differing electronic effects for the two types of bridging group with regard to their influence on the kinetic lability of the water liqands. The triply bridging nature of the capping group would imply that it carries a formal positive charge which for sulfur may suppress its normal tendency to be a better σ-donor than oxygen, a factor presumably responsible for the labilizing effect observed when μ-O is replaced by μ-S. Furthermore UV-visible spectrophotometric and kinetic studies (NCS^- substitution) indicate that the $Mo_3(\mu_3\text{-}S)(\mu\text{-}O)_3^{4+}$ ion may have a slightly larger value for the K_a (0.6 M) than either $Mo_3O_4^{4+}$ (0.2 -0.4 M) or $Mo_3S_4^{4+}$ (0.15 M, see later) and this may reflect an effective electron withdrawing role for the μ_3-S group as opposed to an effective σ-donating role for μ-S. In the NCS^-

substitution study on the complex $[Mo_3(\mu_3\text{-}S)(\mu\text{-}S)_2(\mu\text{-}O)(OH_2)_9]^{4+}$ a two stage process was detected. A statistical factor of two on the slow step was relevant; that is substitution at the two identical molybdenum's with mixed μ-O and μ-S co-ordination spheres was observed to be slower than that at the single molybdenum with all μ-S. This behaviour is also consistent with the differing electronic effects of μ-S *vs* μ-O described above.

1.1.3 Molybdenum-Tungsten Mixed-Metal Trinuclear Aqua Ions $[M_3X_4(OH_2)_9]^{4+}$ (M_3 = Mo_2W or MoW_2 ; X = O or S)

The family of the Mo(IV) and W(IV) aqua ions has been extended as a result of the synthesis of the first mixed-metal aqua ion of oxidation state +4, $[Mo_2WO_4(OH_2)_9]^{4+}$.[19,48] This complex after much sustained effort was finally isolated and characterised, following the reactions of $MoCl_4$ (or $[MoCl_6]^{2-}$) with $K_2[WCl_6]$ in HCl. The UV-visible spectrum of this species is compared with those of the homonuclear Mo(IV) and W(IV) aqua ions in Figure 1.3. Solid derivatives namely $(Me_4N)_3[Mo_2WO_4(SCN)_7(OH_2)_2]$, $(Et_4N)_3[Mo_2WO_4(SCN)_7(OH_2)_2]$ and $Cs_{0.33}Na_{0.67}Mo_2WO_4(MIDA)_8(H_2O)$ have been prepared with satisfactory elemental analysis. Conclusive evidence of the $Mo_2WO_4^{4+}$ core was finally provided by an X-ray crystallographic study of $(Me_4N)_5[Mo_2WO_4(NCS)_9]$.[53] This study has revealed that the molybdenum and tungsten atoms are statistically disordered. The averaged M-M distance in this mixed-metal species (2.521Å)[53] is however similar to those of the homonuclear Mo_3 (2.48Å)[15] and W_3 (2.534Å)[17] species. The presence of the $Mo_2WO_4^{4+}$ core in solution has also been verified by ^{17}O NMR measurements.[53]

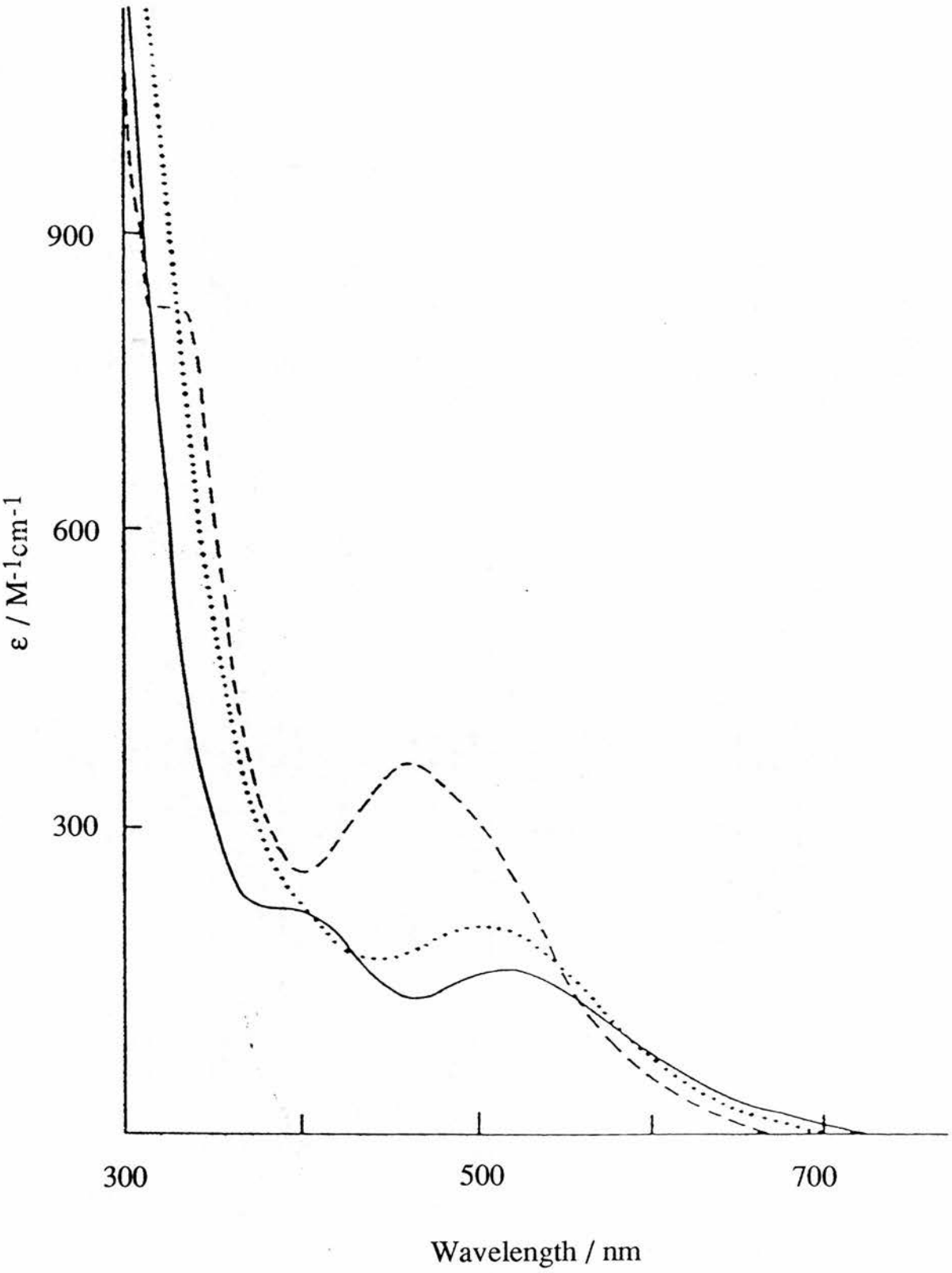

Figure 1.3 : Electronic spectra of trinuclear aqua ions in Hpts solution (2M): (—) $[WMo_2O_4]^{4+}$, (....) $[Mo_3O_4]^{4+}$,(----) $[W_3O_4]^{4+}$.

Having synthesised the $Mo_2WO_4^{4+}$ aqua ion, interest lay in studies of its redox and H_2O substitution behaviour in order to investigate any consequences of the lowering of the three-fold symmetry. Using NCS^- as the incoming ligand, substitution was observed to proceed *via* the monohydroxy form as observed for the homonuclear Mo(IV) and W(IV) species, with a rate constant of 1.82 $M^{-1}s^{-1}$ coupled with an exceptionally high acid dissociation constant of 1.00 M. It is believed that the 1:1 substitution occurred preferentially at the molybdenum sites that are *trans* to the μ-O groups and it is envisaged that deprotonation occurred at a further μ-O group located on the same molybdenum atom being substituted. A statistical factor of two in support of the two identical molybdenum sites was obtained for the rate determining step when values for the k_{eq} from $[M_3^{4+}]$ in excess were compared with those from $[NCS^-]$ in excess. The slightly slower Mo-OH_2 substitution rates (*vs* $Mo_3O_4^{4+}$) and the large K_a value were initially believed to be a consequence of the electron withdrawing tendency of the remote tungsten atom.

Cyclic voltammetric studies have shown that the complex has a reversible wave at - 0.21 V *vs* NHE in 2 M Hpts at 25 °C. This has been assigned to reduction to give the mixed-valence ion Mo_2W(III,III,IV), a fact confirmed following reduction with Eu^{2+} wherein the expected electronic spectrum of the mixed-valence species, with an intervalence band at 880 nm, was generated. The complex is however further reduced by Zn/Hg to give the Mo_2W(III,III,III) species. The large difference in respective reduction potentials is consistent with reduction firstly at molybdenum to give $Mo_2^{III}W^{IV}$ and then at tungsten to give $Mo_2^{III}W^{III}$. The similarity in the appearance of the electronic spectrum of Mo_2W(III,III,IV) to that of the homometal

mixed-valence species (the bands occurring in energy exactly between those of the homometal ions) supports considerable electronic interaction between the two metal centres (Class II behaviour) and a likely molecular structure : $Mo_2W(OH)_4^{6+}$. ^{17}O NMR studies are currently in progress to verify this.

The synthesis of the other mixed tungsten - molybdenum aqua ion $[MoW_2O_4(OH_2)_9]^{4+}$ has so far proved elusive despite many varied attempts in our laboratory and no doubt in others as well. In contrast the family of the corresponding μ-S species $[M_3S_4(OH_2)_9]^{4+}$ (M_3 = Mo_3, Mo_2W, MoW_2,W_3) is complete. This feat was recently achieved with the successful synthesis, characterisation and X-ray structures of the $[M_3S_4(OH_2)_9]^{4+}$ (M_3 =Mo_2W, MoW_2) aqua ions.[49] These mixed-metal species were prepared by reacting $(NH_4)_2WS_4$ with $Na_2[Mo_2O_2S_2(cys)_2].4H_2O$ in the presence of $NaBH_4$ and HCl. The complexes were obtained in the pure form following treatment with Sephadex G-15 and Dowex 50W-X2 cation exchangers in succession. A feature of note is that the $MoW_2S_4^{4+}$ ion is only formed in small amounts which may explain its absence from the μ-oxo system. X-ray structure analysis[49] of the $Mo_2WS_4^{4+}$ and $MoW_2S_4^{4+}$ species revealed the existence of the expected incomplete cubane-type core. These species are isomorphous with the $Mo_3S_4^{4+}$ and $W_3S_4^{4+}$ aqua ions. The molybdenum and tungsten atoms in both crystals are statistically disordered paralleling the behaviour of the $Mo_2WO_4^{4+}$ ion.[53] The averaged metal-metal distances in $Mo_2WS_4^{4+}$ (2.728Å) and $MoW_2S_4^{4+}$ (2.723Å) are fairly similar to those of the homonuclear Mo_3(2.735Å) and W_3(2.724Å)[39] species.

The electronic spectra of these mixed metal sulphido aqua ions are compared with those of the homonuclear aqua sulphido ions in Figure 1.4. None of these four species have any peaks in the near-

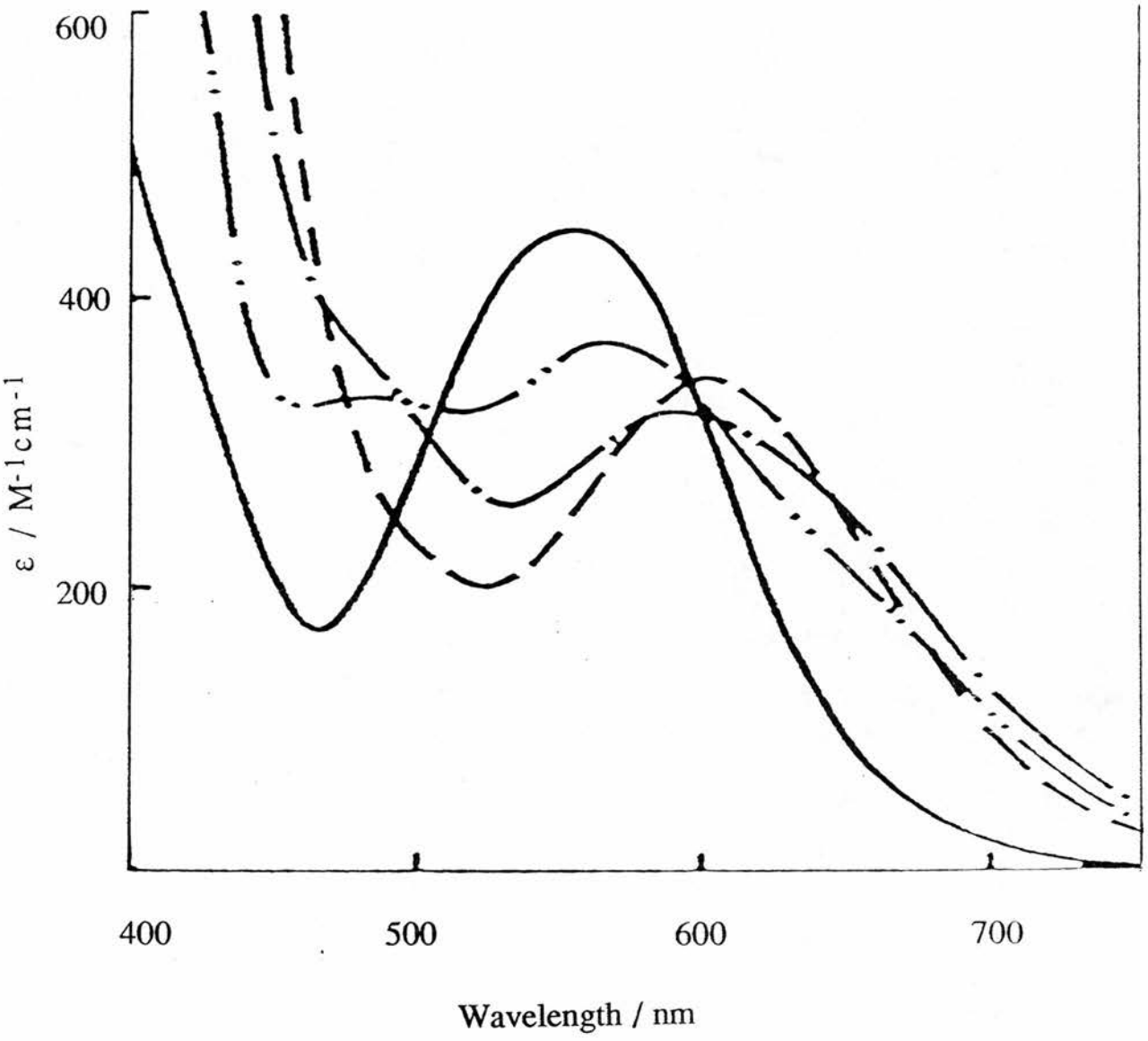

Figure 1.4: Electronic absorption spectra in 2M HPTS :— $W_3S_4(OH_2)_9^{4+}(W_3)$; ---$MoW_2S_4(OH_2)_9^{4+}$ (MoW_2); -·- $Mo_2WS_4(OH_2)_9^{4+}$ (Mo_2W); ---$Mo_3S_4(OH_2)_9^{4+}$ (Mo_3)

infrared region. The figure shows that the mixed metal clusters have fairly large splitting of the absorption peaks and the longer wavelength peak positions of the four aqua ions shift to longer wavelenghts when the tungsten atom is replaced by molybdenum. This splitting is also apparent in the UV-visible spectrum of $Mo_2WO_4^{4+}$ (Figure 1.3).

A controversy was present at the outset of this work concerning the magnitude of K_a for the $Mo_3O_4^{4+}$ and $Mo_3S_4^{4+}$ aqua ions. For both $Mo_3O_4^{4+}$ and $Mo_3S_4^{4+}$, substitution studies using both NCS^- and $HC_2O_4^-$ as incoming ligands have indicated a mechanism involving primarily the monohydroxy ion with a $K_a \sim 0.2$-0.4 M. This seemed at odds with the results obtained from water exchange studies using ^{17}O NMR for c- and d- waters in $Mo_3O_4^{4+}$ and $Mo_3S_4^{4+}$ which indicated formation of the relevant monohydroxy ion consistent with a much lower value for $K_a \leq 0.01$M. For $Mo_3O_4^{4+}$ independent UV-visible spectrophotometric and ^{17}O chemical shift measurements following $[H^+]$ variation were in support of a K_a ~0.2-0.4 M but this had not been similarly substantiated in the case of $Mo_3S_4^{4+}$. In view of the controversy it was thus decided to undertake a repeat kinetic study of NCS^- substitution on $Mo_3O_4^{4+}$ in pts- (conventional timescale) and at the same time attempt a closer investigation of the acid dissociation occurring on $Mo_3S_4^{4+}$. Herein we also report conclusive evidence from a variable $[H^+]$ and temperature spectrophotometric study for a K_a value (25 °C) for $Mo_3O_4^{4+}$ of 0.43 M. In view of these findings we ultimately report a reevaluation of the results obtained from water exchange studies (^{17}O NMR) on the $Mo_3S_4^{4+}$ ion and wish to report the final conclusions reached.

1.2 EXPERIMENTAL

1.2.1 Standardisation of Reactants

Lithium *p*-toluenesulphonate, Lipts, was prepared by neutralising solutions of 4M Hpts (Lancaster Synthesis) with lithium carbonate (BDH, reagent grade) followed by recrystallisation three times from water. Stock solutions of both Lipts and sodium thiocyanate (Fluka) were standardised by cation exchange onto Amberlite IR(H) 120 resin and titration of the liberated H^+ (corresponding to moles M^+ hence X^-) with NaOH (Convol, BDH). The concentrations of $Mo_3O_4^{4+}$ solutions were determined spectrophotometrically at its 505 nm peak (ε = 189 $M^{-1}cm^{-1}$/mol of trimer at 25 °C).[2b] A similar method for standardisation was used for solutions of $Mo_3S_4^{4+}$ (ε= 362 M^{-1} cm^{-1}/mol of trimer for the 603 nm peak).[33] The background $[H^+]$ of the $M_3X_4^{4+}$ (X= O, S) solutions was determined by difference following exchange onto a column of Dowex 50W-X2 resin and titration of liberated H^+ (representing total charge = background H^+ + 4 x $[Mo_3]$) with standard NaOH using phenolphthalein as indicator.

1.2.2 Preparation of Complexes

1.2.2.1 Preparation of Hexachloromolybdate (III)

The hexachloromolybdate (III) solution was prepared by a modification of the method reported by Irving and Steele.[54] A weighed amount of molybdenum trioxide (30 g) was dissolved by heating it with 8 M hydrochloric acid (300 ml) over a 2 hour period. The resulting yellow solution was reduced by electrolysis using a stirred mercury cathode and a carbon anode; the anode compartment was separated from the cathode compartment by a sintered glass partition. Reduction to the

Mo(III) stage required 24 amperes per hour. The reduction process was indicated by the liberation of hydrogen from the cathode and the solution underwent a series of colour changes from yellow through to deep red. Frothing of the anolyte was observed at times during the electrolysis process due to powdering of the carbon electrode, and it was necessary to withdraw the solution periodically and to filter it before returning it to the anode compartment. The temperature of the solution increase during the experiment, and the cell was cooled by ice in order to prevent excessive evaporation.

1.2.2.2 Preparation of Potassium Hexachloromolybdate (III):

The solid was prepared by a modified form of the method of Bucknall *et al.* [55] Potassium chloride (20 g) in deoxygenated water (100 ml) was added to the filtered hexachloromolybdate (III) solution (as described above). Gaseous HCl was then passed through the solution, where upon potassium hexachloromolybdate (III), $K_3[MoCl_6]$, separated as pinkish-red crystals. The mixture was cooled to 0 °C and the crystals filtered off, washed with alcohol and dried in the air.

Yield = 31.5 g

1.2.2.3 Preparation of solutions of $[Mo_3O_4(OH_2)_9]^{4+}$

Two methods have now been established in the literature:

A. This method is based upon that reported by Richens and Sykes.[2b] A mixture of sodium molybdate (2.42g) and potassium hexachoromolybdate (III) (9.5 g) was heated together at 80 °C for 1-2 hours in deoxygenated 2 M HCl solutions (50 ml). The resulting mixture was diluted to a final volume of 500 ml and $[H^+]$ ~0.50 M with

water and Hpts. The solution was then left to stand for 24 hours to allow complete aquation of coordinated chloride. The aqua ion was purified by loading onto a Dowex 50W-X2 cation exchange column (20 cm x 1.5 cm diameter). Before elution of the red aqua ion was commenced any residual Mo(V) and $Mo_3O_4Cl_n^{(4-n)+}$ species were removed by successive washing until the washings were colourless and free of Cl^- (tested with $AgNO_3$). The red aqua ion was then eluted with 3 M Hpts giving stock solutions typically 0.1 M in $Mo_3O_4^{4+}$.

B. Stock solutions of $Mo_3O_4^{4+}$ were also prepared by the method described by Cotton *et al.* [56] This method involves the reaction of amounts of Mo_2^{III} dimer ($Mo_2^{III}(OH)_2^{4+}$) and sodium molybdate in a ratio appropriate for comproportionation to give Mo(IV). The $Mo_2(OH)_2^{4+}$ solution was prepared by reduction of a solution of $Na_2MoO_4.2H_2O$ (0.75 g, 3.1 mmol) in deoxygenated 1 M HCl (310 ml) with zinc amalgam (20 g). The mixture was stirred for 30 minutes after which the Zn/Hg was removed by decantation and the Mo(III) solution added to a deoxygenated solution of $Na_2MoO_4.2H_2O$ (0.38 g, 1.6 mmol) in 1M HCl (50 ml) and the mixture heated for one hour. The solution was then diluted 3-4 times with deoxygenated 1 M Hpts and left to stand under N_2 at room temperature for 2 days to allow complete aquation of coordinated chloride. The red aqua ion was diluted to $[H^+]$ ~0.5 M and loaded onto Dowex 50W-X2 cation exchange column (20 cm x 1.5 cm diameter). Purification of the aqua ion was carried out as described in Method A giving rise to similar stock solutions in Hpts.

1.2.2.4 Preparation of solutions of $[Mo_3S_4(OH_2)_9]^{4+}$

Solutions of the cuboidal ion $[Mo_4S_4(OH_2)_{12}]^{5+}$ in 2 M HCl were first prepared by $NaBH_4$ reduction of the *l*-cysteinato bis (μ-sulphido)

Mo_2^V complex; $Na_2[Mo_2O_2S_2(cys)_2].4H_2O$ as reported in the literature.[45,57] Conversion of dimeric Mo_2S_2 to tetrameric cuboidal Mo_4S_4 occurs during this process. The resulting $Mo_4S_4(OH_2)_{12}]^{5+}$ solution, following DOWEX 50W-X2 cation-exchange chromatography, was heated in 1-2 M HCl on a steam bath at ~90 °C for ~12 hours after which conversion to $[Mo_3S_4(OH_2)_9]^{4+}$ occurred quantitatively.[33] The $Mo_3S_4^{4+}$ aqua ion was then purified by further DOWEX 50W-X2 cation-exchange chromatography. For this the crude solution was diluted to ~0.5 M in $[H^+]$ and then loaded onto the column. Following washing of the column with 1M $HClO_4$ (or 1 M Hpts), which separated the $Mo_3S_4^{4+}$ aqua ion from any remaining $[Mo_4S_4(OH_2)_{12}]^{5+}$, the $Mo_3S_4^{4+}$ species could be then eluted with 4 M $HClO_4$ (or 4 M Hpts). Solutions obtained by eluting with Hpts are observed to be much more concentrated in $[Mo_3]$ by a factor of ≥ 5 than those obtained using $HClO_4$; a consequence it is believed of greater ion-pair association of the aqua ion with the pts^- counter anion than in the case of ClO_4^- (see discussion).

1.2.3 Kinetic study of NCS^- Complexation on $Mo_3O_4^{4+}$

Kinetic runs were on a time scale of $t_{1/2} > 1$ minute and were carried out at 360 nm by conventional UV spectrophotometry on a Perkin-Elmer Lambda 5 instrument (fixed wavelength using an auto cell changer). The study was conducted with the $[NCS^-]$ in large (mole) excess (>10-fold) over the $Mo_3O_4^{4+}$ concentration. For each run the required amounts of Hpts, NaSCN, Lipts and water were added to 1-cm quartz cells (final volume of solutions 3 cm^3). The solution in each cell was deoxygenated by passing a slow stream of N_2 through it (using rubber seals, teflon tubing and stainless steel needles). After

deoxygenating (~15 minutes), the cells were placed inside the cell compartment of the spectrophotometer and allowed to equilibrate to the required temperature. The required amounts of the complex were then added to the cells by means of a Hamilton Syringe (0.50±0.01 cm^3). Following mixing monitoring of the absorbance-time changes was immediately started. The concentrations of thiocyanate were in a range appropriate for 1:1 complex formation at any one metal atom. Even under these conditions small subsequent absorbance changes were observed (believed due to further reaction of SCN^- at a second metal atom).[21] Because of the uncertainity in absorbance infinity (A_∞) values the Swinbourne method (see Appendix) was used to calculate A_∞ for the relevant 1:1 process. First-order equilibration rate constants were evaluated from plots of -ln (A_∞-A_t) versus time which were linear up to at least 3 half-lives. The kinetic study was conducted at 25.0±0.1 °C and the ionic strength maintained at 2.0 M using Hpts and Lipts. The data were treated with the assumption that statistical kinetics apply as reported before.[21] This assumption is based on the idea that rate constants obtained with [NCS^-] in large excess are three times those obtained with [$Mo_3O_4^{4+}$] in large excess at the equivalent concentration such that determination of the forward rate constant (see later) requires division of the [NCS^-] by three in order to allow for this. The kinetic data were evaluated using unweighted linear least-squares fits.

1.2.4 Determination of the Acid Dissociation Constant for the $[Mo_3O_4(OH_2)_9]^{4+}$ Aqua Ion.

The K_a of $[Mo_3O_4(OH_2)_9]^{4+}$ was measured at four temperatures using UV-visible spectrophotometry. For this experiment a stock solution of $Mo_3O_4^{4+}$ was prepared in ~3 M Hpts which was then diluted

with distilled deoxygenated water to achieve an ionic strenght of 2.0 M. At this point the $[Mo_3O_4^{4+}]$ was typically 0.0473 M and the $[H^+]$ was 1.529 M. The measurements of K_a involved the addition, to 1 cm^3 of this solution , aliquots of a deoxygenated 2.0 M Lipts solution measured accurately using the 0.5 cm^3 Hamilton Syringe at near 0 °C in an ice bath. Initially 0.5 cm^3 aliquots of the Lipts solution were added but as the dilution progressed larger volumes (>1 cm^3) were subsequently added to adjust the $[H^+]$. Under these conditions the $[H^+]$ is adjusted by dilution keeping the ionic strength constant at 2.0 M while at the same time keeping the $[H^+]/[Mo_3O_4^{4+}]$ constant at >50 so as to suppress oligomerisation . The solutions after each addition was placed in a 0.1 cm cuvette, and ultimately a 1.0 cm cuvette, and allowed to come to equilibrium at 5 °C, 15 °C, 25 °C and 35 °C. The UV-visible spectrum between 400 and 650 nm was recorded after each adjustment and the absorbance at 505 nm noted after which the absorbance readings were corrected for dilution.

On decreasing the $[H^+]$ between 1.5 and 0.015 M (I=2.0 M, Lipts), small rapid and reversible absorbance changes were detected for solutions of $[Mo_3O_4(OH_2)_9]^{4+}$ between 400 and 650 nm. Typical UV-visible spectral behaviour is depicted in Figure 1.5, for T=15 °C. From the Figure it can be seen that the relative absorbance decreases at the 505 nm peak on decreasing the $[H^+]$ with a progressive shift in the λ_{max} to lower wavelength. An isosbestic point was observed at ~ 550 nm, confirming the presence of two species in equilibrium. This isosbestic point was eventually lost at $[H^+] \leq 0.02$ M and this is believed to be due to the formation of oligomers at these low acidities. The data obtained at the four temperatures were satisfactorily fitted to equation (1.2) and a

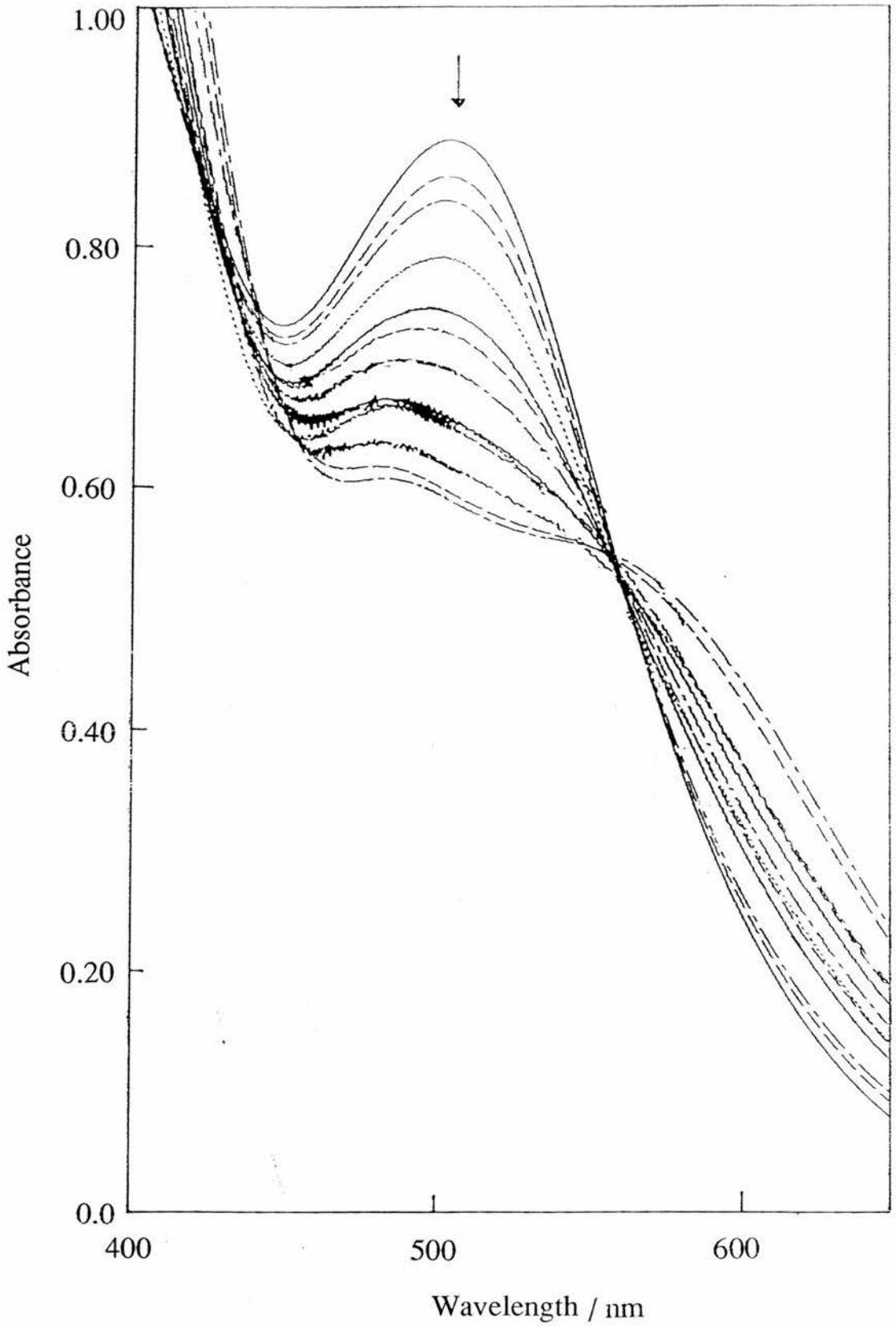

Figure 1.5: UV-visible scan spectra of solutions of $Mo_3O_4^{4+}$ in Hpts (0.03-1.53 M) at I=2.0 M (Lipts), 15 °C. The arrow shows the direction of decreasing $[H^+]$.

$$\varepsilon_{505}^{obs} = \frac{\varepsilon_{505}(Mo_3O_4^{4+}) + \varepsilon_{505}(Mo_3O_4(OH)^{3+}).10^{(pH-pK_a)}}{10^{(pH-pK_a)} + 1} \quad (1.2)$$

representative plot of the pK_a titration curve at 15 °C is shown in Fig. 1.6. The results obtained for the fit of the data to equations (1.2) and (1.3) are shown in Table 1.2.

$$d(\ln K_a)/dT = \Delta H^o_a/RT^2 \quad (1.3)$$

Table 1.2: Results obtained from the UV-visible spectrophotometric study on $[Mo_3O_4(OH_2)_9]^{4+}$ in pts$^-$

	This Study	Previous Study[15]
$\varepsilon_{505}(Mo_3O_4^{4+})$ / $M^{-1}cm^{-1}$	217.7±3.6	193±1
$\varepsilon_{505}(Mo_3O_4OH^{3+})$/ $M^{-1}cm^{-1}$	106±1.1	155±2
K_a^{298} / M	0.43±0.04	0.24±0.04
ΔH^o_a / kJ Mol^{-1}	+3.9±1.5	
I / M	2.0	2.0

These values are believed to be superior and more reliable to those obtained by Richens *et al* [15] from a previous study in which both mixing and equilibration was performed at 25 °C. Under these conditions it is now clear that oligomerisation is more extensive.

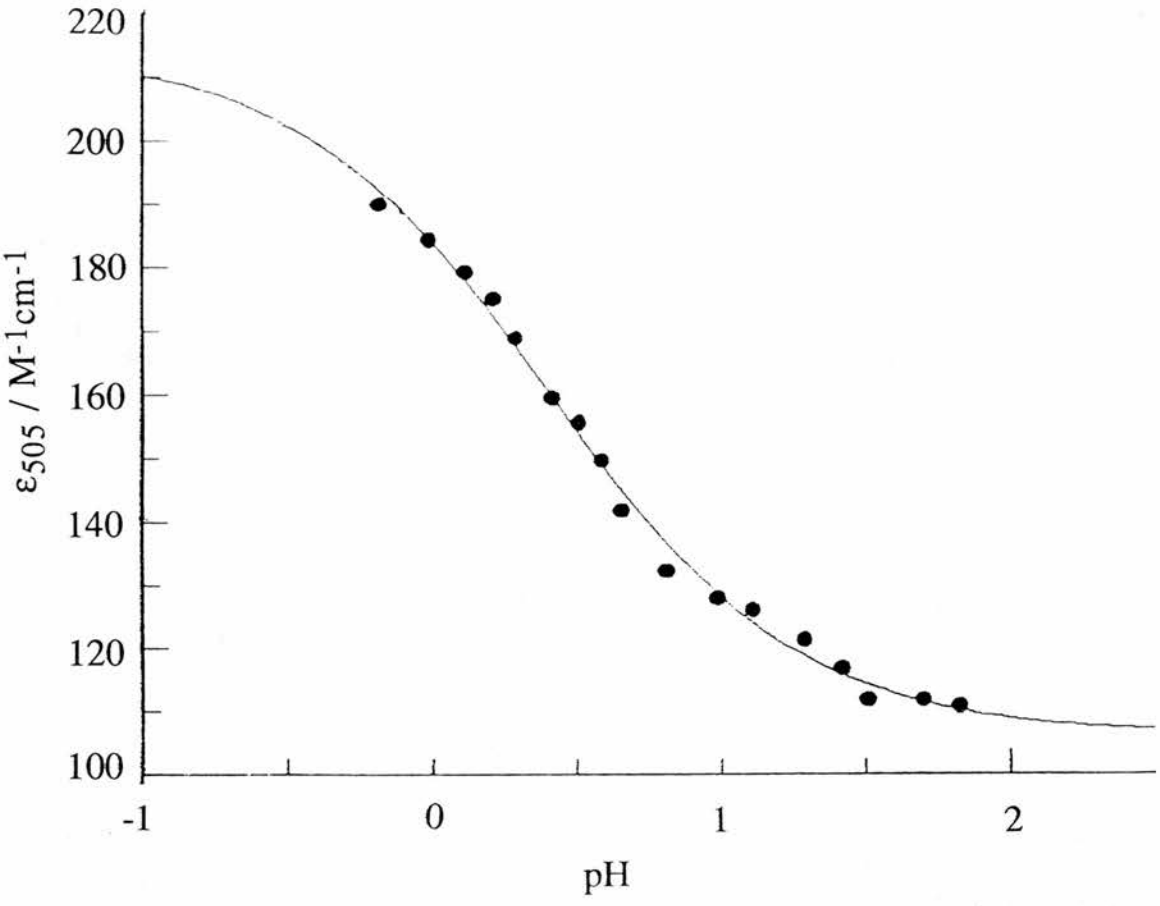

Fig 1.6: Spectrophotometric titration curve showing the variation of ε_{505} with pH for the $Mo_3O_4^{4+}$ aqua ion at 15 °C, I= 2.0 M (Lipts).

1.2.5 Determination of the Acid Dissociation Constant for the $[Mo_3S_4(OH_2)_9]^{4+}$ Aqua Ion

Attempts were made to monitor the acid dissociation during the dilution step to low $[H^+]$ as performed successfully for $Mo_3O_4^{4+}$ but here the scatter of data points proved too much for a reliable measure of the small absorbance changes observed. Instead a solution (50 cm^3) of $Mo_3S_4^{4+}$ was firstly prepared at pH 1.7 (I = 2 M, Lipts) by dilution of a stock solution (0.022 M $Mo_3S_4^{4+}$ in 1.886 M Hpts) into 2 M Lipts

at 0 °C as before. It was then found that accurate addition of aliquots of concentrated (12.2M) $HClO_4$ (Hamilton 0.5 cm^3 syringe) to this solution at 0 °C enabled the extremely small absorbance changes* accompanying the reprotonation of the monohydroxy species : $Mo_3S_4(OH)^{3+}$, to be monitored with satisfactory precision. Corrections to the absorbance readings to take account of dilution were made and the process was followed at five wavelenghts: 366nm (peak), 400nm(rise), 524 nm(min), 600 nm(peak) and 700 nm(rise). The most reliable results were obtained at 400 and 600 nm. As the $[H^+]$ was increased the corrected absorbances at 400 and 600 nm moved in different directions: that at 600 nm increasing in contrast to the decrease at 400 nm (Figure 1.7). An isosbestic point at ~460 nm was observed in support of the presence of the hoped for simple protonation of the monohydroxy form. The $[Mo_3]$ ranged from 0.17 to 0.22 mM during the titration with $HClO_4$. The lowering of the $[Mo_3]$ to below 1 mM within the initial dilution step (keeping the $[H^+] / [Mo_3]$ at ≥ 85) coupled with the use of low temperatures (0 °C (mixing), 5 °C (recording)) contrived to ensure that oligomerisation was suppressed as far as possible during the measurements.

Following these measurements, private communication with Professor Sykes' group at Newcastle University indicated that the absorbance changes as a function of $[H^+]$ observed for $Mo_3S_4^{4+}$ in pts^- solution, although occurring over the same range of $[H^+]$, were not in

---

*Typical delta absorbance changes at several of the wavelengths were as follows: 360 nm (0.008), 400 nm (0.03-largest), 600 nm (0.008) illustrating the size of changes observed. These changes are **much smaller** than those typically characteristic of the corresponding process on $Mo_3O_4^{4+}$.

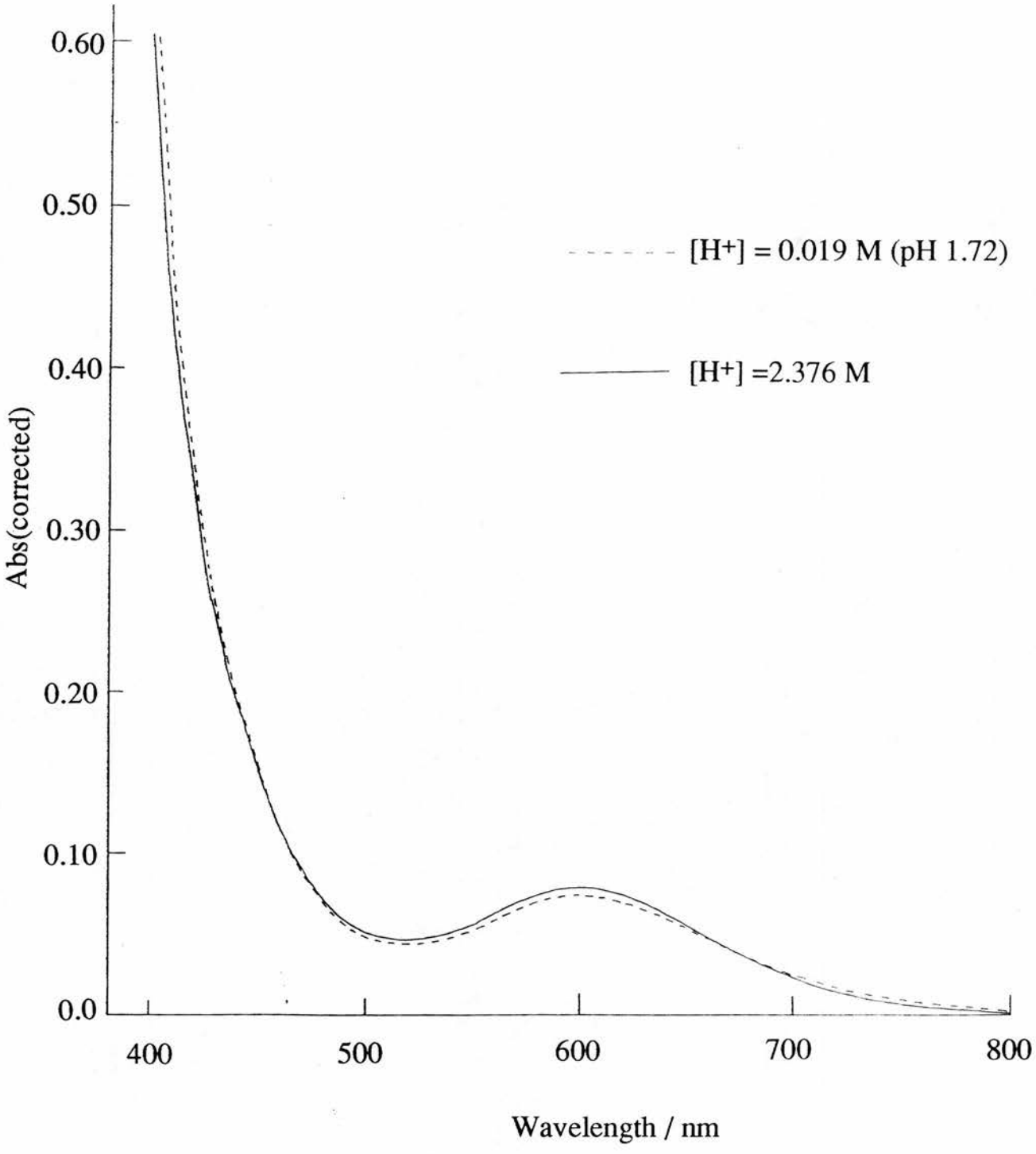

Figure 1.7: Electronic spectra of $[Mo_3S_4(OH_2)_9]^{4+}$ illustrating the small delta absorbance changes at different acidities.

agreement with those correspondingly observed using ClO_4^- as counter ion. It was thus decided to repeat the above measurements in ClO_4^- media. For this study a stock solution of $Mo_3S_4^{4+}$ (3.6 mM) in 3.77 M $HClO_4$ was prepared and diluted to high pH as before using, in this case,a solution of 2 M $NaClO_4$. Because of the lower $[Mo_3]$ of ClO_4^- stock solutions (see discussion), dilution only to pH 1.12 was possible in order to maintain sufficiently high $[Mo_3S_4^{4+}]$. However, as observed by the Newcastle group, the absorbance changes in this medium, after correction for dilution, were different than in pts^- now showing a discernible drop in magnitude between 330 and 440 nm during the dilution to pH 1.12 (Figure 1.8). Reacidification with 12.2 M $HClO_4$

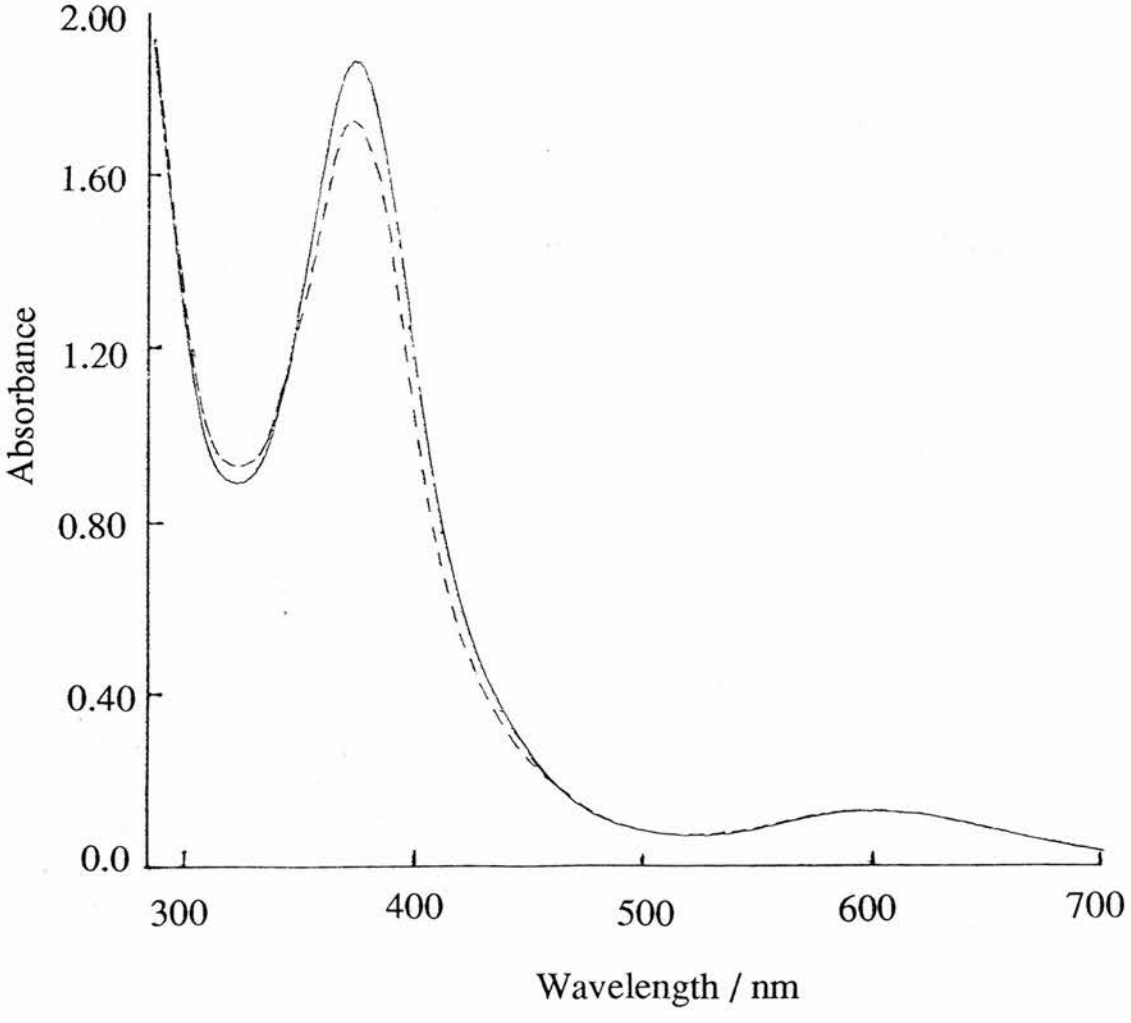

Figure 1.8 : Effect of pH variation on the UV-visible spectrum of $[Mo_3S_4(OH_2)_9]^{4+}$ in aqueous perchlorate solutions : $[H^+]$ = 3.77 M(—); pH=1.12 (---).

showed that these changes were reversible. Again an isosbestic point was observed around 460 nm implying that a similar process to that observed in pts$^-$ media was being followed, namely acid dissociation of the $[Mo_3S_4(OH)_9]^{4+}$ ion. It was concluded from these findings that effects due to the counter anions were playing a role in determining the nature and magnitude of absorbance changes observed between $Mo_3S_4^{4+}$ and $Mo_3S_4(OH)^{3+}$ in the different media.

In the case of $Mo_3S_4^{4+}$ the determination was carried out at a single temperature (5 °C) and as such does not allow an evaluation of ΔH_a^o to be made for comparision with that determined for $[Mo_3O_4(OH_2)_9]^{4+}$. As in the case of the $Mo_3O_4^{4+}$ aqua ion, the K_a value was evaluated using equation (1.2) and the values obtained in pts$^-$ medium at two different wavelengths (600 and 400 nm) were as follows:

400 nm K_a = 0.15 M

(T=5 °C)

600 nm K_a = 0.13 M

The respective plots of absorbance versus pH at the two wavelengths (600 and 400 nm) in pts$^-$ are illustrated in Figures 1.9 and 1.10(a) respectively. The corrsponding plot obtained at 400 nm in ClO_4^- medium is shown in Figure 1.10(b). In ClO_4^- solution a value of ~ 0.23 M for K_a was obtained which is in satisfactory agreement with the two values obtained in pts$^-$ medium, and with the value (0.24 M) reported in a private communication from the Newcastle group.

It was concluded that both $Mo_3O_4^{4+}$ (aq) and $Mo_3S_4^{4+}$ (aq) have high acid dissociation constants in the range 0.1-0.5 M with that for $Mo_3O_4^{4+}$ being somewhat slightly larger than that for $Mo_3S_4^{4+}$. Having established this fact it is now possible to proceed with a discussion of the

kinetic results with respect to the mechanism of replacement (exchange) of the water ligands on the respective two $Mo_3X_4^{4+}$ (X= O,S) aqua ions.

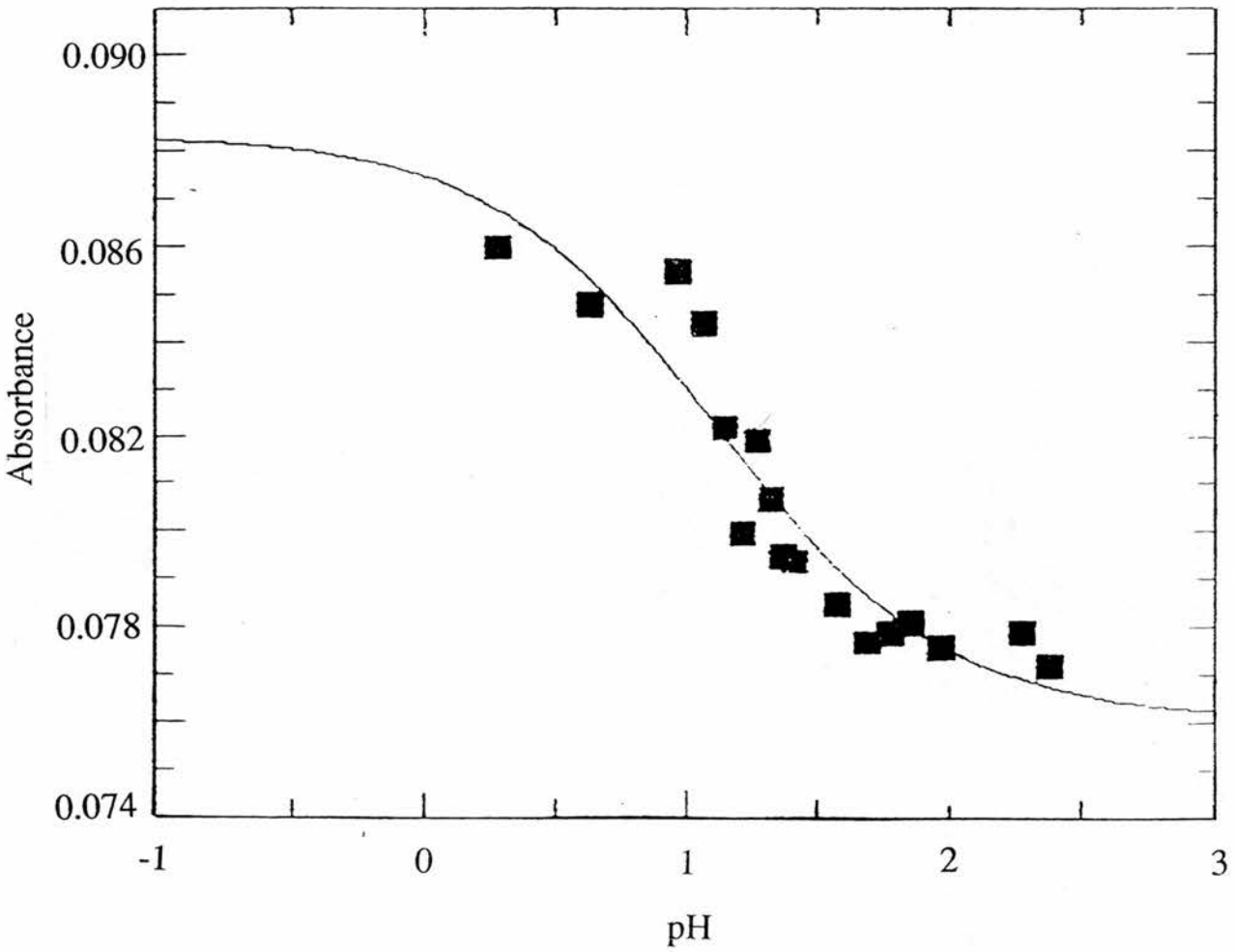

Figure 1.9: Variation of absorbance (at 600 nm) with pH for $[Mo_3S_4(OH_2)_9]^{4+}$ in pts^- solution (I = 2.0 M, Lipts) at 5 °C.

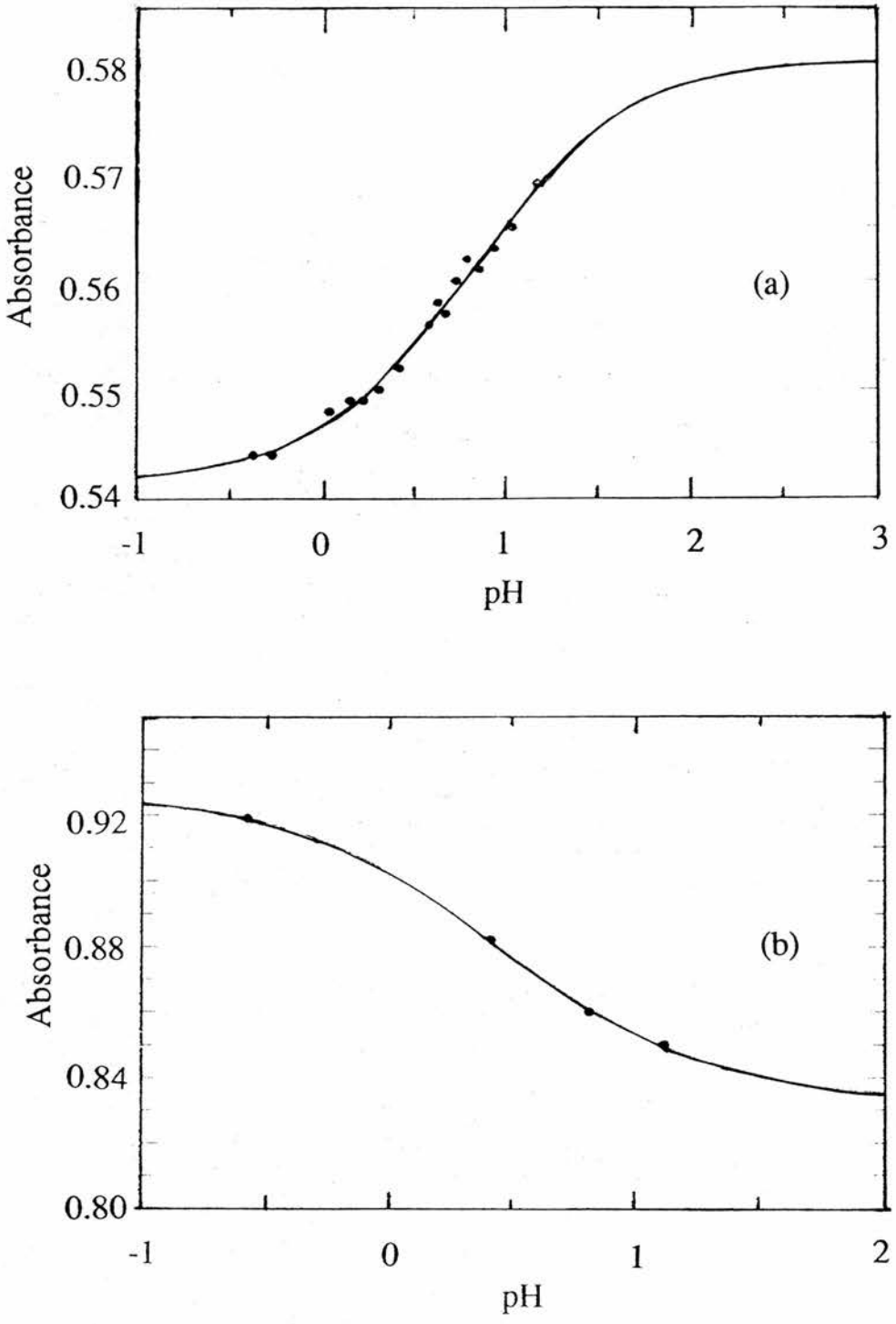

Figure 1.10 : (a) Variation of absorbance (400 nm) with pH for $[Mo_3S_4(OH_2)_9]^{4+}$ in pts^- solution (I= 2.0 M, Lipts) at 5 °C. (b) The corresponding plot of the same aqua ion for readings taken at 400 nm in ClO_4^- solution (I= 2.0 M, $NaClO_4$), T= 5 °C.

1.3 RESULTS

1.3.1 Kinetic study of 1:1 NCS^- substitution on $Mo_3O_4^{4+}$

1.3.1.1 Dependence on Thiocyanate concentration

The dependence of the first-order equilibrium rate constants, k_{eq}, on the thiocyanate concentrations was investigated in a series of runs with [NCS^-] in large excess (>10-fold). The thiocyanate concentration was restricted to the range 1.2×10^{-3} M to 3.5×10^{-3} M to avoid or reduce the chance of any secondary reaction. The results obtained at 25 °C are listed in Table 1.3.

1.3.1.2 Dependence on Hydrogen Ion Concentration

The acid dependence study was investigated in the range 0.25-2.00 M and the variation of k_{eq} values with NCS^- concentration at different H^+ concentrations is shown in Figure 1.11. The figure clearly shows that equilibrium kinetics are relevant and k_{eq} can be expressed as in equation (1.4) which takes into account the statistical factor of three,

$$k_{eq} = k_f [NCS^-] / 3 + k_{aq} \qquad (1.4)$$

with the rate constants corresponding to 1:1 complexing of NCS^- with the molybdenum species. The values of k_f and k_{aq} for formation and

Table 1.3 : First-Order Equilibration Rate Constants (k_{eq}) for the Reaction of $Mo_3O_4^{4+}$ with NCS^- at 25 °C, I = 2.0 M (LiPTS), [Complex] ~ 4.0×10^{-5} M.

$[H^+]$ / M	10^3 $[NCS^-]$ / M	$10^3 k_{eq}$ / s^{-1}	$[H^+]$ / M	10^3 $[NCS^-]$ / M	$10^3 k_{eq}$ / s^{-1}
2.0	1.20	1.76	0.50	1.20	5.69
	1.75	2.02		1.75	6.37
	2.25	2.16		2.75	7.00
	2.75	2.37		3.50	7.81
	3.50	2.55			
1.5	1.20	2.45	0.30	1.20	8.52
	1.75	2.62		1.75	9.31
	2.25	2.87		2.25	9.74
	2.75	3.18		2.75	10.34
	3.50	3.48		3.50	11.07
1.0	1.20	3.08			
	1.75	3.27			
	2.25	3.75			
	2.75	4.00			
	3.50	4.42			
0.70	1.20	4.10			
	1.75	4.63			
	2.25	5.08			
	3.50	5.82			

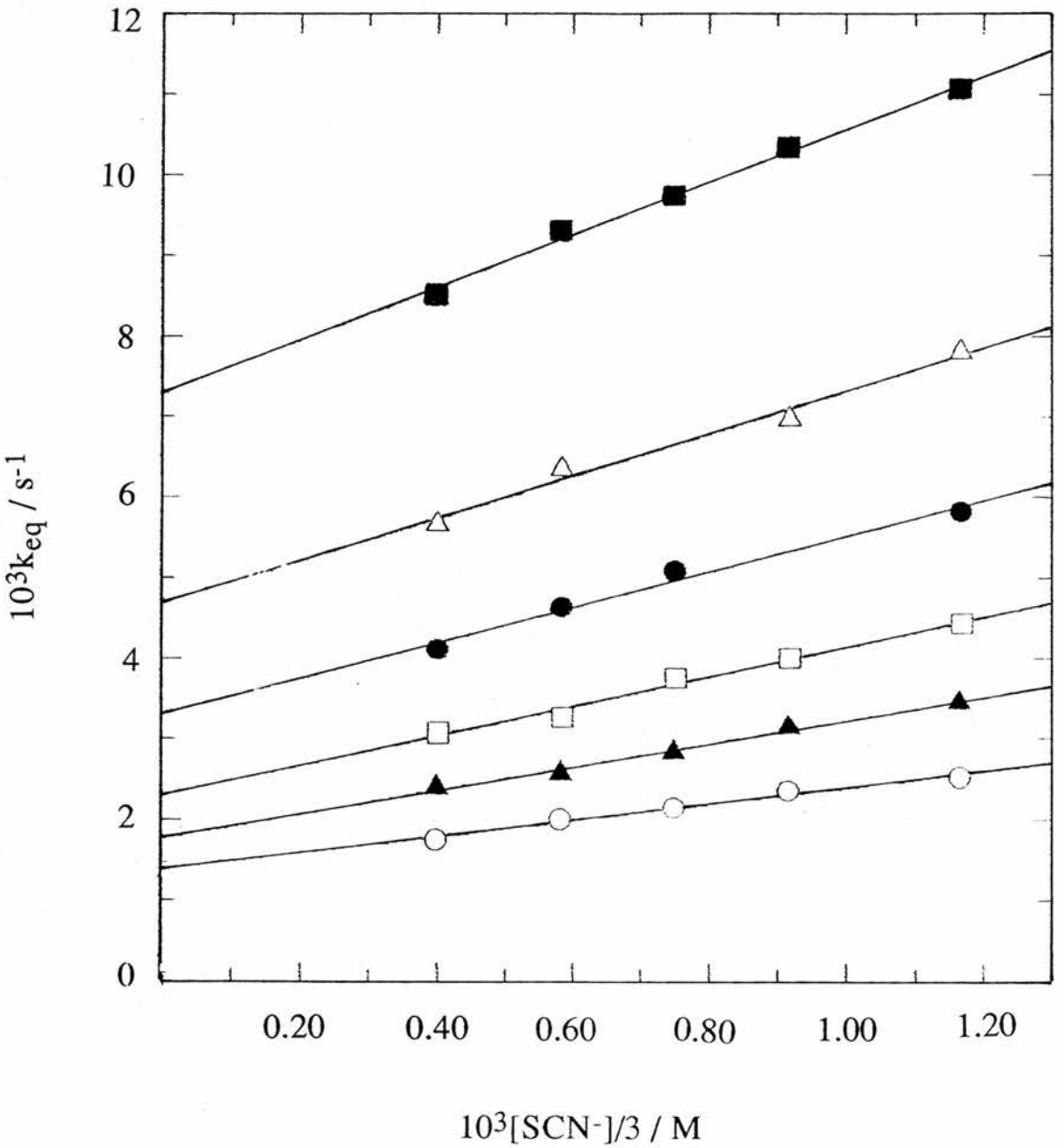

Figure 1.11 : Dependence of First-Order Equilibration Rate Constants (k_{eq}) for the NCS^- anation of $Mo_3O_4^{4+}$ at $[H^+]$ / M = 2.0 (O), 1.5 (▲), 1.0 (❑), 0.70 (●), 0.50 (Δ), 0.30 (■); T= 25 °C, I = 2.0 M (Lipts).

aquation steps involving $Mo_3O_4^{4+}$ and $Mo_3O_4NCS^{3+}$, respectively, are shown in Table 1.4.

Table 1.4 : Formation (k_f) and Aquation (k_{aq}) Rate Constants for the NCS^- anation of $Mo_3O_4^{4+}$ Corresponding to the Slope and Intercepts, Respectively in Figure 11; T= 25 °C, I= 2.0 M (LiPTS).

[H+] / M	k_f / M^{-1} s^{-1}	10^3 k_{aq} / s^{-1}
2.0	1.03±0.04	1.39±0.04
1.5	1.40±0.05	1.85±0.04
1.0	1.82±0.08	2.32±0.06
0.70	2.20±0.12	3.31±0.09
0.50	2.62±0.13	4.71±0.11
0.30	3.35±0.06	7.21±0.05

A plot of k_f against $[H^+]^{-1}$ is curved (Figure 1.12a). The reaction sequence (equations 1.5-1.7), with $Mo_3O_4^{4+}$ here written as Mo_3^{4+},

$$Mo_3^{4+} \underset{}{\overset{K_a}{\rightleftharpoons}} Mo_3OH^{3+} + H^+ \quad (1.5)$$

$$Mo_3OH^{3+} + NCS^- \underset{k_{-1}}{\overset{k_1}{\rightleftharpoons}} Mo_3OH(NCS)^{2+} \quad (1.6)$$

$$Mo_3(NCS)^{3+} \overset{K_{a'}}{\rightleftharpoons} Mo_3OH(NCS)^{2+} + H^+ \quad (1.7)$$

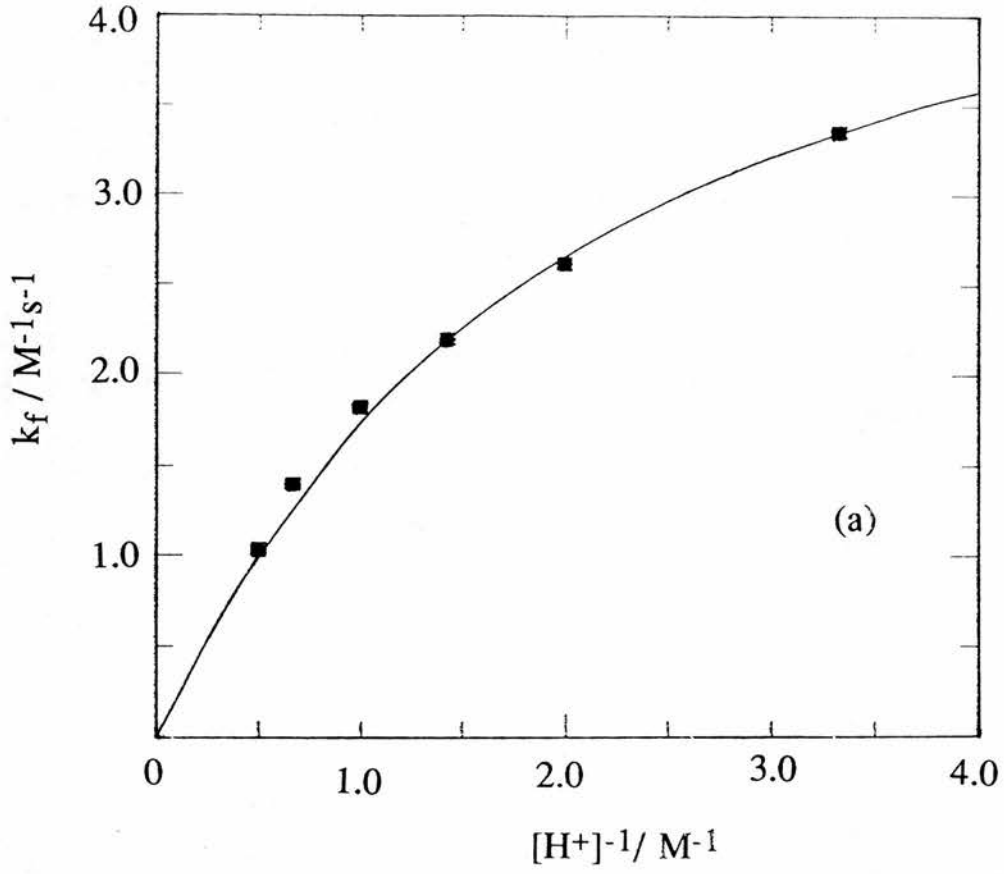

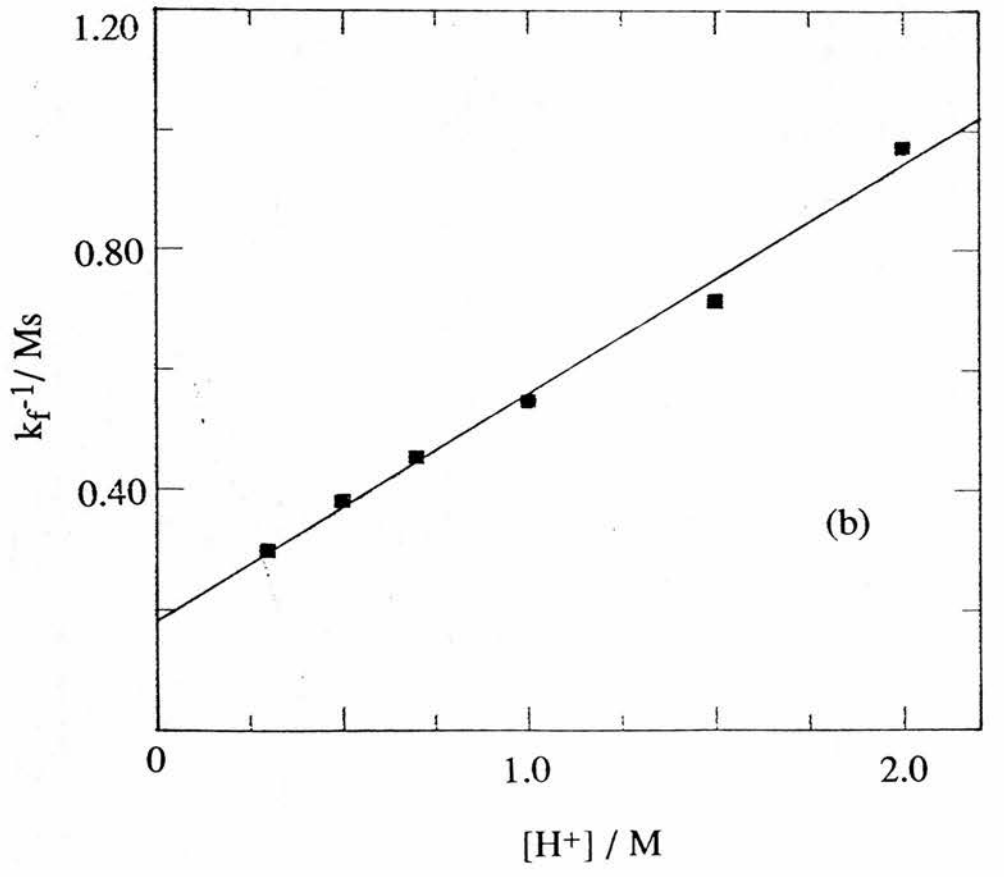

Figure 1.12: (a) Dependence of k_f on $[H^+]^{-1}$ for the 1:1 complexing of $Mo_3O_4^{4+}$ with NCS^-; (b) linear dependence of k_f^{-1} on $[H^+]$ at 25°C, I = 2.0 M (Lipts).

gives a satisfactory fit to the data. As a consequence the forward reaction can be expressed as in eqn. (1.8). The subsequent plot of k_f^{-1}

$$k_f = \frac{k_1 K_a}{[H^+] + K_a} \qquad (1.8)$$

against $[H^+]$ is linear (Figure 1.12b) and by using a non-linear least-squares treatment*, the following values were obtained; K_a = 0.51 ±0.04 M and k_1 = (5.27 ± 0.20) M^{-1} s^{-1}. These values are in very good agreement with those reported previously (K_a = 0.39 M, k_1 = 4.8 $M^{-1}s^{-1}$).[21]

The corresponding plot of k_{aq} against $[H^+]^{-1}$ is also curved (Figure 1.13a), and from reactions (1.6) and (1.7) k_{aq} can be expressed as in equation (1.9).

$$k_{aq} = \frac{k_{-1} K_{a'}}{[H^+] + K_{a'}} \qquad (1.9)$$

A plot of k_{aq}^{-1} versus $[H^+]$ is linear (Figure 1.13b) and similar treatment of the data gives $K_{a'}$= 0.07±0.02 M and k_{-1} = (3.90±0.74) x 10^{-2} s^{-1}. Again these values are close to the previously reported values ($K_{a'}$= 0.19 M and k_{-1} = 1.72 x 10^{-2} s^{-1}).[21]

* R.J.Leatherbarrow (1990) GraFit Version 2.0, Erithacus Software Ltd, Staines, U.K.

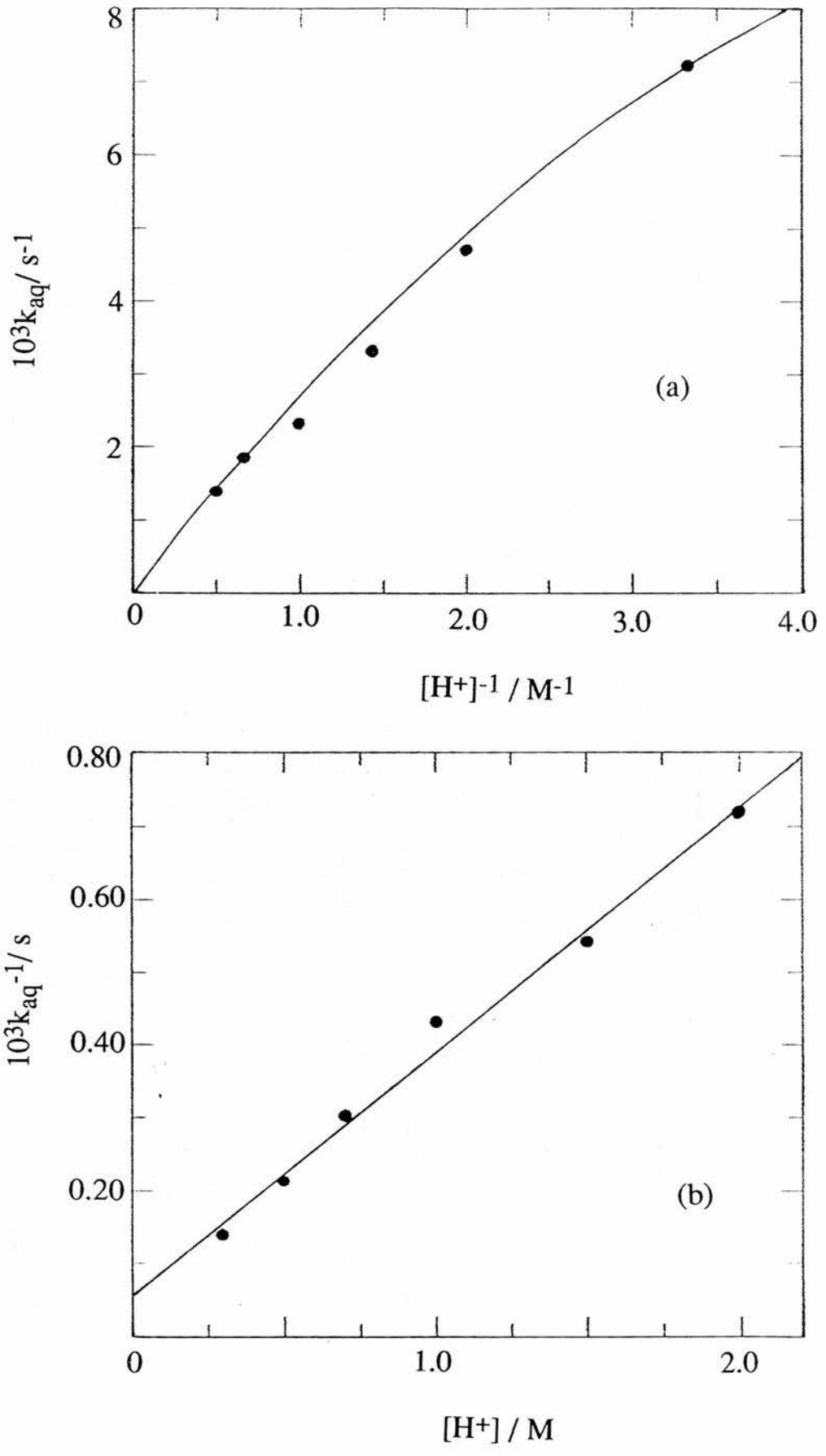

Figure 1.13 : (a) The non linear dependence on $[H^+]^{-1}$ of aquation rate constants (k_{aq}) at 25°C for the $Mo_3O_4^{4+}$ and NCS^- complex; (b) linear dependence of k_{aq}^{-1} on $[H^+]$, I = 2.0 M (Lipts).

1.4 DISCUSSION

The value of K_a (0.43 M, 25 °C) for $Mo_3O_4^{4+}$ determined by spectrophotometric titration is in excellent agreement with the values obtained from kinetic studies with regard to 1:1 complexation with NCS^- (0.51 M, this work and 0.39 M[21]) in which the monohydroxy species $Mo_3O_4(OH)^{3+}$, is the kinetically active form. Separate ^{17}O NMR studies[15] with regard to the chemical shifts of both types of coordinated water, c- and d-(see Figure 1.1), monitored as a function of $[H^+]$ have revealed that the deprotonation to form $Mo_3O_4(OH)^{3+}$ occurs at one of the water ligands *trans* to the bridging oxygen atoms (1.10):

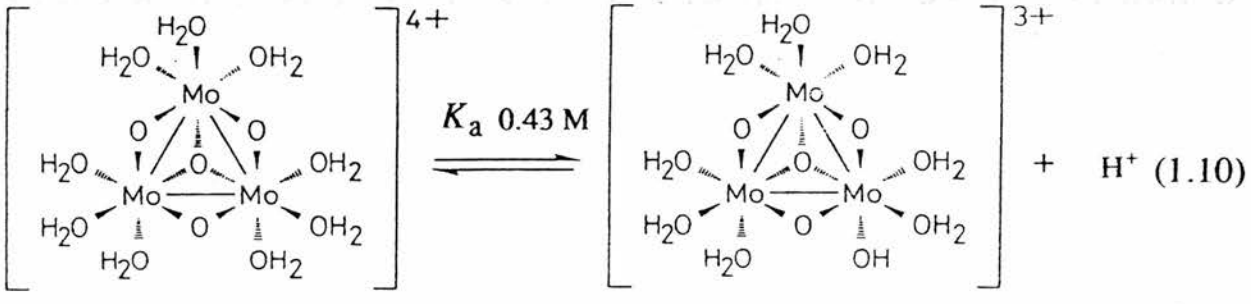

The use of pts^- as an 'inert' medium has now been questioned with regard to parallel investigations of the corresponding acid dissociation on $Mo_3S_4^{4+}$ (aq) conducted in both ClO_4^- and pts^- medium which show different absorbance changes characterising the deprotonation processes. In pts^- solution an increase in absorbance is observed at 400 nm on lowering the $[H^+]$ by dilution: the reverse being observed in ClO_4^- (see Figures 1.7 and 1.8). However in both media an isosbestic point is observed around 460 nm indicating that the same equilibration proesses are involved in each case. This led us to believe that the results in pts^-

are indicative of the acid dissociation occurring but it would appear as if some greater degree of ion-pair outer-sphere association of pts^- with $Mo_3X_4^{4+}$ and $Mo_3X_4(OH)^{3+}$ (X = O, S) (possibly involving hydrogen bonding) versus ClO_4^- is relevant such that the equilibrium represented above should be written as involving ion-pair complexes with the counter anion present in the case of pts^- (see Scheme below)

In ClO_4^- media

$$Mo_3S_4^{4+} \underset{}{\overset{K_a = 0.23\ M}{\rightleftharpoons}} Mo_3S_4(OH)^{3+} + H^+ \qquad (1.11)$$

(greater absorbance at 400 nm)

In pts^- media

$$Mo_3S_4^{4+} + pts^- \rightleftharpoons [Mo_3S_4^{4+}, pts^-] \text{ (ion pair)} \qquad (1.12)$$

$$[Mo_3S_4^{4+}, pts^-] \overset{K_a = 0.15\ M}{\rightleftharpoons} [Mo_3S_4(OH)^{3+}, pts^-] + H^+ \qquad (1.13)$$

(greater absorbance at 400 nm)

The reason for these effects is not immediately clear. The transition at 366 nm has not been fully assigned but if charge transfer in origin, as seems likely from the extinction coeffecient (>5,000), then it is possible that medium effects can modify the appearance of this transition (the band at 600 nm being hardly altered in the two media consistent with its cluster-electron based assignment). An increase in the intensity of the 366 nm band for $Mo_3S_4(OH)^{3+}$ in pts^- is responsible for the increase in absorbance correspondingly at 400 nm (*versus* $Mo_3S_4^{4+}$).

These ion-pair association effects for pts^- are also consistent with other observations namely:

(a) Higher concentrations of ions (up to 10 x) elutable from ion-exchange columns for the same concentration of Hpts *versus* $HClO_4$.

(b) Significantly slower rates of substitution on ions (up to factor of 2) in pts- media *versus* ClO_4^- (e.g. NCS^- substitution on $Mo_3O_4^{4+}$).[23]

(c) Extensive hydrogen-bonding network with bound water ligands in the crystal structure of $Mo_3O_4(OH_2)_9^{4+}$ in pts^-.[15]

(d) Significantly different rate constants for water exchange on $Mo_3S_4^{4+}$ in 1.0 M pts^- *versus* 2.0 M pts^- [58] (although viscosity effects may also be important here.

Studies on $Mo_3O_4^{4+}$ in ClO_4^- are severely limited owing to the slow, but eventual oxidation to Mo(V).[3] The redox stability of $Mo_3S_4^{4+}$ means that corresponding study in ClO_4^- is not a problem here and it is clear that future studies wherever possible should involve ClO_4^- as counter ion. These results have confirmed that both of these aqua ions have a relatively high K_a. In addition a recent report[59] on oxidation-reduction reactions involving the $Mo_3O_4^{4+}$ aqua ion as a reductant has also provided further independent evidence for a high K_a (~0.20 M) for this species. However, it is still puzzling why the acidity is so high given that the effective positive charge per metal atom as only 1.33. This behaviour is however not readily explained on electronic grounds. Both molecular orbital calculations[60] and the very small spectral changes in the visible region of the $Mo_3O_4^{4+}$ on replacing H_2O with OH^- [15] and Cl^- [9] have suggested that the visible electronic transitions are involved with molecular orbitals associated with the metal-metal bonds and thus

little affected by these σ - and π - donor ligands. Richens *et al* [15] proposed that the high acidity of the complex could be due to an electron deficiency at the Mo(IV) atoms; the consequence of this being that available empty π- acceptor orbitals on each Mo(IV) could then readily stabilize a hydroxy ligand in accordance with the general observation among electron-deficient high-oxidation-state metal ions. They also offered an alternative explanation for the high acidity by proposing the stabilization of the hydroxy ligand *via* intramolecular hydrogen bonding with a water molecule on an adjacent Mo centre to form an $H_3O_2^-$ bridge. Sykes and coworkers[41] have recently argued against the involvment of an $H_3O_2^-$ bridge as the likely explanation for the high K_a of these species since K_a varies very little for species having different metal-metal distances. For example the M-M distance is virtually identical for the ions $W_3O_4^{4+}$ (2.52 Å)[17,61] and Mo_3O_4 (2.49Å)[8,12] but different from the μ-sulphido derivatives $W_3S_4^{4+}$ (2.77Å)[38] and $Mo_3S_4^{4+}$ (2.76Å)[37,62] yet they all have K_a values in the range 0.22-0.51 M i.e., 0.22 M[20] for $W_3O_4^{4+}$, 0.39-0.51 M (ref 21 and this work) for $Mo_3O_4^{4+}$, 0.22 M[33] and 0.14 M (this work) for $Mo_3S_4^{4+}$ and 0.35 M[41] for $W_3S_4^{4+}$. Mo-Mo bond distances of 2.49Å for $Mo_3O_4^{4+}$ may be just acceptable for $H_3O_2^-$ bridging, but one of 2.77Å for the $Mo_3S_4^{4+}$ complex is much less so. Moreover, the X-ray crystal structure[15] of $[Mo_3O_4(OH_2)_9](pts)_4.13H_2O$ does not reveal any evidence for hydrogen bonding leading to possible formation of an $H_3O_2^-$ bridge. It should be borne in mind though that the situation in solution may be different to that in the solid state and this idea should perhaps not be ruled out at this stage.

Intermolecular $H_3O_2^-$ bridges have been detected involving carboxylato clusters $[M_3O_2(O_2CR)_6(H_2O)_3]^{2+}$ (M= Mo,W) and in certain mononuclear and polynuclear complexes (see Chapter 2) and

might however be responsible for the formation of oligomeric species in $M_3X_4^{4+}$ (M = Mo,W; X=O, S) solutions at the lower acidities. These species are expected to result in higher cation charges and thus stronger retention on cation-exchange columns which appears to be consistent with observations. The +160 ppm ^{17}O NMR resonance observed in solutions of $Mo_3O_4^{4+}$ (0.04 M) at $[H^+] \leq 0.02$ M has been tentatively assigned[15] to the formation of an intermolecular μ-($H_3O_2^-$) bridge between different trinuclear units.

A further interesting observation has been the trend in lability at the water ligands observed on replacing μ-oxo groups on $Mo_3X_4^{4+}$ successively with μ-sulphido.[52] The μ_3-sulphido cluster ion $[Mo_3(\mu_3\text{-}S)(\mu\text{-}O)_3(OH_2)_9]^{4+}$ has been prepared and shows more inert behaviour at the water ligands versus $Mo_3O_4^{4+}$ coupled with a slightly higher kinetically determined value of K_a (0.60 M). This behaviour is undoubtedly a reflection of the difference in the σ- and π- bonding ability of oxygen versus sulfur. Trends due to σ-and π- bonding effects have been discussed before in relation to Pt(II) square-planar substitution reactions[63] but are more difficult to appraise in these clusters. Nevertheless using this σ- and π- bonding ability of S and O an attempt will be made here to provide an explanation of the high acidity exhibited by these species and the apparent trend in magnitude of K_a, $Mo_3(\mu_3\text{-}S)(\mu\text{-}O)_3^{4+}$ (0.60 M)[64] > $Mo_3(\mu_3\text{-}O)(\mu\text{-}O)_3^{4+}$ > $Mo_3(\mu_3\text{-}S)(\mu\text{-}S)_3^{4+}$ which seems to correlate with an opposite trend in the the lability of the H_2O's in these species. From the acidity trend in the species it would appear as if the capping (μ_3-) atom is involved in a π-acceptor role (S>O) towards promoting the acidity of the waters. The bridging (μ-) atoms on the other hand seem to be promoting acidity through a σ-acceptor behaviour (O>S). If this is a valid explanation then the strongest acid should be $Mo_3(\mu_3\text{-}S)(\mu\text{-}O)_3^{4+}$ and the weakest is $Mo_3(\mu_3$-

S)(μ-S)$_3^{4+}$, as found. So based on this argument it seems as if the acidity is promoted as a result of the σ-withdrawal to the bridging positions or *via* π- withdrawal to the capping groups. On the other hand the lability of the water ligands would seem to be promoted through σ-donation *via* the bridging (μ) positions (S>O) or π-donation *via* the capping position (O>S).

In the case of the mixed-metal cluster ion, $Mo_2WO_4^{4+}$, an exceptionally high K_a (1.0 M) has been found[48] for this species and the above explanation may not be applicable to this cluster due to the mixed-metal effect. It is believed that the high acidity of this species could be partly explained as a result of build up of positive charge on the molybdenum atoms due to electron withdrawal by the more electronegative tungsten atom. It was then suggested that this higher positive charge on the molybdenum centre could be responsible for the observation of slightly more inert water ligands when compared with $Mo_3O_4^{4+}$ towards NCS^- substitution. However, these conclusions would now seem to be at odds with the recent findings from ^{95}Mo NMR and redox studies[53] which suggest rather a build-up of electron density at the Mo atoms *via* electron transfer from tungsten. With these findings in mind an independent verification of the high K_a *via* a spectral study is desirable and studies are planned on this species in the future.

1.4.1 Water Exchange on the $Mo_3O_4^{4+}$ and $Mo_3S_4^{4+}$ Aqua Ions

Some controversy still exists over the interpretation of water exchange data on both the $Mo_3O_4^{4+}$ and $Mo_3S_4^{4+}$ aqua ions determined

using ^{17}O NMR. In the case of both ions it is clear nonetheless that the $Mo_3X_4(OH)^{3+}$ ion (X = O, S) is the active species with regard to water exchange. The problem has been the precise magnitude of the relevant K_a for $Mo_3X_4(OH)^{3+}$ formation consistent with the spectrophotometric and NCS^- complexation results. The slower exchange at the c-water (*trans* to the capping group) was followed by conventional ^{17}O isotopic enrichment. Satisfactory fits have been obtained consistent with a K_a over the entire range from 0.01 to 0.4 M on both ions; it being difficult to be sure of the exact magnitude given the scatter in the data.[65] However, the best fit involving all of the data points (including those at low $[H^+]$ is to a K_a value in line with the spectrophotometric and NCS^- complexation results i.e., between 0.2-0.51 M. Exchange at the more labile ($x10^5$) waters *trans* to the bridging groups on the other hand required measurement by dynamic line broadening above 40°C. This involved measurement of the line width (Hz) of the ^{17}O resonance of the d-H_2O, equivalent to $1/T_2$ (T_2 = transverse relaxation time), over a range of temperatures to allow resolution of the kinetic exchange contribution (k_{ex}) from that of the quadrupolar term ($1/T_{2Q}$) (equation 1.14).

$$\frac{1}{T_2} = \frac{1}{T_{2Q}} + k_{ex} \qquad (1.14)$$

Estimation of the quadrupolar term was also aided by measurement of the line width of the c-H_2O in which the presumed similar quadrupolar term dominates over the entire temperature range >20 °C. Such studies have been recently performed on the $Mo_3S_4^{4+}$ ion by Richens and Merbach[65] at I = 2.0 M (Lipts) to allow an appropriately wide $[H^+]$ range (0.17-1.411 M) to be investigated. Data were taken over the

temperature range 25.7 to 54.8 °C. Initially the data were fitted by a non-linear least squares treatment* as a function of $[H^+]$ and temperature to (eq.1.14) assuming an Erying fit for k_{ex} and an Arrhenius fit for $1/T_{2Q}$. In addition a number of $[H^+]$ dependences for k_{ex} were tested with the best fit being found for data taken over the entire $[H^+]$ range to a $1/[H^+]$ dependence implying a value for the relevant $K_a << [H^+]$.

However, in view of the now strong evidence in support of the higher value of $K_a \sim [H^+]$ it seemed reasonable to reanalyse these data more closely and in particular to start with a consideration of what are likely to be the least reliable of the data, namely those taken at the highest temperatures and lowest acidities. Only data points taken at temperatures $\geq$ 41.4 °C were relevant to the kinetic exchange region. Figure 1.14 shows individual plots of k_{ex} (d-H_2O) / s^{-1} as a function of $[H^+]$ for $Mo_3S_4^{4+}$ ranging from 0.014 M ($[H^+]$= 0.557 M) to 0.03 M ($[H^+]$ =1.411 M) at I= 2.0 M (Lipts) taken at three temperatures: 41.4, 45.3 and 50.8 °C ignoring all data points determined at < 0.5 M $[H^+]$ with the exception of a point at 0.35 M $[H^+]$ for the lowest of the three temperatures. Insufficient points are unavailable at the other temperatures for similar plots to be constructed. As can be seen the data fits easily within random scatter for a dependence involving a non-linear dependence on $[H^+]^{-1}$, i.e. $K_a \sim [H^+]$; the lines drawn being in fact appropriate for an extrapolated value of K_a ~0.13 M at 5 °C. It is conceivable that the anomalously high values of k_{ex} occurring at the lower $[H^+]$ values (leading to the apparent linear fit to a $1/[H^+]$ depend-

*Non-linear least squares programs: ITERAT-general NLSQ Multi parameter fit; ANASPEC- simulation of Lorentzian line shape for estimation of Lorentzian line width. Programs developed at the ICMA, Université de Lausanne, Switzerland.

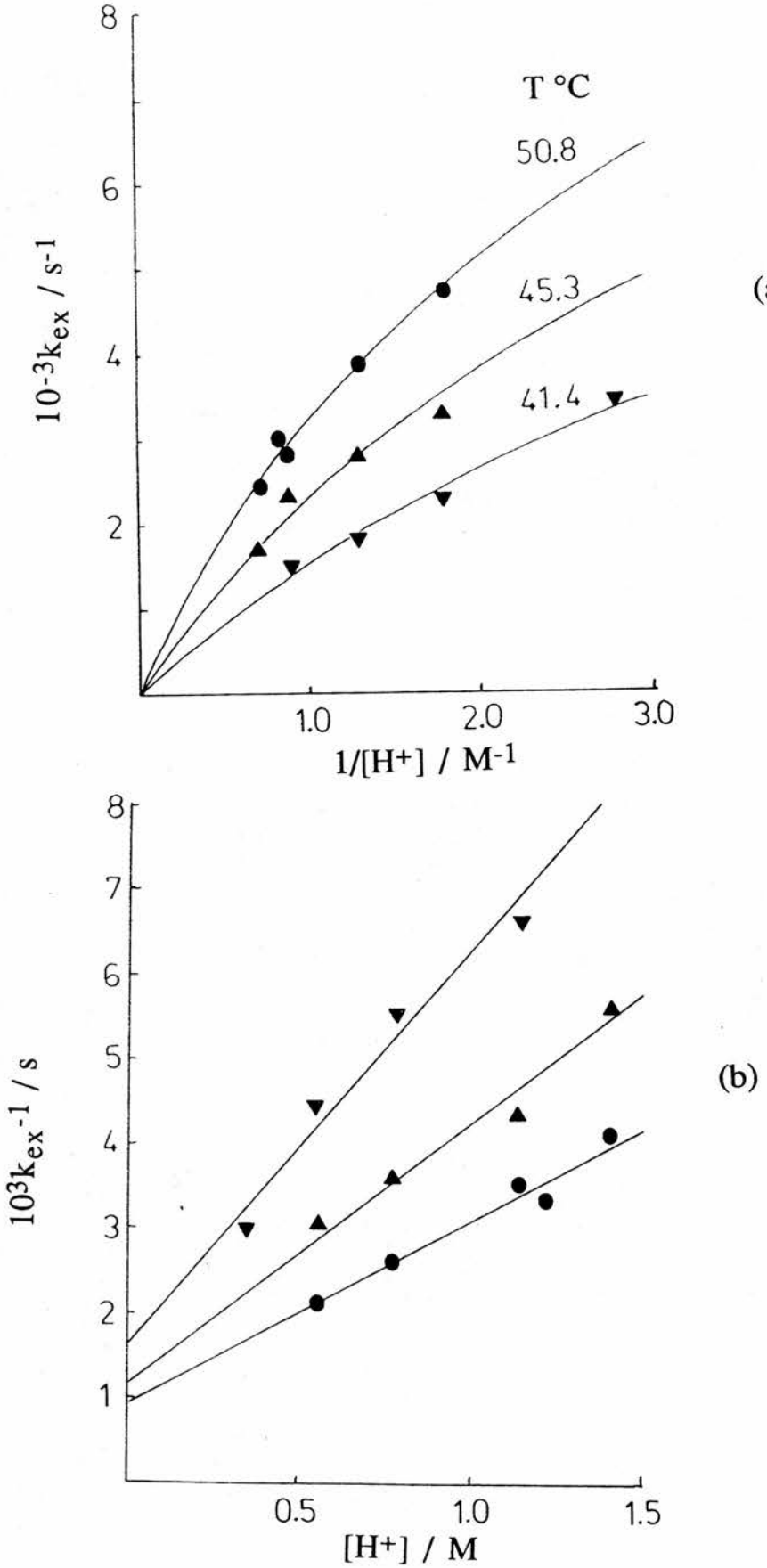

Figure 1.14 : (a) Plot of k_{ex} for the d - H_2O exchange on $[Mo_3S_4(OH_2)_9]^{4+}$ *trans* to the μ_2-oxo against $[H^+]^{-1}$. (b) Linear plot of k_{ex}^{-1} against $[H^+]$ at I =2.0 M(Lipts).

ence and a $K_a < 0.01$ M) are due to the presence of reactive oligomeric products having higher order $[H^+]$ terms and thus not relevant to the species likely to be present at the lower $[Mo_3]$ used for the ligand substitution kinetic studies.

Corresponding consideration of the previous data determined at I=1.0 M (Lipts) on both $Mo_3S_4^{4+}$ [65] and $Mo_3O_4^{4+}$ [15] ions is unfortunately more difficult but similar behaviour seems apparent although here the number of data points at $[H^+] \geq 0.5$ M is severely limited. It appears that the high Mo_3 concentrations necessary for the measurement of the ^{17}O NMR data mean a severe limitation as to range of temperature and particularly $[H^+]$ that can be tolerated. One way around this problem would be to use much higher ^{17}O enrichments (> 8 atom %) so as to allow use of lower $[Mo_3]$ but this is limited by cost. It is unfortunate that the data (determined in pts^-) have not proved to be of a satisfactory quality to pin down the precise magnitude of the relevant K_a. An additional problem has been the high viscosity of sufficiently high ionic strength pts^- solutions to enable the wide variation of $[H^+]$ (0.2 to 1.4 M) to be employed in addition to the clear concerns over the heating up of the $Mo_3X_4^{4+}$ solutions at the concentrations needed for the ^{17}O NMR measurements (>0.01 M in Mo_3). Moreover there are now clear concerns over the use of pts^- as an 'inert' counter ion on the basis of the growing evidence for appreciable ion-pair association of pts^- with both $Mo_3X_4^{4+}$ and $Mo_3X_4(OH)^{3+}$ species. Further studies are being planned on $Mo_3S_4^{4+}$ in ClO_4^- media (where it is at least stable to heating and the viscosity effects should be less of a problem) and it is hoped that superior and thus more meaningful ^{17}O NMR data for water exchange consistent with a K_a >0.1 M will be obtained.

The kinetic results for 1:1 NCS^- complexation on $Mo_3O_4^{4+}$ obtained in this study are in close agreement with those previously reported by Ooi and Sykes.[21] These results lend further support to the dominance of a conjugate-base mechanism for $Mo_3O_4^{4+}$ anation by NCS^-. It is widely recognised that an I_d mechanism[25,26] is appropriate to substitution reactions involving conjugate base forms; an observation that is supported by measurements of volumes of activation.[24] The dominance of conjugate-base pathways suggest that an associative process for water replacement on $Mo_3X_4^{4+}$ is unfavourable , which is of considerable interest in view of the apparent low d-electron population (d^2) at each Mo(IV) centre. This behaviour may be compared with that shown by mononuclear hexaaqua ions of low d-electron population such as Ti(III) ($3d^1$) [66], V(III) ($3d^2$) [67] and Mo(III) ($4d^3$) [25,68] wherein dominating associative interchange (I_a) processes are relevant However, this difference in behaviour is not surprising since each Mo(IV) centre in $Mo_3O_4^{4+}$ has an apparent coordination number of eight (i.e., by counting the metal-metal bonds). As a result of this 'crowding' at each Mo(IV) centre an associative mode of reaction would be expected to be much less favourable. Other evidence in support of the I_d mechanism stems from the similarity of the 1:1 anation rate constant found for oxalate and NCS^- (this work and reference 21) together with the positive $\Delta S^{\neq}$ value (+35 J K^{-1} mol^{-1}) found for the water exchange of a d-H_2O (*ca* .+30 J K^{-1} mol^{-1} was also found from a ^{18}O-exchange study of the water exchange at the c-H_2O).[9]

Within the $Mo_3O_4^{4+}$ cluster ion there are two possible sites on each Mo(IV) atom for 1:1 substitution, the d-H_2O's and the c-H_2O. On the basis of reaction rates existing evidence for NCS^- anation[23] is in favour of substitution at the more labile d-H_2O positions (two on each Mo) *trans* to the μ_2-oxo's group and promoted by conjugate-base

formation involving deprotonation at a d-H_2O presumed on the same Mo atom. 1:1 anation by $HC_2O_4^-$ at a d-H_2O also appears to be consistent with the crystal structure of $[Mo_3O_4(C_2O_4)_3(H_2O)_3]^{2-}$ [8,9] wherein the bidentate oxalate ligands occupy the d-H_2O sites. Murmann and coworkers[9] from their ^{18}O exchange studies had also favoured anation at a d-position since the rates of complexation by both Cl^- and $HC_2O_4^-$ were too fast when compared with the measured rate of water exchange at a c-H_2O. This situation wherein the more labile d-H_2O site is also observed to be the more acidic on these $Mo_3X_4^{4+}$ species would seem to be a remarkable observation but as discussed this is probably a result of the 'two-pronged' donor/acceptor property of the bridging oxo or sulphido groups within the cluster.

The studies performed using mixed oxo-sulphido $Mo_3X_4^{4+}$ clusters in addition to mixed metal (eg., Mo and W) species have shown that electronic properties over the entire cluster influence the acidity and lability of the peripheral water ligands on each metal centre and should lead to furter interesting studies in this area.

The importance of conjugate-base promoted substitution reactions *via* cis-hydroxy-ion formation in these $Mo_3X_4^{4+}$ cluster ions has led to an interest in studying related Mo and W trinuclear clusters having only one water ligand on each metal centre. In this way the possibility of remote conjugate-base effects transmitted through the bridging atoms could be tested. This is the subject of the investigations of Chapter 2.

REFERENCES

1. P. Souchay, M. Cadiot, M. Duhameaux, *C.R. Hebd. Séances Acad. Sci.* 1966, **262,** 1524.
2. (a) D.T. Richens, A.G. Sykes, *Comments Inorg. Chem.* 1981, **1**, 141; (b) *Inorg. Synth.* 1985, **23**, 130.
3. J.F. Ojo, Y. Sasaki, R.S. Taylor, A.G. Sykes, *Inorg. Chem.* 1976, **15**, 1006.
4. M. Ardon, A. Bino, G. Yahav, *J. Am. Chem. Soc.* 1976, **98**, 2338.
5. T. Ramasami, R.S. Taylor, A.G. Sykes, *J. Am. Chem. Soc.* 1975, **97**, 5918.
6. S.P. Cramer, H.B. Gray, Z. Dori, A. Bino, *J. Am. Chem. Soc.* 1979, **101**, 2770.
7. P. Chalilpoyil, F.C. Anson, *Inorg. Chem.* 1978, **17**, 2418.
8. A.Bino, F.A. Cotton, Z. Dori, *J. Am. Chem. Soc* 1978, **100**, 5252.
9. K.R. Rodgers, R.K. Murmann, E.O. Schlemper, M.E. Shelton, *Inorg. Chem.* 1985, **24**, 1313.
10. A. Bino, F.A. Cotton, Z. Dori, *J. Am. Chem. Soc.* 1979, **101**, 3842
11. E.O. Schlemper, M.S. Hussain, R.K. Murmann, *Cryst. Struc. Commun.* 1982, **11**, 89.
12. S. F. Gheller, T.W. Hambley, R.T.C. Brownlee, M. J. O'Connor, M.R. Snow, A.G. Wedd, *J. Am. Chem. Soc.* 1983, **105**, 1527.
13. R.K. Murmann, M.E. Shelton, *J. Am. Chem. Soc.* 1980, **102**, 3984.

14. D.T. Richens, L. Helm, P.A. Pittet, A. E. Merbach, *Inorg. Chim. Acta* 1987, **132**, 85.

15. D.T. Richens, L. Helm, P.A. Pittet, A.E. Merbach, F. Nicolo, G. Chapius, *Inorg. Chem.* 1989, **28**, 1394.

16. A. Müller, R. Jostes, F.A. Cotton, *Angew. Chem. Int. Ed. Engl.* 1980, **19**, 875.

17. M. Segawa, Y. Sasaki, *J. Am. Chem. Soc.* 1985, **107**, 5565.

18. M.R. McMahon, *M. Sc. Thesis*, University of Stirling, 1986.

19. A. Patel. *Ph. D. Thesis*, University of Stirling, 1988.

20. B-L. Ooi, A.L. Petrou, A.G. Sykes, *Inorg. Chem.* 1988, **27**, 3626.

21. B.-L. Ooi, A.G. Sykes, *Inorg. Chem.* 1988, **27**, 310.

22. M.A. Harmer, D.T. Richens, A.B. Soares, A.T. Thornton, A.G. Sykes, *Inorg. Chem.* 1981, **20**, 4155.

23. P. Kathirgamanathan, A.B. Soares, D.T. Richens, A.G. Sykes, *Inorg. Chem.* 1985, **24**, 2950.

24. T.W. Swaddle, A.E. Merbach, *Inorg. Chem* 1981, **20**, 4212.

25. Y. Sasaki, A.G. Sykes, *J. Chem. Soc., Dalton Trans.* 1975, 1048.

26. T.W. Swaddle, '*Advances in Inorganic and Bioinorganic Mechanisms*', A. G. Sykes, Ed., Academic Press; London, 1983, vol 2, p 106.

27. D.T. Richens, A.G. Sykes, *Inorg. Chim Acta* 1981, **54**, L3.

28. D.T. Richens, A.G. Sykes, *Inorg. Chem.* 1982, **21**, 418.

29. M.T. Paffett, F.C. Anson, *Inorg. Chem.* 1983, **22**, 1347.

30. D.T. Richens, M.A. Harmer, A.G. Sykes, *J. Chem. Soc, Dalton Trans.* 1984, 2099.

31 (a) M. Ardon, A. Pernick, *Inorg. Chem.*, 1974, **13**, 2275.
(b) M.A. Harmer, A.G.Sykes. *ibid.*, 1981, **20**, 3963.

32. D.T.Richens, C. Guille-Photin, *J. Chem. Soc. Dalton Trans* 1990, 407

33. B.-L Ooi, A.G. Sykes, *Inorg. Chem.* 1989, **28**, 3799.

34. F.A. Cotton, Z. Dori, R. Llusar, W. Schwotzer, *J. Am. Chem. Soc.* 1985, **107**, 6734.

35. F.A. Cotton, M.P.Diebold, Z. Dori, R. Llusar, W. Schwotzer, *J. Am. Chem. Soc.* 1985, **107**, 6735.

36. H. Akashi, T. Shibahara, H. Kuroya, *Polyhedron*, 1990. **9**. 1671.

37. T. Shibahara, H. Kuroya, *Polyhedron*, 1986, **5**, 357.

38. T. Shibahara, K. Kohda, A. Ohtsuji, K. Yasuda, H. Kuroya, *J. Am. Chem. Soc*, 1986, **108**, 2757.

39. T. Shibahara, A. Takeuchi, A. Ohtsuji, K. Kohda, H. Kuroya, *Inorg. Chim. Acta*, 1987, **127**, L45.

40. V. P. Fedin, M.N. Sokolov, O.A. Geras'ko, M. Sheer, V.Ye. Fedorov, A.V. Mironov, Yu. L. Slovokhotov, Yu. T. Strutchkov, *Inorg. Chim. Acta*, 1989,**165**, 25.

41. M. Nasreldin, A. Olatunji, P.W. Dimmock, A.G. Sykes, *J. Chem. Soc., Dalton Trans.* 1990, 1765.

42. T. Shibahara, T. Yamada, H. Kuroya, E.F. Hills, P. Kathirgamanathan, A.G. Sykes, *Inorg. Chim. Acta* 1986, **113**, L19.

43. P. Kathirgamanathan, M. Martinez, A.G. Sykes, *J. Chem. Soc. Chem. Commun.* 1985, 953.

44. P. Kathirgamanathan, M. Martinez, A. G. Sykes, *J. Chem. Soc. Chem. Commun.* 1985, 1437.

45. M. Martinez, B.-L Ooi, A.G. Sykes, *J. Am. Chem. Soc.* 1987, **109**, 4615.

46. T. Shibahara, A. Takeuchi, T. Kunimoto, H. Kuroya, *Chem. Lett.* 1987, 867

47. T. Shibahara, A. Takeuchi, H. Kuroya, *Inorg. Chim. Acta* 1987, **127**, L39.

48. A. Patel, D.T. Richens, *J. Chem. Soc. Chem., Commun.* 1990, 274.

49. T. Shibahara, M. Yamasaki, *Inorg. Chem.* 1991, **30**, 1687.

50. F. A. Cotton, Z. Dori, R. Llusar, D.O.Marler, W. Schwotzer, *Inorg. Chim. Acta* 1985, **102**, L25.

51. Z. Dori, F.A. Cotton, R. Llusar, W. Schwotzer, *Polyhedron*, 1986, **5**, 907.

52. B.-L Ooi, M. Martinez, A.G. Sykes, *J. Chem. Soc., Chem. Commun.* 1988, 1324.

53. A. Patel, S. Siddiqui, D.T. Richens, *J. Chem. Soc., Dalton Trans.*, 1991 (submitted for publication).

54. R. J. Irving, M. C. Steele. *Aust. J. Chem.*, 1957, **10**, 490.

55. W. R. Bucknall, S. R. Carter, W. Wardlaw, *J. Chem. Soc.*, 1927,512.

56. F. A. Cotton, D. O. Marler, W. Schwotzer, *Inorg. Chem.* 1984, **23**, 3671.

57. B.-L. Ooi, C. Sharp, A. G. Sykes, *J. Am. Chem. Soc.*, 1989, **111**, 125.

58. P. A. Pittet, *Ph. D. Thesis*, University of Lausanne, Switzerland, (1990).

59. S. P. Ghosh, E. S. Gould, *Inorg. Chem.*, 1991, **30**, 3662.

60. B. E. Bursten, F. A. Cotton, M. B. Hall, R. C. Najjar, *Inorg. Chem.* 1982, **21**, 302.

61. R. Mattes, K. Mennemann, *Z. Anorg. Allg. Chem.* 1977, **437**, 175.

62. N. C. Howlader, G. P. Haight, T. W. Humbley, G. A. Lawrence, K. M. Rahmoeller, M. R. Snow, *Aust. J. Chem.*, 1983, **22**, 377.

63. F. A. Cotton, G. Wilkinson, '*Advanced Inorganic Chemistry*,' 5th. Edn., Wiley Interscience, New York, 1988, p.1300.

64. A. G. Sykes, *Private Communication.*

65. D. T. Richens, A. E. Merbach, *unpublished results.*

66. A. D. Hugi, L. Helm, A. E. Merbach, *Inorg. Chem.*, 1987, **26**, 1763.

67. A. D. Hugi, A. Helm, A. E. Merbach, *Helv. Chim. Acta*, 1985, **68**, 508.

68. D. T. Richens, Y. Ducommun, A. E. Merbach, *J. Am. Chem. Soc.*, 1987, **109**, 603.

CHAPTER 2

2.1 INTRODUCTION

2.1.1 Trinuclear Carboxylate Clusters of Tungsten(IV) and Molybdenum(IV)

The preparation[1] and structural characterisation[2] of quadruply bonded binuclear molybdenum (II) compounds with bridging carboxylate ligands (Figure 2.1) was reported more than 25 years ago.

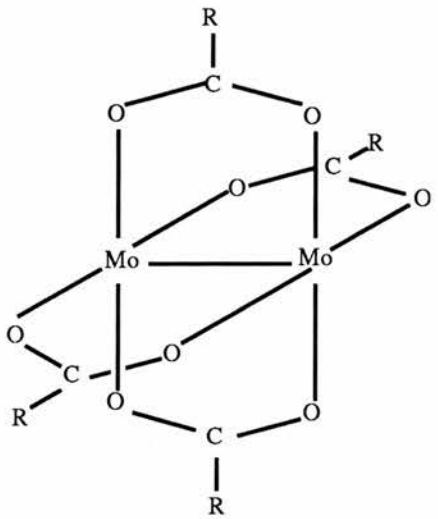

Fig 2.1: Structure of $[Mo_2(O_2CR)_4]$

These yellow complexes were obtained by reacting $Mo(CO)_6$ with the appropriate carboxylic acid. In the reaction with acetic acid for example, $Mo_2(OAc)_4$ is produced in approximately 20% yield (although it can be made much higher by using other solvents such diglyme) and the fate of the rest of the molybdenum products remained unknown for quite some time. It is interesting to note that the analogous reaction of $W(CO)_6$ produces no $W_2(OAc)_4$ and the products that were formed were not correctly identified. However it was not until 1976 that Bino *et al* [3] reported that the dark brown solution remaining after the separation of the $Mo_2(OAc)_4$ solid contained trinuclear triangular

clusters of molybdenum. Since then much progress has been made in understanding these reactions and it is now well established that both molybdenum and tungsten have marked tendency to form trinuclear, triangular cluster compounds in mean formal oxidation states in the range III-V.

While these cluster species are all based on an equilateral M-M bonded triangle of metal atoms there are four different structural types with respect to the ligand arrangements. These are shown in Fig. 2.2.

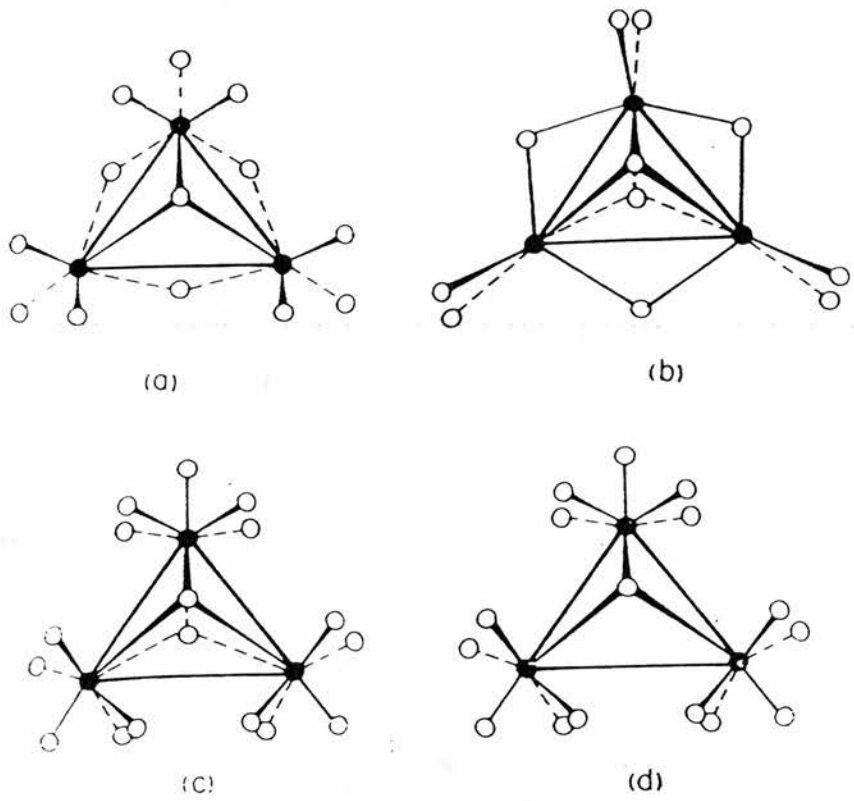

Fig 2.2: Prototypal representations of the four types of trinuclear cluster structures known for Mo and/or W compounds.

Structure (a) is that of the incomplete cuboidal type of which the aqua ions, $[M_3O_4(OH_2)_9]^{4+}$ (M = Mo or W) are typical examples. Another type of equilateral triangular molybdenum cluster has been reported by Chisholm *et al* .[4] This is represented schematically by (b) in Fig. 2.2 and typical examples are $[Mo_3(\mu_3\text{-}O)(\mu_3\text{-}OR)(\mu\text{-}OR)_3(OR)_6]$, where

R=$(CH_3)_2CH$ or $(CH_3)_3CCH_2$. Both the electronic and spectroscopic properties of such compounds have been elucidated by physical and theoretical studies.[5] Trinuclear clusters of type (c) have the general formula $[M_3X_2(O_2CR)_6L_3]^{n+}$. In such a unit there is a central trigonal-bipyramidal $M_3(\mu_3\text{-}X)_2$ unit, with one of the capping groups above and the other below the trinuclear plane of the metal-metal bonded framework. In addition each pair of metal atoms is bridged by two carboxylates and the coordination sphere is completed by a radial ligand which is bonded to each metal atom. Typical and well characterised examples of this structure type are $[M_3O_2(OAc)_6(H_2O)_3]^{2+}$ (M = W[6], Mo[7]). The basic structural unit is shown in Figure 2.3. The homo-

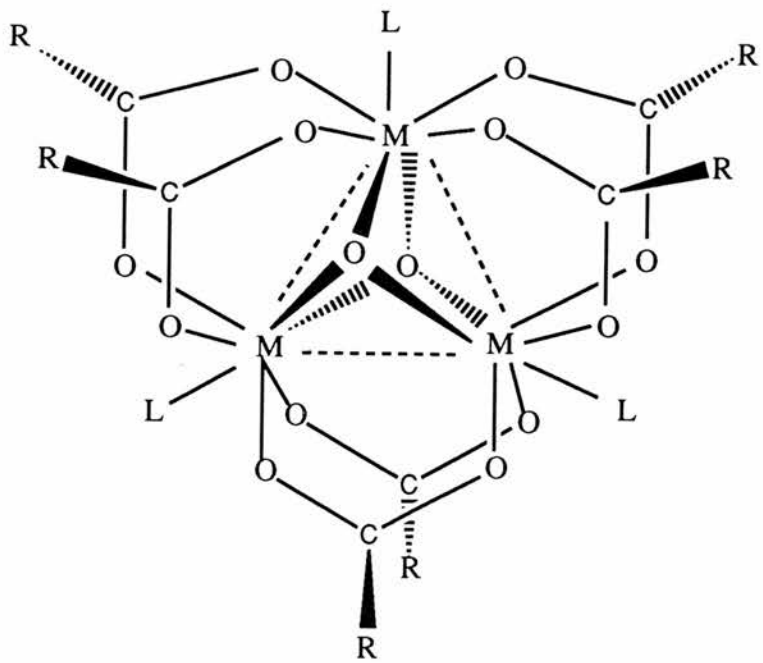

Fig 2.3: Structure of $[M_3O_2(OAc)_6(H_2O)_3]^{2+}$ (M = Mo or W)

metal trimolybdenum and tritungsten compounds are very similar to one another and in the case of the triflate salts they are isomorphous with similar Mo-Mo and W-W distances; 2.757Å in the former and 2.747Å in the latter which are consistent with the existence of M-M single bonds. As evident from the structure shown in Fig 2.3 these species have a coordination number of nine, counting the neighbouring metal atoms as well as the coordinated oxygen atoms.

A surprising feature of this chemistry has been that there are species of this structural type in which one or both capping groups are alkylidyne groups.[7-12] The presence of the capping alkylidyne groups in these species has been confirmed through crystallographic analysis, by ^{1}H and ^{13}C NMR studies. The source of the ethylidyne group in the $[Mo_3O(CCH_3)(OAc)_6(H_2O)_3]^+$, for example, was shown by ^{13}C tracer study to arise by reduction of an acetate ion.[8]

The electronic structure of type (c) triangular cluster species has been analysed by molecular-orbital methods and a basic understanding of the metal-metal bonding has been achieved.[13] These bicapped clusters can accommodate a maximum of six cluster electrons, whereby three M-M single bonds are formed. In several compounds there are only 5 or 4 such electrons. In the +1 bicapped ethylidyne complex, $[Mo_3(CCH_3)_2(OAc)_6(H_2O)_3]^+$,[9] for example, there are 5 electrons for the trimolybdenum cluster, the Mo-Mo bond orders are 5/6 and the mean Mo-Mo distance is 2.814Å. This species also exists as the 2+ cation[9] which has 4 electrons and hence a bond order of 2/3. A noticeable increase in the bond length (*ca.* 0.06Å) accompanies each decrease of 1/6 in the bond order. The oxidation state of the trimoybdenum species is thus Mo(IV, IV, V) in the +1 cation and Mo(IV, V, V) in the 2+ cation.

Although these alkylidyne compounds contain Mo-C bonds they

are very stable toward oxygen, aqueous acids and even toward permanganate which, however, oxidises the compounds but leave the structure intact. The origin of the stability of these Mo-C bonds towards oxidative and hydrolytic attack may be kinetic in nature. In the case of tungsten no bi-alkylidyne capped tritungsten species have yet been reported but the mono alkylidyne species, $[W_3(\mu_3\text{-}O)(\mu_3\text{-}CCH_3)(OAc)_6(H_2O)_3]^{2+}$ has been reported.[12] Whereas both of the molybdenum alkylidyne compounds can be easily obtained from the reaction of $Mo(CO)_6$ with glacial acetic acid or a mixture of the acid and its anhydride (depending on the reaction conditions and workup procedures) the corresponding tungsten analogues cannot be prepared using this method. Thus the tungsten species $[W_3O(CCH_3)(OAc)_6(H_2O)_3]^{2+}$ was prepared by a different route.[12] The complex was obtained by the reaction of $W(CO)_4(pip)_2$ and a mixture of acetic acid and acetic anhydride. This cluster differs in having one electron fewer than its stable molybdenum analogue: $[Mo_3O(CCH_3)(CH_3CO_2)_6(H_2O)_3]^{+}$.[8] The molybdenum species shows no tendency to be oxidised to the 2+ species in neutral or acid solution. The tungsten compound, however, undergoes oxidation in 0.1 M $HClO_4$ (even in the absence of oxygen) and is also easily reduced in acidic or ethanolic solution to the diamagnetic six electron system, $[W_3O(CCH_3)(OAc)_6(H_2O)_3]^{+}$. The 2+ tungsten cation can also be reduced to the +1 cation electrochemically, and a reversible wave centered at 0.2 V(*vs* Ag/AgC1) has been reported.[12] The unipositive tungsten cation is reported to be stable for several days in acidified ethanol solution, from which it can be obtained as a solid on cooling. This +1 compound has been characterised by ^1H NMR.[12] The W-W bond lengths were estimated for the +1 ion to be shorter than the +2 ion by about 0.062Å. This increase for a W-W bond order change of 1/6 is very similar to

that found in the molybdenum systems.[9] Thus, despite the redox and chemical differences between the trimolybdenum and tritungsten systems, their stereoelectronic properties are very similar.

As mentioned earlier the bioxo-capped species can be obtained by refluxing either $Mo(CO)_6$ or $W(CO)_6$ with the appropriate carboxylic acid or mixtures of the corresponding acid and anhydride. Further studies[14] have shown that $Na_2MoO_4.2H_2O$ is a very useful starting reagent for the preparation of these bicapped molybdenum species. This method employs either zinc or $W(CO)_6$ as the reductant. It was found that the initial product of these preparative reactions was $Na[Mo_3O_2(OAc)_9]$. In acid solution rapid hydrolysis occurs with replacement of the three monodentate equatorial acetate ions by H_2O molecules. In neutral aqueous solution the product is the neutral compound: $[Mo_3O_2(OAc)_6(H_2O)(OH)_2].16H_2O$, which has been characterised by X-ray crystallography.[14] The corresponding tungsten compound[15] is also known which is isostructural with its molybdenum analogue; the double salt $[W_3O_2(OAc)_6(H_2O)(OH)_2].KBr.15H_2O$ is also known.[15]

The isostructural molybdenum and tungsten cluster units deviate significantly from threefold symmetry and Cotton *et al* [14] explained these deviations in the dihydroxo molybdenum compound by assuming that the stronger the M-O (equatorial) bond is the weaker will be the adjacent M-M bonds. Accordingly, the distance (HO)M-M(OH) (2.796Å) should be longer than (H_2O)M-M(OH) (2.773Å) since the M-OH bond (1.979Å in $[Mo_3O_2(OAc)_6(H_2O)(OH)_2].16H_2O$) is shorter and presumed stronger than M-OH_2 (2.083 - 2.144Å[16]). This pattern is retained in the isostructural dihydroxo tungsten cluster but interestingly not in the double salt wherein the (HO)W-W(OH) distance (2.7883Å) is shorter than the other two (HO)W-W(OH_2) distances, 2.8005Å and

2.7980Å. The W-W bond lengths are however significantly longer than the W-W distance in the triaqua complex, $[W_3O_2(OAc)_6(H_2O)_3]^{2+}$ (2.746Å).[14] Bino and Gibson[15] proposed that M-M and M-O bonds are not exclusively determined by the nature of the equatorial ligands (OH^- or H_2O) but are susceptible to intramolecular forces such as hydrogen bonding and electrostatic interactions in the lattice. They also proposed an alternative explanation by assuming that some of the extra negative charge in the clusters, relative to the +2 triaqua ion, $[W_3O_2(OAc)_6(H_2O)_3]^{2+}$, flows to metal-metal molecular orbitals with anti-bonding nature.[15]

Finally, we have structure (d) of Figure 2.2 which might be considered as a variant of the bicapped structure (c) in which one capping group is absent and is therefore called the monocapped structure. This structural form is represented by the dark blue tungsten cluster, $[W_3O(OAc)_6(H_2O)_3]^{2+}$ as well as $[W_3O(OAc)_5(OCH_3)(H_2O)_3]^{2+}$.[17,18] Surprisingly there is so far no report of an analogous molybdenum species. The monocapped complex, $[W_3O(OAc)_6(H_2O)_3]^{2+}$, was first isolated[17] as a minor product in the preparation of the bicapped $[W_3O_2(OAc)_6(H_2O)_3]^{2+}$ complex. An improved method to prepare the monocapped cluster with greater ease and in better yield was later reported.[18] Instead of using $W(CO)_6$ as the starting material, as in the case of the bicapped cation, the new method begins with sodium tungstate and employs zinc as a reducant.

The dark blue species, $[W_3O(OAc)_6(H_2O)_3]^{2+}$, has been characterised by X-ray crystallography. The structure is shown in Fig. 2.4. In this complex, two of the W-W distances are equal (2.693Å); the third is in a statistical sense different, at 2.712Å which is significantly different from that of 2.75Å in the bicapped species. This is clearly a significant difference in both the statistical and chemical senses. The

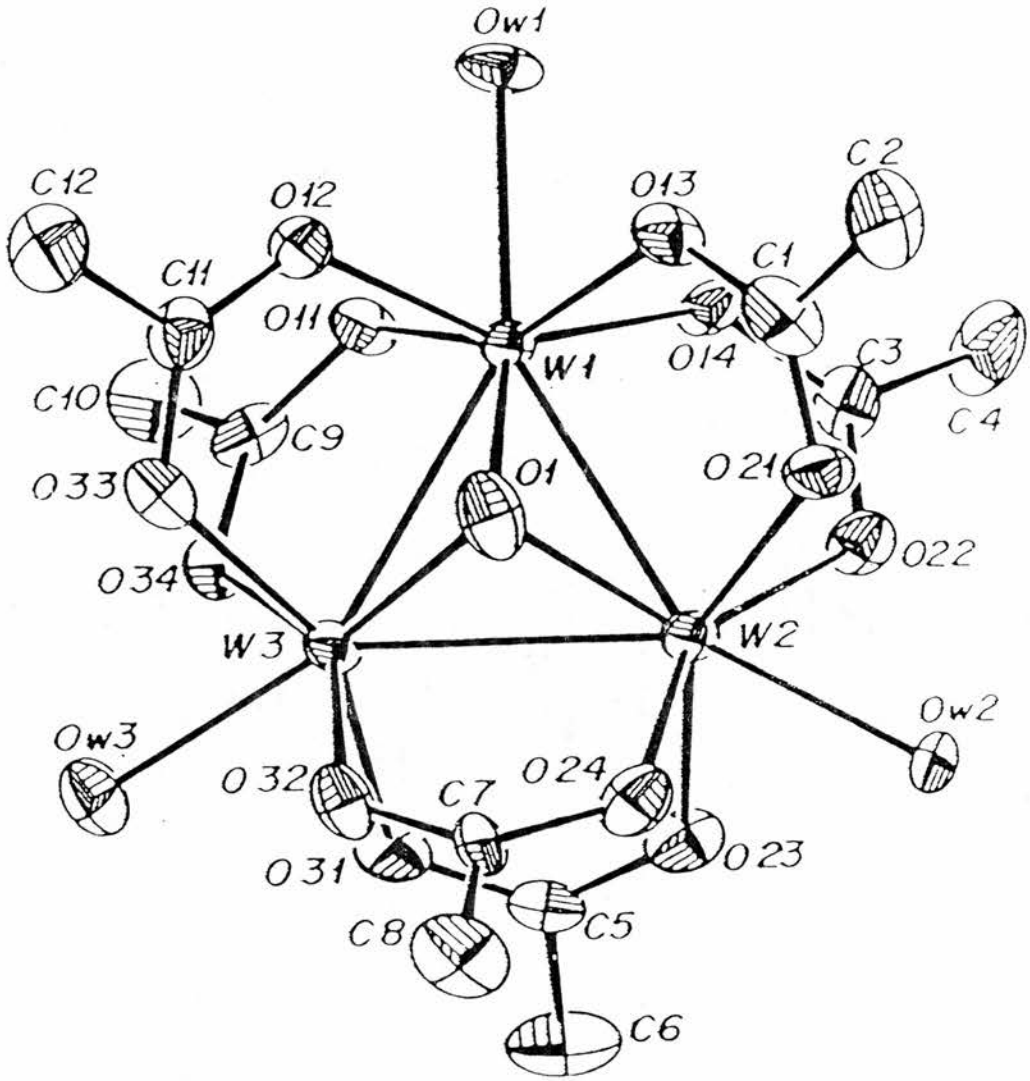

Figure 2.4: Structure of the $[W_3O(OAc)_6(H_2O)_3]^+$ cation.

structure also shows that the three W-(μ_3-O) distances are equal within their esds and have an average value of 1.98Å. In addition to the crystal structure, a ^{1}H NMR study shows two methyl resonances thus providing confirmation that only a single capping oxygen is present.[18]

The electronic structure, bonding and visible spectrum were well accounted for by a Fenske-Hall type molecular orbital calculation, which shows that in addition to six M-M bonding electrons comparable to those in the bicapped species, there is an empty e orbital and a filled a_1 orbital with weakly M-M bonding character.[17]

2.1.2 Molybdenum-Tungsten Mixed-Metal Trinuclear Carboxylate Clusters : $[M_3O_2(OAc)_6(H_2O)_3]^{2+}$ (M=Mo_2W or MoW_2)

In addition to the homonuclear, trinuclear carboxylate clusters $[M_3O_2(OAc)_6(H_2O)_3]^{2+}$ (M=Mo[7,14] or W[6]), the mixed molybdenum-tungsten clusters, namely dimolybdenum-tungsten and molybdenum-ditungsten compounds are now known.[19] This was the first complete series of trinuclear metal-metal bonded non-carbonyl clusters involving two metal ions. There exists however the series for $[M_3(\mu_3\text{-}O)(\mu\text{-}OAc)_6(H_2O)_3]^+$ (M = *e.g.* Fe(III) and Cr(III)) but these species have no metal-metal bond.[20] Also the trinuclear mixed-metal molybdenum-tungsten complexes, $[Mo_2W(\mu_3\text{-}O)(\mu_3\text{-}O\text{-}Pr^i)(\mu\text{-}O\text{-}Pr^i)_6(O\text{-}Pr^i)_3]$[21] and $[Mo_2W(\mu_3\text{-}CCH_3)(\mu_3\text{-}O\text{-}Pr^i)(\mu\text{-}O\text{-}Pr^i)_6(O\text{-}Pr^i)_3]$[22] have been reported, but interestingly their MoW_2 analogues were only poorly characterised or not known.

The preparation[19] of these molybdenum-tungsten mixed-metal species was carried out by refluxing a mixture of sodium molybdate, sodium tungstate and zinc dust in acetic anhydride for 24 h, followed by

purification using SP-Sephadex C-25 cation exchange resin. It is believed that it is important to add the Na_2MoO_4 some fifteen minutes after the initiation of the reflux of tungsten in acetic anhydride. However, the purification process is rather tedious as it took nearly a month for complete separation of the complexes using three columns of 4 cm. in diameter and 140 cm. in length. The homonuclear tritungsten analogue is also obtained in this method of preparation. The MoW_2 species can be prepared as a secondary product in fairly god yield *via* refluxing Na_2MoO_4 in acetic acid/acetic anhydride in the presence of $W(CO)_6$ (see experimental section).

Both the orange red Mo_2W and orange MoW_2 clusters are well characterised structurally.[19] A comparison of some crystal structure data of these complexes with the homonuclear species is given in Table 2.1. The table shows that the corresponding parameters of all four species are almost identical except for the crystal densities. From this data it is expected that all four species should have almost identical structural parameters. This is reflected in the metal-metal bond lengths

Table 2.1 : Some Crystallographic Data of $[Mo_nW_{3-n}(\mu_3\text{-}O)_2(OAc)_6(H_2O)_3]Br_2.H_2O$

Complex	a/Å	α	V/Å^3	Z	ρ_{obs} gcm^{-3}	ρ_{calcd} gcm^{-3}	Ref
Mo_3	11.784	106.34	1386.58	2	2.18	2.17	16
Mo_2W	11.809	106.37	1394.5	2	2.33	2.35	19
MoW_2	11.812	106.34	1396.5	2	2.54	2.57	19
W3	11.787	106.30	1388.93	2	>2.7	2.80	23

for example, with the Mo_2W being 2.73Å[23] which is very close to those

of the Mo_3 (2.759Å)[16] and the W_3 complex (2.746Å).[24] The X-ray study indicated that the molybdenum and tungsten atoms are statistically disordered in the crystal lattice producing the same crystal symmetry as that of the homonuclear Mo_3 analogue.

Perhaps the most convincing evidence that these species are mixed-metal clusters and not a mixture of the two homonuclear trimers was provided by ^1H NMR[19] (Fig 2.5). Whereas the Mo_3 and W_3

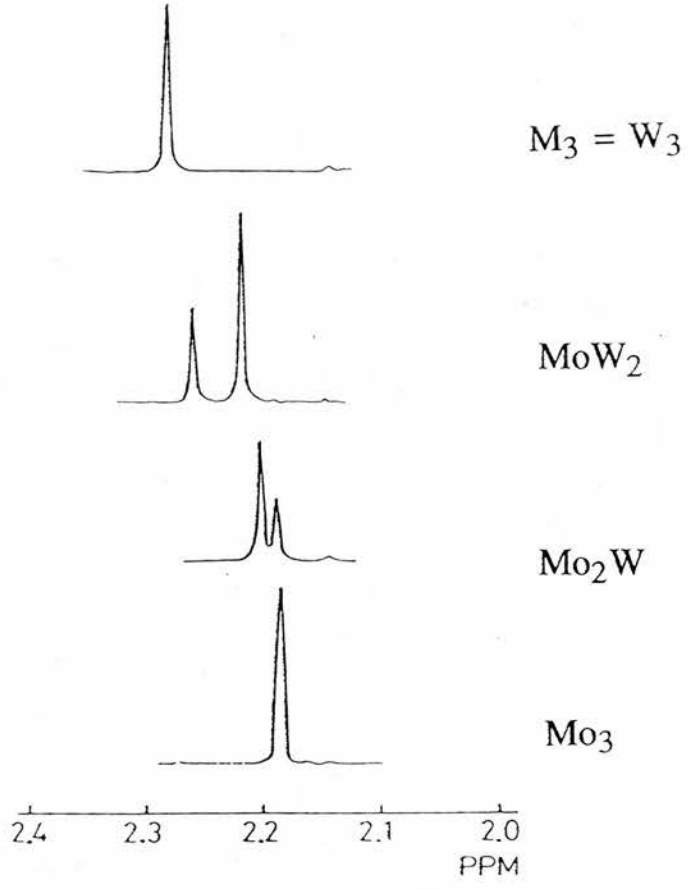

Fig. 2.5: ^1H NMR spectra of $[M_3O_2(OAc)_6(H_2O)_3]^{2+}$ complexes in aqueous solution

species gave one sharp methyl singlet the mixed species gave two new methyl singlets in a 2:1 ratio. It is clear from the figure that the

chemical shifts appear at lower field as the molybdenum atom is replaced by tungsten. The metal NMR spectra (^{183}W and ^{95}Mo) of these species have also been studied and the chemical shifts are summarised in Table 2.2, together with those of other clusters of molybdenum and tungsten. It is known from ^{95}Mo NMR that the

Table 2.2: ^{183}W and ^{95}Mo Chemical Shifts of Some Di-andTrinuclear Cluster Complexes.[a] in D_2O*

Complex	Oxid. State	δ(^{183}W ppm	δ(^{95}Mo) ppm
$[W_2Cl_9]^{3-}$	3	3539*	
$[W_3O_4(NCS)_9]^{5-}$	4	2063*	
$[W_3O_4(H_2O)_9]^{4+}$	4	1138	
$[W_3O_2(CH_3CO_2)_6(H_2O)_3]^{2+}$	4	1005	
$[MoW_2O_2(CH_3CO_2)_6(H_2O)_3]^{2+}$	4	897	1360
$[Mo_2WO_2(CH_3CO_2)_6(H_2O)_3]^{2+}$	4	848	1224
$[Mo_3O_2(CH_3CO_2)_6(H_2O)_3]^{2+}$	4		1061
$[W_2O_4(edta)]^{2-}$	5	798	
$[MoWO_4(edta)]^{2-}$	5	549	877
$[Mo_2O_4(edta)]^{2-}$	5		612

[a]Data taken from reference 23
*measured in CH_3CN

chemical shift of di- and poly-nuclear clusters appears at lower field as the oxidation number decreases.[25] Table 2.2 shows that there is a similar trend for the ^{183}W NMR. It was concluded that molybdenum in the mixed-metal trinuclear clusters is in a somewhat lower oxidation state and tungsten in a somewhat higher oxidation state than the oxidation states of these metal ions in the homonuclear Mo_3 and W_3

complexes.[26] The same conclusion was derived from the X-ray photoelectron spectral (XPS) studies.[27]

The UV-visible spectra[19] of the mixed-metal species are compared with the homonuclear cluster in Fig. 2.6. The complexes all exhibit two peaks in the visible region except for the Mo_2W species which shows one broad band with a distinct shoulder at lower energy. A systematic trend is observed among the complexes W_3, MoW_2 and Mo_3 that the corresponding transitions shift to higher energies with an increase in the extinction coefficient as molybdenum is replaced by tungsten. The Mo_2W species however seems to be somewhat exceptional.

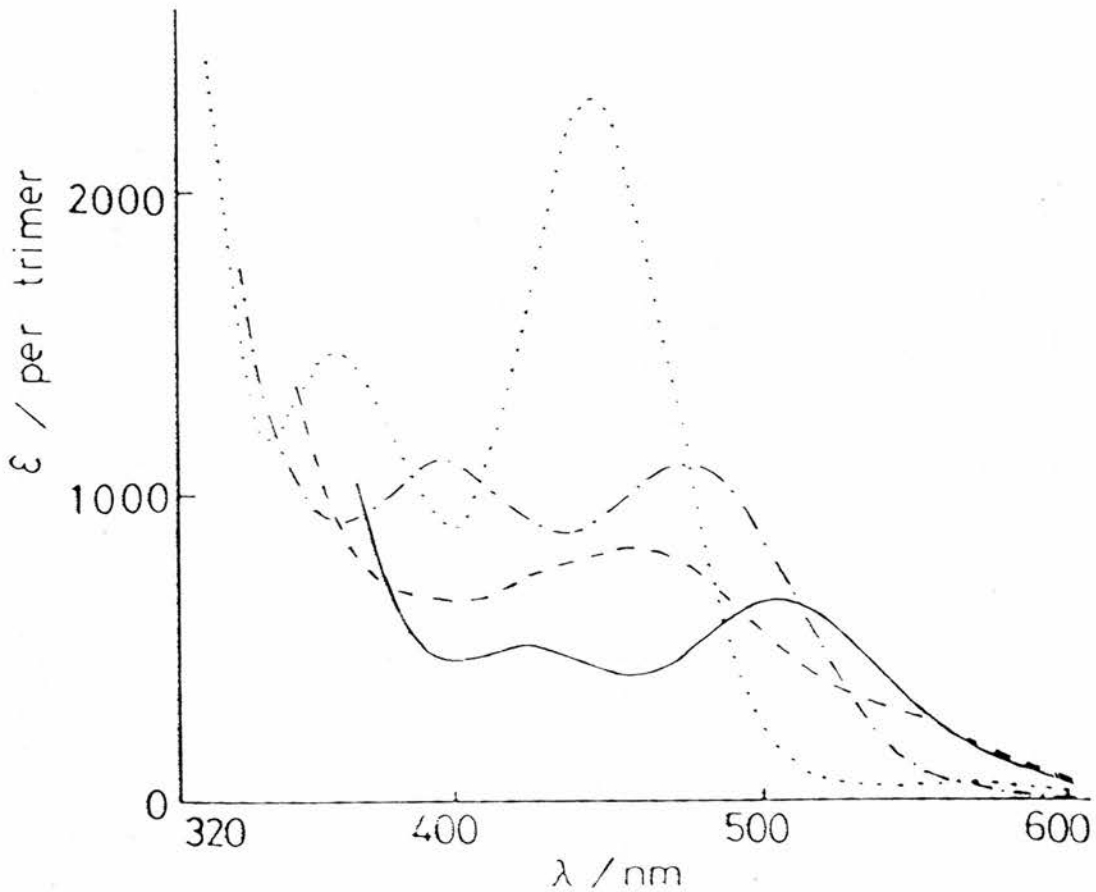

Fig. 2.6: Electronic absorption spectra in 1 M $HClO_4$ of $[Mo_3O_2(OAc)_6(H_2O)_3]^{2+}$ (—), $[Mo_2WO_2(OAc)_6(H_2O)_3]^{2+}$, (---), $[MoW_2O_2(OAc)_6(H_2O)_3]^{2+}$, (·--), and $[W_3O_2(OAc)_6(H_2O)_3]^{2+}$, (···)

2.1.3 The $H_3O_2^-$ Bridging Ligand in Mo(IV) and W(IV) Trinuclear Carboxylate Clusters

The hydrated hydroxide ion has been the subject of a number of investigations, [28-30] and the existence of species such as $H_2O_2^-$, $H_6O_4^{2-}$, $H_7O_4^-$, etc. was proposed on the basis of spectroscopic results.[28,29] Since then the mixed salt $Na_2[Et_3MeN]\{Cr[PhC(S)=N(O)]_3\}$-$.1/2Na(H_3O_2).18H_2O$ was isolated by Raymond *et al* [31] and has afforded the first example of a crystalline substance containing the $H_3O_2^-$ ion as a discrete entity in a crystal lattice. However, the existence of the hydrogen oxide bridging ligand ($H_3O_2^-$) between metal atoms was not reported until about a decade later in 1981, in Mo(IV) and W(IV) trinuclear, triangular clusters.[32-34]

It is well known that $M(OH)^{(n-1)+}$, the primary product of hydrolysis of a metal aqua ion $M(OH_2)^{n+}$ often undergoes condensation reactions to form hydrolytic dimers and polymers.[35] It is generally assumed that the metal atoms in these dimers and polymers are bridged by μ-oxo ligands.[36,37] These bridges are formed by elimination of a water molecule from a pair of ions (eqs 2.1 and 2.2).

$$M(OH)^{(n-1)+} + (H_2O)M^{n+} \longrightarrow (M\text{-}OH\text{-}M)^{(2n-1)+} + H_2O \quad (2.1)$$

$$M(OH)^{(n-1)+} + (HO)M^{(n-1)+} \longrightarrow (M\text{-}O\text{-}M)^{(2n-2)+} + H_2O \quad (2.2)$$

Bridging by the $H_3O_2^-$ ligand in these Mo(IV) and W(IV) clusters is different, however, and may be accomplished by formation of a strong hydrogen bond between the hydroxo ligand of one metal ion and the water ligand on the other ion. These strong hydrogen bonds stabilise the bridge towards subsequent elimination of a water molecule (eqn. 2.3)

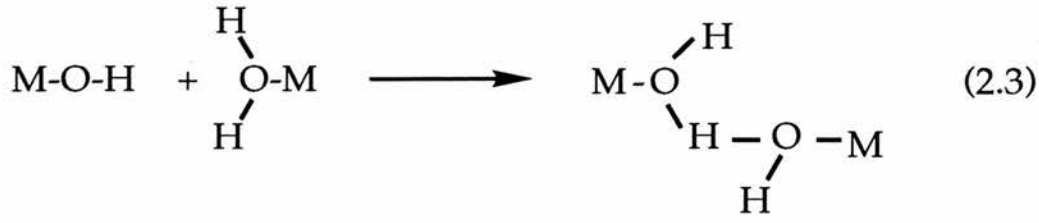

(2.3)

For this $H_3O_2^-$ ligand the bond energy of the hydrogen bond is in the region of 100 kJ mol^{-1} and the bond length is, in most cases, less than 2.47Å.[38,39] As such the hydrogen bond of the $H_3O_2^-$ bridging ligand belongs to the class of "very strong" H-bonds.[40-42] The strength of a hydrogen bond A-H-B is most conveniently defined by the distance between the atoms A and B. If their distance is shorter than the sum of their van der Waals radii, by more than 0.5Å, the bond is classed "very strong". A difference between 0.3Å and 0.5Å defines a "strong" H-bond, while <0.3Å characterises a "weak" H-bond.[41] For the homonuclear O-H-O bond, the corresponding separations are : smaller than 2.5Å for a "very strong" bond, 2.5 to 2.5Å for a "strong"bond and over 2.7Å for a "weak" bond.

The $[M_3O_2(O_2CR)_6(H_2O)_3]^{2+}$ (M = Mo or W) cluster compounds are usually prepared by elution of the 2+ cation from a cation exchange column with acids such as HBF_4, CF_3SO_3H and $HClO_4$, followed by slow evaporation of the eluate. It has been found that if the elution is carried out with various KX salts ($X=NCS^-$, Br^-, Cl^-, I^-) or HBr the H_3O_2 bridging compounds[33] can be obtained with different degrees of polymerisation. It is believed that the co-ordinated water ligand in the cluster $[M_3O_2(O_2CR)_6(H_2O)_3]^{2+}$ (called "monocluster") undergoes acid dissociation to produce an acidic solution (2.4). The hydroxo species I then reacts with a monocluster to form the 3+ cation, $\{[M_3O_2(O_2CR)_6(H_2O)_3]_2(H_3O_2)\}^{3+}$ (called "dicluster") by means of the H_3O_2 bridging ligand (eqn. 2.5).

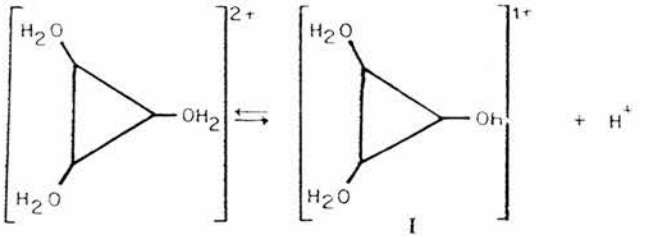

(2.4)

I

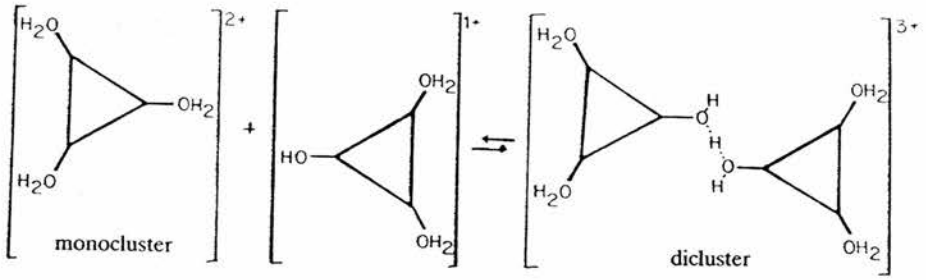

Similarily the reaction of several I with each other may form an infinite chain of M_3 clusters bridged by $H_3O_2^-$ ligands (referred to as "polycluster") (eqn. 2.6)

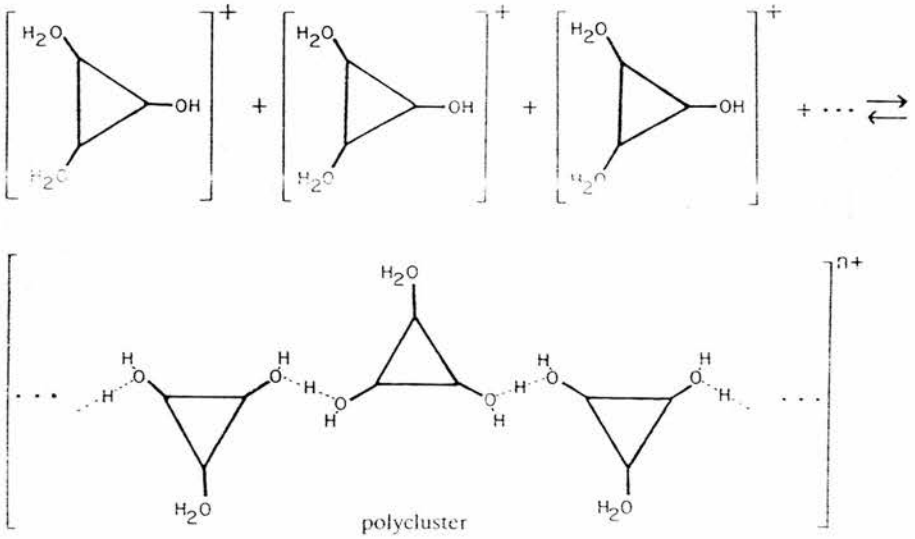

For a given total concentration of cluster, the relative concentration of these species depends on the H^+ concentration. The concentration of the dicluster increases at low pH and reaches its maximum at pH ~ pK_a. With increasing pH the equilibrium in solution shifts towards the polycluster.[43] Several of these Mo(IV) and W(IV) species have been isolated and characterised crystallographically and some structural information are given in Table 2.3. The table shows that these species all have short O-O($H_3O_2^-$) bond distances but are significantly longer than in the previously reported free ion (2.29Å).[31] This is due to the fact that the oxygen atoms of the $H_3O_2^-$ ligand are co-ordinated to the metal atoms donating a pair of electrons to the metal orbitals and hence becoming more positively charged.[33] The structure of the $\{[Mo_3O_2(pr)_6(H_2O)_2]_2(H_3O_2)\}^{3+}$ dicluster[32] is depicted in Figure 2.7

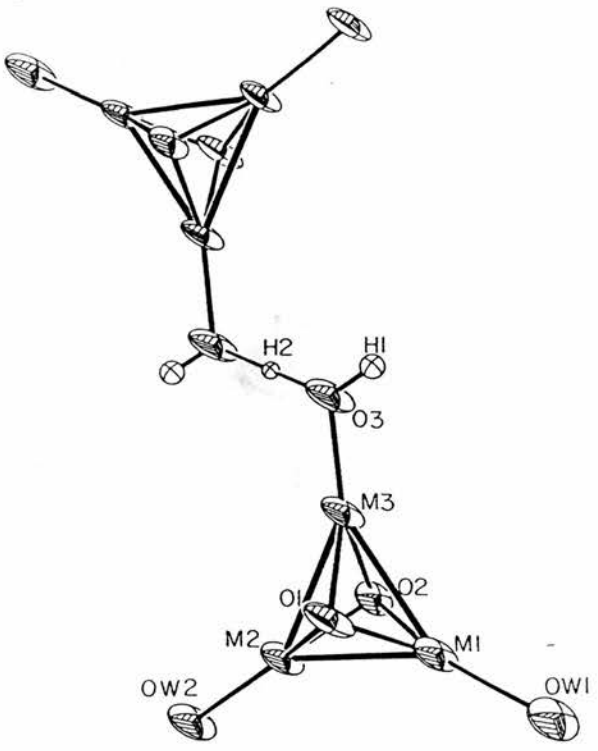

Fig 2.7: Skeletal Structure of $\{[M_3O_2(pr)_6(H_2O)_2]_2(H_3O_2)\}^{3+}$ dicluster (M = Mo or W). The propionato groups are omitted for the sake of clarity.

Table 2.3: Structural Data for $H_3O_2^-$ Bridging ligands in Trinuclear Mo(IV) and Tungsten (IV) Clusters

Complex	Type	O-O(H_3O_2), Å	M-O(H_3O_2), Å	M-M Å	M-O-O(H_3O_2) deg	M-O-O-M torsional angle deg	Ref
$\{[Mo_3O_2(pr)_6(H_2O)_2]_2(H_3O_2)\}Br_3{\cdot}6H_2O$	dicluster	2·52	2·009	5.63	117·1	180	32
$\{[W_3O_2(pr)_6(H_2O)_2]_2(H_3O_2)\}Br_3{\cdot}6H_2O$	dicluster	2·50	1·99	5·64	119·4	180	32
$\{[W_3O_2(pr)_6(H_2O)_2]_2(H_3O_2)\}(NCS)_3{\cdot}H_2O$	dicluster	2·46	2·04	5·73	120·3	180	33
$\{[Mo_3O_2(pr)_6(H_2O)_2(H_3O_2)\}(NCS)_3{\cdot}H_2O$	dicluster	2·52	2·01	5·71	119·9	180	33
$[W_3O_2(pr)_6(H_2O)(H_3O_2)]NCS$	polycluster	2·44	2·02	5·95	132·9	156·1	33
			2·07		130·0		
$[W_3O_2(OAc)_6(H_2O)(H_3O_2)]NCS$	polycluster	2·44	2·06	5·81	126·5	149·6	33
			2·03		126·2		

while the H_3O_2 unit is illustrated in Fig. 2.8.[33] Careful examination of

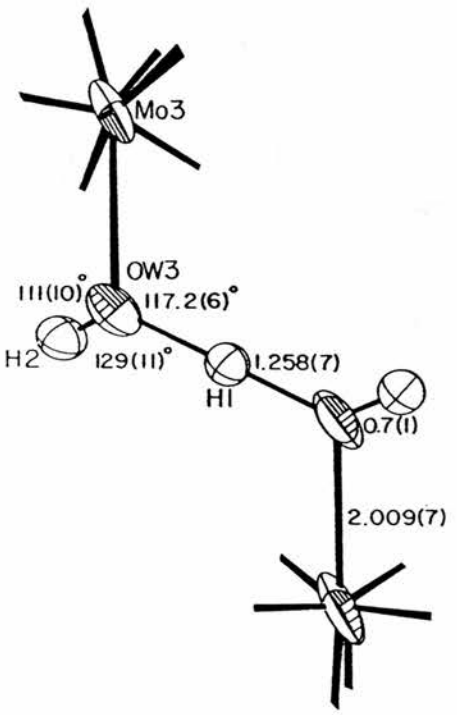

Fig. 2.8: The structure and dimensions of the Mo-O(H)HO(H)-Mo portion of the dicluster (the $H_3O_2^-$ bridging ligand).

the M-M distances within the trimer showed that the M_3 triangles are not equilateral but isosceles. This distortion was a result of a displacement of the bridged metal atom towards the negatively charged $H_3O_2^-$ ligand.

X-ray studies have shown that he $H_3O_2^-$ ligand exists not only in Mo(IV) and W(IV) clusters[32-34] but also in classical co-ordination compounds.[43] In addition to the crystallographic evidence of H_3O_2 bridges in these species, vapour tensiometry[44] and Mössbauer spectroscopy[45] have provided indirect evidence for $H_3O_2^-$ bridge formation in solutions of chromium and iron complexes. However, these experiments are neither structurally definitive nor, in the case of

the Mössabauer work, necessarily representative of aqueous solutions. Direct evidence was however obtained for the existence of $H_3O_2^-$ bridges in a tungsten species in aqueous solution using the differential anamalous X-ray scattering technique (DAS).[46] This ligand obviously plays a fundamental role in the structure of primary hydrolysis products of metal ions and may be important in relation to redox and substitution reaction mechanisms.

This chapter now describes substitution studies with regard to replacement (exchange) reactions at the terminal water ligands on four of these complexes namely the bioxo capped M(IV) species; $[Mo_3O_2(OAc)_6(OH_2)_3]^{2+}$, $[MoW_2O_2(OAc)_6(OH_2)_3]^{2+}$ and $[W_3O_2(OAc)_6(OH_2)_3]^{2+}$ and the monooxo capped mixed-valence W(III, III, IV) species; $[W_3O(OAc)_6(OH_2)_3]^{2+}$. Within this series of complexes it was viewed possible to explore four separate effects:

(i) the rates of substitution of the lone water ligand at the metal in a series of trimetal (IV) cluster ions; M = Mo, W for comparison with the $[M_3X_4(OH_2)_9]^{4+}$ (X = O, S) series of cluster ions as described in Chapter 1. Also the effect of a lower overall charge on the complex (2+);

(ii) the substitution behaviour at Mo on replacing Mo atoms in the bicapped cluster structure with W atoms;

(iii) substitution at W compared to substitution at Mo in the same system ;

(iv) the effect of a different average valency and moreover a single capping ligand in the case of $[W_3O(OAc)_6(OH_2)_3]^{2+}$.

At the outset of this work, little or no substitution studies had been reported on any of these trimetal carboxylate complexes.

2.2 EXPERIMENTAL

2.2.1 Reagents

Sodium thiocyanate (Fluka), $Mo(CO)_6$ (BDH, reagent grade), $W(CO)_6$ (BDH, reagent grade), sodium molybdate, $Na_2MoO_4.2H_2O$ (Fisons), glacial acetic acid (May and Baker, Pronalys), acetic anhydride (Aldrich), sodium tungstate, $Na_2WO_4.2H_2O$ (BDH, reagent grade), perchloric acid (BDH, AnalaR), sulphuric acid (May and Baker, reagent grade), zinc pellets (BDH), mercury (triple distilled, Aldrich), trifluoromethanesulphonic scid, CF_3SO_3H (Fluorochem) and oxalic acid (BDH, AnalaR) were used without further purification. Samples of $H_2{}^{17}O$ (12.5 atom%) were obtained from Yeda Isotope Co., Rehovot, Israel. The sodium salt of CF_3SO_3H, was prepared by neutralisation of 4M CF_3SO_3H with sodium carbonate (BDH, reagent grade), followed by recrystallisation two or three times from water. Solutions of Ce(IV) were obtained by dissolving ammonium cerium(IV) sulphate (BDH, AnalaR) in 1M sulphuric acid. Manganese triflate was prepared by neutralisation of CF_3SO_3H with manganese carbonate (May and Baker, reagent grade) followed by recrystallisation two or three times from water.

2.2.2 Standardisation of Reactants

Solution of oxalic acid was titrated against standard sodium hydroxide (Convol, BDH) with phenolphthalein as indicator. Sodium thiocyanate and sodium triflate (CF_3SO_3Na) solutions were standardised by ion exchange onto Amberlite IR(H) 120 resin (BDH, analytical

grade) and titration of the H^+ released with standard sodium hydroxide. Ce(IV) solutions were standardised by titrating with standard ammonium ferrous sulphate solution using ferroin as indicator.

2.2.3 Measurement of pH

The pH of the solutions was measured by using a Radiometer PHM82 pH meter and a Russell CWR/320/757 narrow stem glass/Ag/AgCl electrode. No buffers were used. The pH meter was calibrated with solutions at I=1.0 M (CF_3SO_3Na).

2.2.4 Spectrophotometry

Ultraviolet and visible spectra were recorded on a Perkin Elmer Lambda 5 recording spectrophotometer using 1.0-cm quartz cells with electronic thermostatting (± 0.1 °C) and auto-cell change facilities for kinetic measurements.

2.2.5 Oxygen-17 NMR measurements

These were carried out on solutions containing 0.01-0.02 M complex at 40.68 MHz in 10-mm o.d. tubes on a Bruker AM-300 instrument. Manganese (II) triflate (0.01 M) was added to the solutions to remove the large ^{17}O resonance line of bulk water by paramagnetic exchange broadening. Corrections for small shifts in the bound oxygen resonances due to the presence of added Mn^{2+} were made by assuming a value for ClO_4^- +288 ppm *vs* bulk water (ClO_4^- was used as reference). Oxygen-17 enrichments of ~6 atom% were used. The temperature of the NMR probe was calibrated using ethylene glycol by measuring the

chemical shift between H and OH (the value of which varies with temperature) over a wide temperature range (15 - 80 °C). Thus by comparing these values with the standard ones (Bruker) the correct temperatures can be obtained.

Water exchange runs were carried out for all the complexes at a fixed ionic strength, I, of 1.0 M, using $Mn(trif)_2$ and conc. $HClO_4$ solution (12.2 M) in addition to the required amounts of normal and ^{17}O-enriched water made up to a volume of 2 cm^3 ($[H^+]$ of solutions ~0.60 M). For runs involving the air-sensitive complexes $[W_3(\mu_3\text{-}O)_2(\mu\text{-}OAc)_6(H_2O)_3]^{2+}$ and $[MoW_2(\mu_3\text{-}O)_2(\mu\text{-}OAc)_6(H_2O)_3]^{2+}$ the solutions were deoxygenated by passing argon through them and the tube then sealed under vacuum.

Spectra were taken at preset timed intervals involving between 20,000 - 50,000 transients accumulated over a sweep width of 62,500 Hz using a 90° pulse width of 27 μs and the peak heights of the exchanging bound H_2O of the complex were measured and normalised against the peak of the non-exchanging ClO_4^- counter ion (the height of which remained constant). The ratio of the height of the bound H_2O peak to the height of the ClO_4^- peak thus gives the exponential increase of the exchanging H_2O^{17} for the bound H_2O. An example of such a plot, showing the gradual increase in the height of the H_2O^{17} peak is shown in Figure 2.9(a). The water exchange rate constants (k_{ex}) were calculated by fitting the data to a first-order exponential curve using the computer program GraFit. A typical trace is displayed in Figure 2.9(b).

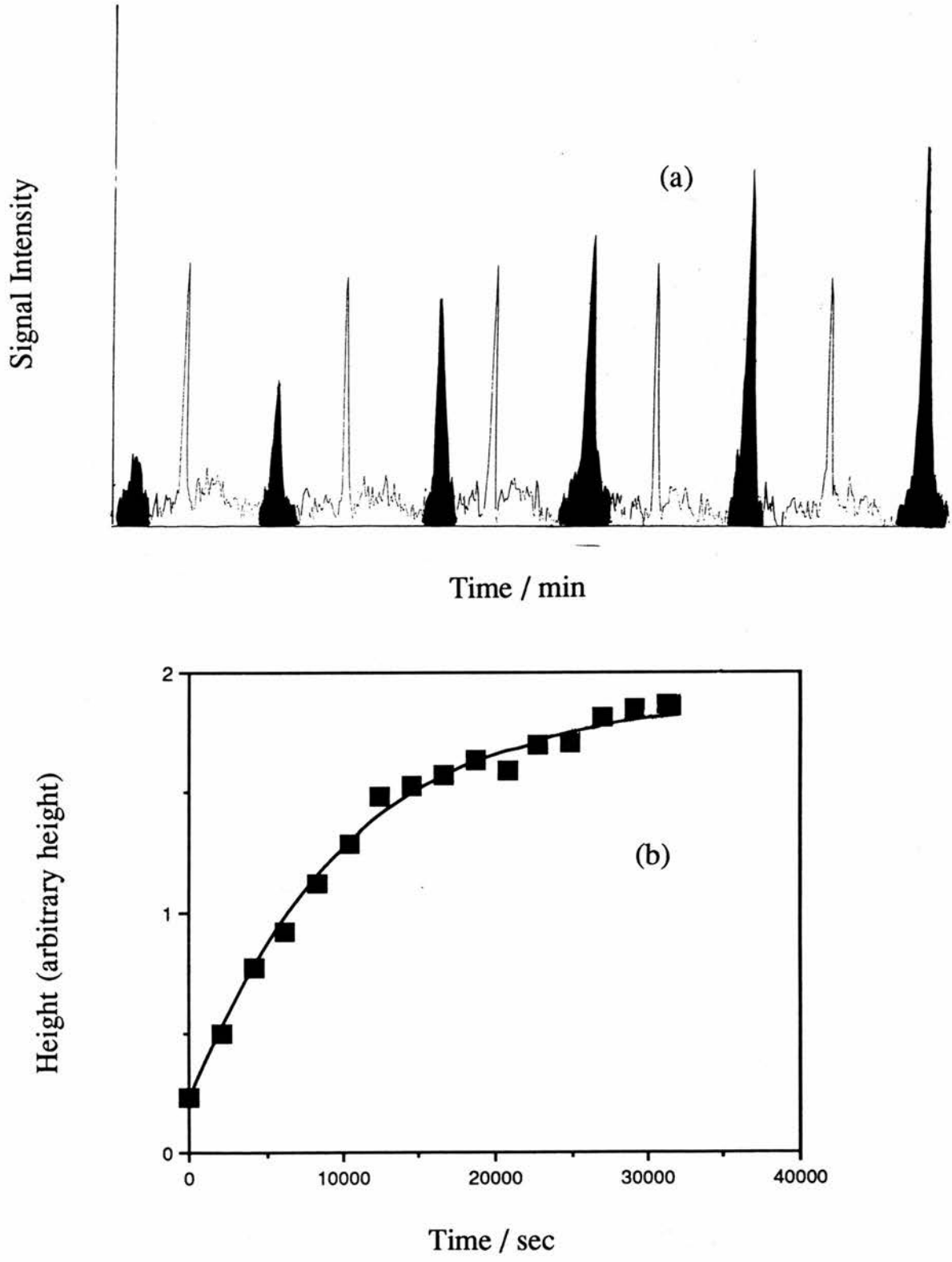

Figure 2.9: (a) Plot showing the gradual increase in height of the exchanging water (shaded) with time for the water exchange reaction of $[Mo_3O_2(OAc)_6(H_2O)_3]^{2+}$, T = 41 °C; ClO_4^- (unshaded) was used as reference , the height of which remains fairly constant. (b) Plot showing the normalised exponential increase of the exchanging H_2O peak height (arbitrary unit) with time for the reaction illustrated in (a).

2.2.6 Preparation of Complexes

2.2.6.1 Preparation of (μ_3-dioxo) hexakis (μ-acetato) triaquatri-molybdenum (IV) perchlorate, $[Mo_3O_2(OAc)_6(H_2O)_3](ClO_4)_2$

(A) 1 g of $Mo(CO)_6$ was refluxed in 100 ml of a 1:1 mixture of acetic acid and acetic anhydride for 24 hours with constant bubbling of oxygen.[7] The solution was then cooled, filtered, diluted with water (5-fold dilution) and then passed down a Dowex 50W-X2 cation exchange resin column. A red band was found to adhere to the resin but in very low amounts. Three bands were subsequently eluted from the column using 0.5 M $HClO_4$, the first was reddish-yellow in colour, the visible spectrum of which differed significantly from that of the $[Mo_3O_2(OAc)_6(H_2O)_3](ClO_4)_2$ species reported. The second band was of a very light pink colour and again the visible spectrum indicated little or no $[Mo_3O_2(OAc)_6(H_2O)_3]^{2+}$ species. The third band was of a deep reddish-pink colour, the electronic spectrum of which indicated the presence of pure $[Mo_3O_2(OAc)_6(H_2O)_3]^{2+}$. After elution of the $[Mo_3O_2(OAc)_6(H_2O)_3]^{2+}$ band a further red band was retained on the column which could not be eluted with higher acid thus indicating a higher charged species possibly consisting of polymeric material.

The preparation was subsequently repeated but this time without the bubbling of oxygen through the solution but with the mixture gently refluxed for 36 hours. Following the same procedure as above *i.e.* cooling, filtering and diluting the solution, the mixture was passed down the column. Again a very intense red band was found to adhere to the column but this time in much greater yield. (It appears that the bubbling of oxygen through the solution might not be as important as the reflux

time). The red band was eluted with 0.5 M $HClO_4$. The UV-visible spectrum of the eluate was fairly close to that of the $[Mo_3O_2(OAc)_6(H_2O)_3]^{2+}$ complex but was probably contaminated with a yellowish species. The eluted solution was diluted with water (5-fold dilution) and again passed down a Dowex 50W-X2 cation exchange resin column to separate the species present. The red ion was again eluted with 0.50 M $HClO_4$. Beautiful red crystals were subsequently obtained by allowing the solution to slowly evaporate. The complex was characterised by its UV-visible spectrum in 1 M $HClO_4$: λ_{max} = 505 nm (ε = 695 $M^{-1}cm^{-1}$ per trimer) and 430 nm (ε = 500 $M^{-1}cm^{-1}$ per trimer). These values correspond well with the published values:[19] λ_{max} ~ 505 nm (ε ~ 700 $M^{-1}cm^{-1}$) and ~ 430 nm (ε ~ 500 $M^{-1}cm^{-1}$)

(B) A mixture of reagent grade sodium molybdate dihydrate (2g), tungsten hexacarbonyl (4 g) and acetic anhydride (200 ml) was refluxed under N_2 for 5 1/4 hours. The mixture was cooled and then filtered. The solid obtained was found to be a mixture of red and blue species (the reported preparation[14] required the $Na_2MoO_4.2H_2O$ to be pure (freshly recrystallised) otherwise an initial blue product rather than red may be obtained). The solid mixture was dissolved in water whereupon the solution turned red. Some blue material remained undissolved which was filtered. It was also observed that more blue material precipitated from the filtered red solution on standing. The red solution was passed down a Dowex 50W-X2 cation exchange column. A yellow solution was found to pass straight through the column. Elution was carried out with 2 M $HClO_4$. During the elution process it became apparent that there were two bands, a red one followed by an orange one. The red band was eluted first with probably some of the orange species. The first fraction containing predominantly the red complex was diluted to

$[H^+]$~0.10 M and recolumned (Dowex 50W-X2 resin). Again 2 M $HClO_4$ was used as the eluant. The Dowex resin could not provide complete separation of the species and as such the first part of the red band was collected to avoid contamination from the orange species. Likewise the latter part of the orange band was collected to avoid contamination from the red species. The electronic spectrum of the red species compared very well with that of $[Mo_3O_2(OAc)_6(H_2O)_3]^{2+}$ and that of the orange species was very similar to that of the mixed metal complex, $[MoW_2O_2(OAc)_6(H_2O)_3]^{2+}$. The complex was characterised by its UV-visible spectrum in 1 M $HClO_4$: λ_{max} = 485 nm (ε = 1100 $M^{-1}cm^{-1}$ per trimer) and 395 nm (ε = 1110 $M^{-1}cm^{-1}$ per trimer). These values correspond well with the published values:[19] λ_{max} ~ 485 nm (~ 1100 $M^{-1}cm^{-1}$) and ~395 nm (ε ~ 1110 $M^{-1}cm^{-1}$). The mixed Mo-W complex was also characterised by elemental analysis.

Analysis:

	C	H
Calcd. for $MoW_2C_{12}H_{24}O_{25}C_{l2}$	13.07	2.19
Found	12.50	1.95

Perhaps the most convincing evidence that the orange species was genuinely the mixed-metal complex was provided by ^1H NMR of the CH_3 resonances of the acetate groups. The ^1H NMR spectrum shows two peaks in a 2:1 ratio similar to that reported by Sasaki and coworkers.[19] The ^1H NMR spectrum of this complex maybe compared with those of the homonuclear Mo_3 and W_3 analogues in Figure 2.10.

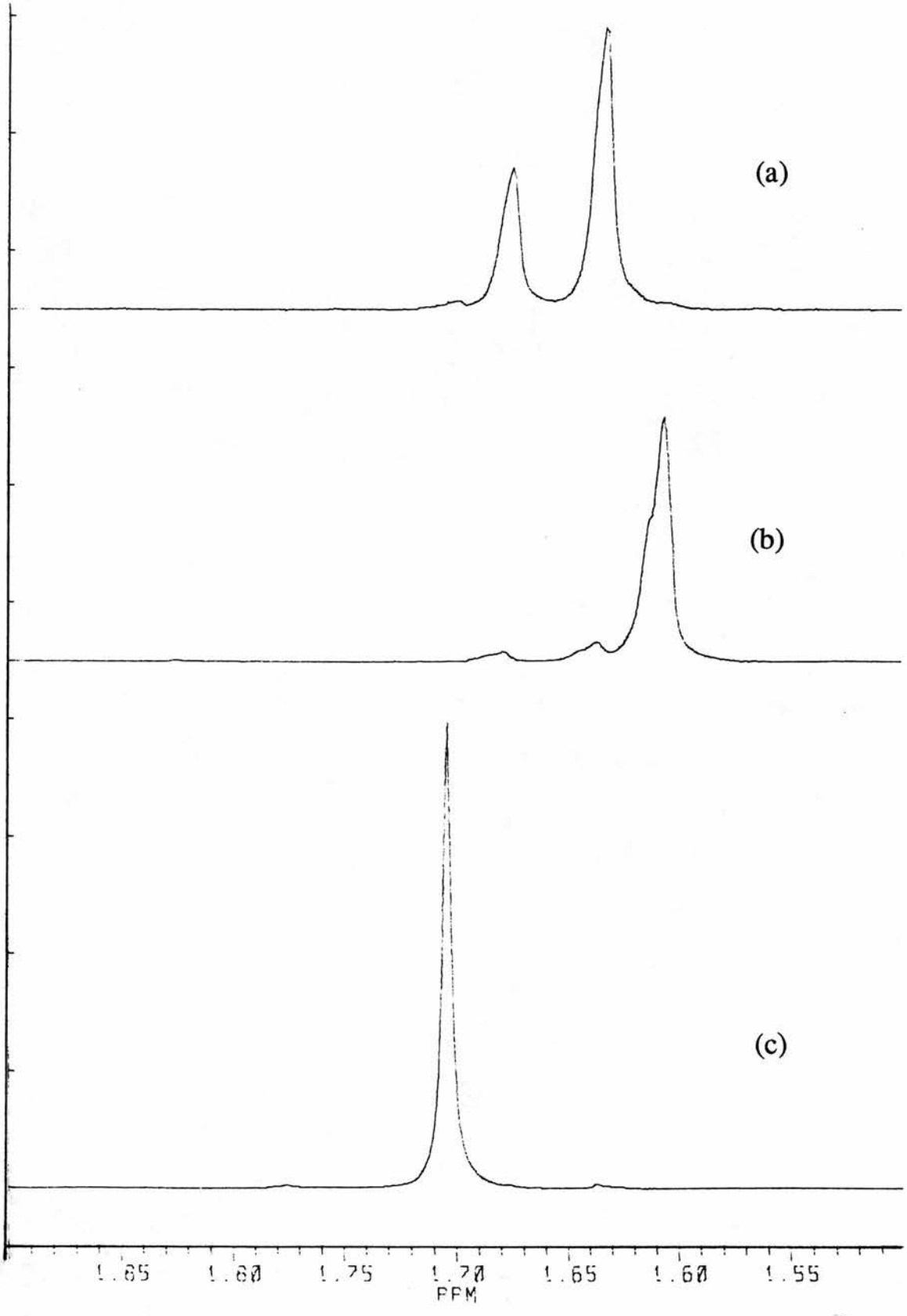

Figure 2.10: ^1H NMR spectra (CH_3 resonances of acetate) of $[M_3O_2(OAc)_6(H_2O)_3]^{2+}$ complexes in aqueous solution: (a) $M_3 = MoW_2$, (b) Mo_3, (c) W_3

2.2.6.2 Preparation of (μ_3-dioxo)hexakis(μ-acetato)triaqua-tritungsten (IV) perchlorate, $[W_3O_2(OAc)_6(H_2O)_3](ClO_4)_2$

This complex was prepared following the published method.[6] 1g of $W(CO)_6$ was refluxed overnight with 50 ml acetic acid and 50 ml of acetic anhydride. The solution was allowed to cool and a yellow precipitate that formed was filtered off. The clear filtrate was diluted with 100 ml of water and passed down a cation exchange column (Dowex 50W-X2 resin). A yellow band was absorbed onto the resin which was eluted with 2 M $HClO_4$. Yellow crystals of the title complex were obtained by allowing the eluate to evaporate slowly. The complex was characterised by its UV/visible spectrum, which agrees very well with that reported in the literature,[19] and by elemental analysis. λ_{max} = 445 nm (ε = 2300 $M^{-1}cm^{-1}$ per trimer) and 350 nm (ε = 1480 $M^{-1}cm^{-1}$ per trimer). The corresponding literature values are as follows: λ_{max} ~ 445 nm (ε ~ 2300 $M^{-1}cm^{-1}$) and λ_{max} ~ 350 nm (ε ~ 1500 $M^{-1}cm^{-1}$).

Analysis:

	C	H
Calcd. for $W_3C_{12}H_{24}O_{25}Cl_2$	12.10	2.03
Found	12.00	2.24

2.2.6.3 Preparation of (μ_3-oxo)hexakis(μ-acetato)triaqua-tritungsten(IV) perchlorate, $[W_3O(OAc)_6(H_2O)_3](ClO_4)_2$.

The monocapped complex was prepared[18] by refluxing a mixture of sodium tungstate (5.0 g) and granular zinc(5.0 g) in 60 ml of acetic anhydride for 10 hours. On cooling to room temperature, a

greenish-yellow precipitate was formed, which was filtered and washed with ethanol and ether. The solid was dissolved in water and the solution then filtered. The filtrate was passed down a cation exchange column (Dowex 50W-X2 resin) which retained a blue ion, while a yellow solution containing the anion $[W_3O_2(OAc)_9]^-$, passed through the column. After the column was washed with water to remove any trace of the yellow anion, the blue band containing the title complex was then eluted with 2 M $HClO_4$. Crystals of the solid complex were obtained by evaporation of the eluate as before. The crystals were washed with ether and air-dried. Crystals of the triflate salt were also prepared following the same procedure, except that the final elution was carried out using 2M CF_3SO_3H. The complex was characterised by its UV-visible spectrum which agrees well with the published values.[17] Wavelength maxima are in nm and the extinction coefficients ($M^{-1}cm^{-1}$) in parentheses: 668(1245), 508(630), 404(1010), 340(2370). The corresponding literature values are as follows: 668(1250), 508(625), 404(1016), 340(2375).

2.2.7 Kinetic Studies

2.2.7.1 Anation by NCS^- on $[Mo_3O_2(OAc)_6(H_2O)_3]^{2+}$

For the reaction of NCS^- with $[Mo_3O_2(OAc)_6(H_2O)_3]^{2+}$, a large absorbance change occurred below 400 nm. The $[NCS^-]$ was maintained at very large excess (≥ 10-fold) over the concentration of complex. For each run the required amounts of NaSCN and distilled water were added to a 1-cm quartz cuvette (final volume = 3 cm^3). The ionic strength was kept constant at 1.0 M by adding the appropriate amount of $NaCF_3SO_3$

to the solution in the cuvette. The cuvette was then placed in the thermostatted compartment of the UV-visible spectrophotometer for 30 minutes to equilibrate. The required amount of the solid complex was then added to the cuvette and shaken to facilitate its dissolution. The cuvette was returned to the cell compartment of the spectrophotometer and the solution was allowed to fully equilibrate for a further 10-15 minutes before absorbance *versus* time readings at 400 nm were commenced. The pH of run solutions (~3.0) was then measured before and after collection of kinetic data and was in close agreement (± 0.05 pH unit).

2.2.7.2 Anation by Oxalate on $[Mo_3O_2(OAc)_6(H_2O)_3]^{2+}$

For oxalate complexation on $[Mo_3O_2(OAc)_6(H_2O)_3]^{2+}$ the reaction was followed at 340 nm in the presence of an excess (>10 fold) of oxalate over the complex in order to permit pseudo first-order kinetics. Runs were followed over 10-20 hour periods at between 40 and 55 °C using 1.0 cm quartz cuvettes. Each solution was kept at an ionic strenght, I, of 1.0 M using $NaCF_3SO_3$. For each run the appropriate amounts of $NaCF_3SO_3$ and oxalic acid (the source of oxalate) were added to the cuvette. The solution was then adjusted to the required pH using dilute HCF_3SO_3 and/or dilute NaOH as required. For these reactions no buffer was necessary since the oxalate species served as a convenient self-buffering system. The calculated amount of the complex was then added and the solution made up to 3-cm^3 with distilled water. The filled cuvette was then placed in the thermostatted compartment of the spectrophotometer and allowed 15 minutes to fully equilibrate at the set temperature before the absorbance *versus* time

readings were taken. The pH of each solution was measured at the end of the runs and showed close agreement with the starting pH. The average pH was recorded and used in the evaluation of the kinetic data.

2.2.7.3 Anation by NCS^- on $[MoW_2O_2(OAc)_6(H_2O)_3]^{2+}$

The rate measurements were made at an ionic strength of 1.0 M ($NaCF_3SO_3$) and at 55 °C. The solutions were all adjusted to 0.01M $[H^+]$ by adding the appropriate amount of triflic acid. The $[NCS^-]$ was kept in fairly large excess (≥10-fold excess) over the concentration of complex. Each solution was made up in a 1-cm^3 quartz cuvette by adding the required amount of NaSCN to the solution of triflic acid and sodium triflate. A weighed amount of the complex was then added to the cuvette and the solution made up to 3-cm^3 with distilled water. Each cuvette was then sealed with a septum cap and the solution deoxygenated by bubbling N_2 through the solution for 10 minutes using teflon tubing inserted *via* a hollow stainless steel needle. The cuvette was then placed in the thermostatted compartment of the spectrophotometer and allowed to equilibrate for 15 minutes before the absorbance changes *versus* time was recorded at 370 nm. The pseudo-first order rate constants, k_{obs}, were computed by fitting the data to a first-order exponential curve using the GraFit program.

2.2.7.4 Anation by Oxalate on $[W_3O_2(OAc)_6(H_2O)_3]^{2+}$

Here, the kinetic study was conducted in a manner similar to that described above for the corresponding molybdenum complex. As in the

case of the mixed-metal complex, however, deoxygenation of the solutions was required. As before the appropriate amounts of $NaCF_3SO_3$ and oxalic acid were added to each cuvette and the solution adjusted to the desired pH. The weighed amount of complex was then added and the solution made up to the mark (final volume = 3 cm^3). Each cuvette was then sealed with a septum cap and the solution vigorously deoxygenated by bubbling N_2 through the solution using teflon tubing inserted *via* a hollow stainless steel needle. The cuvette was allowed to equilibrate in the thermostatted compartment of the spectrophotometer for ~30 minutes at the set temperature (55 °C) before the absorbance *versus* time readings were commenced. The pH of the solutions was measured at the end of the run and again close agreement was found between the starting and final pH. The average pH values were recorded (± 0.05).

2.2.7.5 Anation by NCS^- on $[W_3O(OAc)_6(H_2O)_3]^{2+}$

A similar method was used to that employed for the $NCS^-/[MoW_2O_2(OAc)_6(H_2O)_3]^{2+}$ anation study. The only difference was that the required amount of NaNCS solution was added just before commencement of the run in order to ensure that as little of the reaction as possible had elapsed before absorbance *versus* time readings were recorded. This was accomplished by first making up a solution in a 1-cm quartz cuvette with the required amounts of triflic acid, distilled water, $NaCF_3SO_3$ and the complex. The cuvette was then sealed with a septum cap and deoxygenated as described previously. Afterwards the cuvette was allowed to equilibrate for 15-20 minutes at the required temperature (50 °C) in the compartment of the spectrophotometer. The

cuvette was then taken out and the calculated amount of deoxygenated NaSCN solution was rapidly added using a Hamilton Syringe (0.5 cm^3). The cuvette was rapidly shaken and placed back into the compartment of the instrument and allowed to fully equilibrate for a further 5 minutes. Absorbance *versus* time readings were then commenced by monitoring the progress of the reaction at 390 nm. The pseudo-first order rate constants, k_{obs}, were calculated as perfomed for the $[MoW_2O_2(OAc)_6(H_2O)_3]^{2+}/SCN^-$ study by fitting a first-order exponential curve using GraFit.

2.3 Results

2.3.1 Thiocyanate Anation of $[Mo_3O_2(OAc)_6(H_2O)_3]^{2+}$

2.3.1.1 Dependence on Thiocyanate Concentration

The variation of the anation rate constant on thiocyanate concentration was carried out with thiocyanate concentration in very large excess (>>10-fold) over the complex concentration. The thiocyanate concentration was varied from 0.1 M to 1.0 M. It was necessary to use very high concentration of the ligand because the complex was found to be extremely inert to substitution.

A spectral scan of the complex with SCN^- under the conditions shown in Figure 2.11 illustrates a gradual decrease in absorbance of the complex λ_{max} at 505 nm and a large increase in absorbance in the UV region. These spectral changes are accompanied by the formation of two fairly well defined isosbestic points at ~ 490 nm and ~ 560 nm. The absorbance-time changes at a fixed wavelength (400 nm) indicated two stages for the reaction. A representative plot is shown in Figure 2.12(a). Towards the end of the reactions there were noticeable small

decreases in the absorbance readings corresponding to possible decomposition of the product and/or some other secondary reactions. Although this stage was ignored (which is slow), its existence ensured that the absorbance corresponding to completion of the second stage had to be estimated. These 'infinity' values were thus estimated using the method of Swinbourne (see Appendix 1). A consecutive reaction treatment of the kind applying to a sequence A --> B--> C was used to treat the data. Figure 2.12(b) shows a a typical plot of $\ln(A_\infty - A_t)$ *versus* time for the NCS^- anation of the complex. From the straight line portion of the curve, the first-order rate constant for the slower reaction (k_2) was obtained. When the logarithm of the difference between the extrapolated straight-line portion and the experimental curve was plotted *versus* time (inset , Figure 2.12(b), the rate constant of the more rapid reaction (k_1) was obtained. The observed rate constants, k_1 and k_2, for the different temperatures are collected in Table 2.4. As discussed in Chapter 1, three identical metal sites are available for 1:1 anation by SCN^- in this complex and so a statistical factor involving division of the [SCN-] by three has been assumed for the purpose of evaluating the anation rate constant at any one metal centre. A plot of k_{obs} *versus* $[SCN^-]/3$ for the first stage of the reaction is shown in Figure 2.13. From the figure it is clear that saturation behaviour occurs at sufficiently high NCS^- concentration ($\geq$ 0.50 M). The data are consistent with an interchange mechanism involving the rapid formation of a precursor outer-sphere species in a pre-equilibrium step followed by rate-determining interchange (or substitution) between outer and inner spheres of the aqua trimer complex (Scheme 2.2).

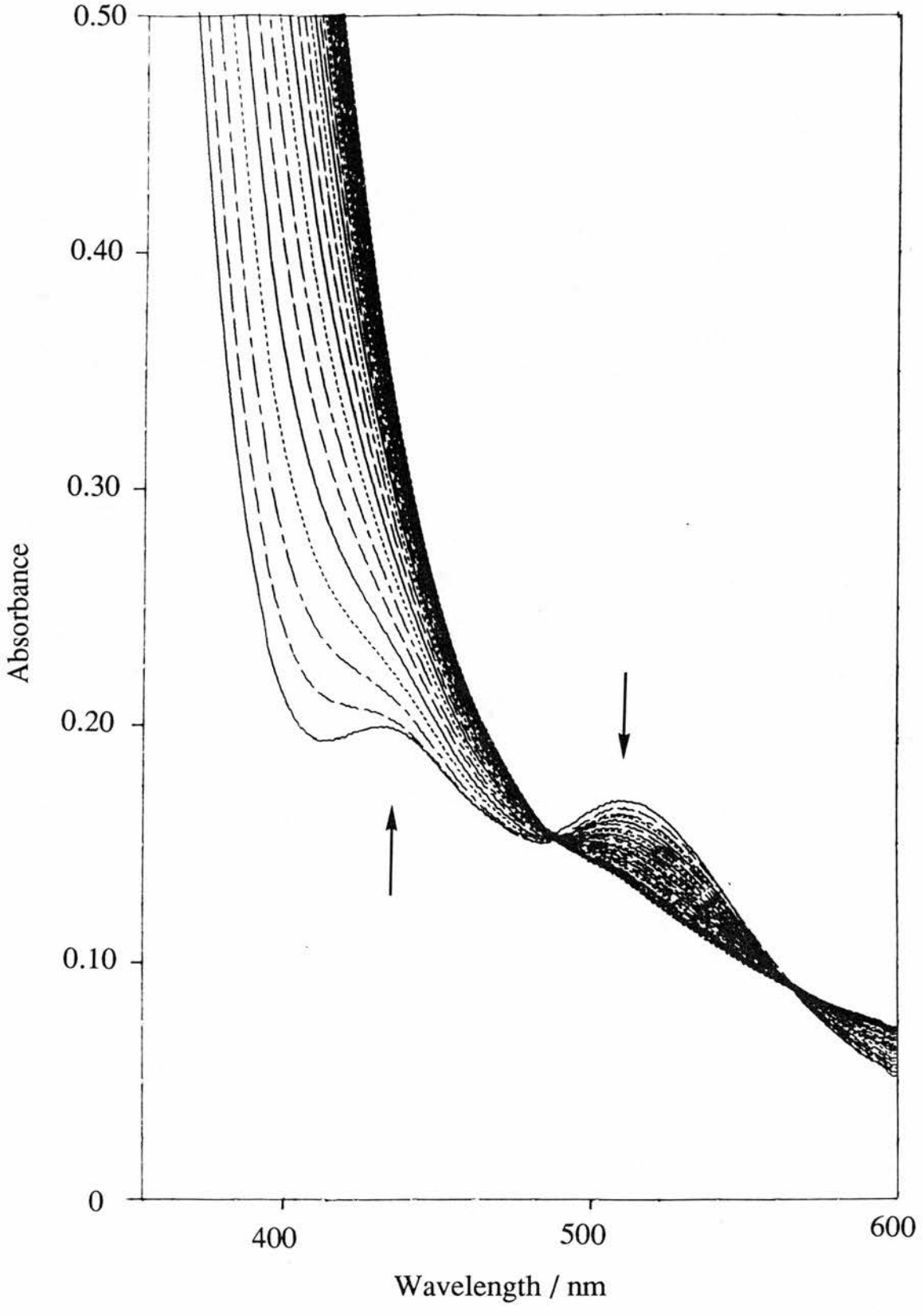

Figure 2.11: Changes in the electronic spectrum of $[Mo_3O_2(OAc)_6(H_2O)_3]^{2+}$ during reaction with SCN^-. [Complex] ~ 4 x 10^{-4} M, T= 47 °C, time interval = 60 min., [SCN^-] = 0.90 M and I= 1.0 M (CF_3SO_3Na).

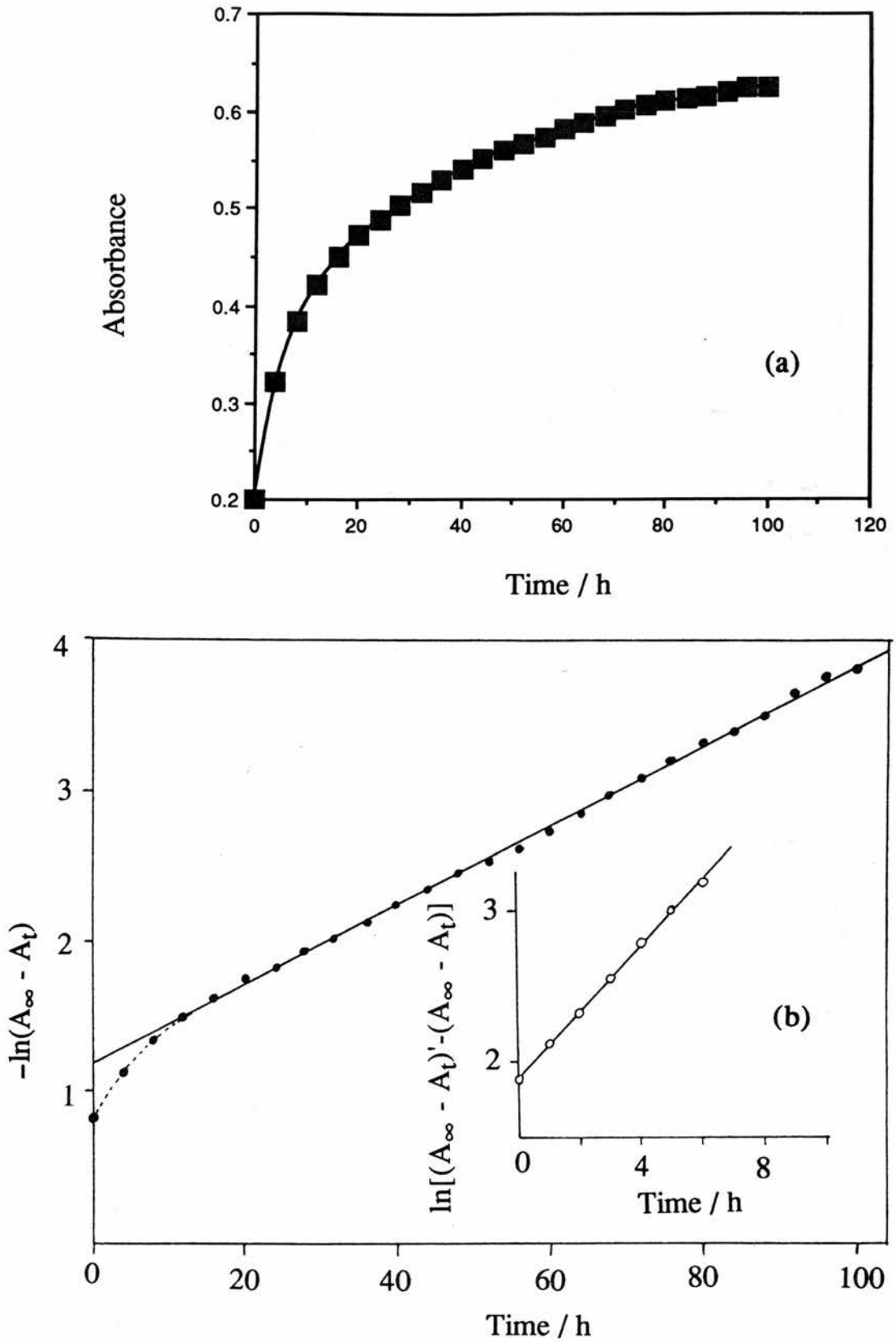

Figure 2.12: (a) A representative plot of absorbance *versus* time for the reaction of $[Mo_3(\mu_3\text{-}O)_2(\mu\text{-}OAc)_6(H_2O)_3]^{2+}$ with SCN^- ; (b) plot of the experimental data of the same reaction : pH ~3.0 , T= 47 °C, λ_{max} = 400 nm, $[NCS^-]$ = 0. 1M and [complex] = 4 x 10^{-4} M.

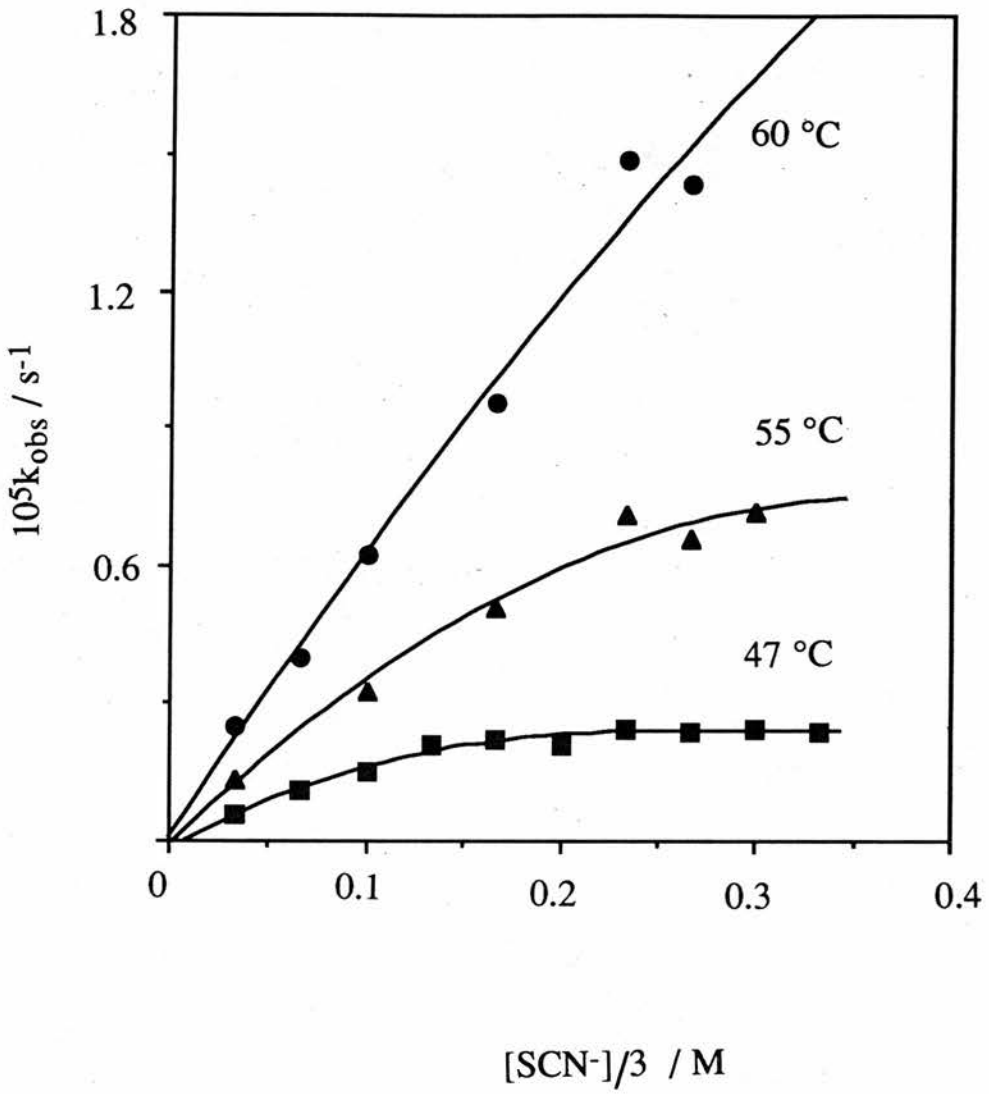

Figure 2.13: A plot of k_{obs} against [SCN⁻]/3 for the first stage of the reaction between $[Mo_3(\mu_3\text{-}O)_2(\mu\text{-}OAc)_6(H_2O)_3]^{2+}$ and SCN^- at different temperatures.

Table 2.4: Pseudo-First-Order Rate Constants for the Two Stages in the Reaction of Thiocyanate with $[Mo_3(\mu_3\text{-}O)_2(\mu\text{-}OAc)_6(H_2O)_3]^{2+}$ (2.0×10^3) at Different Temperatures, I = 1.0 M (CF_3SO_3Na) λ_{max} = 400 nm.

Temperature /°C	$[SCN^-]$/M	$10^4k_1/s^{-1}$	$10^5k_2/s^{-1}$
47	0.10	0.57	0.72
	0.20	1.08	1.00
	0.30	1.53	1.43
	0.40	2.07	2.07
	0.50	2.19	2.42
	0.60	2.11	3.33
	0.70	2.44	3.50
	0.80	2.35	3.67
	0.90	2.42	4.34
	1.00	2.36	4.87
55	0.10	1.33	1.35
	0.30	3.27	4.18
	0.50	5.10	6.96
	0.70	7.12	9.61
	0.80	6.60	11.53
	0.90	7.20	13.00
60	0.10	2.50	2.64
	0.20	4.00	5.09
	0.30	6.25	8.83
	0.50	9.56	13.70
	0.70	14.90	20.00
	0.80	14.33	22.08

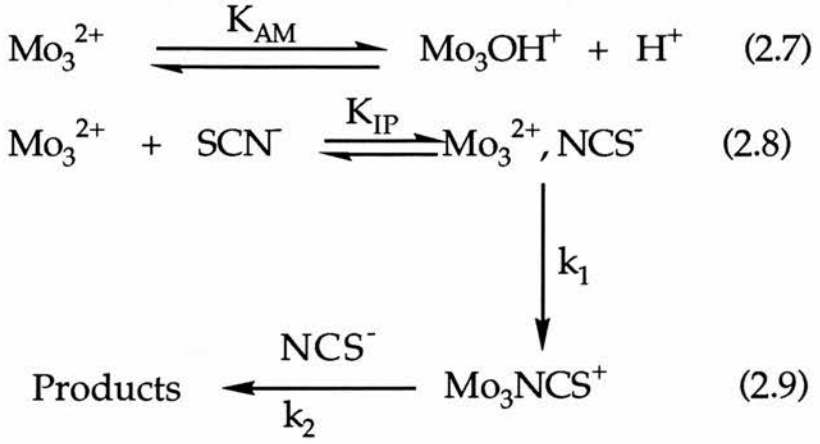

($[Mo_3O_2(OAc)_6(H_2O)_3]^{2+}$ written as Mo_3^{2+} for the sake of clarity)

Scheme 2.1

Separate studies have indicated that the $[Mo_3O_2(OAc)_6(OH_2)_3]^{2+}$ complex undergoes acid dissociation at one of the coordinated water ligands with a p*K*a ~ 4.[34] Thus at the reaction pH ~3 for the SCN^- runs a significant amount of the monohydroxy form is expected to be present. It follows from this scheme that

$$k_{obs} = \frac{k_1 K_{IP}[NCS^-]/3[H^+]}{(1+K_{IP}[NCS^-]/3)([H^+] + K_M)} \qquad (2.10)$$

The full derivation of the rate law (2.10) is shown in Appendix 2. At $[H^+] \sim K_M$ *i.e.* at pH ~3, equation (2.10) can be rearranged into equation (2.11)

$$\frac{1}{k_{obs}} = \frac{3(1+ K_{IP}[NCS^-]/3)([H^+] + K_M)}{k_1 K_{IP}[NCS^-]/3[H^+]} \qquad (2.11)$$

It follows from equation (2.11) that

$$\frac{1}{k_{obs}} = \frac{3([H^+] + K_M)}{k_1 K_{IP}[NCS^-][H^+]} + \frac{([H^+] + K_M)}{k_1[H^+]} \qquad (2.12)$$

From equation (2.12) it can be seen that

$$\frac{1}{k_{obs}} = \frac{slope}{[NCS^-]} + int \qquad (2.13)$$

Thus if a plot of $1/k_{obs}$ *versus* $1/[NCS^-]$ is made, a straight line should be obtained with intercept as $3([H^+] + K_M)/[H^+]k_1$, hence k_1. This treatment is illustrated in Figure 2.14, where data at three temperatures from Table 2.4 are shown as $1/k_{obs}$ *versus* $1/[SCN^-]$ plot. The value of K_{IP} can be obtained by dividing the intercept by the slope. The values of k_1 and K_{IP} thus obtained along with the corresponding activation parameters are summarised in Table 2.5.

Table 2.5: Summary of Kinetic Parameters for the First Step of the Rection Between SCN^- and $[Mo_3(\mu_3\text{-}O)_2(\mu\text{-}OAc)_6(H_2O)_3]^{2+}$, I= 1.0 M ($NaCF_3SO_3$).

Temperature/ °C	$10^4k_1/s^{-1}$	K_{IP}/M
47.0	4.96	1.5
55.0	18.61	0.9
60.0	40.45	0.7
$\Delta H^{\neq}$ = 140.7 ± 0.9 kJ mol^{-1}		$\Delta H°$ = -52.4 ± 2.7 kJ mol^{-1}
$\Delta S^{\neq}$ = 130.6 ± 2.7 J K^{-1}mol^{-1}		$\Delta S°$ = -160.4 ± 8.2 J K^{-1} mol^{-1}

Attempts to carry out a pH variation study (adjusting the pH with dilute triflic acid and/or dilute NaOH) at a fixed $[NCS^-]$ were unsuccessful due to failure of the solutions to maintain the pH. Unfortunately no

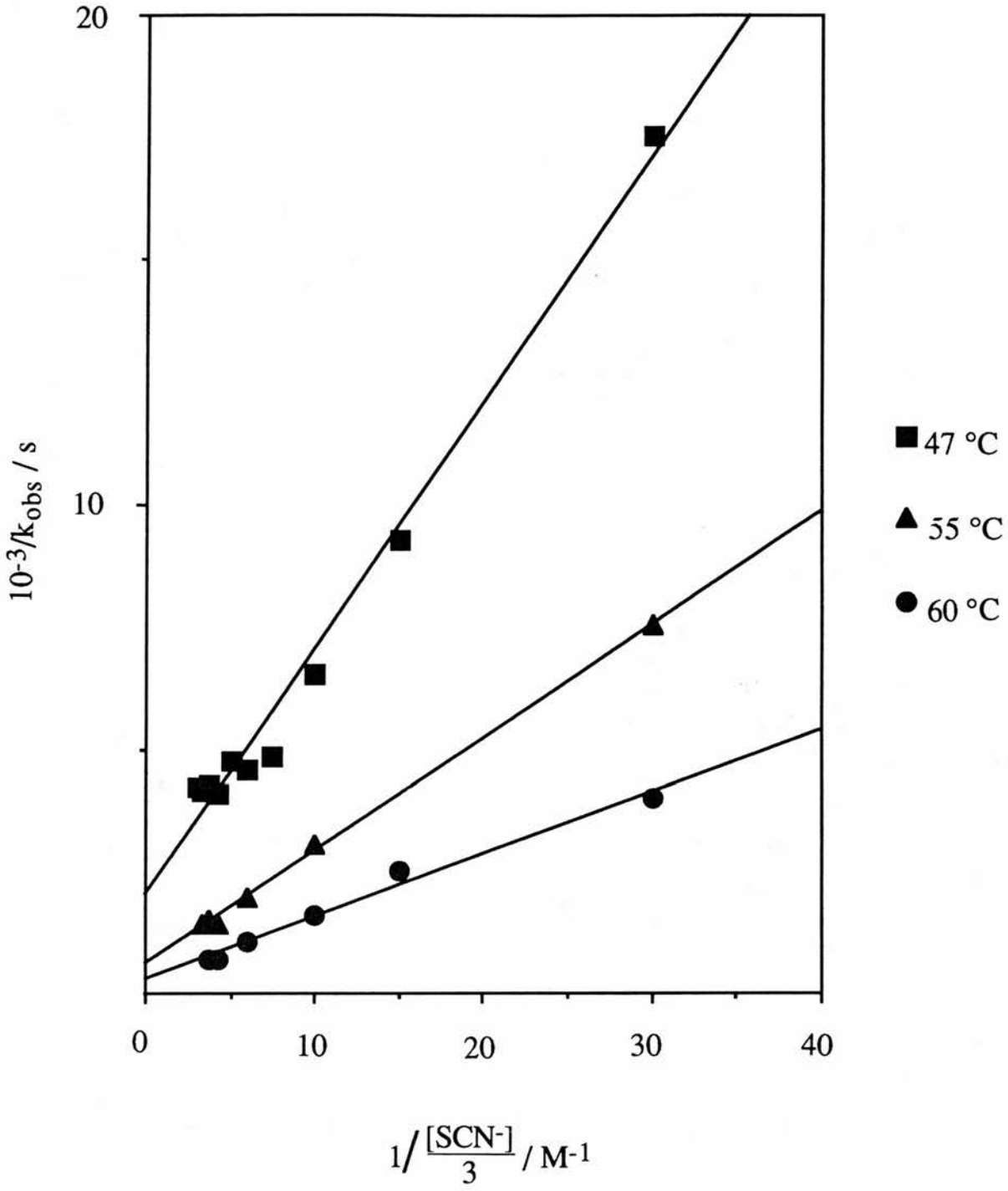

Figure 2.14: Plot of $1/k_{obs}$ *vs* $[SCN^-]^{-1}$ for the first step of the reaction between $[Mo_3O_2(OAc)_6(OH_2)_3]^{2+}$ and SCN^-.

satisfactory buffers for this reaction could be found. Interestingly an attempt to use acetate as buffer causes complete retardation of the substitution, presumably due to strong ion-pair association perhaps involving hydrogen bonding with the aqua ligands.

The results for the second stage of the reaction between $[Mo_3O_2(OAc)_6(H_2O)_3]^{2+}$ and SCN^- are shown in Table 2.4 and represented as plots of k_{obs} *vs* $[SCN^-]/2$ in Figure 2.15. Here it is assumed that a statistical factor of two is operative for reaction with the diaqua monothiocyanate trimeric complex. Here a simple linear dependence on $[NCS^-]/2$ is observed passing through the origin with no evidence of curvature indicating negligible ion-pairing of SCN^- with the monothiocyanate complex. Simple bimolecular rate constants were obtained according to (2.14) as a function of temperature and are listed in Table 2.6.

$$k_{obs} = k_2 \frac{[NCS^-]}{2} \qquad (2.14)$$

Table 2.6: Kinetic Parameters for the Second Stage of the Reaction Between $[Mo_3O_2(OAc)_6(H_2O)_3]^{2+}$ and SCN^-

Temp / °C	$10^5 k_2$ / M^{-1}	$\Delta H^{\neq}$ kJ mol^{-1}	$\Delta S^{\neq}$ /J $K^{-1}mol^{-1}$
47.0	9.342	120.1 ± 0.6	52.6 ± 1.7
55.0	28.94		
60.0	56.42		

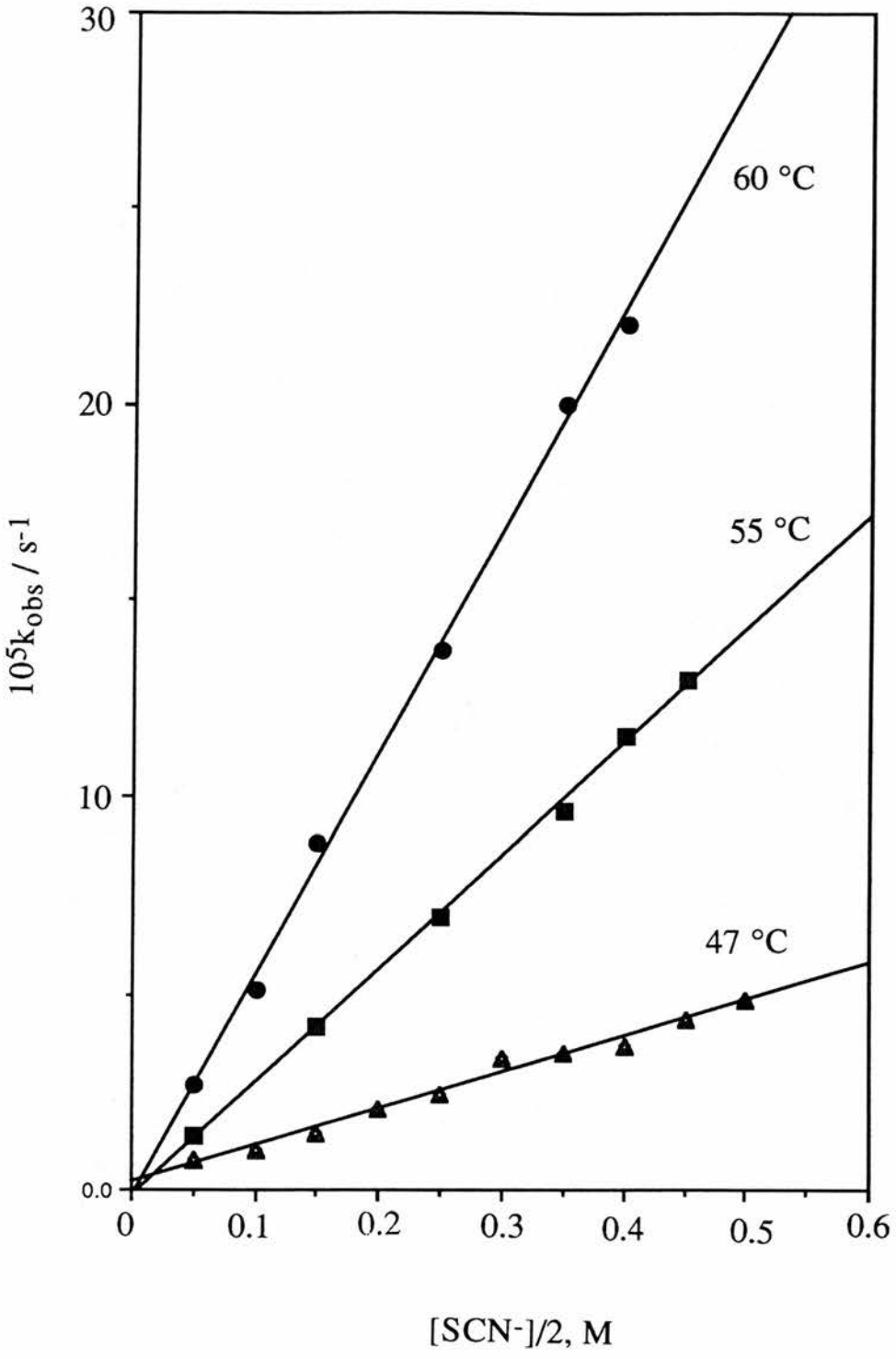

Figure 2.15: Dependence of k_{obs} on [SCN⁻]/2 at different temperatures for the second stage of the reaction between $[Mo_3(\mu_3\text{-}O)_2(\mu\text{-}OAc)_6(H_2O)_3]^{2+}$ and SCN^-.

2.3.2 Oxalate Anation of $[Mo_3O_2(OAc)_6(H_2O)_3]^{2+}$

2.3.2.1 Dependence on Total Oxalate Concentration

The reaction of $[Mo_3O_2(OAc)_6(H_2O)_3]^{2+}$ with oxalate shows a small shift in λ_{max} to higher wavelength with an increase in absorbance corresponding to the oxalate anation process (Figure 16). This small shift in the λ_{max} to higher wavelengths is what one would except based on the position of oxalate with respect to H_2O in the spectrochemical series. Also since both species bond through oxygen atoms not much change is expected in the overall spectrum as is observed.

The dependence of the anation rate constant on the oxalate concentration was studied in a series of runs with $[oxalate]_T$ in large excess (>10-fold). The total oxalate concentration was varied from 0.01 M to 0.05 M. However, use of higher concentrations of oxalate comparable to those used for the NCS^- study was not possible due to solubility problems. There were uncertainties in the absorbance values at the end of the reaction (A_∞) due to small decreases in absorbance readings. This could possibly be due to slight decomposition of the product and/or due to some other secondary process. Values for k_{obs} were thus calculated from $-\ln(A_\infty - A_t)$ *versus* time plots using A_∞ estimated by the Swinbourne method (see Appendix 1). Such plots were linear up to at least three half-lives. A typical absorbance *versus* time plot is shown in Figure 2.17(a) and the corresponding first-order plot is shown in Figure 2.17(b). Under the conditions of study a first-order dependence of k_{obs} on total oxalate concentration was found passing through an intercept and a representative plot *i.e.* of k_{obs} *versus* $[Ox]_T$ at 40 °C is shown in Figure 2.18. This behaviour suggests that equilibrium kinetics are in operation and can be represented by equation (2.15). Again a statistical factor of three has been assumed

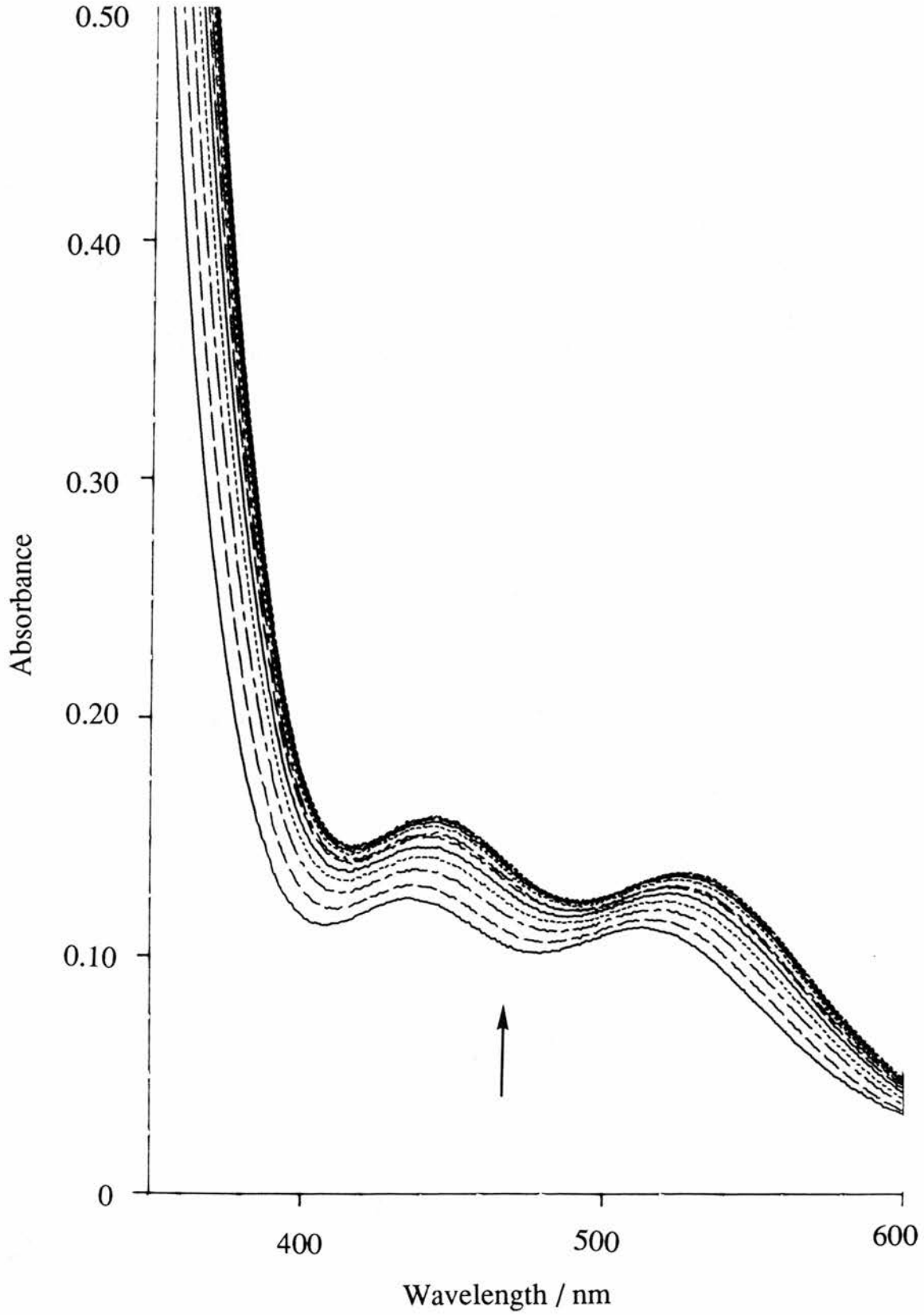

Figure 2.16: Scan spectra of the reaction (47 °C) of oxalate (0.10 M) with $[Mo_3O_2(OAc)_6(H_2O)_3]^{2+}$ (~ 2 x 10^{-4} M) at pH 3.2. Time interval between spectra 20 minutes, I=1.0 M ($NaCF_3SO_3$)

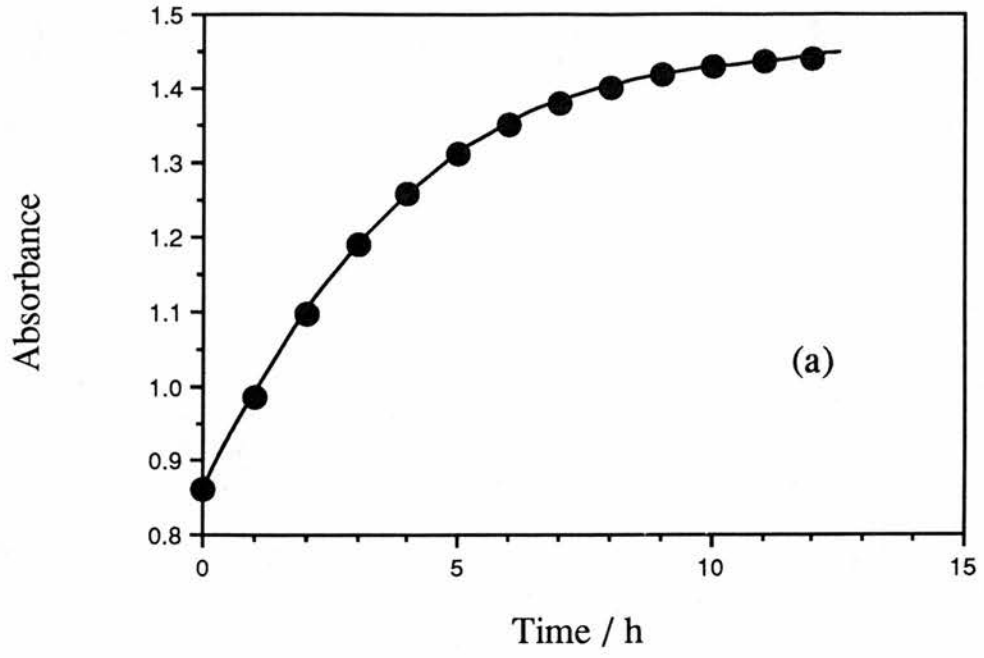

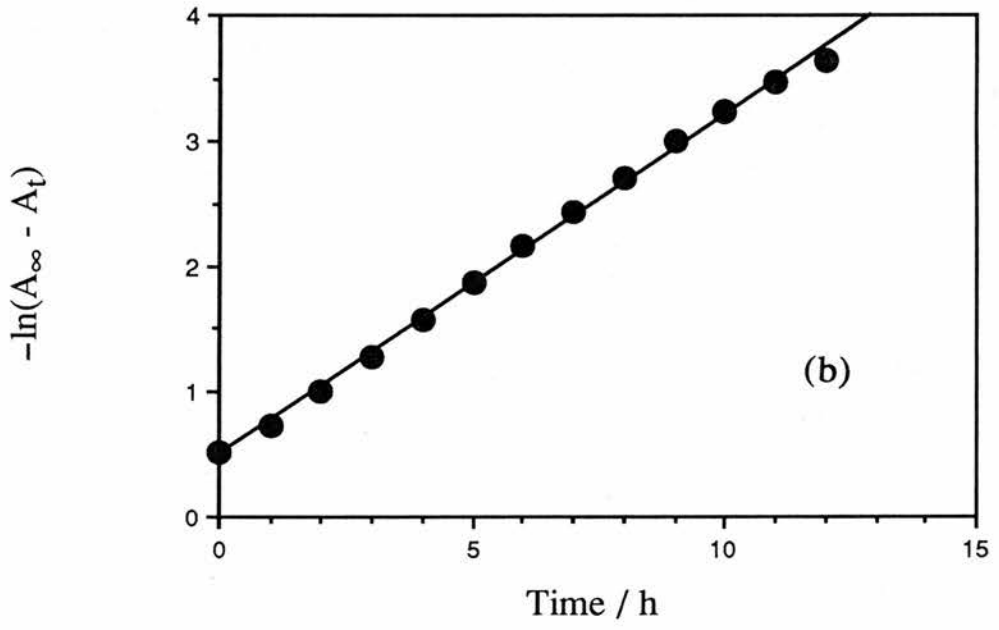

Figure 2.17 (a): Graph of absorbance *versus* time for the reaction of $[Mo_3O_2(OAc)_6(H_2O)_3]^{2+}$ with oxalate (λ = 340 nm, T=47 °C, [Ox] = 0.02 M [Complex] = 4 x 10^{-4} M, pH = 3.10 and I=1.0 M ($NaCF_3SO_3$). (b) Plot of $-\ln(A_\infty - A_t)$ *versus* time for the reaction between $[Mo_3O_2(OAc)_6(H_2O)_3]^{2+}$ and oxalate under the conditions displayed in Figure 2.17(a).

$$k_{obs} = k_f\left[\frac{Ox}{3}\right]_T + k_b \qquad (2.15)$$

for 1:1 complex formation. The results obtained at three different temperatures are tabulated in Table 2.7.

2.3.2.2 Dependence on Hydrogen Ion Concentration

Oxalic acid was used as the source of oxalate. This acid undergoes two successive acid dissociations as shown in equations (2.16) and (2.17), the respective acid dissociation constants are K_1 and K_2.

$$H_2C_2O_4 \overset{K_1}{\rightleftharpoons} HC_2O_4^- + H^+ \qquad (2.16)$$

$$HC_2O_4^- \overset{K_2}{\rightleftharpoons} C_2O_4^{2-} + H^+ \qquad (2.17)$$

The corresponding thermodynamic parameters for K_1 and K_2 calculated from previously reported data at ionic strength 1.0 M are as follows: for K_1, ΔH^o = -15.76 ±0.47 kJ mol^{-1} and ΔS^o = -318.3±1.40 J K^{-1}mol^{-1}, and for K_2, ΔH^o= -6.03 ± 0.04 kJ mol^{-1} and ΔS^o = -333.2 ± 0.10 J K^{-1} mol^{-1}.[47]

For the conditions used in this study (2.5 < pH < 3.9) the amounts of the fully protonated form, $H_2C_2O_4$, may be neglected and the total oxalate concentration may be represented as consisting of the monodeprotonated form, $HC_2O_4^-$ and the dianion, $C_2O_4^{2-}$. Thus, the

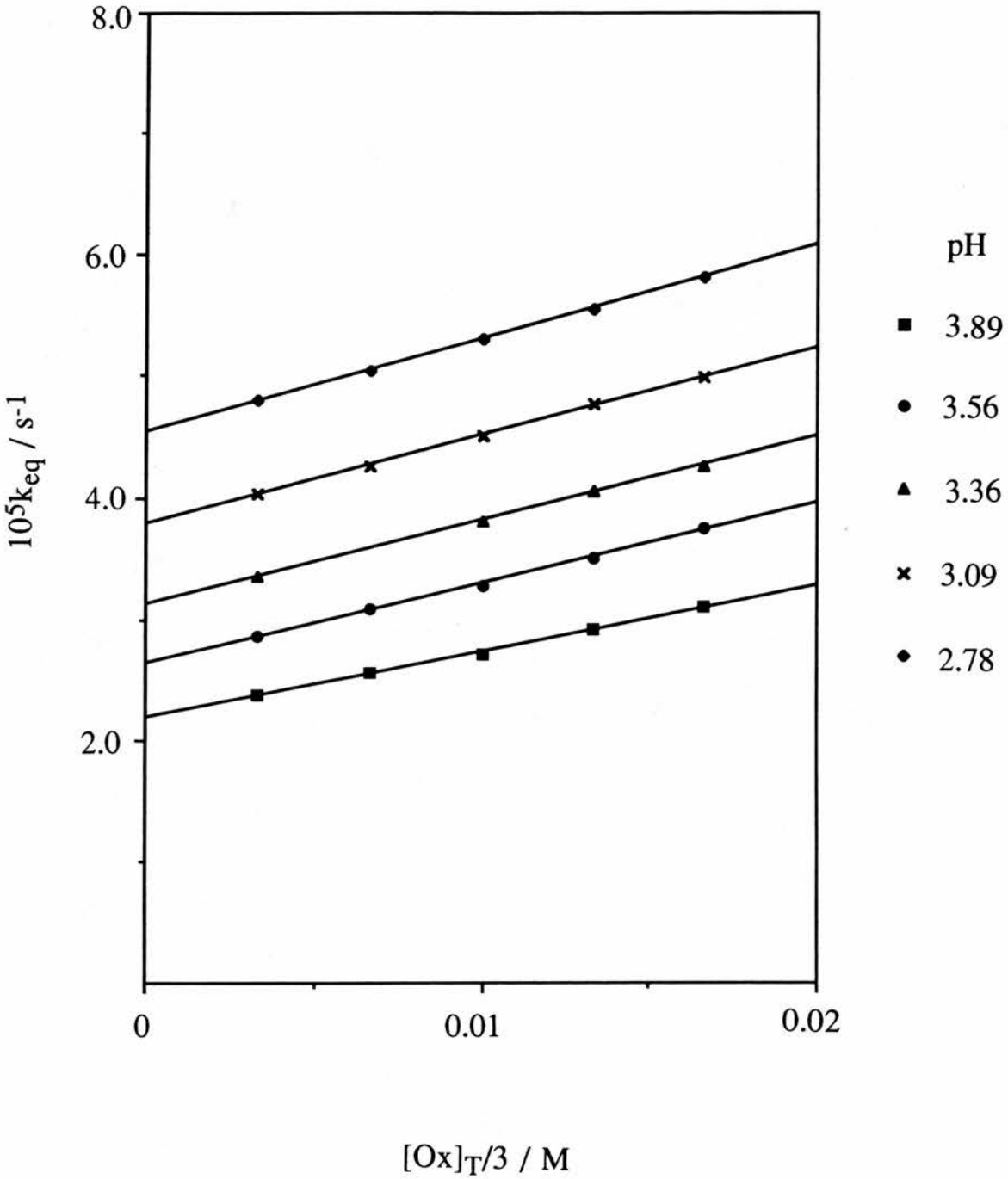

Figure 2.18: Equilibration rate constants (k_{eq}) *versus* $[Ox]_T$ at 40 °C (I=1.0 M (CF_3SO_3Na)) for the reaction of $[Mo_3O_2(OAc)_6(H_2O)_3]^{2+}$ with oxalate at pH different pHs.

Table 2.7: First-Order Equilibration Rate Constants (k_{eq}), Formation (k_f) and Aquation (k_{aq}) Rate Constants for the Reaction of $[Mo_3(\mu_3\text{-}O)_2(\mu\text{-}OAc)_6(H_2O)_3]^{2+}$ with Oxalate at various pH's and Different Temperatures [Complex]= 4x 10^{-4} M, λ_{max}=340 nm, I=1.0 M ($NaCF_3SO_3$).

Temp/°C	pH	$[Ox]_T$/M	10^5k_{obs}/ s^{-1}	$10^4k_f/M^{-1}$ s^{-1}	$10^5k_{aq}/s^{-1}$
40	2.78	0.01	2.38	5.46	2.19
		0.02	2.56		
		0.03	2.71		
		0.04	2.92		
		0.05	3.11		
	3.09	0.01	2.87	6.54	2.64
		0.02	3.09		
		0.03	3.27		
		0.04	3.51		
		0.05	3.75		
	3.36	0.01	3.36	6.75	3.13
		0.03	3.81		
		0.04	4.04		
		0.05	4.26		
	3.56	0.01	4.03	7.56	3.78
		0.02	4.26		
		0.03	4.50		
		0.04	4.76		
		0.05	4.99		
	3.89	0.01	4.80	7.62	4.54
		0.02	5.04		
		0.03	5.31		
		0.04	5.56		
		0.05	5.81		

47	2.65	0.01	0.45	12.00	4.10
		0.02	0.49		
		0.03	0.52		
		0.04	0.57		
		0.05	0.61		
	2.82	0.01	0.58	13.80	5.30
		0.02	0.61		
		0.03	0.66		
		0.04	0.71		
		0.05	0.76		
	3.10	0.01	0.71	17.10	6.50
		0.02	0.76		
		0.03	0.82		
		0.04	0.87		
		0.05	0.94		
	3.51	0.01	0.94	19.50	8.80
		0.02	1.01		
		0.03	1.07		
		0.04	1.14		
		0.05	1.20		
	3.75	0.01	1.10	24.00	10.20
		0.02	1.18		
		0.03	1.26		
		0.04	1.34		
		0.05	1.42		

55	2.54	0.01	1.77	25.50	16.90
		0.02	1.86		
		0.03	1.96		
		0.04	2.03		
		0.05	2.11		
	2.78	0.01	1.95	30.90	18.50
		0.02	2.05		
		0.03	2.17		
		0.04	2.26		
		0.05	2.36		
	3.11	0.01	2.58	41.70	24.50
		0.02	2.73		
		0.03	2.87		
		0.04	3.00		
		0.05	3.14		
	3.48	0.01	3.37	52.80	31.90
		0.02	3.53		
		0.04	3.89		
		0.05	4.07		
	3.84	0.01	4.25	59.10	40.60
		0.02	4.46		
		0.03	4.66		
		0.04	4.83		
		0.05	5.05		

total oxalate concentration may be written as in equation (2.18):

$$[Ox]_T = [HC_2O_4^-] + [C_2O_4^{2-}] \quad (2.18)$$

By making use of the different equilibria represented in equations (2.16) and (2.17) it is possible to express the concentrations of $HC_2O_4^-$ and $C_2O_4^{2-}$ as a function of total oxalate as shown below:

$$[HC_2O_4^-] = \frac{[H^+]\,[Ox]_T}{[H^+] + K_2} \qquad (2.19)$$

$$[C_2O_4^{2-}] = \frac{K_2[Ox]_T}{[H^+] + K_2} \qquad (2.20)$$

The H^+ concentration was varied in order to determine whether $HC_2O_4^-$ or $C_2O_4^{2-}$ or indeed both species were involved as reactants with the metal species.

The results clearly show (see Figure 2.18) that the k_{obs} values increase as the acidity is decreased, suggesting that the dianion ($C_2O_4^{2-}$) is either the dominant anating reactant or reacts at a much faster rate than the monodeprotonated form ($HC_2O_4^-$). In the pH range of study the participation of the monohydroxy form of the complex as a reactant is also likely. As such it is necessary to try fitting the acid dependence to various rate laws which account for the involvement or exclusion of the diferent species.The first and simplest one to consider was a plot of the slope (k_f) against $1/[H^+]$. Such a plot is curved and the subsequent plot of $1/k_f$ *versus* $[H^+]$ was also found to be curved. Representative plots are shown in Figures 2.19(a) and 2.19(b), respectively. It therefore follows that the rate law was of a much more complicated form and not that corresponding to just a simple reaction between the fully protonated form of the complex and the dianion, $C_2O_4^{2-}$ as might be envisaged from the acid dependence.

Another attempted fit involved the participation of both oxalate species, the monoanion ($HC_2O_4^-$) and the dianion ($C_2O_4^{2-}$) with the

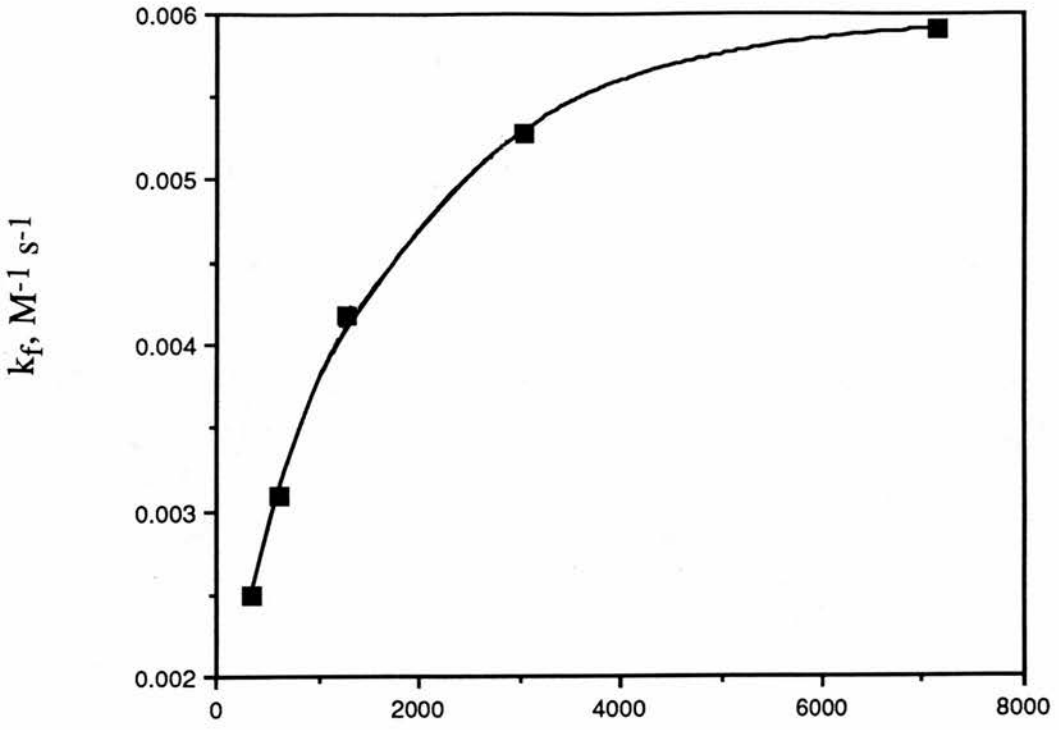

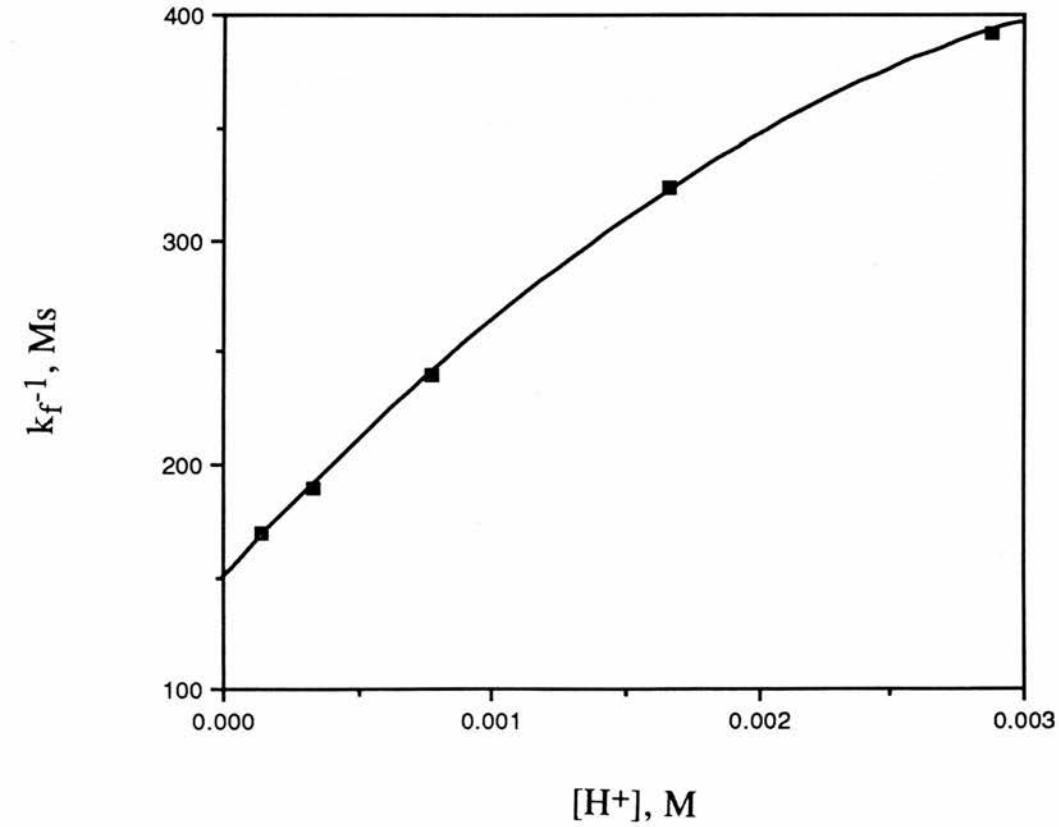

Figure 2.19: (a) Variation of k_f (55 °C) , for the oxalate and $[Mo_3O_2(OAc)_6(H_2O)_3]^{2+}$ formation step, with $[H^+]^{-1}$ at I=1.0 M ($NaCF_3SO_3$). (b) Plot of k_f^{-1} *versus* $[H^+]$ for the same reaction and conditions as in Figure 2.19(a).

triaqua form of the complex. The derived rate law is shown in equation (2.21). By rearranging this equation i nto the linear form of equation

$$k_f = \frac{k_1[H^+] + k_2K_2}{[H^+] + K_2} \qquad (2.21)$$

$$k_f([H^+] + K_2) = k_1[H^+] + k_2K_2 \qquad (2.22)$$

(2.22), a plot of $k_f([H^+] + K_2)$ *versus* $[H^+]$ should give a straight line with slope k_1 and intercept k_2K_2. This plot is shown in Fig. 2.20 and again curvature

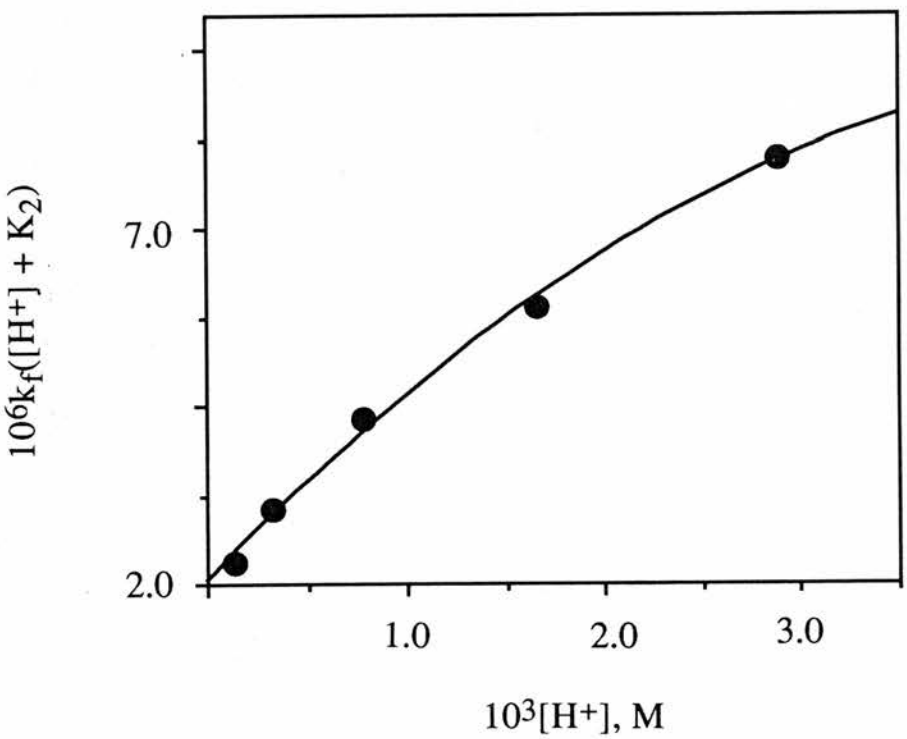

Figure 2.20 : Plot of $k_f([H^+] + K_2)$ *versus* $[H^+]$ for the reaction between $[Mo_3O_2(OAc)_6(H_2O)_3]^{2+}$ and oxalate at 55 °C, I =1.0 M (CF_3SO_3Na).

was obtained. It then became apparent that the monohydroxy form of the trimer might be playing a role in the reaction. It is recognised that between pH 2-4 appreciable amounts of the monohydroxy form of the complex would be present (estimated pK_a~4) and as such a rate law was derived on the basis that the deprotonated form was the reacting species. The proposed rate law is shown in equation 2.23.

$$k_f = \frac{k_{ox}[H^+]K_{AM}}{([H^+] + K_{AM})([H^+] + K_2)} \qquad (2.23)$$

This rate law was derived assuming the reaction is between the monohydroxy form of the complex and the monoanion ($HC_2O_4^-$) or between the triaqua form of the complex and the dianion ($C_2O_4^{2-}$). In any case if such a rate law is relevant plotting a graph of $k_f([H^+] + K_{AM})([H^+] + K_2)$ against $[H^+]$ should give a straight line passing through the origin and with slope equal to $k_{ox}K_{AM}$ if the former situation is relevant. The same plot would also be applicable if the fully protonated form of the trimer and $C_2O_4^{2-}$ are the reacting species but now with slope $k_{ox}K_2$. However, such a plot was found to be noticeably curved (Figure 2.21) thus eliminating either of these reactions as the only pathways. The appearance of Figure 2.21 suggests that a term in $[H^+]^2$ may be involved. With this in mind other rate laws were investigated assuming the triaqua form of the complex to be the reacting species with both $HC_2O_4^-$ and $C_2O_4^{2-}$. The derived rate law for this situation is shown below (see Appendix 3 for full derivation)

$$k_f = \frac{k_1[H^+]^2 + k_2K_2[H^+]}{([H^+] + K_{AM})([H^+] + K_2)} \qquad (2.24)$$

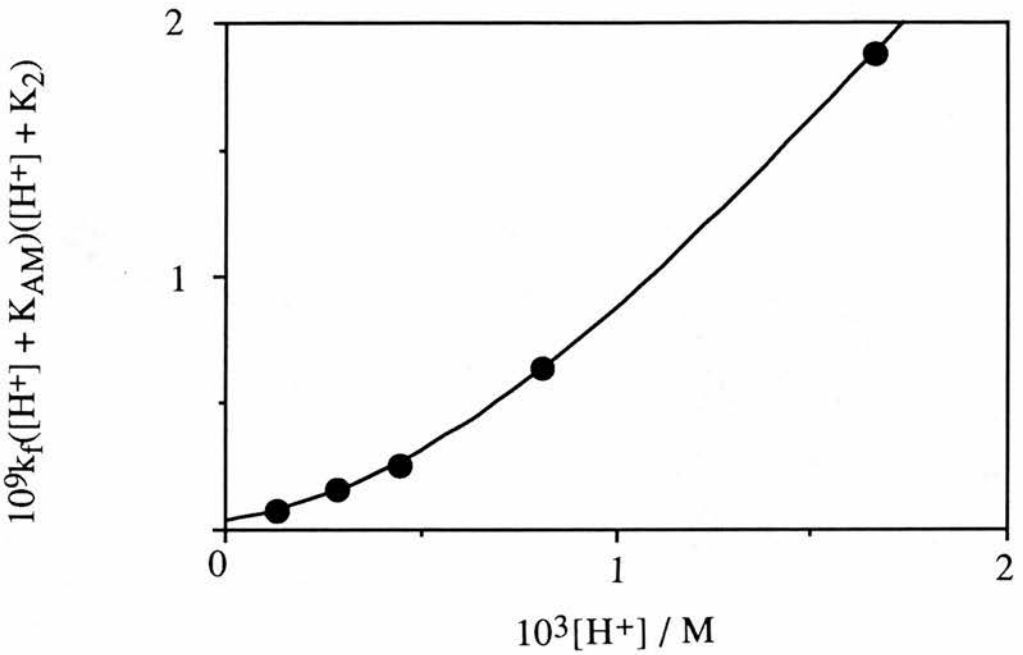

Figure 2.21 : Plot of $k_f([H^+] + K_{AM})([H^+] + K_2)$ *versus* $[H^+]$ for the reaction of oxalate with $[Mo_3O_2(OAc)_6(H_2O)_3]^{2+}$, T = 40 °C and I=1.0 M (CF_3SO_3Na).

This rate law was derived from the following reaction scheme:

$$HC_2O_4^- \underset{}{\overset{K_2}{\rightleftharpoons}} C_2O_4^{2-} + H^+ \qquad (2.25)$$

$$Mo_3^{2+} \overset{K_{AM}}{\rightleftharpoons} Mo_3OH^+ + H^+ \qquad (2.26)$$

$$\begin{array}{ccc} Mo_3^{2+} + HC_2O_4^- & \overset{k_1}{\underset{k_{-1}}{\rightleftharpoons}} & Mo_3C_2O_4H^+ \\ K_2 \uparrow\downarrow & & \uparrow\downarrow K_{AMOX} \\ Mo_3^{2+} + C_2O_4^{2-} & \overset{k_2}{\underset{k_{-2}}{\rightleftharpoons}} & Mo_3C_2O_4 \end{array} \qquad (2.27)\ (2.28)$$

($[Mo_3O_2(OAc)_6(H_2O)_3]^{2+}$ written as Mo_3^{2+} for the sake of simplicity)

Scheme 2.2

Eqn. (2.24) can be rearranged into the linear form of equation (2.29)

$$\frac{k_f([H^+] + K_{AM})([H^+] + K_2)}{[H^+]} = k_1[H^+] + k_2K_2 \qquad (2.29)$$

From this equation a plot of $k_f([H^+] + K_{AM})([H^+] + K_2)/[H^+]$ *versus* $[H^+]$ should give a straight line with slope k_1 and an intercept of k_2K_2. These plots at three temperatures are shown in Fig. 2.22 and are indeed

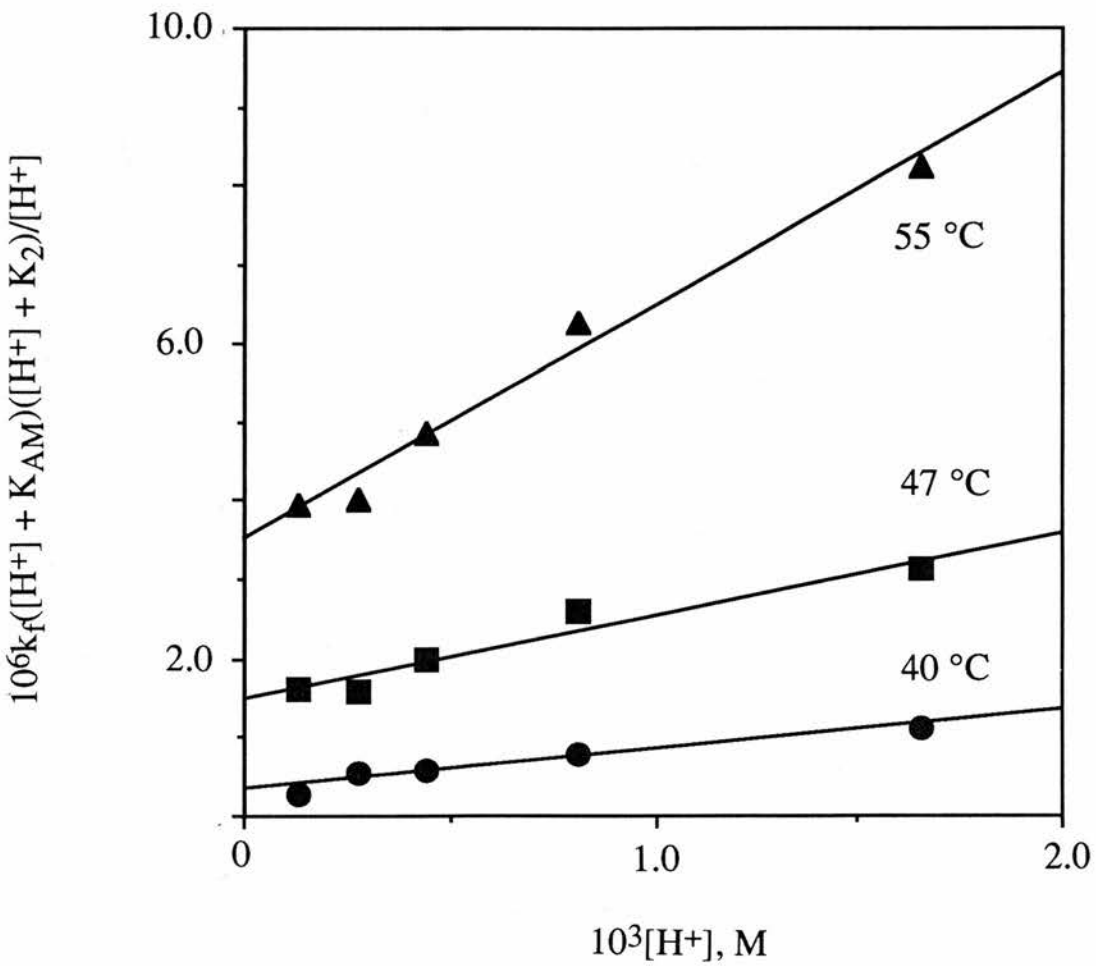

Figure 2.22 : Graph of $k_f([H^+] + K_{AM})([H^+] + K_2)/[H^+]$ *versus* $[H^+]$ at different temperatures for the reaction of $[Mo_3O_2(OAc)_6(H_2O)_3]^{2+}$ with oxalate.

satisfactorily linear, thus verifying the derived rate expression. The values of k_1 and k_2 obtained at three temperatures are listed in Table 2.8 together with the appropriate activation parameters. Values of K_2 at each temperature were calculated from the $\Delta H_2°$ and $\Delta S_2°$ values (page 108).

Table 2.8: Kinetic Parameters for the Reaction Between $[Mo_3O_2(OAc)_6(H_2O)_3]^{2+}$ and Oxalate in Aqueous Solution.

Temp./ °C	$10^4\, k_1$/ $M^{-1}s^{-1}$	$10^3\, k_2$/ $M^{-1}s^{-1}$	$10^4 K_2$ / M
40.0	4.08	1.67	2.61
47.0	7.95	5.36	2.54
55.0	16.29	14.47	2.45

$\Delta H_1^{\neq} = 76.2 \pm 0.3$ kJ mol^{-1}; $\Delta H_2^{\neq} = 120.0 \pm 8.6$ kJ mol^{-1}

$\Delta S_1^{\neq} = -67.0 \pm 0.9$ J K^{-1} mol^{-1}; $\Delta S_2^{\neq} = +85.0 \pm 26.8$ $JK^{-1}mol^{-1}$

From the proposed reaction scheme, the rate law (2.30) for the back reaction (aquation) can be derived from equations (2.27) and (2.28):

$$k_b = \frac{k_{-1}[H^+] + k_{-2}K_{AMOX}}{[H^+] + K_{AMOX}} \qquad (2.30)$$

This equation can be rearranged into the linear form of equation (2.31).

$$k_b([H^+] + K_{AMOX}) = k_{-1}[H^+] + k_{-2}K_{AMOX} \qquad (2.31)$$

From equation (2.31) a plot of $k_b([H^+] + K_{AMOX})$ *versus* $[H^+]$ should give a straight line of slope k_{-1} and intercept $k_{-2}K_{AMOX}$. However to make such a plot it is necessary to estimate a value for K_{AMOX}. It is

expected that pK_{AMOX} should not be very different from the second pK_a of oxalic acid, K_2, if anything greater due to the effect of the metal centre which might cause increased polarisation of the oxalate ligand. Using a value for K_{AMOX} of 4 x 10^{-4} M, one can achieve satisfactory fits to the experimental data, as shown in Figure 2.23. The derived rate

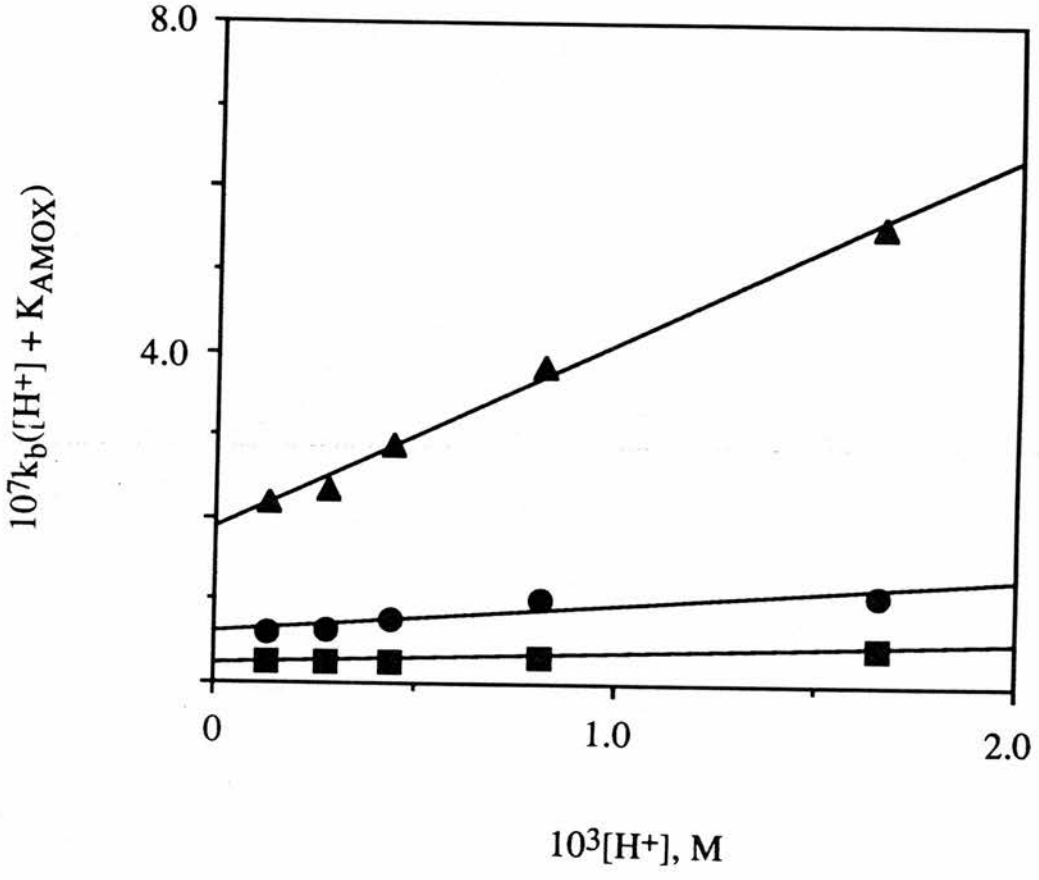

Figure 2.23: Plot of $k_b([H^+] + K_{AMOX})$ *versus* $[H^+]$ for the aquation of the $[Mo_3O_2(OAc)_6(H_2O)_3]^{2+}$ and oxalate complex at I =1.0 M (CF_3SO_3Na).

constants, k_{-1} and k_{-2} together with the corresponding activation parameters are listed in Table 2.9.

Table 2.9: Kinetic Parameters for the Back Reaction (Aquation) of the $[Mo_3O_2(OAc)_6(H_2O)_3]^{2+}$ and Oxalate Complex in Aqueous Solution

Temperature / °C	10^4k_1/ s^{-1}	10^4k_2 / s^{-1}
40.0	0.14	0.53
47.0	0.25	1.41
55.0	1.22	4.86

$\Delta H_{-1}^{\neq}$ = 121.4 ± 30.0 kJ mol^{-1}; $\Delta H_{-2}^{\neq}$ = 123.7 ± 5.4 kJ mol-1

$\Delta S_{-1}^{\neq}$ = 48.0 ± 93.6 J K^{-1} mol^{-1}; $\Delta S_{-2}^{\neq}$ = 67.5 ± 16.8 J K^{-1} mol-1

2.3.3 Thiocyanate Anation of $[MoW_2O_2(OAc)_6(H_2O)_3]^{2+}$

2.3.3.1 Dependence on [SCN^-]

The dependence of the anation rate constant (k_{obs}) on the thiocyanate concentration was investigated in a set of runs with [NCS^-] in very large excess (>>10-fold) over the complex. As in the case of the homonuclear Mo_3 species a high concentration of the incoming ligand (up to 1.0 M) and high temperature were necessary in order to speed up the rate of substitution. The gradual formation of the thiocyanate species is shown in Figure 2.24. The spectral scans show that the λ_{max} at 475 nm decreases gradually with time while the other λ_{max} at 390 nm increases with time. There is strong absorption below 400 nm which is characteristic for these systems and is probably due to NCS^- ---> M_3^{4+} charge transfer. Under the conditions of this study a linear first-order dependence of k_{obs} on [NCS^-] was found passing through an intercept. This behaviour can be represented by equation (2.32)

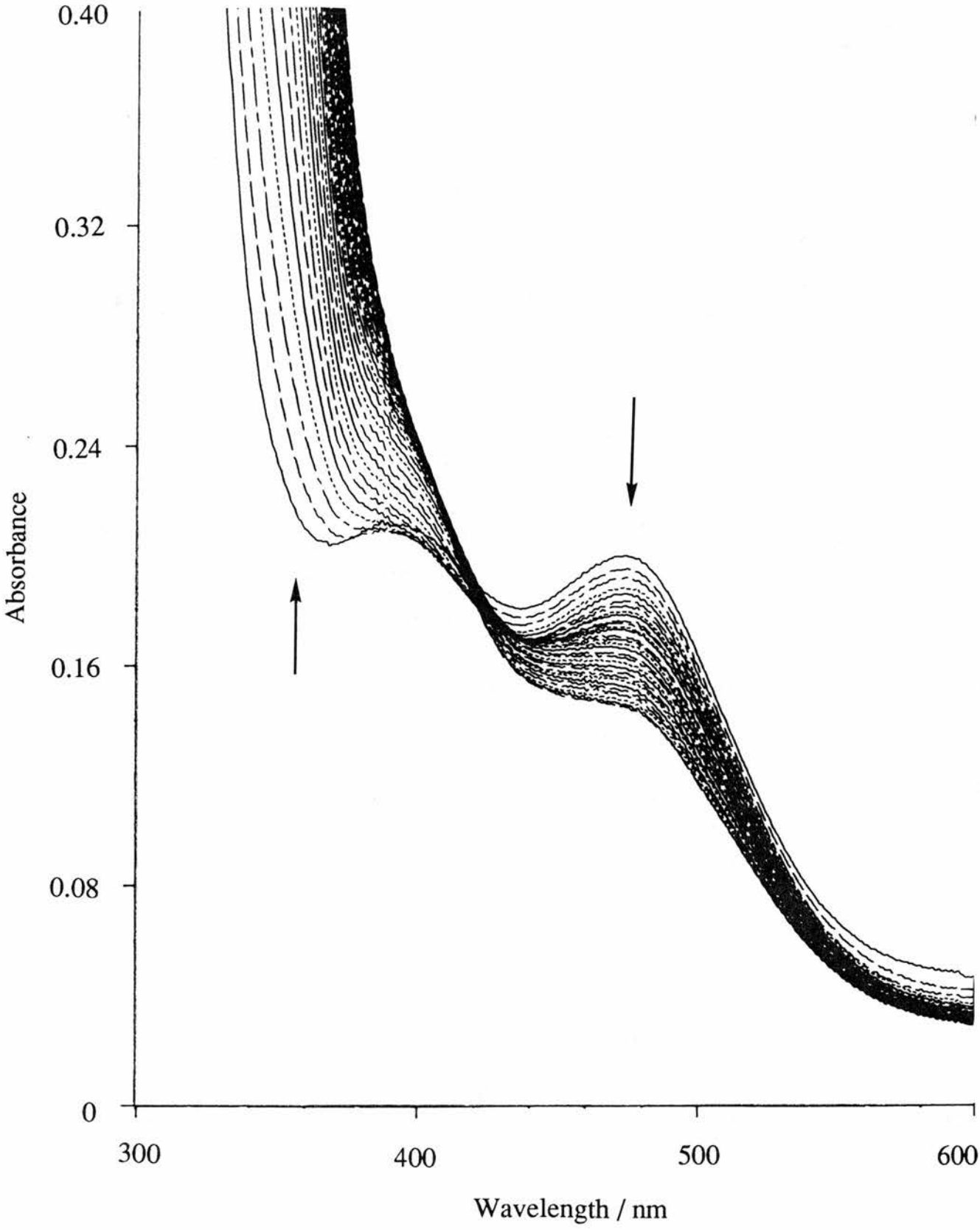

Figure 2.24: Repetitive scan at 30 min. intervals for the reaction between $[MoW_2O_2(OAc)_6(H_2O)_3]^{2+}$ (~ 2 x 10^{-4} M) and SCN^- (0.95 M) at 50 °C under air free conditions, I= 1.0 M (CF_3SO_3Na).

$$k_{obs} = k_f[NCS^-] + k_b \qquad (2.32)$$

This means that equilibrium kinetics are relevant for this process. The results obtained at 55 °C are displayed in Table 2.10 and graphically illustrated as a plot of k_{obs} *versus* [SCN^-] in Figure 2.25. This behaviour is rather different to that observed in the case of the homonuclear Mo_3 species in which a similar plot to Figure 2.25 (see Figure 2.13) indicated saturation kinetics with the curve passing through the origin. It is not clear at this stage why the mixed-metal species should behave differently from the homonuclear Mo_3 cluster. Values of k_f and k_b obtained for the MoW_2 cluster at 55 °C are respectively; 9.4 x 10^{-5} $M^{-1}s^{-1}$ and 4 x 10^{-5} s^{-1}. Values of k_f are presumed made up of the usual composite term, kK_{IP}, where K_{IP}, the ion-pair association constant for NCS^- appears to be much smaller than in the case of Mo_3 cluster.

Table 2.10: Pseudo-First Order Rate Constants for SCN^- Anation of $[MoW_2O_2(OAc)_6(H_2O)_3]^{2+}$, pH ~2.0, T= 55 °C, λ_{max} = 370 nm, I =1.0 M ($NaCF_3SO_3$).

[SCN^-] /M	$10^5k_{obs}/s^{-1}$
0.20	5.35
0.40	8.03
0.60	9.10
0.80	11.02
1.00	13.40

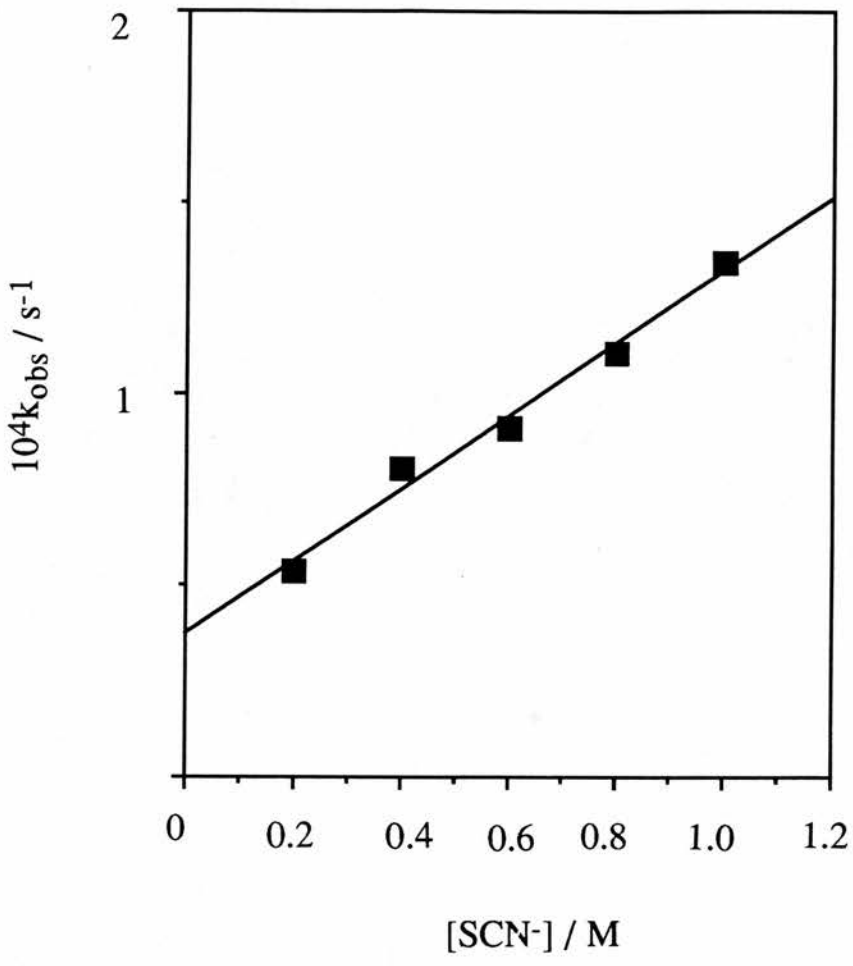

Figure 2.25: Plot of k_{obs} *versus* [SCN^-] for the reaction between SCN^- and $[MoW_2O_2(OAc)_6(H_2O)_3]^{2+}$; conditions as in Table 2.10

It is worth emphasising that under the conditions of this study only one stage was observed for the reaction, presumably corresponding to susbstitution of the H_2O at the single molybdenum centre. This is in accordance with fairly well behaved infinity readings (small but noticeable decrease in absorbance readings were however observed with time) and the absorbance *versus* time data were satisfactorily fitted to a single exponential curve. It is expected that substitution at the tungsten atoms is also possible but apparently this requires more forcing conditions (*e.g.* higher temperature) might be necessary (*cf* substitution studies on $[W_3O_2(OAc)_6(OH_2)_3]^{2+}$ to follow and water exchange studies

on the $[MoW_2O_2(OAc)_6(OH_2)_3]^{2+}$ later.

One thing that is clear from these studies is that substitution of H_2O at the molybdenum site in the mixed-metal complex is approximately an order of magnitude slower for substitution of H_2O in the homonuclear Mo_3 cluster after allowance for statistical factors. It is believed that this behaviour is due to effective electron donation from tungsten to molybdenum introducing more 'd_3' behaviour at the molybdenum centre (see discussion).

2.3.4 Oxalate Anation of $[W_3O_2(OAc)_6(H_2O)_3]^{2+}$

2.3.4.1 Dependence on Total Oxalate Concentration

A series of runs studying the dependence of the anation rate constants on $[oxalate]_T$ for the bicapped tungsten trimer was made at a fixed pH. Unlike the Mo_3/oxalate study no pH variation was made in this study. The oxalate concentration was varied from 0.01-0.05 M but still in large excess over the complex concentration. A gradual change to the original spectrum of the triaqua complex was observed with significant absorbance changes below 400 nm. A family of spectra (Figure 2.26) collected during the course of the reaction of the complex with 0.01M oxalate reveals the overall sequence of the reaction. The peak a 450 nm shows a small shift to higher wavelengths as in the corresponding reaction of the molybdenum trimer with oxalate. This small shift in λ_{max} is consistent with what would be expected for replacement of O-bonded water by O-bonded oxalate. The shift of the λ_{max} to higher wavelengths corresponding to the formation of the

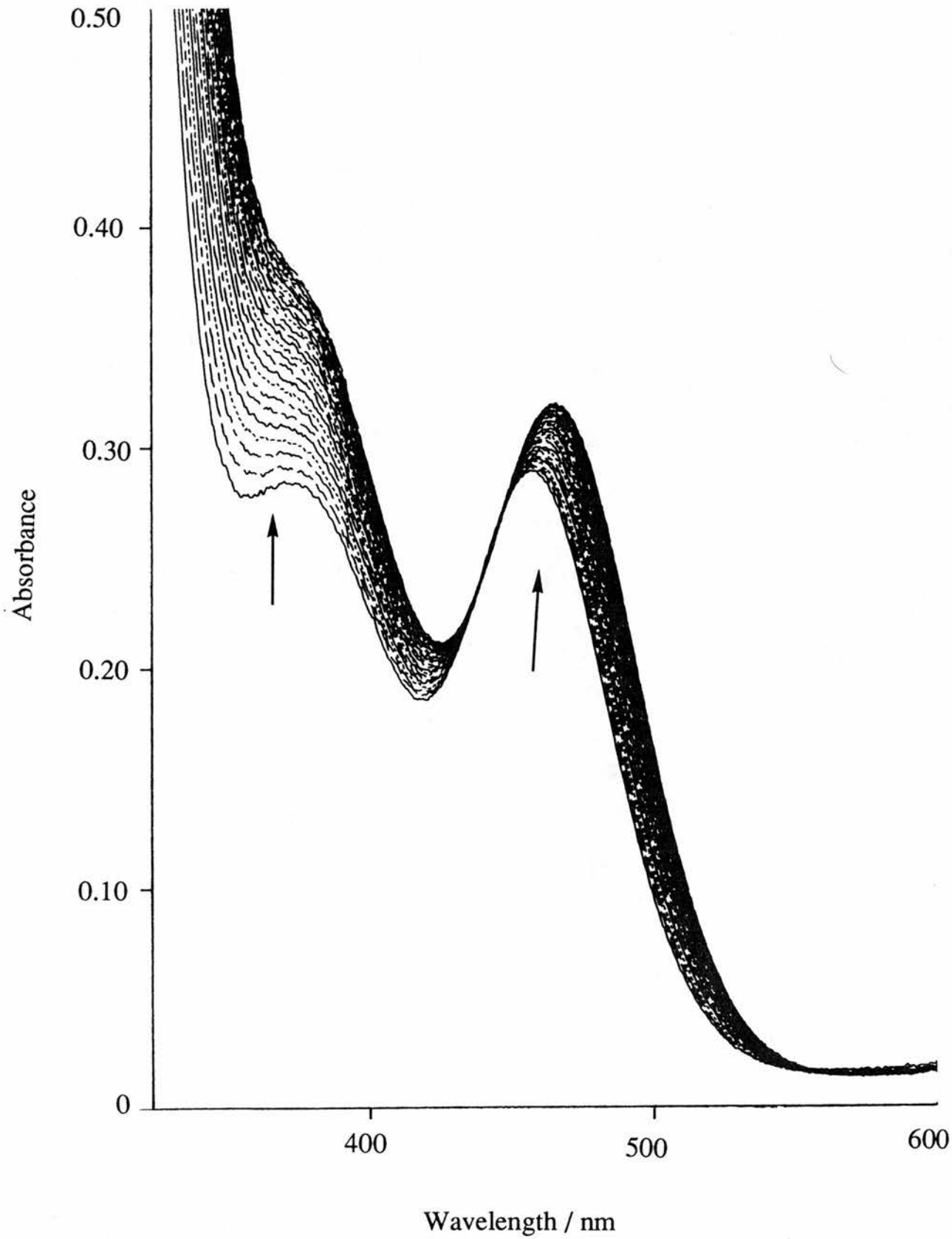

Figure 2.26: Spectral changes during the reaction of $[W_3O_2(OAc)_6(H_2O)_3]^{2+}$ in oxalate solution under air free conditions. [Complex] ~ 1.5 x 10^{-4} M at 55 °C, scanning interval = 60 min., pH ~ 4.0.

oxalato species is also consistent with the position of oxalate in relation to H_2O in the spectrochemical series. In contrast the absorbance at the 350 nm λ_{max} increase more strongly with the formation of a shoulder, but again only a slight shift in λ_{max} is observed.

Due to the long reaction times required to reach infinity the absorbance values at infinite time (A_∞) were estimated by the Swinbourne method. The k_{obs} values were subsequently computed from $\ln(A_\infty - A_t)$ *versus* time plots which produced linear plots up to at least three half-lives. The first-order rate constants (k_{obs}) are listed in Table 2.11 as a function of oxalate concentration and the corresponding plot of k_{obs} *versus* $[Ox]_T$ is displayed in Figure 2.27 assuming as before

Table 2.11: Observed Rate Constants for the Reaction of $[W_3O_2(OAc)_6(H_2O)_3]^{2+}$ with Oxalate Under the Following Conditions: [Complex] = 4×10^{-4} M, pH = 3.83, T = 55 °C and I = 1.0 M ($NaCF_3SO_3$)

$[Ox]_T$ / M	$10^5\ k_{obs}/s^{-1}$
0.01	1.06
0.02	1.18
0.03	1.28
0.04	1.34
0.05	1.44

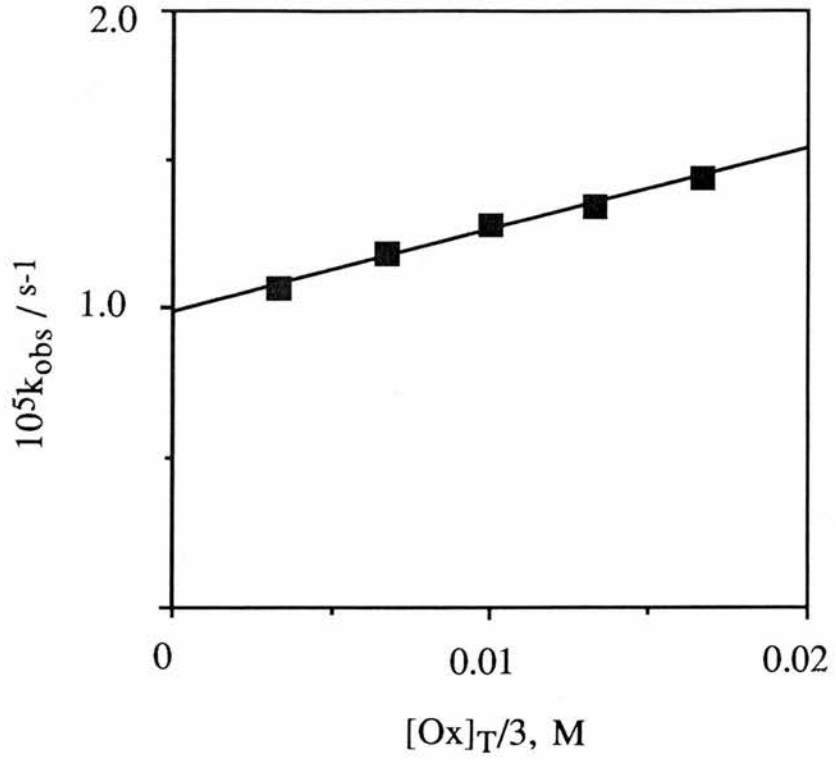

Figure 2.27: Plot of k_{obs} against $[Ox]_T$ for the reaction between $[W_3O_2(OAc)_6(H_2O)_3]^{2+}$ and oxalate; conditions as in Table 2.11.

a statistical factor of three. As evident from the plot, equilibrium kinetics are in operation as in the analogous molybdenum reaction and can be represented by equation (2.33). Likewise as in the case of the moly-

$$k_{obs} = k_f[Ox]_T + k_b \qquad (2.33)$$

bdenum study there is no evidence of saturation behaviour under the conditions used in these studies; presumably higher concentrations of oxalate are required to see such behaviour. Although a full kinetics study was not conducted on this system it is nevertheless clear that the bicapped tungsten complex is much more inert to substitution than the molybdenum analogue, consistent with the typical behaviour of the two elements. A comparision of the forward rates (k_f) for the two reactions

under similar conditions has revealed that substitution at tungsten occurs approximately 40 times slower than at molybdenum. Values of k_f and k_b determined at 55 °C for reaction of oxalate with the tritungsten complex are respectively; (2.76 ± 0.17) x 10^{-4} $M^{-1}s^{-1}$ and (9.84 ± 0.19) x 10^{-6} s^{-1}.

2.3.5 Thiocyanate Anation studies on $[W_3O(OAc)_6(H_2O)_3]^{2+}$

The $[W_3O(OAc)_6(H_2O)_3]^{2+}$ complex has only one capping group and a different oxidation state from the bicapped species, $[M_3O_2(OAc)_6(H_2O)^{2+}]$ (M= Mo_3, W_3, Mo_2W, MoW_2) and as such offers a chance to probe the effect of the capping group and of the different oxidation states on the reactivity of these species. Ideally more useful comparative information could be gained by studying a series of related species with different capping groups such as $-CCH_3$, but unfortunately time prevented such a study to be made.

Thiocyanate was chosen as the incoming anating ligand to enable a direct comparison with the bicapped Mo_3 and MoW_2 cluster complexes. The kinetic runs were conducted at 0.01 M H^+ using a large excess of SCN^- (>> 10-fold excess) over the complex at 50 °C. Typical scan spectra for a run at 0.2 M SCN^- is shown in Figure 2.28. Rate constants (k_{obs}) were obtained by studying the absorbance change at 400 nm with time with SCN^- varied between 0.2 and 0.95 M. Values of k_{obs} were found to obey eqn. (2.34)

$$k_{obs} = k_1 \frac{[NCS^-]}{3} \qquad (2.34)$$

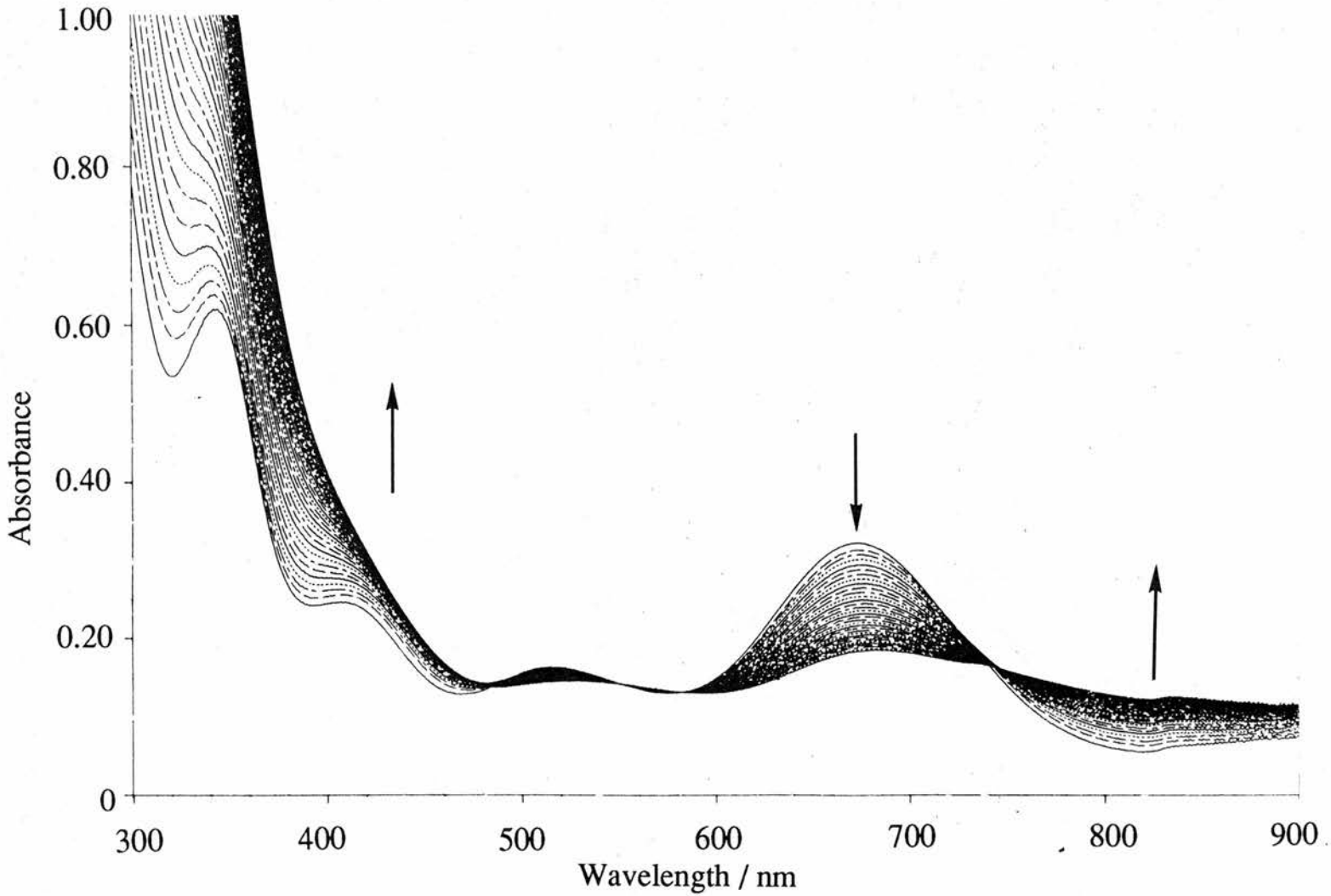

Figure 2.28: Spectral changes during the reaction between SCN^- and $[W_3O(OAc)_6(H_2O)_3]^{2+}$ under air free conditions at 50 °C, [complex] = 2.5×10^{-4} M, $[SCN^-]$ = 0.20 M, pH ~ 2.0, time interval = 30 min., I= 1.0 M (CF_3SO_3Na).

showing a linear dependence (Fig. 2.29) passing through or discernably near to the origin (no saturation or equilibrium kinetics). At 50 °C k_1 had the value ~2.4 x 10^{-4} $M^{-1}s^{-1}$.

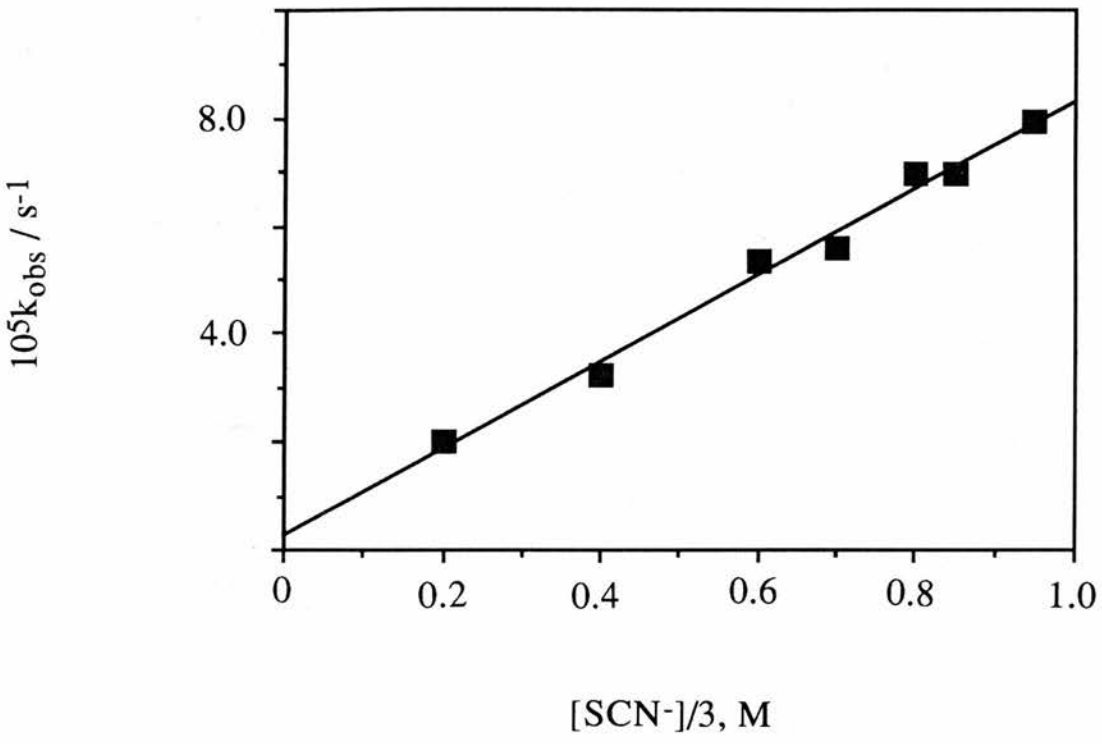

Figure 2.29: Plot of k_{obs} *vs* [SCN^-]/3 for the reaction of SCN^- with $[W_3O(OAc)_6(OH_2)_3]^{2+}$ (1 x 10^{-4} M) and SCN^-, T = 50 °C, I = 1.0 M ($NaCF_3SO_3$).

The large absorbance changes occurring below 400 nm are believed due to the development of intense charge-transfer bands in the UV-visible region as observed on the other trimetal aqua complexes. A series of isosbestic points is apparent from Fig. 2.28 occurring at ~745 nm, ~580 nm, ~550 nm and ~480 nm which ultimately become lost in the latter stages of the reaction due presumably to decomposition of the thiocyanato complex on prolonged heating.

The question may arise within this mixed-valence W(III, III, IV) as to at which tungsten centre, W(III) or W(IV) is substitution occurring. It is likely that on such a slow time scale electronic equivalence between the tungsten centres has occurred through rapid electron transfer and as a result a statistical factor of three should be relevant as assumed in Fig. 2.29 and in the calculation of k_1. Such a situation would be consistent with the uniphasic first order kinetics found for this system consistent with substitution at one of three identical and independent tungsten sites. The absence of a second stage due to further SCN^- complexation reaction is also intriguing and could be due to a loss of the three-fold equivalence within the 1:1 NCS^- complex leading to promotion of a valence-localised structure. Marked changes to the electronic spectrum of the $[W_3O(OAc)_6(OH_2)_3]^{2+}$ complex in the visible / near infra-red region are observed upon initial SCN^- complexation (Fig. 2.28). However, further experiment would be required to substantiate the possible change to a more localised valence-trapped system.

Water Exchange

Variable temperature H_2O-exchange studies have been conducted on the trinuclear, carboxylate complexes $[M_3(\mu_3\text{-}O)_2(\mu\text{-}OAc)_6\text{-}(H_2O)_3]^{2+}$(M = Mo, W) and $[W_3(\mu_3\text{-}O)(\mu\text{-}OAc)_6(H_2O)_3]^{2+}$. Water exchange studies have also been carried out on the mixed-metal complex, $[MoW_2(\mu_3\text{-}O)_2(\mu\text{-}OAc)_6(H_2O)_3]^{2+}$ at 50 °C in order to determine the rate of exchange of the H_2O at the molybdenum centre and at 70 °C to obtain the rate of exchange of H_2O at the tungsten centres, as described in the experimental section. A summary of the water exchange rate constants (k_{ex}) is given in Table 2.12 together with

the activation parameters for the relevant ions. An Eyring plot of the water exchange of $[Mo_3(\mu_3\text{-}O)_2(\mu\text{-}OAc)_6(H_2O)_3]^{2+}$ is presented in Figure 2.30.

Table 2.12: A Summary of the Kinetic Parameters Obtained for the Water Exchange Reactions of the Trinuclear Carboxylate Complexes, $[M_3(\mu_3\text{-}O)_2(\mu\text{-}OAc)_6(H_2O)_3]^{2+}$ (M = Mo_3, W and MoW_2) and $[W_3(\mu_3\text{-}O)(\mu\text{-}OAc)_6(H_2O)_3]^{2+}$.

Complex	T / °C	$10^4k_{ex}/s^{-1}$	$\Delta H^{\neq}$ /kJ mol^{-1}	$\Delta S^{\neq}$ / J K^{-1} mol^{-1}
Mo_3	37.0	0.38 ± 0.04	125.85 ± 9.62	76.58 ± 30.03
	43.5	1.14 ± 0.21		
	50.0	3.77 ± 0.30		
	59.0	9.84 ± 0.51		
W_3	53.5	0.09 ± 0.01	58.30 ± 8.39	-164.3 ± 24.9
	64.5	0.16 ± 0.01		
	76.0	0.38 ± 0.01		
MoW_2*	50.0	2.13 ± 0.35		
	76.0	0.31 ± 0.23		
W_3	15	2.46 ± 0.12	51.31 ± 2.94	-135.5 ± 9.9
(monocapped)	25	5.54 ± 0.36		
	33	9.15 ± 0.94		

* value at 50 °C corresponds to exchange of H_2O at the Mo centre and the value at 76 °C correponds to exchange of H_2O at the W atom

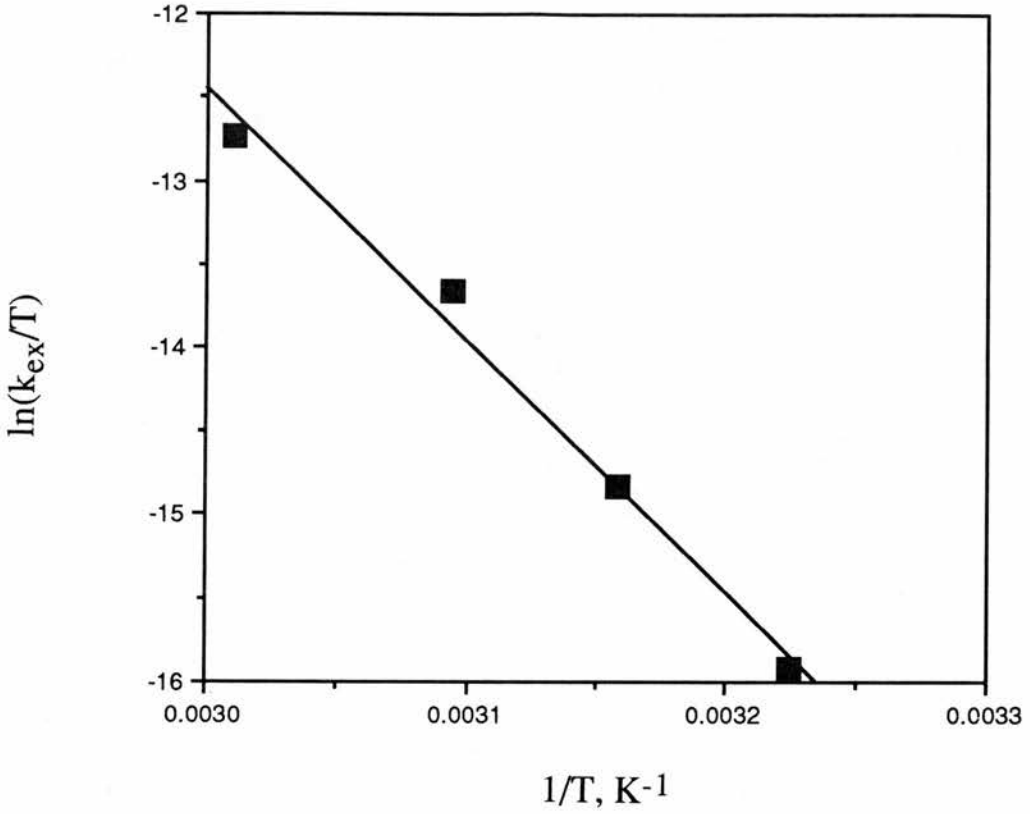

Figure 2.30: Eyring plot for the water exchange reaction of $[M_3(\mu_3\text{-}O)_2(\mu\text{-}OAc)_6(H_2O)_3]^{2+}$

2.4 DISCUSSION

2.4.1 $[Mo_3O_2(OAc)_6(OH_2)_3]^{2+}$

With regard to the NCS^- anation two distinct stages were observed consistent with a stepwise substitution of two H_2O ligands. For the first stage saturation behaviour is observed which has been successfully assigned to an ion-pair preassociation step prior to interchange of H_2O and SCN^- ligands. Ion-pair constants were found to be in the range expected for 2+ and 1- reactants at ionic strength 1.0 M. Activation parameters for the interchange step show large positive $\Delta H^{\neq}$ (141 kJ mol^{-1}) and $\Delta S^{\neq}$ (+ 131 J K^{-1} mol^{-1}) implying the existence of a dissociative mechanism. Support for this is also apparent from measurement of the water exchange rate constant which has a value (25

°C) of 5.6 x 10^{-6} s^{-1} comparable to that of the SCN^- interchange step (25 °C) (9.4 x 10^{-6} s^{-1}) and in which large and positive $\Delta H^{\neq}$ (+ 126 kJ mol^{-1}) and $\Delta S^{\neq}$ (+77 J K^{-1} mol^{-1}) values are also obtained.

These rate constants are many orders of magnitude smaller (x 10^6) than corresponding rate constants for SCN^- substitution and water exchange on the ion $[Mo_3O_4(OH_2)_9]^{4+}$.[48,49] This finding provides further support for the dominating conjugate-base assigned mechanism for substitution at the incomplete cubane $M_3X_4^{4+}$ (X = O, S) cluster ions involving *cis*-labilisation by an adjacent deprotonated water rather than the alternative mechanism involving charge reduction at the Mo centre. An additional factor in the present case would be the considerably greater steric hindrance to approach of the incoming ligand due to the position of the acetate groups (Fig. 2.31) which, when

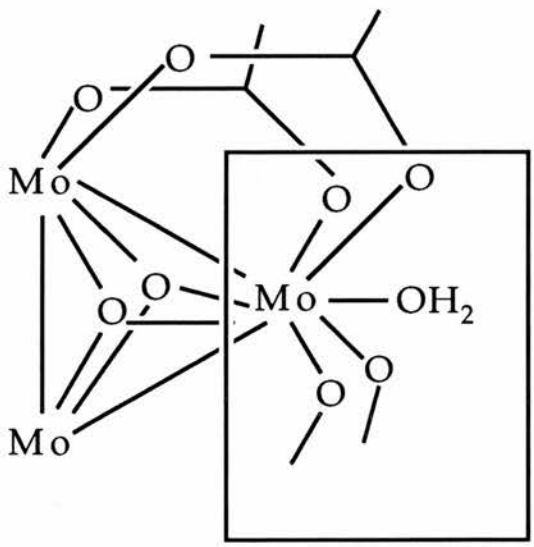

Fig. 2.31: Structure of the $[Mo_3O_2(OAc)_6(OH_2)_3]^{2+}$ ion showing the high coordination number at a Mo atom.

coupled with the high apparent coordination number of 9 at

molybdenum, would tend to promote a mechanism dominated by Mo-OH_2 bond cleavage.

For the second stage (substitution of a second SCN^- ligand) there was no evidence of saturation behaviour (up to $[SCN^-] = 1.0$ M) implying a much smaller value for the relavant ion-pair constant for the 1+ / 1- reactants; presumed also responsible for the smaller rate constants observed (factor of 1/10). For each stage reactions were observed to proceed to completion indicating a high equilibrium constant for formation of the mono and bis thiocyanato complexes. The overall sequence of reactions is summarised below (scheme 2.3):

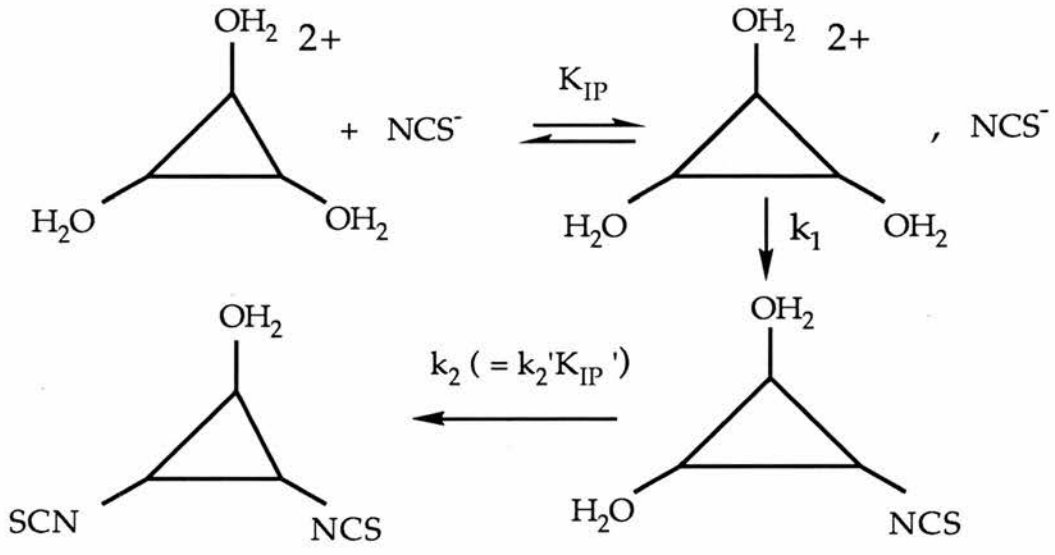

Scheme 2.3

Complexation of oxalate however appears to involve a somewhat different process wherein both $HC_2O_4^-$ and $C_2O_4^{2-}$ (both relevant to the pH range studied) are involved in an equilibrium reaction with the trimolybdenum aqua complex. Well characterised forward and back reactions are apparent with rate constants for each observed to increase

with increasing pH. The absence of saturation kinetics, which characterises the 1:1 complexation with SCN^-, is probably characteristic of the lower concentration range of oxalate available (only up to 0.05 M) owing to solubility problems at higher oxalate concentrations at I = 1.0 M.

The most striking feature of the complexation reaction however are the markedly differing activation parameters characterising the two paths. For the pathway involving $HC_2O_4^-$, the value of $\Delta H^{\neq}$ (76 kJ mol^{-1}) is noticeably smaller than the values characterising water exchange (126 kJ mol^{-1}) and SCN^- anation (141 kJ mol^{-1}) and together with the markedly nagative $\Delta S^{\neq}$ value (-67 J K^{-1} mol^{-1}) are reminiscent of the values obtained by van Eldik and Harris[50] characterising complexation by both $HC_2O_4^-$ and $H_2C_2O_4$ on $[Co(NH_3)_5(OH_2)]^{3+}$. Taube and co-workers[51] had earlier proposed a C-O bond breaking process as providing the dominant mechanism for acid catalysed aquation in $[Co(NH_3)_5(HC_2O_4)]^+$ and led van Eldik and Harris[50] to propose a similar process for the 'reverse' complexation reaction. Conceivably a similar process cannot be ruled out here wherein complexation by $HC_2O_4^-$ proceeds *via* a type of concerted process involving release of a water molecule *via* C-O(oxalate) bond breakage rather than Mo-$O(OH_2)$ bond breakage. Such a possible mechanism is illustrated below.

Rate parameters for a number of oxalate complexation reactions with aqua metal ions are collected in Table 2.13 together with parameters for water exchange necessitating M-OH_2 bond cleavage. In the case of $[Mo_3O_2(OAc)_6(OH_2)_3]^{2+}$, rate constants (25 °C) for water exchange are comparable to those for C-O bond breakage making mechanistic distinctions difficult on the basis of rate data alone. It should also be borne in mind that in calculatuing rate constants for both the SCN^- and oxalate reactions, a temperature independent value for

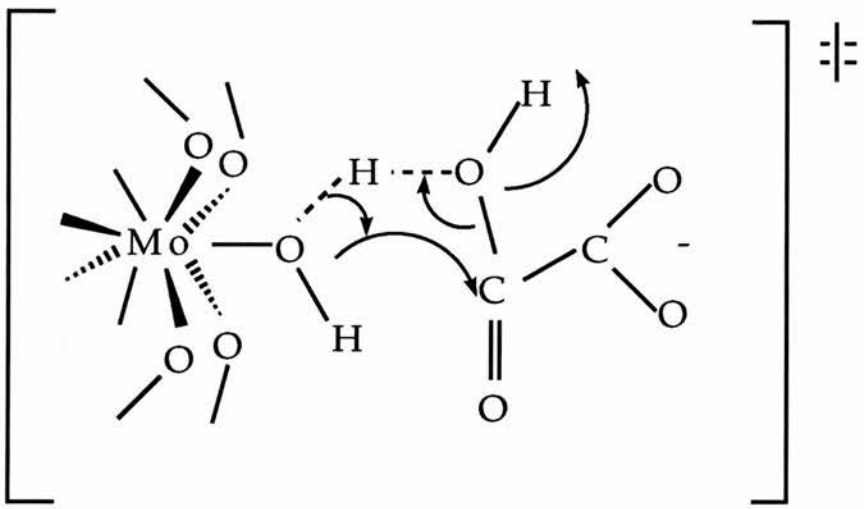

K_{AM} of 1 x 10^{-4} M was assumed. This is a reasonable assumption given the relatively temperature independent value for K_{AM} observed for the $[Mo_3O_4(OH_2)_9]^{4+}$ ion ($\Delta H_a°$ +3.9 kJ mol^{-1}) (Chapter 1).

Regarding apparent anation by the dianion, $C_2O_4^{2-}$ the situation is more difficult to evaluate owing to the so called 'proton ambiguity' problem. Conceivably the reactants here could be Mo-OH_2, $C_2O_4^{2-}$ or Mo-OH, $HC_2O_4^-$ or a combination of both; the similarity in acid dissociation constants (~ 10^{-4} M) rendering all four possible reactants equally relevant in the pH range studied (2.5 - 3.9). Consideration of sole involvement of Mo-OH_2 with $C_2O_4^{2-}$ gives an evaluated bimolecular rate constant (25 °C) of 1.64 x 10^{-4} $M^{-1}s^{-1}$ apparently well in excess of that obtained for water exchange and for anation by SCN^- (k_1 = 9.4 x 10^{-6} s^{-1}). Values of $\Delta H^{\neq}$ (120 kJ mol^{-1}) and $\Delta S^{\neq}$ (+85 J K^{-1} mol^{-1}) so determined are, on the other hand, rather similar to those obtained for water exchange in contrast to the pathway involving $HC_2O_4^-$. The bimolecular rate constant, 1.6 x 10^{-4} M^{-1} s^{-1}, according to Eigen and Wilkins[57], is however likely to be a composite term of the interchange rate constant and ion-pair association equilibrium constant and as such its value will also reflect the value of the ion-pair constant.

Such values for 2+ / 2- reactants are likely to be relatively large, perhaps as high as ~ 10 M^{-1}, implying an actual interchange rate constant for the dianion step of ~ 1.6 x 10^{-5} s^{-1} comparable now to the rate constant for water exchange and only twice that for SCN^- anation. A similar dissociative interchange mechanism is thus likely and cannot be ruled out.

Consideration of the other extreme situation requires knowledge of the temperature dependence of the acid dissociation constant for the trimolybdenum complex for which no data is available. A similar rigorous evaluation is thus not possible here. However, if a temperature independent value of 1 x 10^{-4} M is assumed for K_{AM}, then values of k_3 respectively at 40, 47 and 55 °C are: 4.37 x 10^{-3} $M^{-1}s^{-1}$, 13.60 x 10^{-3} $M^{-1}s^{-1}$ and 35.46 x 10^{-3} $M^{-1}s^{-1}$ giving rise to k_3 (25 °C) = 4.62 x 10^{-4} $M^{-1}s^{-1}$, $\Delta H^{\neq}$ = 116.4 ± 8.8 kJ mol^{-1} and $\Delta S^{\neq}$ = 81.4 ± 27.3 J K^{-1} mol^{-1}.

The increase in aquation rate for the presumed monodentate oxalate complex with pH is intriguing in that it implies a 'base-catalysed' process. Possibilities (shown Fig. 2.32) include attack of $H_2O(OH^-)$ either at the metal (reverse of $C_2O_4^{2-}$ path) or at the proximal carboxyl carbon polarised through metal coordination (reverse of $HC_2O_4^{2-}$ path). One would favour the second possibility given the likely steric hindrance at the metal and from the fact that a back reaction is uniquely observed in the case of the oxalate ligand. However rate constants and activation parameters (Table 2.13) for both reverse processes are comparable to those for water exchange at the triaqua complex and imply that attack at the metal is also a distinct possibility that cannot be ruled out.

Taube and co-workers[51] proposed C-O bond cleavage during acid-catalysed aquation of $[Co(NH_3)_5(HC_2O_4)]^{2+}$ (interestingly 'normal' Co-O bond cleavage is observed at higher pH's). Since then ^{18}O-label-

Table 2.13: Rate Parameters for Complexation of Oxalate Compared to Water Exchange on a Number of Aqua Metal Ions at 25 °C.

Complex		10^5k	$\Delta H^{\neq}$	$\Delta S^{\neq}$	Ref
		$M^{-1}s^{-1}$	kJ mol^{-1}	J K^{-1} mol^{-1}	
$[Mo_3O_2(OAc)_6(OH_2)_3]^{2+}$	$HC_2O_4^-$	8.94	76.2	-67.0	This work
	H_2O*	0.56	125.9	+76.6	This work
$[Co(NH_3)_5(OH_2)]^{3+}$	$HC_2O_4^-$	~1.0	93.7	-37.6	50
	$H_2C_2O_4$	~1.0	57.3	-150.6	50
	H_2O*	0.57	111	28	52
$[Rh(OH_2)_6]^{3+}$	$H_2C_2O_4$	1.21	76.7	-81.7	53
	H_2O*	0.00022	131.2	+29.3	54
$[Ir(OH_2)_6]^{3+}$	$H_2C_2O_4$	1.30	73.1	-94.0	55
	H_2O*	$\sim10^{-11}$	—	—	56

*units of s^{-1}

ling studies[58] of the base hydrolysis of *cis*-$[Co(en)_2(C_2O_4)]^+$ have demonstrated that C-O bond cleavage processes can also be relevant to alkaline solution. Similar O-isotope labelling studies would be relevant in the present case in order to confirm which precise mechanism is involved.

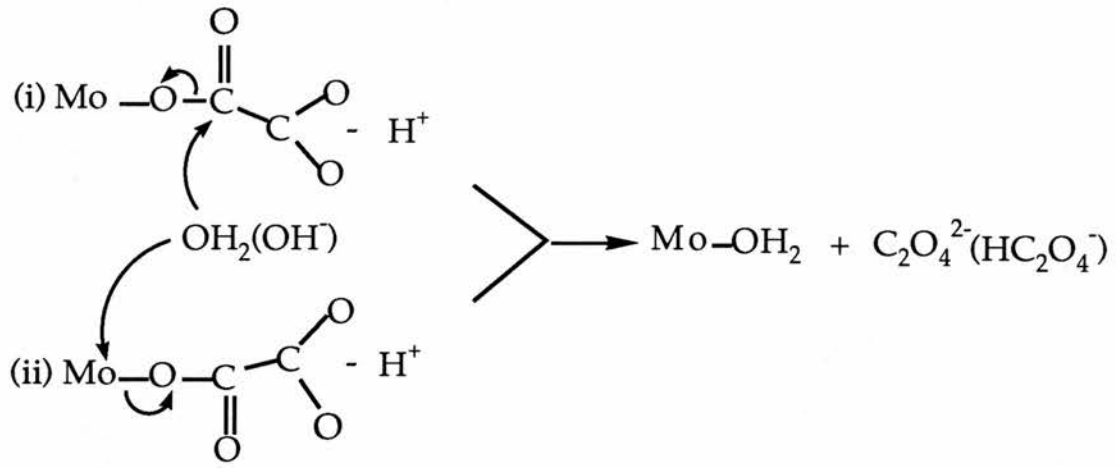

Fig. 2.32: Possible mechanisms involved in the aquation of $[Mo_3O_2(OAc)_6(OH_2)_2(C_2O_4H)]^+$.

2.4.2 $[MoW_2O_2(OAc)_6(OH_2)_3]^{2+}$

Kinetic studies with regard to substitution on this mixed Mo-W complex have allowed an opportunity to monitor the effect of substituting molybdenum atoms by tungsten in the bicapped cluster unit upon the substitution / exchange of water at molybdenum. The results show a distinct lowering in the rate constants for both water exchange and SCN^- substitution at molybdenum *versus* the trimolybdenum complex (allowance made for statistical factors). Water exchange rate constants (compared at 50 °C) are respectively 3.3×10^{-4} s^{-1} (Mo_3) and 2.1×10^{-4} s^{-1} (MoW_2). This trend is exactly mirrored in the SCN^- substitution bahaviour; rate constants here compared at 55 °C being respectively 18.6×10^{-4} s^{-1} (Mo_3) and 0.72×10^{-4} s^{-1} (MoW_2, assuming a similar K_{IP} value to Mo_3). These results imply that metal-metal interactions are important in affecting the substitution lability at a given metal centre in these complexes. Evidence from ^{95}Mo and ^{183}W NMR studies of a shift in electron density from W to Mo in these mixed metal species was mentioned earlier. Additional evidence has come from XPS

measurements[27] of the binding energies of Mo 3d, W 4d and W 4f electrons in these clusters which have shown a significant difference of 0.5 - 1 eV between values obtained for the Mo_2W and MoW_2 clusters *versus* those obtained for homometal Mo_3 and W_3 cluster (Table 2.14).

Table 2.14: Binding Energies (eV) of Molybdenum and Tungsten in the Trinuclear Carboxylate Clusters, $[M_3(\mu_3\text{-}O)_2(\mu\text{-}OAc)_6(H_2O)_3]^{2+}$ Determined by XPS.

Complex	Mo-$3d_{3/2}$	Mo-$3d_{5/2}$	W-$4f_{5/2}$	W-$4f_{7/2}$	W-$4d_{3/2}$	W-$4d_{5/2}$
Mo_3	234.1	231.1	-	-	-	-
Mo_2W	233.8	230.6	36.7	34.8	258.4	245.9
MoW_2	233.5	230.4	36.2	34.2	258.0	245.0
W_3	-	-	36.1	34.0	257.5	245.0

The greater inertness of the single Mo site in the MoW_2 cluster could be viewed as reflecting increased Mo(III) 'd_3' character as a consequence the shift in electron density from W to Mo.

Water exchange at tungsten in the MoW_2 complex was followed during a single run at 70 °C allowing comparison with the homotritungsten species to be described below. Rate constants here though were comparable, within experimental errors, (see Table 2.12) reflecting the almost identical binding energies (Table 2.14) of the W 4d and 4f electrons between the MoW_2 and W_3 clusters.

Finally, significantly lower rate constants (~ 60 %) were observed for substitution at molybdenum on the Mo-W cluster ion; $[Mo_2W(\mu_3\text{-}O)(\mu_2\text{-}O)_3(OH_2)_9]^{4+}$, *versus* the trimolybdenum analogue, correlating

with similar ^{95}Mo NMR evidence of an increase in electron density at molybdenum *versus* the trimolybdenum species (shift to lower field).

2.4.3 $[W_3O_2(OAc)_6(OH_2)_3]^{2+}$

Complexation of oxalate with this species was studied at a single temperature (55 °C) which nonetheless allows a direct comparison with a run performed on the trimolybdenum cluster under identical conditions. It is observed that rate constants for substitution on the tritungsten species are some 40 x smaller than those for the trimolybdenum analogue. Increased inertness at tungsten also characterises substitution reactions on the $[M_3X_4(OH_2)_9]^{4+}$ ions (M = Mo, W; X = O, S), a general phenomenon believed to relate to the so-called relativistic expansion effect[59] resulting in increased 5d participation and stronger W-W and W-OH_2 bonds. Whilst the lower rate for tungsten in the present case may also correlate with this general trend (the dissociative character of the $C_2O_4^{2-}$ path discussed earlier possibly responsible) such a supposition is however not consistent with the surprising rate parameters found for water exchange on the tritungsten complex (Table 2.12). Here, despite the slower rates (factor of 20 x) versus the trimolybdenum species, the values of $\Delta H^{\neq}$ (58.3 kJ mol^{-1}) and $\Delta S^{\neq}$ (-164.3 J K^{-1} mol^{-1}) appear to be rather more consistent with an 'associative' process. A consequence of this is that at 25 °C, water exchange rate constants for both the trimolybdenum and tritungsten complexes differ by only a factor of 5, with the values for the trimolybdenum complex rising sharply as the temperature is raised.

This remarkable apparent 'changeover' in mechanism, if genuine is unprecedented in magnitude between a second and third row element and all the more remarkable here given the closeness in molecular structure between the trimolybdenum and tritungsten species.

Independent verification of this will undoubtedly be required, for example, *via* measurements of the volumes of activation. One might suppose that the dissociative mechanism has become unfavourable for tungsten due to the remarkable strength of the W-OH_2 bonds and as such might allow the alternative associative mechanism to successfully compete. Furthermore the more 'expanded' empty 5d/5f orbitals on tungsten might help to facilitate attack by the incoming water molecule. Further conclusive evidence is required in order to verify these suppositions.

2.4.4 $[W_3O(OAc)_6(OH_2)_3]^{2+}$

Studies of substitution on this species allow an opportunity to compare the effect of a different formal valency at the metal (here W(III, III, IV) and the effect of only one μ_3-capping oxo group.

Of all the species studied in this work the mono(oxo)-capped W(III, III, IV) complex is by far the most labile which is intriguing in view of the earlier supposition of more inert behaviour for lower valent species. It might be concluded therefore that the lability of the complex is related to electronic effects arising from the presence of only one capping oxo group. The observation of uniphasic processes characterising both SCN^- substitution and water exchange suggests that the tungsten atoms are electronically equivalent in the triaqua complex but that electronic changes may occur (lack of evidence of successive SCN^- substitutions) following initial 1:1 SCN^- complexation as a result of loss of the three-fold symmetry. However, the most remarkable finding again relates to the measured rate parameters for water exchange: k(25 °C) 5.32 x 10^{-4} s^{-1}, $\Delta H^{\neq}$ 51.3 kJ mol^{-1}, $\Delta S^{\neq}$ -135.5 J K^{-1} mol^{-1} strongly suggestive, as with the bicapped tungsten complex (500 x slower), of an 'associative' process. Low $\Delta H^{\neq}$ and highly negative $\Delta S^{\neq}$

values appear to characterise exchange on both of the two tungsten complexes lending further support to a link with specific properties of the tungsten centres. A comparison with rate data for SCN^- substitution on the W_3O complex is possible at 50 °C wherein values obtained are: k_{ex} 2.5 x 10^{-3} s^{-1} and $k_1(NCS^-)$ 1.5 x 10^{-4} s^{-1}, assuming $K_{IP} = 1.5$ M^{-1}. Here, the smaller rate constant for entry of SCN^- may reflect steric hindrance to associative attack of the larger SCN^- ligand at the tungsten centre. On the other hand, associative attack by a water molecule may be facilitated by H-bonding through the acetate groups (Fig. 2.33) although it remains unclear as to why this process appears to be so unique to the tungsten species.

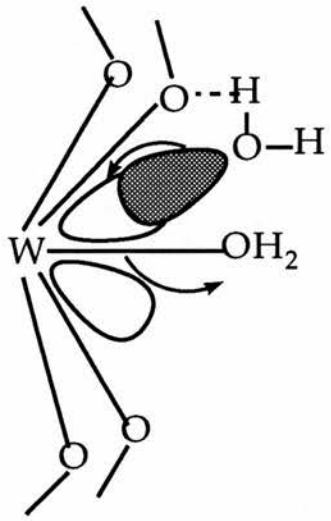

Fig. 2.33: A view of the 'expanded' 5d or 6p orbital on W and the proposed hydrogen bonding between the acetate groups and an incoming H_2O molecule.

Recently a paper by Nakata *et al*[60] has reported variable temperature kinetic studies with regard to CD_3OD substitution of H_2O using ^1H NMR on the complexes; $[Mo_3(\mu_3\text{-}CCH_3)(\mu_3\text{-}$

$O)(OAc)_6(OH_2)_3]^{+}$ ($Mo(IV)_3$) and the mono(oxo)-capped $[W_3O(OAc)_6(OH_2)_3]^{2+}$ together with brief mention of one or two measurements with regard to the bi(oxo)-capped trimolybdenum and tungsten complexes. Here an I_D or even D mechanism was assigned for all terminal ligand substitution reactions on these trinuclear carboxylate complexes.

For $[W_3O(OAc)_6(OH_2)_3]^{2+}$, Nakata *et al*[60] detected a stepwise substitution process corresponding to successive replacement of the water ligands. The first-order rate constant for the initial stage at 25 °C was 5.5 x 10^{-5} s^{-1}, some 10 x smaller than the value for water exchange (5.3 x 10^{-4} s^{-1}). Activation parameters; $\Delta H^{\neq}$ (113 kJ mol^{-1}), $\Delta S^{\neq}$ +56 J K^{-1} mol^{-1}) supported the proposition of a dissociative mechanism. These findings again appear to suggest that water exchange occurs *via* a rather unique process on these trinuclear tungsten carboxylate complexes. The single rate constant reported for CD_3OD substitution on $[Mo_3O_2(OAc)_6(OH_2)_3]^{2+}$ (k(44.8 °C) 1.1 x 10^{-5} s^{-1}) is also ~10 x smaller than the values for water exchange (1.38 x 10^{-4} s^{-1}) and SCN^- substitution at this temperature. CD_3OD substitution on $[W_3O_2(OAc)_6(OH_2)_3]^{2+}$ was reported to be ≥ 20 x slower than on the molybdenum species and ≥ 10^3 x slower than on the mono(capped) tungsten complex (this overall trend paralleling the findings here).

A further significant finding in the reported studies by Nakata *et al*[60] was the detection of a greater *trans*-labilising effect from the CH_3C^{3-} cap versus the oxo cap with respect to CD_3OD substitution of water, amounting to a factor of 10^5 at 44.8 °C for the trimolybdenum complexes.

A number of pieces of evidence were presented by Nakata *et al*[60] for a favoured dissociative mechanism on these trinuclear carboxylate complexes:

(i) Stereochemical considerations favour the dissociative mechanism. The O(acetate)-M-O(OH_2) angle of *ca.* 75° shows that the acetates truly bend towards the substitution side making associative attack of the incoming ligand less likely than in the case of a regular octahedral site.

(ii) In pyridine exchange reactions on the complex [Mo(μ_3-CCH_3)(μ_3-O)$(OAc)_6(py)_3]^+$ (Mo IV,IV,IV), the rate constant was observed to be independent of [d^5-pyridine] suggestive of a D mechanism.

(iii) A significant dependence on the nature of the leaving group (H_2O or py) was taken as indicative of an importance of bond breaking at least in the trimolybdenum complexes.

(iv) Large positive $\Delta H^{\neq}$ and $\Delta S^{\neq}$ were found for all substitution and pyridine exchange reactions studied.

These findings may however be qualified. It appears that a dissociative mechanism (I_D or D) is probably relevant for SCN^- and CD_3OD substitution together with water and pyridine exchange on the bicapped trimolybdenum complexes with capping μ_3-CH_3C^{3-} promoting a stronger *trans*-labilising effect than capping μ_3-oxo. Rate constants for SCN^- and $C_2O_4^{2-}$ substitution on $[Mo_3O_2(OAc)_6(OH_2)_3]^{2+}$ correlate well with the water exchange rate constant providing further support for the dissociative mechanism. It appears that protonated oxalate ($HC_2O_4^-$) may react differently in a 'concerted' mechanism in which a water molecule is released in a C-O bond breaking rather than a Mo-O(OH_2) bond breaking process.

Substitution processes at the water ligands on the bicapped(oxo) trimolybdenum carboxylates occur a million times slower than those on the incomplete cubane type cluster aqua ion $[Mo_3O_4(OH_2)_9]^{4+}$, despite a lower overall charge, verifying the importance of a true conjugate-base

cis-labilising effect in the latter (Chapter 1) stemming from activation *via* a deprotonated adjacent water molecule on the same molybdenum atom being substituted. Remote conjugate base labilising effects from deprotonated water molecules on the remote metal centres in the trinuclear carboxylate complexes are not relevant.

Remarkable activation parameters have been obtained characterising water exchange on the bioxo-capped and monooxo-capped tritungsten acetate complexes pointing strongly towards a unique associative mechanism. Rate constants for the mono(oxo) cap tritungsten complex show it to be the most labile system studied, a fact possibly related to the presence of only one oxo cap although the lower formal oxidation state at tungsten (3 $^{1}/_{3}$) may also be relevant. Possible labilisation resulting from a favoured associative mechanism seems however at odds with similar activation parameters (low $\Delta H^{\neq}$ and highly negative $\Delta S^{\neq}$) found for the bioxo capped tritungsten complex which is by far the most inert of the four complexes studied. Clearly further work is required in order to substantiate these findings. Particularly desirable would be a high pressure study of water exchange on the complexes to estimate the relevant activation volumes involved. If such a dramatic mechanistic changeover is relevant on going from molybdenum to tungsten in these systems then this should manifest itself in a change of sign of activation volume from a positive value (Mo) to a negative value (W). Finally Table 2.15 has collected all the available substitution rate data on trinuclear carboxylate complexes of molybdenum and tungsten for comparison.

Table 2.15: Rate Parameters for Substitution / Exchange Reactions at Trinuclear Carboxylate Complexes of Molybdenum and Tungsten.

Complex	Incoming Ligand	$k_{298}/M^{-1}s^{-1}$	$\Delta H^{\neq}$/ kJ mol^{-1}	$\Delta S^{\neq}$ /J K^{-1} mol^{-1}	Mechanism	Reference
$[Mo_3O_2(OAc)_6(OH_2)_3]2+$	H_2O	5.6 x 10^{-6}[a]	126	+77	I_D or D	This work
	SCN^-	9.4 x 10^{-6}[a]	141	+131	D	"
	$C_2O_4^{2-}$	~1.6 x 10^{-5}[a]	120	+85	I_D or D	"
	$HC_2O_4^-$	8.94 x 10^{-5}	76	-67	'concerted'	"
	CD_3OD	1.1 x 10^{-5}[b]	—	—	I_D	60
$[Mo_3O(CCH_3)(OAc)_6(OH_2)_3]^+$	CD_3OD	1.2[b]	93	+49	I_D or D	60
$[Mo_3O(CCH_3)(OAc)_6(py)_3]^{2+}$	py-d^5	8.6 x 10^{-4}[c]	112	+77	D	60
$[MoW_2O_2(OAc)_6(OH_2)_3]^{2+}$	H_2O	2.1 x 10^{-4}[d]	—	—		This work
	SCN^-	0.72 x 10^{-4}[e]	—	—		"
$[W_3O_2(OAc)_6(OH_2)_3]^{2+}$	H_2O	1.02 x 10^{-6}[a]	58	-164	I_A or A?	This work
	CD_3OD	< 5 x 10^{-7}[b]	—	—		60
$[W_3O(OAc)_6(OH_2)_3]^{2+}$	H_2O	5.3 x 10^{-4}[a]	51	-135	I_A or A?	This work
	SCN^-	1.5 x 10^{-4}[f]	—	—		"
	CD_3OD	5.5 x 10^{-5}[g]	113	113	I_D or D	60

a- s^{-1}, I =1.0 M ($NaCF_3SO_3$); b- s^{-1}, 44.8 °C in neat CD_3OD; c- s^{-1} in CD_3NO_2 containing py-d^5; d- s^{-1} at 50 °C; e- $s^{-1}(k_1)$ at 55 °C, I = 1.0 M ($NaCF_3SO_3$); f- $s^{-1}(k_1)$ at 50 °C, I = 1.0 M ($NaCF_3SO_3$); g- s^{-1} at 24.5 °C in neat CD_3OD.

2.5 Studies on the Redox Chemistry of the $[M_3O_2(OAc)_6(H_2O)_3]^{2+}$ (M = Mo, W, MoW_2) and $[W_3O(OAc)_6(H_2O)_3]^{2+}$ Complexes.

2.5.1 INTRODUCTION

The incomplete cuboidal type ions; $[M_3O_4(OH_2)_9]^{4+}$ (M_3 = Mo_3, W_3, Mo_2W) are characterised as having a well defined redox chemistry characterising reduction to M(III) and / or mixed valence M(III-IV) oxidation states.[61,62] It was of interest therefore to study whether these trinuclear carboxylate complexes had any comparable redox chemistry involving these lower valent states. Furthermore, it was not clear why the trimolybdenum mono(μ_3-oxo) capped complex $[Mo_3O(OAc)_6(OH_2)_3]^{2+}$ was hitherto unknown given that a number of mixed-valence Mo(III,III,IV) trinuclear complexes, such as $[Mo_3OCl_3(OAc)_3(OH_2)_3]^{2+}$ [63] and $[Mo_3(OH)_4(OH_2)_{10}]^{6+}$,[61] are well characterised and that the corresponding tritungsten mono(μ_3-oxo) capped complex was well established and moreover relatively stable in solution. It was envisaged that electrochemical or chemical reduction of $[Mo_3O_2(OAc)_6(OH_2)_3]^{2+}$ might ultimately provide evidence for formation of the mono(μ_3-oxo) capped species *via* reductive 'protonation' of the bicapped complex. Studies are also reported regarding the bicapped tritungsten analogue, mixed MoW_2 complex and the mono(μ_3-oxo) tritungsten complex itself. Some intriguing findings have resulted.

2.5.2 Experimental

2.5.2.1 Electrochemistry

Cyclic voltammetry measurements were carried out by using a

standard three-electrode cell design employing glassy-carbon working electrode (area 0.2 cm^3), platinum-wire counter and saturated calomel reference electrode, with a Princeton Applied Research Model 170 electrochemistry system.

Controlled potential electrolyses were carried out using either a mercury pool or platinum gauze (area ~ 4.0 cm^3) working electrode in the three electrode cell design as described above.

Chemical reduction was carried out using amalgamated zinc prepared by mixing zinc beads (~ 0.3 cm diameter) with purified distilled mercury.

2.5.3 Results and Discussion

2.5.3.1 $[Mo_3O_2(OAc)_6(OH_2)_3]^{2+}$

Figure 2.34 shows a cyclic voltammogram for a 5 mM solution of the above complex in 0.1 M CF_3SO_3H recorded at a glassy carbon working electrode at 0.2 Vs^{-1}. The cathodic scan was commenced at + 0.8 V (*vs* S.C.E.) wherein no reduction process was observed until an irreversible reduction wave was seen at -0.8 V. However on return anodic scan, two successive oxidation waves were observed at +0.05 V ($E_{1/2}$, reversible) and + 0.48 V (irreversible). The second cathodic scan revealed that the wave corresponding to the reductive portion of the reversible process at +0.05 V had all but disappeared. However the irreversible reduction wave at -0.8 V was regenerated. These observations can be interpreted initially in terms of an ECEC process. Furthermore, although comparisons of peak heights between irreversible and reversible processes is dangerous, it appears qualitatively that the -0.8 V, +0.05 V and +0.48 V waves respectively correspond to a three electron reduction, to give $Mo(III)_3$, followed by successive one electron reversible (to Mo(III, III, IV)) and two electron

irreversible (to $Mo(IV)_3$) processes.

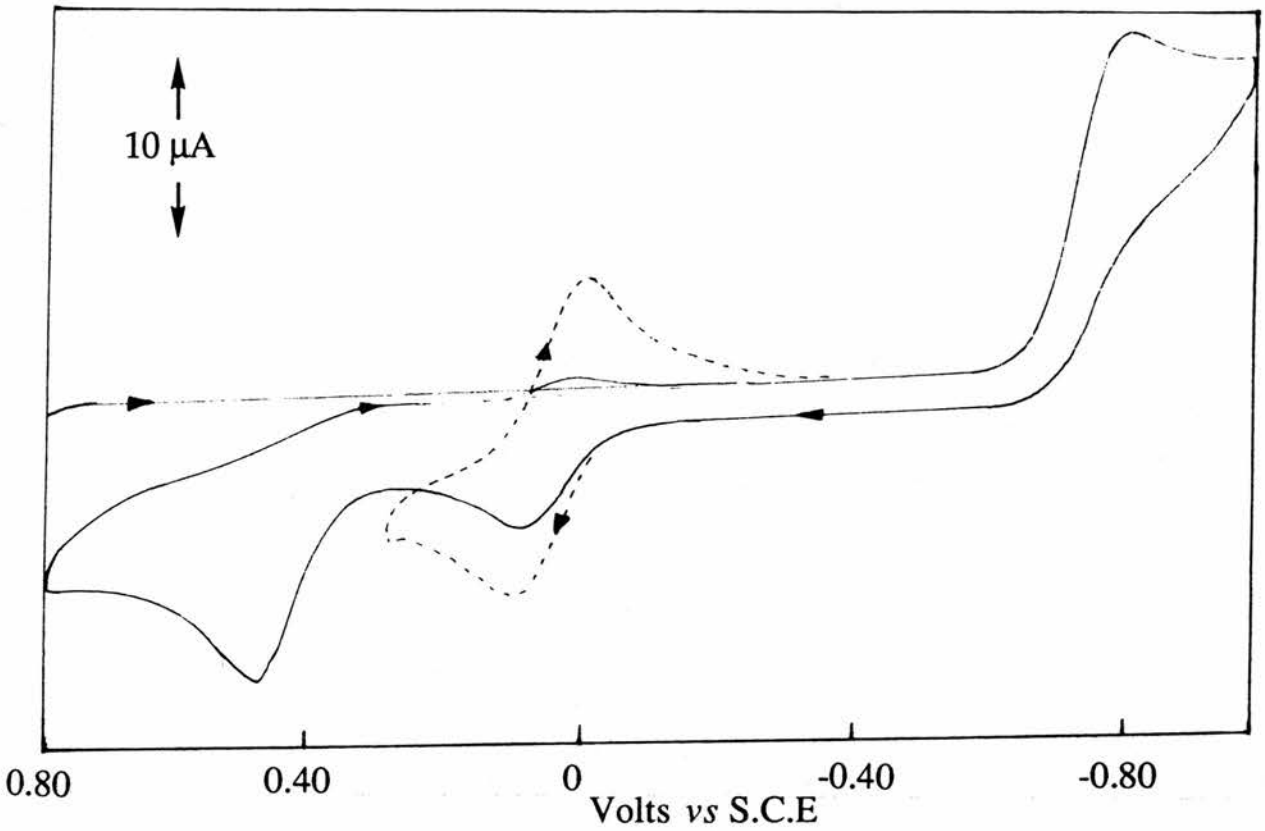

Figure 2.34: Cyclic voltammogram of $[Mo_3O_2(OAc)_6(H_2O)_3]^{2+}$ in 0.10 M triflic acid.

If true, is the $Mo(IV)_3$ species generated irreversibly at +0.48 V the original starting bicapped complex and what is the nature of the structural changes presumably involved in the irreversible redox processes? To answer these questions, controlled chemical and / or electrochemical reduction of $[Mo_3O_2(OAc)_6(OH_2)_3]^{2+}$ proved difficult owing to the negative potential and highly reducing nature of the product. Successful reduction was however carried out chemically using a stirred slurry of amalgamated zinc pellets.

2.5.4 Chemical Reduction of $[Mo_3O_2(OAc)_6(H_2O)_3]^{2+}$

For the chemical reduction of the complex a sample was weighed

out to make up a 5 mM solution in 0.10 M triflic acid in the presence of a slurry of zinc pellets and mercury. The solution was stirred continuously under a stream of N_2 for a period of 2-3 hours wherein an emerald-green solution formed. It was believed that this emerald-green species corresponded to that being generated at the irreversible reduction wave observed at -0.8 V *vs* S.C.E.

2.5.4.1 Estimation of the Formal Oxidation State for Mo in the Emerald-Green Solution Obtained on the Chemical Reduction of $[Mo_3O_2(OAc)_6(H_2O)_3]^{2+}$

A dilute Ce(IV) stock solution in 1 M H_2SO_4 (~0.01 M was standardised by titrating a known volume with standard solution of ammonium ferrous sulphate). A sample of the emerald-green solution (accurately measured using a Hamilton Syringe) was added to a 100 fold excess of Fe(III) as $Fe_2(SO_4)_3$ in 1 M H_2SO_4. The solution was then stirred and kept under N_2 for 15 minutes. After this time the mixture was opened to the air and then titrated with Ce(IV) using ferroin as indicator. An oxidation state per Mo atom of 3+ was obtained in accordance with the following redox reactions

$$Mo^{3+} + 3Fe^{3+} \longrightarrow Mo^{6+} + 3Fe^{2+} \quad (2.35)$$

$$3Mo^{2+} + 3Ce^{4+} \longrightarrow 3Fe^{3+} + 3Ce^{3+} \quad (2.36)$$

$$\therefore Mo^{3+} \equiv 3\ Ce^{4+} \quad (2.37)$$

A sample of the emerald-green solution was transferred (0.5 cm^3 Hamilton syringe) to a deoxygenated 1-cm quartz cell covered with a septum cap and the electronic spectrum recorded. The spectrum shows a distinct band at 595 nm (ε= 346 $M^{-1}cm^{-1}$ per Mo_3; Figure 2.35) . A

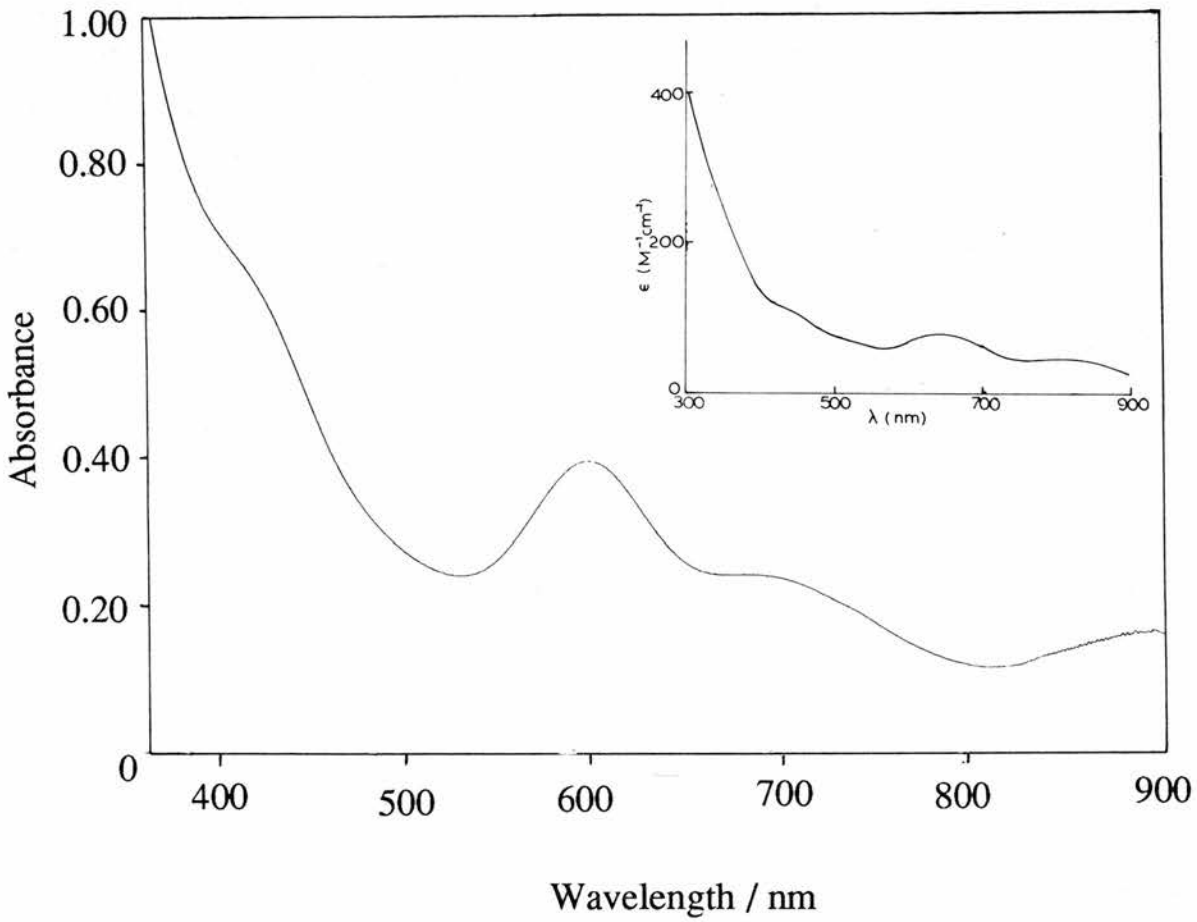

Fig. 2.35: UV-visible spectra of reduced $[Mo_3O_2(OAc)_6(OH_2)_3]^{2+}$ and reduced $[Mo_3O_4(OH_2)_9]^{4+}$ (inset).

sample of the reduced species was then exposed to the air and its changes monitored spectrophotometrically (Figure 2.36). As can be seen from the figure the final spectrum does not correspond to the red starting complex , $[Mo_3O_2(OAc)_6(H_2O)_3]^{2+}$, instead a species of very

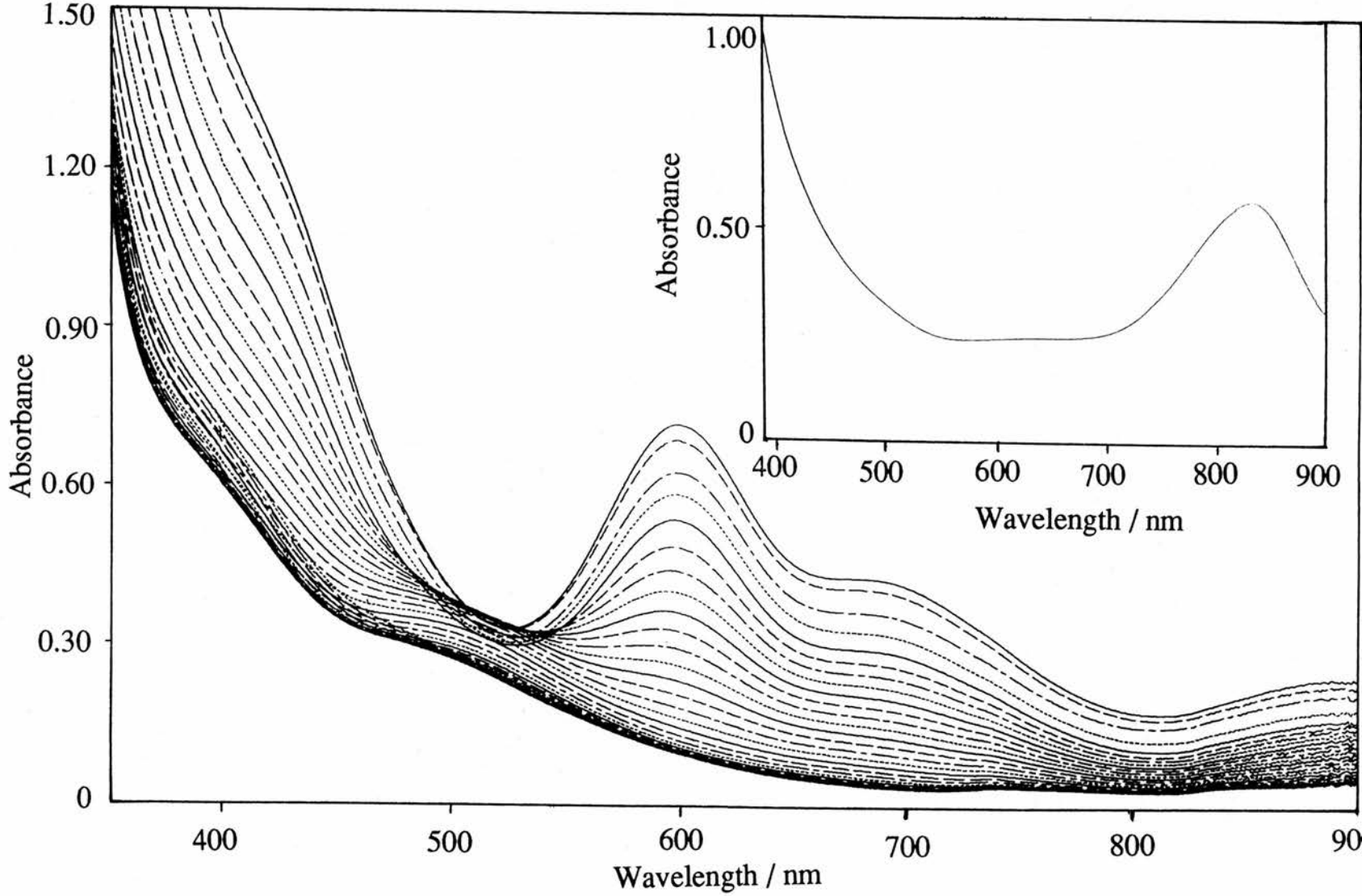

Fig. 2.36: Spectral changes observed on exposing the emerald-green species to air.

low absorbance in the visible region was obtained. Furthermore this resulting solution, when left standing for a few days took on a green tinge with a λ_{max} at 831 nm (inset Figure 2.36) indicative of small amounts of Mo(V) species. The electronic spectrum of the emerald-green species (Fig. 2.35) has certain features, in particular the λ_{max} at 595 nm (ε = 346 $M^{-1}cm^{-1}$), reminiscent of the $Mo_3^{III}(OH)_4^{5+}$ aqua ion (λ_{max} = 635 nm, ε = 240 $M^{-1}cm^{-1}$) (inset, Fig. 2.35) generated on reducing the $Mo_3O_4^{4+}$ aqua ion.[61] However, the lack of regeneration of the original bicapped trimolybdenum complex on air-oxidation is consistent with the irreversible nature of the wave at -0.8 V which suggests that some break up of the bicapped trinuclear core has resulted upon its generation, a process that does not appear to be reversed upon exposure to air (O_2). To prove the nature of these presumed structural changes, controlled potential oxidation (mercury pool) was carried out at +0.3 V to investigate the nature of the reversible oxidation process. The formal oxidation state of this species was found to be Mo(III, III, IV) by redox titration with Ce(IV)/Fe(III)/ferroin as described for the $Mo(III)_3$ species and confirms the one-electron nature of the redox process. The most remarkable finding however was the controlled potential oxidation (platinum gauze) at +0.8 V (*vs* S.C.E.) which was found to regenerate the original $[Mo_3O_2(OAc)_6(OH_2)_3]^{2+}$ complex (in 90 % yield following column chromatography) which showed that the gross triangular structure of the carboxylate complex had not been destroyed during the redox changes.*

*Some accompanying decomposition characterised these electrolyses if carried out over too long a time span (> 1-2 hours) believed to relate to the products obtained on air oxidation.

These findings lead to the intriguing tentative conclusion that the species responsible for the reversible process centred at +0.05 V are non other than the hitherto unknown mono(μ_3-oxo) trimolybdenum complexes; $[Mo_3O(OAc)_6(OH_2)_3]^{2+/+}$. Reversible loss of one of the capping μ_3-oxo groups could thus be responsible for the irreversible generation of the $Mo(III)_3$ species (favoured by having one less oxo cap) at -0.8 V. Irreversible oxidation of mono to bicapped species is presumed responsible for the wave at +0.48 V. A scheme of possible reactions may thus be described below:

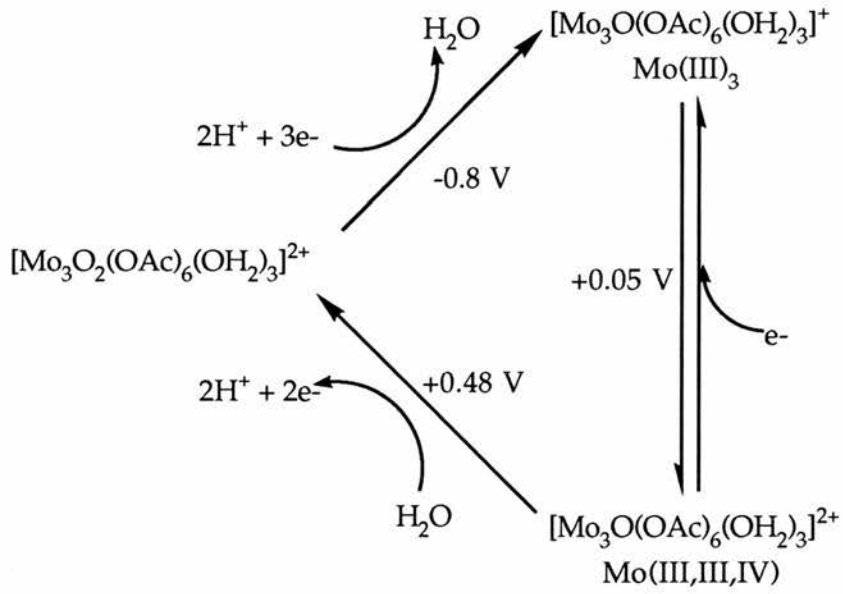

Scheme 2.4: Possible redox interconversions of mono(oxo) and bi(oxo) capped trinuclear carboxylate species.

Further supportive information comes from redox studies on the other complexes.

2.5.4.2 $[W_3O_2(OAc)_6(H_2O)_3]^{2+}$

Similar chemical reduction to that described above was attempted on the corresponding tungsten complex. However even after several hours no distinct change in the colour of the solution was observed suggesting that the complex cannot be reduced under these conditions. Cyclic voltammograms also failed to show any evidence of a redox process prior to the cathodic limit.

2.5.4.3 $[W_3O(OAc)_6(OH_2)_3]^{2+}$

The redox chemistry of the corresponding mono-capped (μ_3-oxo) compound, $[W_3O(OAc)_6(H_2O)_3]^{2+}$ proved to be more interesting than its bicapped analogue This ion was studied electrochemically using cyclic voltammetry and a single reversible reduction wave was observed, centred at -0.92 V *vs* S.C.E. at 25 °C (Fig. 2.37). This process is believed

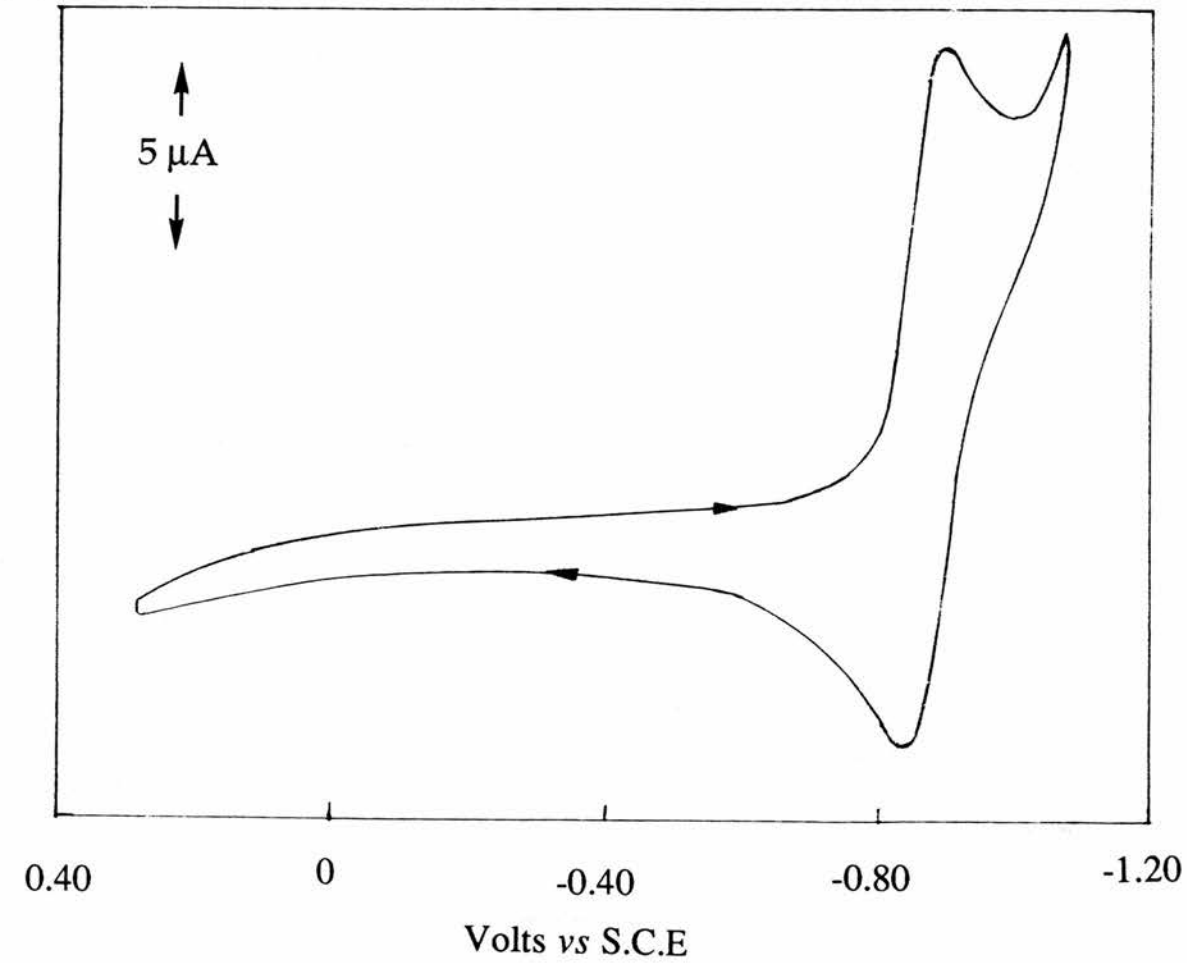

Figure 2.37: Cyclic voltammogram of $[W_3O(OAc)_6(H_2O)_3]^{2+}$ (2 x 10^{-3} M) in 0.10 M triflic acid, scan rate = 0.2 Vs^{-1}.

to be due to conversion of the W(III, III, IV) species to the reduced W(III,III,III).species. This result is very significant and probably represents the **first W(III, III, III) trinuclear species to be electrochemically generated.** The electrochemical reversibility strongly suggests that the basic trinuclear unit is retained in solution during the electrochemical process. Why this species is reduced electrochemically to the W(III, III, III) form whereas the corresponding bicapped analogue under similar conditions shows no redox chemistry could be due to the fact that the monocapped species has an empty e orbital and as a consequence is able to accommodate an extra electron. Attempts to reduce the monocapped species with Zn/Hg was not successful since the reduction potential for this species is observed to be more negative than that of Zn/Hg. However, attempts were made to generate this reduced W(III, III, III) species by controlled potential electrolysis.

2.5.4.4 Attempted Controlled Potential Reduction of $[W_3O(OAc)_6(H_2O)_3]^{2+}$

A controlled potential reduction experiment on $[W_3O(OAc)_6(H_2O)_3]^{2+}$ was attempted using a mercury pool working electrode. The experiment was carried out in a two-compartment cell separated by a fine sinter (No.4). Separation of the anodic and cathodic compartments was essential to avoid side reactions occurring as a result of contamination. The potential was set at -1.0 V *vs* S.C.E. and the reduction was followed by measuring the current as a function of time. A current /time graph allows in theory the calculation of the number of electrons involved. Such a plot was found to be very noisy and of

unsatisfactory quality to provide a meaningful value due to efficient background reduction of H_3O^+. The blue solution of the starting tungsten complex took on a greenish colouration after approximately an hour. A sample was syringed into a 0.10 cm deoxygenated quartz cell covered with a septum cap and the electronic spectrum taken. The spectrum was however very similar to that of the starting $[W_3O(OAc)_6(H_2O)_3]^{2+}$ species. It was thus concluded that if any reduction had occurred the species was unstable and rapidly reoxidised to the +2 ion by H_3O^+.

These results for the mono(μ-oxo) tritungsten complex in providing evidence for a reversible electrochemical reduction to give a W(III, III, III) species at -0.90 V *vs* S.C.E. provide further supportive evidence for the analogous molybdenum process occurring at +0.05 V *vs* S.C.E. This is summarised by eqn. 2.38.

$$\underset{\text{M(III, III, IV)}}{[Mo_3O(OAc)_6(H_2O)_3]^{2+}} + e^- \longrightarrow \underset{\text{M(III, III, III)}}{[Mo_3O(OAc)_6(H_2O)_3]^{+}} \quad (2.38)$$

$$E^o\,(Mo) = +0.05 \text{ V } vs \text{ S.C.E.}$$

$$E^o\,(W) = -0.90 \text{ V } vs \text{ S.C.E.}$$

The more negative reduction potential by ~ 0.9 V for tungsten *vs* molybdenum is typical of the behaviour observed between the two metals in other systems.

However, if the molybdenum monocapped species exists, it is strangely unstable when compared to the tungsten analogue. A possible reason why the presumed monocapped molybdenum species is unstable compared to that of tungsten may lie in the strength of the M-M bonding. It is known that stronger M-M bonding exists in the lower valent species for tungsten *vs* molybdenum[64] with typical examples

being the halo species, $M_2X_9^{3-}$. In $W_2X_9^{3-}$ (W-W, 2.45Å) the bonding is stronger than in the corresponding $Cs_3Mo_2Cl_9$ and $Cs_3Mo_2Br_9$ species where the Mo-Mo distances are 2.67Å and 2.78Å, respectively. Indeed the W-W bonds are noticeably shorter (Å) in the mono(μ_3-oxo) capped tungsten complex than in the bi(μ_3-oxo) capped tungsten (Å) analogue reflecting stronger W-W bonds in the mixed-valence species.

Further work is being planned for the future to monitor the possible reversible nature of the bicap-monocap interconversion in the molybdenum system. Such a study might involve oxygen isotopic labelling prior to reoxidation in order to detect the presence of the labelled μ_3-capping group. Detection of the labelled capping group would verify rapid incorporation *via* oxidation of the monocapped species.*

In view of the similarity of the UV-visible spectrum of the $Mo(III)_3$ species with that of $Mo_3(OH)_4^{5+}$ (Fig. 2.35) it is thus possible that the $Mo(III)_3$ species could have a protonated capping oxygen (μ_3-OH) as well. This idea could be tested by doing a $[H^+]$-dependence study of the Mo(III, III, IV) / $Mo(III)_3$ reversible redox process. The reduction of ^{17}O-labelled $[Mo_3{}^{17}O_2(OAc)_6(H_2O)_3]^{2+}$ to $Mo(III)_3$ would probably allow the detection of the μ_3-OH group in $Mo(III)_3$ to be made *via* NMR. The detection of the μ_3-OH group might be rather straightforward based on the knowledge that the signal for this group occur upfield from typical μ_3-O groups.[61]

---

*Separate studies have demonstrated the highly 'inert' nature of the capping oxo groups in the bi(oxo) capped complexes.

2.5.4.5 $MoW_2O_2(OAc)_6(OH_2)_3]^{2+}$

The mixed-metal ion $[MoW_2O_2(OAc)_6(OH_2)_3]^{2+}$ shows little evidence of an extensive redox chemistry reminiscent of the homo-trinuclear bicapped species. Figure 2.38 shows a cyclic voltammogram recorded for a 5 mM solution in 0.1 M triflic acid. An irreversible reduction wave at ~ 1.4 V *vs* S.C.E. is the only feature observed. There is no evidence of an accompanying reversible oxidation process corresponding to a mono(oxo)-capped system on an anodic scan up to +0.3 V. It is conceivable that the wave is due to irreversible reduction at molybdenum which if true would be consistent with the negative charge shift[27] from tungsten to molybdenum along the metal-metal bond in this complex such that the single molybdenum atom is in a lower formal oxidation state and hence more difficult to reduce than in the case of the homotrimolybdenum (IV) species (-0.8 V *vs* S.C.E).

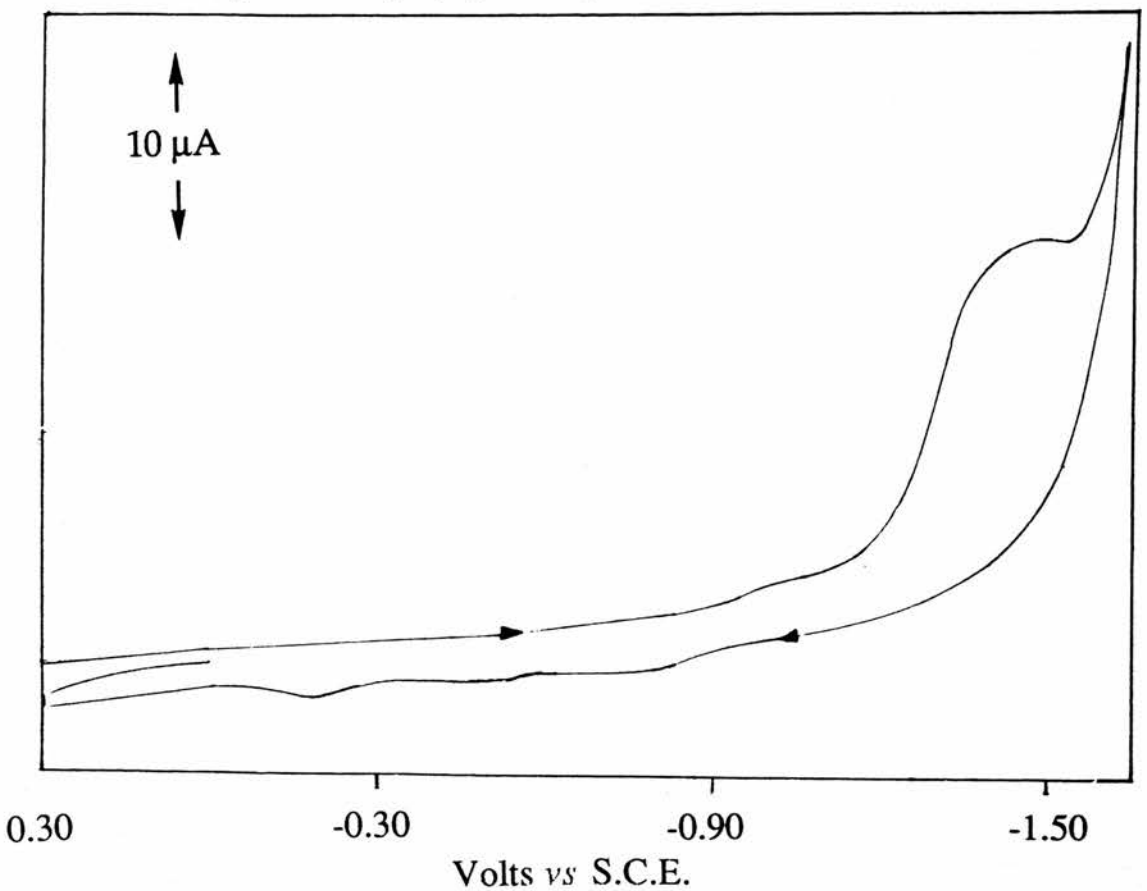

Figure 2.38: Cyclic voltammogram of $[MoW_2O(OAc)_6(H_2O)_3]^{2+}$ in 0.10 M triflic acid, scan rate = 0.2 Vs^{-1}.

2.6 REFERENCES

1. T. A. Stephenson, E. Bannister, G. Wilkinson, *J. Chem. Soc.* 1964, 2538.
2. (a) D. Lawton, R. Mason, *J. Am. Chem. Soc.* 1965, **87**, 921.
   (b) F. A. Cotton, Z. C. Mester, T. R. Webb, Acta. Crystallogr. 1974, B30, 2768.
3.. A. Bino, M. Ardon, I. Maor, M. Kaftory, Z. Dori, *J. Am. Chem. Soc.* 1476, **98**, 7093.
4. M. H. Chisholm, K. Folting, J. C. Huffman, C. C. Kirkpatrick, *J. Am. Chem. Soc.* 1981, **103**, 5967
5. M. H. Chisholm, F. A. Cotton, A. Fang, E. M. Kober, *Inorg. Chem.* 1984, **23**, 749.
6. A. Bino, F. A. Cotton, Z. Dori, S. Koch, H. Kuppers, M. Miller, J. C. Sekutowski, *Inorg. Chem.* 1978, **17**, 3245.
7. A. Bino, F. A. Cotton, Z. Dori, *J. Am. Chem. Soc.* 1981, **103**, 243.
8. A. Bino, F. A. Cotton, Z. Dori, B. W. S. Kolthammer, *J. Am. Chem. Soc.* 1981, **103**, 5779.
9. M Ardon, A. Bino, F. A. Cotton, Z. Dori, M. K. Kaftory, B. W. S. Kolthammer, M Kapon, G. Reisner, *Inorg. Chem.* 1981, **20**, 4083.
10. A. Bino, F. A. Cotton, Z. Dori, L. R. Falvello, G. M. Reisner *Inorg. Chem.* 1982, **21**, 3750.
11. A. Bino, D. Gibson, *Inorg. Chim. Acta* 1982, **65**, L37
12. F. A. Cotton, Z. Dori, M. Kapon, D. O. Marler, G. M. Reisner, W. Schwotzer, *Inorg. Chem.* 1985, **24**, 4381.
13. B. E. Bursten, F. A. Cotton, M. B. Hall, R. C. Najjar, *Inorg. Chem.* 1982, **21**, 302.

14. A. Birnbaum, F. A. Cotton, Z. Dori, D. O. Marler, G. M. Reisner, W. Schwotzer, M. Shaia, *Inorg. Chem* 1983, **22**, 2723.

15. A. Bino, D. Gibson, *Inorg. Chim. Acta*, 1985, **104**, 155.

16. M. Ardon, A. Bino, F. A. Cotton, Z. Dori, M. Kaftory, G. Reisner, *Inorg. Chem.* 1982, **21**, 1912.

17. M. Ardon, F. A. Cotton, Z. Dori, A. Fang, M. Kapon, G. M. Reisner, M. Shaia, *J. Am. Chem. Soc.* 1982, **104**, 5394.

18. A. Bino, F. A. Cotton, Z. Dori, M. Shaia-Gottlieb, M. Kapon, *Inorg. Chem.* 1988, **27**, 3592.

19. B. Wang, Y. Sasaki, A. Nagasawa, T. Ito, *J. Am. Chem. Soc* 1986, **108**, 6059.

20. J. Catterick, P. Thornton, *Adv. Inorg. Chem. Radiochem*, 1977, **20**, 291. See also: B. P. Straughan, O. M. Lam, *Inorg. Chim Acta*, 1985, **98**, 7.

21. M. H. Chisholm, K. Folting, J. C.Huffman, E. M. Kober, *Inorg. Chem.* 1985, **24**, 241.

22. M. H. Chisholm, K. Folting, J. A. Heppert, D. M. Hoffman, J. C. Huffman, *J. Am. Chem. Soc.* 1985, **107**, 1234.

23. B. Wang, Y. Sasaki, A. Nagasawa, T. Ito, *J. Coord. Chem.* 1988, **18**, 45.

24. A. Bino, K.-F. Hesse, H. Kuppers, *Acta Crystallogr., Sect B: Struct Crystallogr. Cryst. Chem.* 1980, **B36**, 723.

25. M. Minelli, J. H. Enemark. R. T. C. Brownlee, M. J. O'Connor, A. G. Wedd, *Coord. Chem. Rev.* 1985, **68**, 169.

26. A. Nagasawa, Y. Sasaki, B. Wang, S. Ikari, T, Ito, *Chem. Lett.* 1987, 1271.

27. B. Wang, Y. Sasaki, S. Ikari, K. Kimura, T. Ito, *Chem. Lett.* 1987. 1955.

28 G. Zundel, "*The Hydrogen Bond, Recent Developments in Theory and Experiment. Structure and Spectroscopy*"; P. Shuster, G. Zundel, C. Sandorty, Eds.; North Holland Publishing Co: Amsterdam, 1979; Vol II, Chapter 15.

29 (a) I. Gennick, K. M. Harmon, J. Hartwig, *Inorg. Chem.* 1977, **16**, 2241.

(b) K. M. Harmon, I. Gennick, *ibid.* 1975, **14**, 1840.

(c) K. M. Harmon, I. Gennick, *J. Mol. Struct.* 1977, **39**, 39.

30 M. D. Joesten, L. J. Schaad, "*Hydrogen Bonding*"; Marcel Dekker: New York, 1974; Chapter 2.

31 (a) K. Abu-Dari, K. N. Raymond, D. P. Freyberg, *J. Am. Chem. Soc.* 1979, **101**, 3688.

(b) K. Abu-Dari, D. P. Freyberg, K. N. Raymond, *Inorg. Chem.* 1979, **18**, 2427.

32. A. Bino, D. Gibson, *J. Am. Chem. Soc.* 1981, **103**, 6741.

33. A. Bino, D. Gibson, *J. Am. Chem. Soc.* 1982, **104**, 4343.

34. A. Bino, D. Gibson, *Inorg. Chem.* 1984, **23**, 109.

35. J. Burgess, "*Metal Ions in Solution*"; E. Harwood: Chichester, 1978; pp 290-305.

36. F. A. Cotton, G. Wilkinson, "*Advanced Inorganic Chemistry*", 4th Ed; Wiley: New York, 1980; pp 152-153.

37. C. F. Baes, Jnr., R.E. Mesmer, "*The Hydrolysis of Cations*"; Wiley: New York, 1976; pp 419-421.

38. C. L. Rohlfing, L. C. Allen, M. C. Cook, *J. Chem. Phys.* 1983, **78**, 2498.

39. B. O. Roos, W. P. Kraemer, G. H. F. Diercksen, *Theor. Chim. Acta.* 1976, **42**, 77.

40. J. Emsley, *Chem. Soc. Revs.* 1980, **9**, 91.

41. J Emsley, D. J. Jones, J. Lucas, *Reviews in Inorganic Chemistry* 1981, **3**, 105.

42. D. Hadzi, *J. Mol. Struct*, 1983, **100**, 343.

43. M. Ardon, A. Bino, *Structure and Bonding*. 1987, **65**, 1.

44. M. Ardon, B. Magyar, *J. Am. Chem. Soc*. 1984, **106**, 3359.

45. C. J. Carrano, K. Spartalian, G. V. N. Appa Rao, V. L. Pecoraro, M. Sundaralingam, *J. Am. Chem. Soc*. 1985, **107**, 1651.

46. R. D. Lorentz, A. Bino, J. E. Penner-Hahn, *J. Am. Chem. Soc*. 1986, **108**, 8116.

47. G. Davies, K. O. Watkins, *Inorg. Chem*. 1970, **9**,2735.

48. B.-L. Ooi, A. G. Sykes, *Inorg. Chem*. 1988, **27**, 310.

49. D. T. Richens, L. Helm, P.-A. Pittet, A. E. Merbach, F. Nicolo, G. Chapius. *Inorg. Chem*. 1989, **28**, 1394.

50. R. van Eldik, G. M. Harris, *Inorg. Chem*. 1978, **14**, 10.

51. C. Andrade, R. B. Jordan, H. Taube, *Inorg. Chem*. 1970, **9**, 711.

52. H. R. Hunt, H. Taube, *J. Am. Chem. Soc*. 1958, **80**, 2642.

53. A. Patel, P. Leitch, D.T. Richens, *J. Chem. Soc. Dalton Trans*. 1991, 1029.

54. I. Rapaport, G. Laurenczy, D. Zbinden, A. E. Merbach, *unpublished work*.

55. I. Rapaport, P. Bernhard, L. Helm, A.Ludi, A. E. Merbach, *Inorg. Chem*. 1988, **27**, 878.

56. S. E. Castillo-Blum, H. Gamsjager, A. G. Sykes, *Polyhedron* 1987, **6**, 101.

57. M. Eigen, R.G. Wilkins, *Adv. Chem. Ser*. 1965, **49**, 55.

58. G. M. Miskelly, D. A. Buckingham, *Comments on Inorganic Chemistry*, eds. N. Sutin and P. Gütlich, Gordon and Breach, London, 1985, Vol. 4, p. 163 and refs. therein.

59. (a) P. Pykko, J. P. Desclaux, *Acc. Chem. Res*. 1979, **12**, 276.

(b) D. R. McKelvey, *J. Chem. Ed.* 1983, **60**, 112.

60. K. Nakata, A. Nagasawa, N. Soyama, Y. Sasaki, T. Ito, *Inorg. Chem.* 1991, **30**, 1575.

61. D. T. Richens, C. Guille-Photin, *J. Chem. Soc. Dalton Trans.* 1990, 407.

62. A. Patel, D. T. Richens, *J. Chem. Soc. Chem. Commun.* 1990, 274.

63. A. Bino, F. A. Cotton, Z. Dori, *Inorg. Chim. Acta* 1979, **33**, L133.

64. R. Saillant, R. A. D. Wentworth, *Inorg. Chem.* 1969, **8**, 1226.

CHAPTER 3

3.1 GENERAL INTRODUCTION

3.1.1 Trinuclear μ_3-Oxo Carboxylate-Bridged Complexes

The trinuclear, oxo-centred carboxylate-bridged unit: $[M_3O(RCO_2)_6L_3]^{n+}$ (Figure 3.1) is remarkably common[1] in transition metal

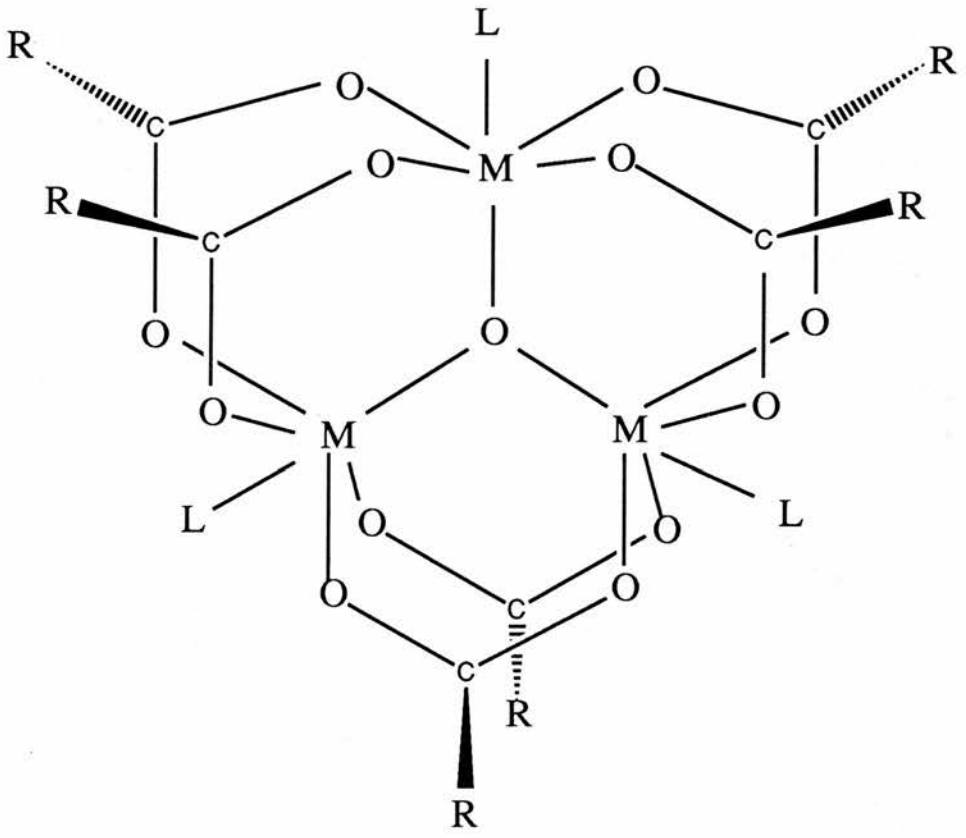

Fig 3.1: General structure of the μ_3-oxo trinuclear carboxylate complexes, $[M_3O(O_2CR)_6L_3]^{n+}$

chemistry. Complexes of this type are known for a diverse range of metals (V,[2] Cr,[3] Mn,[4] Fe,[5] Co,[6] Ru,[7,8] Rh,[9,10] and Ir,[11] R groups and terminal ligands L (H_2O, pyridine, CH_3OH, THF, DMF, PPh_3). When R = CH_3, they form the series of so-called 'basic' acetates, perhaps the most common examples and certainly the earliest to be documented. In

addition to the oxo-centred carboxylate complexes other related complexes are known with a central nitrogen atom[12] (M_3S clusters also exist but the sulphur atom is out of the plane [13,14]). The M_3X (X = O or N) group is planar and equilateral with D_{3h} symmetry but slight deviations from this trigonal symmetry are found in certain complexes. It is of interest to note that the planar M_3O units are also found in certain basic salts of mercury (II) with $[O(Hg Cl)_3]Cl$ and $[O(Hg CH_3)_3]ClO_4$ as examples.[14] Other examples are found in certain copper (II) chelate[15-17] complexes as well as the platinum (II) complex, $K_2[Pt_3(NO_2)_6O]$ (Vèze's red salt).[18] A number of mixed-valence compounds $[M_2^{III}M^{II}O(OAc)_6L_3]$ (M=V,[2b] Cr,[19] Mn,[20-22] Fe,[23,24] Ru[25]) as well as mixed-metal complexes $[M_2M'O(OAc)_6L_3]^{n+}$ [26-30] are also known with this trigonal structure.

The history of these carboxylate species is long and as early as 1908 the first preparative results on work conducted on those of chromium were reported by Weinland[31,32] and Werner.[33] They believed that a trinuclear unit was maintained during a number of substitution reactions in these species and they also believed they possessed six carboxylate groups and two hydroxide ions tightly held and not replaceable by acid. It was not until 1928 before the correct triangular geometry was proposed by Welo, based on magnetic data evidence.[34,35] However, this structure was not fully accepted until 1960 when Orgel[36] also postulated such a structure, which was soon resolved when X-ray crystallography confirmed[3b] the postulated structure of Orgel. Since then much progress has been made in this area of chemistry.

Interest in these compounds has arisen on several accounts:

(i) They form an unusual and perhaps rare class of compounds by elements from all regions of the transition series; early, middle

and late; first, second and third row and as such allows a unique opportunity for comparative studies.

(ii) The polynuclear structure, lending itself to the formation of variable valence, mixed-valence and mixed-metal derivatives has allowed a unique opportunity to study electronic and magnetic interactions between homo and heterometal centres in close proximity.

(iii) Several of the complexes are now well established as possessing catalytic activity towards a number of important and interesting transformations including:

(a) C-H activation and air oxygenation in cyclic aliphatic[37] and aromatic[6] hydrocarbons (M=Fe, Ru, Co)

(b) Oxidation of alcohols[38] (M=Ru)

(c) Epoxidation of olefins[39] (M=Fe)

(d) Hydrogenation of olefins[40] (M=Ru)

(e) Isomerisation of terminal olefins[40] (M=Ru)

(f) Hydroxylation of saturated hydrocarbons[41] (M=Mn)

(g) Reduction of aromatic nitro compounds[42] (M=$Fe_2^{III}Fe^{II}$ and several heteronuclear analogues (Fe_2Co, Fe_2Mn, Fe_2Ni)).

(h) Intramolecular conversion of unsaturated carbinols to saturated ketones[43] (M=Ru)

(i) Intramolecular oxidative transfer dehydrogenation[44] (M=Ru).

Certain aspects of (a) will be highlighted later .

In view of the nature of reactions catalysed, most attention has focused on the redox properties of these trinuclear complexes. Surprisingly little attention has been paid to a consideration of ligand substitution processes with very few, if any, reports of kinetic studies

with regard to the rates of complexation at the terminal L positions at the time this work was commenced. As mentioned before most interest has tended to focus on aspects of electronic structure, magnetic and redox properties.

3.1.1.1 Electronic Spectra

The first-row transition metal μ_3-oxo carboxylate complexes are known to have large metal-metal separations (typical values ~3.3 - 3.4 Å) as well as small antiferromagnetic coupling. As a consequence the electronic spectra of these species can be interpreted to a good approximation in terms of 3d-3d transitions within the individual metal ions, in addition to ligand-metal charge transfer. However, in some cases intensity enhanced absorption bands are observed which can be correlated with exchange interactions in such species resulting in reduced magnetic moments. In the case of mixed-valence species, additional absorption bands observed in the complexes can often be assigned to intervalence charge transfer thus leading to useful information as to the nature and extent of the electronic interaction between the metal centres.

The chromium (III) trinuclear complexes have been much studied, as a result their spectra are fairly well understood.[26c,45,46] In contrast the visible spectra of the trinuclear iron (III) analogues are poorly resolved and less well understood, the problem being ligand-metal charge transfer absorptions extending well into the visible region so obscuring the very weak, spin forbidden d-d absorption bands.[47] However, Blake *et al* [26c] have studied the diffuse-reflectance spectra of $[Fe_3O(OAc)_6L_3]^+$ (L = H_2O or py) complexes between 6,000 and 40,000 cm^{-1} at room temperature and were able to assign the transitions responsible for three of the bands occurring at *ca*

10,000 cm^{-1} ($^6A_{1g} \longrightarrow {}^4T_{1g}$), 18,000 cm^{-1} ($^6A_{1g} \longrightarrow {}^4T_{2g}$) and 21,000 cm^{-1} ($^6A_{1g} \longrightarrow {}^4A_{1g} + {}^4E_g$), on the basis of shifts with varying ligands L

3.1.1.2 Vibrational Spectra

A lot of work has been performed over the years in order to try understanding the vibrational spectra of the trinuclear μ_3-oxo complexes and much interest is still being generated in this area. Much progress has been made in establishing frequency trends in these species by systematically altering the metal ions and the R groups. The use of isotopic substitution, especially deuteration of the attached ligands, and in some cases substitution of the central bridging ion, ^{15}N for ^{14}N or ^{18}O for ^{16}O has proven to be a valuable technique. An example is provided by $[Fe_3(^{18}O)(OAc)_6py_3]^+$ in which ^{18}O-substitution has enabled assignments to be made of both in-plane (ν_{as} Fe_3O) and out-of-plane (σ_s, Fe_3O) vibrations of the oxo unit.[48] In fact most of the principal stretching modes and some of the deformations have now been assigned.

There are certain features which are common to most complexes and these are represented by the complex, $[Cr_3O(OOCCD_3)_6(OD_2)_3]Cl.xD_2O$[49] in Figure 3.2. The frequency range above 800 cm^{-1} is usually dominated by vibrations of the organic ligands, which can be assigned readily. Below 400 cm^{-1}, the only stretching frequencies are those of the central $M_3O_{13}L_3$ framework (L = terminal ligand directly bonded to the metal). To a first approximation these can be reduced into vibrations of the planar (or almost planar) MO_4 units, the central triangle, and the M-L bonds. For the majority of carboxylate complexes the strong angle deformation and out of plane deformation of the RCO_2 group are

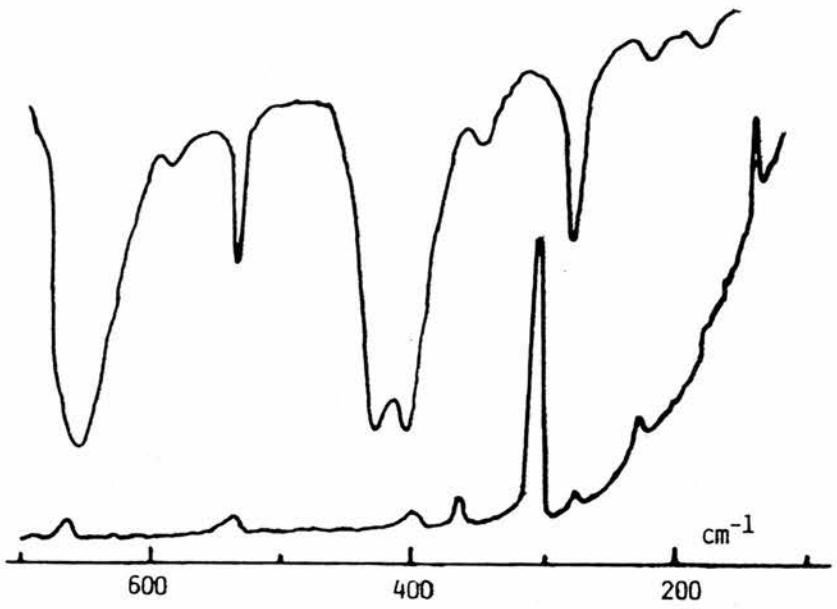

Fig.3.2: Infrared and Raman spectra of $[Cr_3O(OOCCD_3)_6(OD_2)_3]Cl.xD_2O$

found between the two frequency ranges previously mentioned. The asymmetric stretch $\nu_{as}(M_3O)$ is also found in or near this region.

3.1.1.3 Electrochemistry

The electrochemical behaviour of selected oxo-centred trinuclear species has been reported by Uemura *et al.*[11] Their results indicate that the $[Cr_3O(OAc)_6L_3]^+$ (L = H_2O, CH_3OH, py, β-picoline) species do not show any reduction or oxidation waves in the range +2.0 to -1.8 V *vs* S.C.E. However, the corresponding pyridine and β-picoline manganese complexes and the pyridine analogue of iron all exhibit an irreversible reduction peak
at *ca.*. +0.3 and -0.03 V *vs* S.C.E, respectively. These reduction processes were found to involve one-electron as confirmed by controlled potential coulometery experiments. The β-picoline complex of cobalt and the rhodium species (L = H_2O, py) all showed a single irreversible reduction wave at +0.13 V and *ca.* -0.9 to -1.0 V *vs* S.C.E., respectively. The reduction process in the case of the cobalt complex was found to involve one electron while controlled potential

coulometry on the rhoduim species gave only rhodium metal and the n values were not reproducible. The iridium complexes, $[Ir_3O(OAc)_6L_3]^{2+}$ were also studied and shown to undergo an irreversible reduction from Ir(IV, III, III) to Ir(III, III, III).

With the exception of the chromium complexes all these species showed some form of reduction in the presence of hydrogen (2 atm.) and platinum oxide catalyst or sodium borohydride in ethanol. The aqua, pyridine and β-picoline complexes of Mn, Fe and Co were readily reduced to the corresponding metal (II) ions. The rhodium complexes were reduced to the metal instead. The Ir(IV, III, III) complexes were reduced in stages, first to the Ir(III, III, III) species, and then to the Ir(I) analogues and/or metal.

Uemura *et at* [11] concluded that the electrochemical reduction of Mn, Fe and Co complexes by one electron suggests that the reduced species retain the trinuclear structure in solution. Unfortunately all attempts[11] to isolate these reduced species proved unsuccessful. Physical evidence of their structures would be very welcome.

More recently cyclic voltammetric studies [29b] were carried out on the series $[Cr_nFe_{3-n}O(gly)_6(H_2O)_3]^{7+}$ (n = 0, 1, 2, 3). It was found that both the Cr_3 and $FeCr_2$ species showed no redox processes in ethanolic solution in the region +2.0 to -2.0 V *vs* S.C.E. while the Fe_2Cr complex produced an irreversible peak at -0.5 V *vs* S.C.E. The Fe_3 species, however, produced the most interesting redox properties, showing a reversible wave at +0.05 V *vs* S.C.E. This was a one-electron process and it was concluded that the triiron complex retains its trinuclear structure on reduction in solution. The electrochemical process was explained using the following equilibrium (3.1):

$$Fe_3^{III}O(gly)_6(H_2O)_3]^{7+} \rightleftharpoons [Fe_2^{III}Fe^{II}O(gly)_6(H_2O)_3]^{6+} \qquad (3.1)$$

This mixed-valence complex has been synthesised but not as yet characterised crytallographically.[29b]

3.1.1.4 Magnetic Susceptibility

Extensive magnetic susceptibility measurements as a function of temperature have been carried out on the class of trinuclear μ_3-oxo compounds, $[M_3O(OAc)_6L_3]^+$, in particular those of M = Cr(III) and Fe(III). Magnetic coupling is observed between the metal centres in these species. The Fe(III) and Cr(III) complexes have been shown crystallographically to have a D_{3h} symmetry which leads to a spin Hamiltonian[50] having a single coupling constant to describe the interaction of the metal ions (eqn 3.2)

$$H = -2J(S_1 \cdot S_2 + S_2 \cdot S_3 + S_3 \cdot S_1) \qquad (3.2)$$

where J = coupling constants and S_1, S_2 and S_3 are spin operators.

The expression derived for the variation of magnetic susceptibility with temperature for both Fe_3O and Cr_3O acetate complexes have not been entirely successful in simulating the experimental data, the deviations being greatest at the lowest temperatures. However, this same approach, *i.e.* assuming an equilateral arrangement of the three metal atoms has been used successfully in explaining the magnetic properties of the Mn_3O acetate species (L=py).[22]

Better fits for such expressions (in the case of the Fe_3O and Cr_3O complexes) have however, been achieved by using a variety of approaches.[51] One of which, and perhaps the most popular theory, is that in which the metal ion triangles are distorted to an isosceles arrangement.[50] This model has been applied to many Cr(III) and Fe(III) complexes. Another theory that has been proposed is one

which considers coupling between trimer units.[3c,52] There is also a dynamic model proposed by Jones *et al* [51] which assumes that the metal triangle is slightly distorted from equilateral, but that the distortion rapidly fluctuates so that the time average seen by crystallography is equilateral.

Studies so far seem to indicate that the antiferromagnetic exchange interaction for the Fe_3O acetate complexes are greater than for the Mn_3O species. The value for manganese is comparable to that found in the Cr_3O systems (d^3) as shown by these values: ($-J = 10.2$ cm^{-1}, 11 cm^{-1} and 30 cm^{-1} for Mn_3O, L=py;[22] Cr_3O, L = H_2O;[26c] and Fe_3O, L = H_2O,[26c] respectively). This was explained[22] in terms of the greater occupancy of d_z2 orbital directed towards the bridging O^{2-} ion in Fe(III), which is high spin d^5 ($t_{2g}^3e_g^2$), than for Cr(III) (d^3, t_{2g}^3) or Mn(III) (d^4, $t_{2g}^3e_g^1$)

The mechanism for exchange in these systems is considered as a 'super-exchange' process involving participation of the metal d orbital interaction with the p orbitals of oxygen. Thus there are two possible superexchange pathways in these μ_3-oxo systems: the central oxygen atom and the carboxylate groups (the metal-metal distance *ca.* 3.3 Å, is too great for significant direct overlap). Blake *et al* [26c] have, however, showed that the μ_3-oxo atom provides the main superexchange pathway in these trinuclear carboxylate complexes, whereas exchange *via* the bridging carboxylates can be largely negleted. The overall conclusion is that overlaps between d_z^2, d_{xz} and d_{yz} orbitals of the metal ions *via* in-plane p orbitals of the central oxygen atoms are the most effective mechanism of superexchange in the M_3O systems. Because of this mechanism a larger interaction is possible with occupancy of the d_z^2 metal orbitals.

3.1.2 Mixed-Metal Trinuclear (μ_3-O) Carboxylate Complexes

As far back as 1909, the first mixed-metal complexes $Cr_2^{III}Fe^{III}$ and $Cr^{III}Fe_2^{III}$ were reported by Weinland and Gussmann[53] and later in 1928, *i.e* before the constitution of the "basic acetate" complexes $[M_3O(OAc)_6L_3]^{n+}$ was recognised, mixed metal hydroxy acetates of Fe(III) with various divalent transition metal ions were reported by Weinland and Holtmeier.[54] They assigned to these hydroxy species misleading formulae such as $M_4^{II}[Fe_9^{III}(OH)_9(OAc)_{26}].23H_2O$ and $M_3^{II}[Fe_6^{III}O_3(OH)\text{-}(OAc)_{17}].12py$, and believed them to contain Fe_3(III) units of the type found in basic iron(III) acetate. Following the procedures described by Weinland and Holtmeier, Blake and co-workers[26a,b] have isolated crystalline products, which were found to be analogues of the (μ_3-O) bridged compounds.

Various combinations of mixed-metal analogues of the trinuclear oxo compounds $[M_2^{III}M^{II}O(RCO_2)_6L_3]^{n+}$ have now been prepared[26] where M and M' are different trivalent and divalent transition metals respectively, R = CH_3, L = H_2O, py and n = 0. As well as existing with acetate groups[26c,27] the mixed-metal combinations of $Fe_2^{III}Cr^{III}$ and $Cr_2^{III}Fe^{III}$ have been prepared with carboxylate bound glycine.[28,29] In addition to these species a $Ru_2^{III}Rh^{III}$ acetate complex (n=1 and L=H_2O, py) is also known.[30]

3.1.2.1 Preparation

For the synthesis of these complexes the required amounts of the metal salts are reacted with an excess of a carboxylate salt in aqueous solution. Most of the species are only sparingly soluble in the medium thus facilitating their precipitation. The corresponding pyridine complexes can be prepared readily by interaction of the aqua species

with pyridine. In the case of the chromium(III) series, chromium(II) acetate is generally used in the presence of the other metal (II) acetate, although $Cr^{III}Fe^{III}$ complexes have also been prepared by reacting appropriate Cr(III) and Fe(III) salts. The $Fe^{III}Cr^{III}M^{II}$ complexes can be prepared by reacting Cr(II) acetate with the corresponding preformed complex, $Fe_2^{III}M^{II}$.

3.1.2.2 Electronic Spectra

Studies have shown that there is a lowering of the ligand field strength in $[M_3O(OAc)_6L_3]^+$ when a trivalent ion is being replaced by a divalent one, and shifts to lower frequencies are observed for d-d transitions associated with the Cr(III) and Fe(III) ions [26b,c] For the $Cr^{III}Fe^{III}M^{II}$ complexes a striking feature is their purple colour, which contrasts with the green colour of most of the Cr_2M^{II} and Fe_2M^{II} species. The colour appears to be associated with an intense band at *ca.* 19,000 cm^{-1}.[26c] Whereas the Cr_3(III) and Fe_3(III) complexes are grey-green and olive-green respectively, the $Cr_2^{III}Fe^{III}$ is purple-red and it has intense bands at 18,000 and 25,500 cm^{-1} which do not appear to correspond to any bands in the Cr_3 and Fe_3 complexes. The $CrFe_2$ complex is red-brown in colour and shows less well defined absorptions, the spectrum of which is somewhat like that of a mixture of Ce_2Fe and Fe_3 complexes, although the intensities of bands are greater than for a simple mixture of species.

Blake *et al* [26] have suggested this colour difference between the homonuclear and mixed-metal species is due to simultaneous (Cr^{3+}, Fe^{3+}) double excitations.

3.1.2.3 Structural Studies

Various mixed-metal (μ_3-O) compounds have been structurally characterised as well as several mixed-valence homotrinuclear species, the properties of which might be expected to relate to mixed-metal species of similar valence distribution. Hence it is appropriate to consider the mixed-valence species together with these mixed-metal complexes. The $[Fe^{III}Cr_2^{II}O(OAc)_6H_2O)_3]^+$ species has been structurally analysed by different workers[27,55] and although confirming the similarity of its structure to those of the homonuclear Fe(III) and Cr(III) species they were unable to distinguish between the individual metal ions and a statistical distribution of the ions was indicated. The M-O bond distances were also vary similar to the Cr_3O species. In the case of the $Fe_2^{III}Cr^{III}$ glycinato complex[28] an ordered arrangement of the metal ions in the crystal was observed.

In a $[M_3O(OAc)_6L_3]$ complex containing $M_2^{III}M^{II}$ oxidation states the M^{III}-(μ_3-O) bond distances would be expected to differ from that of the M^{II}-(μ_3-O) based on symmetry. However, no difference between the three metal ions was detected in a variety of such mixed valence species except for $[Mn_2^{III}Mn^{II}O(OAc)_6(3\text{-Clpy})_3]$.[21] In this complex an isosceles triangular arrangement is formed by the metal ions indicating the position of an Mn(II) ion. In other cases where the crystal structure data indicate an equivalence of the metal ions, a rapid electron transfer between the metal ions, possibly *via* the central oxygen atom or delocalisation of the metal and oxygen electrons over the M_3O cluster is indicated. The diamagnetism observed in the $Ru_2^{III}Ru^{II}$ complex, for example, is believed to be due to such a delocalisation.[25] Another possibility is that there is a statistical distribution of $M_2^{III}M^{II}$ units throughout the crystal, causing each metal site to appear equivalent. In the species, $[Fe_2^{III}Fe^{II}O(OAc)_6L_3]S$

(L = py, 4-Et-py, S=L);[24] (L = 4-Me-py, S = benzene),[23] two doublets of area ratio 2:1 (Fe^{III}:Fe^{II}) are present in the Mössbauer spectra at low temperatures (to 11K). As the sample temperature is increased, spectral changes occur until, at *ca.* 300K, only a single averaged spectrum can be seen, in accordance with the X-ray structural studies, which indicate that the Fe sites are equivalent at room temperature. It is believed that at room temperature the valencies have become equivalent by a rapid electron transfer process and the longer time scales of X-ray diffraction or Mössbauer spectroscopy are unable to detect the oxidation state differences between the iron atoms.[56]

Very recently a unique trinuclear μ_3-oxo mixed-valence complex, $[Fe_2^{III}Fe^{II}O(OAc)_6(TACN)]\cdot 2CHCl_3$, (Figure 3.3) was reported.[57] It was synthesised by air oxidation of iron(II) acetate in the presence of TACN (1, 4, 7 - triazacyclononane). X-ray crystallography at 195K has shown that in this species only one pair of adjacent iron atoms is bridged by two bidentate acetate ligands with the other two pairs bridged by only one such ligand. The terminal positions of two of the three iron atoms are occupied by a rare bidentate acetate ligand while the third atom is bonded to the tridentate TACN ligand. This structure is stabilised by internal hydrogen bonding between the NH protons of

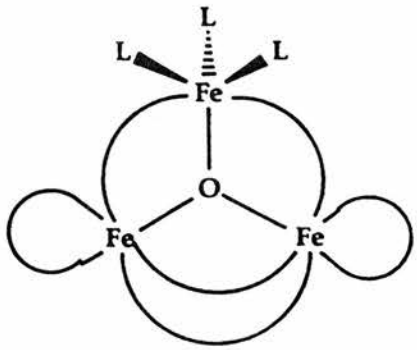

Fig 3.3: Structure of $[Fe_2^{III}Fe^{II}O(OAc)_6(TACN)]\cdot 2CHCl_3$

the TACN ligand and the bidentate terminal acetate ligands. Analysis of the iron-ligand bond lengths has indicated that this iron species has a localised structure. A comparison of the three Fe-(μ_3-oxo) distances shows that the two Fe^{III}-O distances (1.862Å and 1.867Å) are shorter than the Fe^{II}-O distance (1.998Å)

A localised structure for the $[Fe_3O(OAC)_6(TACN)]\cdot 2CHCl_3$ was also confirmed by Mössbauer spectroscopic studies in the range 4.2 - 295K, which revealed the Fe(III) and Fe(II) sites with an intensity ratio of ~2:1. The magnetic susceptibility of this complex was also studied, in the range 2-300K, and the data were successfully fitted by using a model with only two different spin exchange coupling constants. This complex is also of interest because of its terminal chelating carboxylate ligands, a feature of the diiron(III) oxo core in the ribonucleotide reductase B2 subunit.[58]

3.1.2.4 Vibrational Spectra

Infrared spectra (800 - 130 cm^{-1}) of the mixed-metal and mixed valence complexes $[Fe_2^{III}M^{II}O(OAc)_6L_3]$ (M = Mn, Fe, Co, Ni; L = H_2O, py), and Raman spectra on the aqua adducts, have been reported and assigned by using a variety of isotopic substitutions.[59,60] The aim of such a study was to try to establish the 'true' molecular symmetry of $Fe_2^{III}Fe^{II}$ systems, employing a method whereby the spectra of mixed-valence complexes were compared with those of corresponding mixed-metal complexes of C_{2v} symmetry. In C_{2v} symmetry, the asymmetric vibration associated with the $Fe_2M^{II}O$ unit would be split into two components, A_1 and B_2, and such bands have been assigned[59,60] for the range of mixed metal species mentioned above. The frequencies were found to increase in the order Mn<Co<Ni, parallel to the Irving-Williams series of stabilities of metal-ligand

complexes, and also parallel to frequency trends in other metal-pyridine complexes. These assignments have allowed the assignment of the related bands in the mixed-valence complexes (M=Fe) at room temperature. It was concluded that in these mixed-valence iron species the oxidation states are partially localised on the vibrational time scale.[59]

Although major advances have been made in establishing the 'true' nature of these species, more work is needed with respect to some. For example, isotopic substitution studies and /.or other spectroscopic techniques seem relevant in confirming the results of earlier work conducted by Johnson *et al* [61] on the mixed-valence complexes $[Ru_3O(OAc)_6L_3]$ ($L=H_2O$, PPh_3) and by Cleare and Griffith[62] on normal and (^{15}N) substituted $[Ir_3N(SO_4)_6(OH_2)_3]^{4-}$. The results of both studies indicate delocalised systems, but Mössbauer spectroscopic studies carried out on the iridium complex at 4.3K indicate distinct valencies.[63]

3.1.2.5 Magnetic Susceptibility

Blake *et al* [26c] have conducted a variable temperature study on the series of mixed-metal μ_3-oxo acetate species $Cr_2^{III}M^{II}$ and $Fe_2^{III}M^{II}$ (M = Ni, Mn, M_g). It was found that in the $Fe_2^{III}M^{II}$ species the Fe-Fe coupling constant is about twice the value of in the symmetrical Fe_3^{III} systems. A similar result was obtained for the $Cr_2^{III}M^{II}$ systems when compared with Cr_3^{III}. It was also found that these results were almost independent of the nature of M(II) providing clear evidence that coupling through the central oxygen is important.

Detailed magnetic studies[29b] have also been carried out on the series of oxo-centred trinuclear glycinate species $[Cr_nFe_{3-n}O(gly)_6(H_2O)_3]^{7+}$ (n=0, 1, 2, 3) and attempts were made to fit the

data to a susceptibility expression on the assumption of an isosceles triangle of atoms. This method involved the use of a factor representing the ratio of two integrals such that $J_{12} = J_{23} = \alpha J_{13}$. The values of J and α were varied in an attempt to obtain the best fit for the data. The best fits to the data for the Cr_3 and Cr_2Fe species were obtained with $\alpha = 1$, indicating that these species approximated closely to an equilateral triangle of metal atoms. In contrast the Fe_3 complex gave a very poor fit with $\alpha = 1$ but good fits with $\alpha = 0.7$ and 1.57 indicating that something less than an equilateral triangle fitted the arrangement of the iron atoms. The Fe_2Cr species, however, was less sensitive to the arrangement of the metal ions. The same method was also applied to the mixed-valence species, $[Fe_2^{III}Fe^{II}O(gly)_6(H_2O)_3]^{6+}$, with a rather interesting result. The best fit was obtained when the complex was regarded as a binuclear Fe_2^{III} unit with virtually no interaction from the Fe^{III} ion. This result could suggest that a great deal of spin localisation is present in this species as opposed to most other $Fe_2^{III}Fe^{II}$ complexes studied.

3.1.3 Trinuclear Ruthenium μ_3-Oxo Carboxylate-Bridged Complexes

The history of the ruthenium (III) carboxylate complex chemistry, like so much of the chemistry of ruthenium is characterised by early confusion and a number of false identifications, later clarified by improved physical techniques.

Ruthenium carboxylate complexes were first studied by Mond[64] who obtained a series of acetate species, formulated as binuclear $[Ru_2(OAc)_4(OH)_2(OH_2)_2]$. These species were obtained by refluxing a

hydrated ruthenium (III,IV) oxide ("ruthenium (III) hydroxide") with the acid. However, this work has proved irreproducible.[65] Stephenson and Wilkinson[65] later reported that $[Ru_2(OAc)_4(H_2O)_2]$ (but containing chloride ion as an impurity) could be isolated from the green solution formed by the reaction between 'commercial ruthenium trichloride' and acetic acid / acetic anhydride. Attempts to purify the complex using silver acetate, or to repeat the preparation using '$Ru(OH)_3$' instead of '$RuCl_3.xH_2O$', resulted in a product believed to be $[Ru_2(OAc)_{4.5}(H_2O)_{1.5}]$. Legzdins *et al* [66] later reported an improved method of preparing dinuclear $[Ru_2(OAc)_4]$, which involved the reaction between ruthenium (III) chloride and sodium acetate in a mixture of acetic acid and ethanol. Soon after it was proved that this earlier product, thought to be $[Ru_2(OAc)_4]$. as well as the main product of Mond's reaction and the products reported above as $[Ru_2(OAc)_4(H_2O)_2]$ and $[Ru_2(OAc)_{4.5}\text{-}(H_2O)_{1.5}]$ are all impure forms of the complex $[Ru_3O(OAc)_6\text{-}(H_2O)_3]OAc$.[7,67] The pure complex can be obtained by recrystallisation from methonal/acetone mixtures[7], Sephadex[7,67] or Dowex[30] cation exchange chromatography. Furthermore the variety of products obtained from Mond's reaction between '$Ru(OH)_3$' and acetic acid have now been rationalised in terms of the following equilibrium (3.3);

$$[Ru_3O(OAc)_6(H_2O)_3]^+ \rightleftharpoons [Ru_3O(OAc)_6(OAc)_3]^{2-} \qquad (3.3)$$

in which unidentate acetate is involved in the stepwise replacement of water.[7] There were further complications, this time involving the product obtained by Martin[68] from the reaction of RuO_4 by acetaldehyde in acetic acid/carbon tetrachloride solutions. Martin thought the complex was $[Ru_3(OAc)_6(OH)_2]OAc.7H_2O$, which was

later incorrectly reformulated as $[Ru_3O(OAc)_6(H_2O)_3]OAc.5H_2O$ by Stpehenson and Wilkinson[65] and its Raman spectrum interpreted on this assumption.[69] Although the structure of Martin's acetate, as it is called, is not known its properties are not consistent with a trimeric μ_3-oxo centred structure and a polymeric species has been suggested instead.[7]

The structre of the triaqua complex has been established by crystallography and is reported herein (see Results and Discussion section). In addition, structural characterisation of a trinuclear μ_3-oxo ruthenium (III,III,III) acetate with phosphine ligands has been reported (see Section 3.1.3.4). Prior to the crystal structure determination the correct formulation of the aqua complex was established by a combination of molecular weight determinations, paper electrophoresis, pH titration and elecrochemical measurements and by analogy with the well characterised Cr(III), Mn(III) and Fe(III) complexes.[7,67]

The $[Ru_3O(OAc)_6(H_2O)_3]^+$ complex is very soluble in water and the aqua ligands have been shown to be weakly acidic. In acid solutions it is a cation and in alkaline solutions an anion with the first two protons deprotonating at ~ pK_a 4.35 and the third at pK_a >12.[7] In contrast to the more labile aqua ligands the acetate ligands are tightly held as shown by the lack of exchange with trifluoroacetic acid even on boiling for 48 hours.[7] However, chloroacetate derivatives, namely $CH_nCl_{3-n}CO_2H$ (n=0,1 or 2) have been prepared.[70] These species are also very interesting from a practical viewpoint and Sasson and Rempel have shown that $[Ru_3(OAc)_6(H_2O)_3]OAc$ is an active catalyst for the intramolecular conversion of unsaturated carbinols to saturated ketones.[43]

$$RCH{=}CHCH(OH)R' \longrightarrow RCH_2CH_2C(O)R' \qquad (3.3)$$

They also showed that it will catalyse an intramolecular oxidative transfer dehydrogenation [44]

$$\begin{array}{lll} RCH{=}CHCH(OH)R' & & RCH{=}CHC(O)R' \\ + & \longrightarrow & + \\ CH_2{=}CHC(O)R' & & CH_3CH_2C(O)R'' \end{array} \qquad (3.4)$$

Among the trinuclear oxo-centred carboxylates $[M_3O(CO_2R)_6L_3]^+$ (M=V,Cr,Mn,Fe,Co,Ru,Rh or Ir, L=H_2O, CH_3OH, py, etc.) the ruthenium complexes are unique in undergoing reduction first by an electrochemically reversible one-electron step, and secondly by an irreversible two electron reduction that involves loss of the central oxygen atom and which is reversed by oxygen.[7] The dark green $[Ru_3(OAc)_6(H_2O)_3]OAc$ is readily reduced in H_2O or CH_3OH by hydrogen (2 atm/PtO_2), first to a light green solution and then to a yellow solution. The reduction is much faster in CH_3OH, the first stage takes ~1 hour and the second ~3 hours after which a yellow precipitate slowly forms. In water the first stage takes ~ 4 hours giving a light green precipitate which is insouble in water, and ~ 24 hours for reduction to the yellow insoluble complex. Both the light green complex and the yellow precipitate have been isolated and identified, the former is $[Ru_3O(OAc)_6(H_2O)_3]$ and the latter is $[Ru_3(OAc)_6(L)_3]$ (L=H_2O or MeOH) depending on whether it is isolated from H_2O or MeOH.[7] The yellow species in solution are very air sensitive, reacting instantly to form the pale green complex, which

is then more slowly reoxidised back to the dark green complex. Evidence for the lack of the central oxygen atom was obtained in the case of the pyridine derivative.

The reduction of the aqua complex was also studied electrochemically.[7] The first stage of the reduction to the light green species was confirmed to be a reversible one-electron process but the second stage of the reduction , producing the yellow species, could not be inverstigated because of the electrolytic reduction of the solvent.

3.1.3.1 Pyridine and Pyrazine Derivaties

The water molecules in $[Ru_3O(OAc)_6(H_2O)_3]^+$ are readily replaced by pyridine to give the blue complex, $[Ru_3O(OAc)_6(py)_3]^+$ Interestingly , this complex was first reported[66] as $[Ru_3O(OAc)_6(py)_2]$ but was later reassigned correctly as the trimer.[7,67]

The electrochemical behaviour of the pyridine derivative has been established [7] and found to be very similar to that establised by the aqua complex as illustrated in Scheme 3.1. As in the case of the aqua species the first stage of the reduction is a reversible one-electron process to a light green complex. This is followed by an irreversible two electron reduction process to form the yellow complex, $[Ru_3(OAc)_6(py)_3]$. Similarly to the corresponding aqua species this yellow complex can be oxidised to $[Ru_3O(OAc)_6(py)_3]^+$, a process which requires the re-insertion of the bridging oxygen atom. Positive proof for this was obtained for the pyridine derivatives. The experiment was conducted[7] with the butanoate complex, $[Ru_3(O_2CC_3H_7)_6(py)_3]$, which is very soluble in CH_3OH. The complex was treated with a stoichiometric amount of pyridine-*N*-oxide

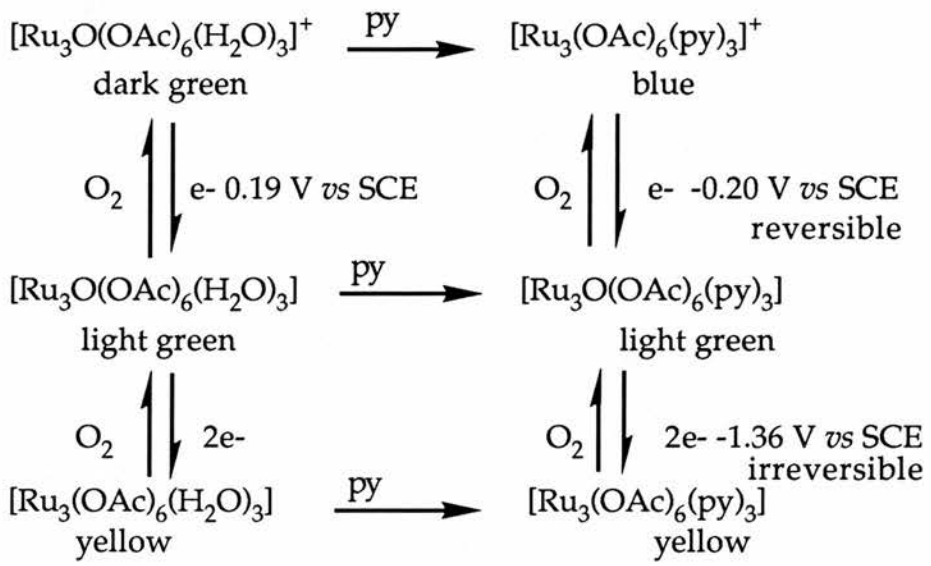

Scheme 3.1:

under air free conditions and within a few minutes the yellow butanoate complex was oxidised to the light green complex. The presence of free pyridine was detected by g.l.c. The possibility of pyridine being derived from the dissociation or decomposition of the complex was ruled out by repeating the experiment using pyridine-*N*-oxide to oxidise the 3-methyl pyridine butanoate analogue. Again g.l.c. measurements showed that the expected amount of free pyridine was formed.

Spencer and Wilkinson[7] have prepared a series of ruthenium trinuclear species in which both the bridging carboxylates and the terminal ligands (L) have been varied systematically to give symmetrically substituted species of the type $[Ru_3O(OAc)_6L_3]^+$. Baumann *et al* [8] later developed a route which would allow for sequential substitution at the terminal site of the complexes. Such a route led to the preparation of the unsymmetrically substituted complexes $[Ru_3O(OAc)_6(py)_2L]^+$ (L = pyr, 4,4' - bpy, BPE, BPA). Their synthetic starting material is $[Ru_3O(OAc)_6(py)_2(CH_3OH)]^+$; the

BPE BPA

methanol group which is weakly bound can be readily replaced by excess ligand (L) under mild conditions. Both the complexes, $[Ru_3O(OAc)_6(py)_2pyr]^n$ (n=+2, 0) have also been isolated following chemical or electrochemical oxidation or reduction of the +1 complex. These species have been characterised by UV-visible spectroscopy, IR, ^1H NMR and X-ray photoelectron spectroscopy. These complexes have an extensive reversible electron-transfer chemistry in CH_3CN, allowing them to exist in a series of redox states, $[Ru_3O(OAc)_6L_3]^n$ (n = +3, +2, +1, 0, -1, -2) A more or less typical cyclic voltammogram of these complexes is represented by that of $[Ru_3O(OAc)_6(py)_2BPE]^+$ in Figure 3.4. The choice of solvent for studying the electrochemical

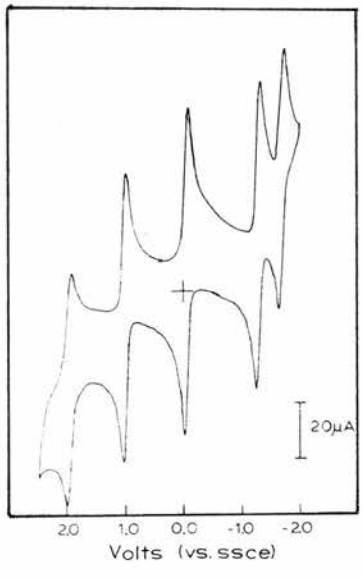

Fig 3.4. Cyclic voltammogram of $[Ru_3O(OAc)_6(py)_3BPE]^+$ at room temperature in 0.1 M TBAH-CH_3CN at scan rate of 500 mV/s.

properties of these species is very important and the use of CH_3CN has allowed Baumann *et al* [8] to identify a series of reversible couples for $[Ru_3O(OAc)_6(py)_3]^+$, in addition to the reversible +/0 couple previously observed by Spencer and Wilkinson[7] using acetone as solvent. In addition to not extending their potential sweep far enough to observe the 2+/1+ couple, the 3+/2+ couple is beyond the solvent limit in acetone. They also reported an irreversible two-electron reduction past the +/0 wave.

UV-visible spectral studies have shown that the +2, +1 and 0 complexes absorb light strongly in the visible region, and the absorption extends into the very near-infrared region for the neutral species. The changes in optical spectra with changes in complex electronic content are very small and suggest that electrons must be gained or lost from extensively delocalised molecular orbitals. ESCA studies have also been done and revealed that all three $[Ru_3O(OAc)_6(py)_3]^n$ (n = 0, +1, +2) complexes have a single Ru $3d_{5/2}$ binding energy and surprisingly only slight shifts in binding energies were observed upon oxidation of the 0 complex to the +1 and +2 species. These results also suggest that the ruthenium sites are equivalent and the complexes are delocalised on the ESCA time scale which is consistent with the UV-visible spectral results.[8]

A more detailed qualitative molecular orbital scheme for the Ru_3O system (Figure. 3.5) based on that first proposed by Cotton and Norman[25] was used to explain the electronic properties of the $[Ru_3O(OAc)_6L_3]^n$ (n = 0, +1, +2)[8] The redox and spectral properties of the complexes can be understood in terms of a series of delocalised, cluster-based π-bonding, π-non-bonding , and π-antibonding levels which are largely Ru-Ru and Ru-O-Ru in character. In the neutral complex, $[Ru_3O(OAc)_6L_3]$, the A_2' level, which is metal-metal anti-

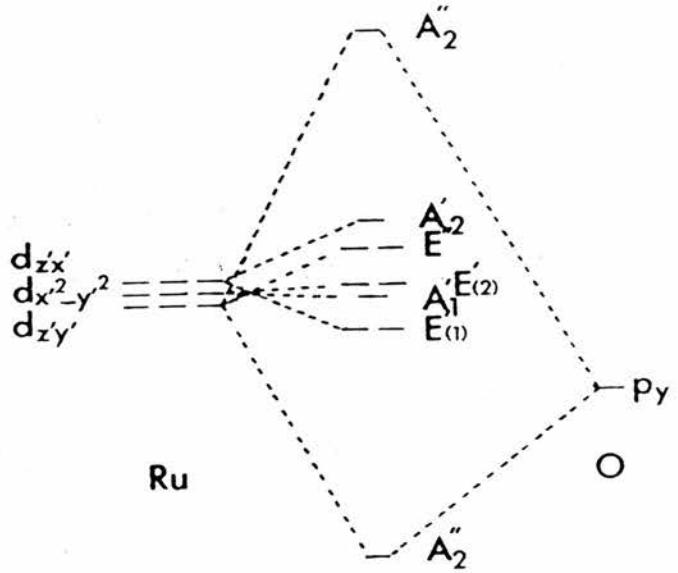

Figure 3.5: Qualitative molecular orbital scheme for the cluster π system in D_{3h} symmetry.

bonding in character, is filled. Oxidation to the +1 and +2 species involves stepwise loss of electrons from the A_2' level. Loss of a third electron to give the 3+ ion occurs at the degenerate E'' levels which are Ru-O-Ru nonbonding in character. Reduction of the neutral complex to the -2 species probably involves electron occupancy firstly of the vacant Ru-O-Ru antibonding A_2'' level, followed closely by occupancy of π^* orbitals deriving from the ligands. Spectral deconvolution studies have shown that the lowest energy visible absorption band consists of three well defined components for the 0, +1 and +2 complexes. These have been assigned to the symmetry allowed $E'' \rightarrow A_2''$ and $A_1' \rightarrow A_2''$ transitions and to the $E_{(1)}' \rightarrow A_2''$ electric dipole-forbidden transition.

The rather interesting complex, $[Ru_3O(OAc)_6(py)_2CO]$, first synthesised by Spencer and Wilkinson[71] has quite different chemical and physical properties from related species. They proposed the unsymmetrical structure in Figure 3.6 on the basis of IR and NMR

evidence and the fact that the complex undergoes an unsymmetrical splitting reaction with PPh_3 to give the dimer $[Ru_2O(OAc)_3(CO)(PPh_3)]$. However, the proposed structure of Fig. 3.6

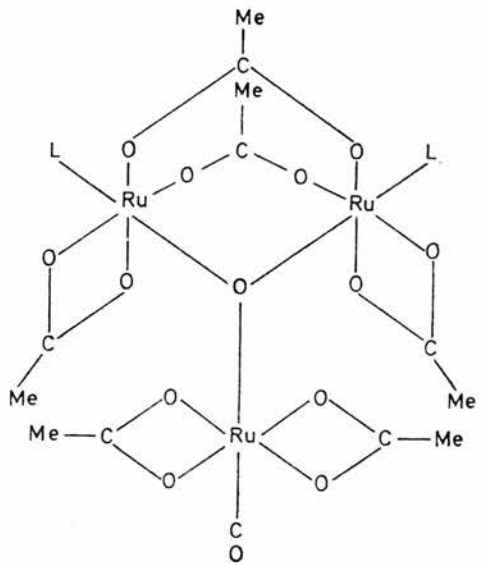

Fig. 3.6: Structure of $Ru_3O(OAc)_6(CO)L_2]$ proposed by Spencer and Wilkinson.[71]

was later challenged by Meyer and coworkers[8] in favour of a more conventional symmetrical structure. The latter group believed that the two carboxylate bands in the asymmetrical stretching region at 1565 and 1599 cm^{-1} may be due to a lowering of the symmetry of the complex and not due to a change from the symmetrical structure to the asymmetrical structure. Their argument is based on comparison of the IR spectrum of the CO complex with those of $[Ru_3O(OAc)_6(py)_6pyr]$, which has an intense band at 1580 cm^{-1} but is absent in $[Ru_3O(OAc)_6(py)_3]$ A similar argument was used to explain its two methyl resonances in the ^1H NMR spectrum. Further support for the retention of the symmetrical structure in the CO complex was provided by chemical reactions. It is prepared from symmetrical

complexes by simple displacement reactions under mild conditions (eqn 3.6).

$$[Ru_3O(OAc)_6(py)_2L] + CO \longrightarrow [Ru_3O(OAc)_6(py)_2CO] \quad (3.6)$$

(L = py or solvent)

Cyclic voltammetric studies[8] have shown that it undergoes two reversible one-electron oxidation. The first oxidation is followed by slower loss of CO to give the complexes $[Ru_3O(OAc)_6(py)_2S]^+$ (S = CH_3OH or CH_3CN) where again the basic cluster structure is retained as shown by their redox and spectral properties.

Although the basic structure unit of the complex may by maintained the CO group has a marked effect on its properties. For example, there are large positive shifts in its $E_{1/2}$ values compared to the tris(pyridine) species. Also the optical spectrum is different and the consistent pattern of cluster electronic transitions is no longer observed in the CO complex. Its unique properties are believed to be due to strong, localised back-bonding from Ru to CO at the single Ru-CO site in the complex.[8] The importance of Ru → CO back-bonding is seen in the lability of the CO group following oxidation to the +1 complex, $[Ru_3O(OAc)_6(py)_2CO]^+$, where the π-electron content has been lowered and the CO group labilised toward substitution. Since CO is bound to a single ruthenium site, the symmetrical electronic structure assumed in the qualitative MO treatment in Fig 3.5 is no longer appropriate.[8]

3.1.3.2 Ligand Bridged Trinuclear Ruthenium Clusters

Baumann *et al* [72] also reported the preparation of the ligand bridged trimeric cluster $\{[(py)_2Ru_3O(OAc)_6(pyr)]_2\{Ru_3O(OAc)_6$-

$(CO)]\}^{2+}$ which involves the replacement of weakly co-ordinated methanol groups either from $[Ru_3O(OAc)_6(CO)(CH_3OH)_2]$ by $[Ru_3O(OAc)_6(py)_2(pyr)]^+$ (eqn 3.7) or from $[Ru_3O(OAc)_6$-$(py)_2(CH_3OH)]^+$ by $[Ru_3O(OAc)_6(CO)(pyr)_3]$ (eqn 3.8)

$$[Ru_3O(OAc)_6(CO)(CH_3OH)_2]^+ + 2[Ru_3O(OAc)_6(py)_2(pyr)]^+ \longrightarrow \{[(py)_2Ru_3O(OAc)_6(pyr)]_2[Ru_3O(OAC)_6(CO)]\}^{2+} + 2CH_3OH \quad (3.7)$$

$$[Ru_3O(OAc)_6(CO)(pyr)_2] + 2[Ru_3O(OAc)_6(py)_2(CH_3OH)]^+ \longrightarrow \{[(py)_2Ru_3O(OAc)_6(pyr)_2[Ru_3O(OAc)_6(CO)]\}^{2+} + 2CH_3OH \quad (3.8)$$

The pyrazine containing starting complexes can act as ligands by being able to bridge through the free nitrogen atom of the pyrazine ligand.

This ligand-bridged complex has a very interesting electrochemistry, revealing a series of ten one-or-two reversible electron waves in the potential region from +2.2 to -1.7 V (*vs* SSCE) in CH_3CN. Both the optical and the redox properties have shown that when its electron content is low (eg +2 oxidation state) that the properties of the cluster are those expected for isolated cluster units where inter-cluster electronic interactions are weak. However the electrochemical results have shown that at negative potential where the electron content of the cluster is high, electronic coupling between the cluster sites is increased. In this potential region the detection of a series of closely spaced, one-electron waves is believed to signal the appearance of band-like behaviour in the cluster.[72]

Baumann *et al* [73] have also reported a series of ligand-bridged cluster dimers of the type $[(py)_2Ru_3O(OAc)_6(L)Ru_3O(OAc)_6(py)_2]^{2+}$ (L = pyr, 4, 4'-bpy, BPE, BPA, py). Their method of preparation is

related to that previously mentioned for the ligand bridged trimer complex $\{[(py)_2Ru_3O(OAc)_6(pyr)]_2[Ru_3O(OAc)_6(CO)]\}^{2+}$ and utilises the lability of the CH_3OH group in $[Ru_3O(OAc)_6(py)_2(CH_3OH)]^+$. Equimolar amounts of this bis(pyridine) methanol complex and $[Ru_3O(OAc)_6(py)_2(L)]^+$ (L = pyr, 4,4'-bpy, BPE, BPA) will lead to the respective bridged dimers. The oxidised and reduced forms of the dimers can be prepared readily by chemical or electrochemical oxidation or reduction.[73] The mixed - valence cluster dimers like $[(py)_2Ru_3O(OAc)_6(pyr)Ru_3O(OAc)_6(py)_2]^+$ can also be prepared, by simply mixing solution containing the corresponding 0 and +2 dimers and the 3+ can be prepared by mixing equimolar amounts of the 4+ and 2+ ions.

Cyclic voltammetry has shown that the extensive reversible redox chemistry of the individual clusters also appears in the dimers, but is even more complex. Both the UV-visible spectral and redox potential data suggest that the delocalised intramolecular electronic structure of the cluster sites is maintained in the dimers.[73] Relative to the strong electronic coupling within the clusters, intercluster interactions are relatively weak and depend on the bridging ligand and on the electron content of the clusters. As shown by cyclic voltammetry the $[(py)_2Ru_3O(OAc)_6(pyr)Ru_3O(OAc)_6(py)_2]^{2+}$ complex shows broad waves at anodic potentials (+2.05 and +1.07 V *vs* SSCE) corresponding to two slightly separated one-electron waves and are indicative of weak cluster-cluster interaction across the ligand. However, as the electron content of the system increases *i.e.* at more cathodic potentials, two pairs of electrochemically reversible one-electron waves appear indicating significant cluster-cluster interactions. In the mixed-valence dimers $[(py)_2Ru_3O(OAc)_6(pyr)$-$Ru_3O(OAc)_6(py)_2]^{n+}$ (n = 1,3) it is believed that discrete, localised

($[Ru_3O]^+$ and $[Ru_3O]^o$ or $[Ru_3O]^{2+}$ and $[Ru_3O]^+$) cluster sites exist and evidence for low-energy cluster-cluster charge transfer or intervalence transfer (IT) absorption bands were provided by difference spectra in the near-IR region. However, the authors did not make any attempt to look for new low-energy bands for the +1 or +3 dimers where the bridging ligand is 4,4' -bpy, BPE or BPA. The reason being that if IT bands exist in the dimer for these ligands they are expected to be weaker and occur at higher energies than for L = pyr and obscured by the intramolecular cluster transitions. Further support in favour of discrete, localised $[Ru_3O]^+$ and $[Ru_3O]^o$ in the +1 pyr dimer was provided by the ESCA studies. Although not definitive, the IR spectrum of the solid indicated localised redox sites. However, the situation might be different in the -1 pyr dimer; intercluster electronic coupling increases with electron content and there may be enough in this to cause delocalisation. Unfortunately, reliable optical spectra of the reduced species could not be obtained due to their extreme air sensitivity.[73]

3.1.3.3 Isonicotinamide Derivatives

Fairly recently, Toma and Cunha[74] have reported the electrochemical and spectroelectrochemical properties of the water soluble trinuclear complex, $[Ru_3O(OAc)_6(iso)_3]$, in both aqueous and acetonitrile solutions. As in the case of the substituted pyridines and related complexes previously discussed, this complex also has an extensive irreversible electron transfer chemistry. As revealed by cyclic voltammetric studies, it gives five successive reversible electron transfer waves in the region of -1.5 to +2.3 V (*vs* SHE) in acetonitrile (Figure 3.7).[74] These waves have been assigned to the successive μ-

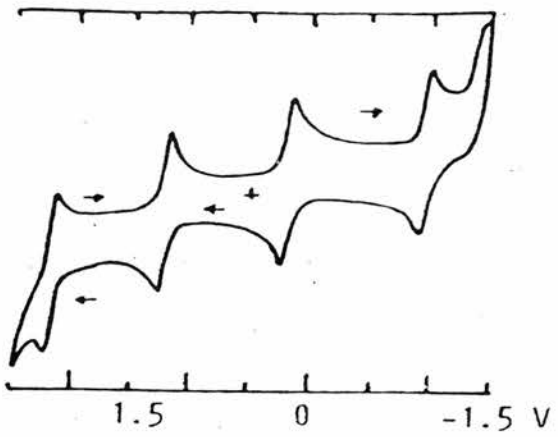

Fig 3.7: Cyclic voltammogram of $[Ru_3O(OAc)_6(iso)_3]$ in acetonitrile, $[NEt_4ClO_4] = 0.10$ M, [Complex] = 2×10^{-3} M, scan rate = 100 mVs^{-1}

oxo $Ru^{IV}Ru^{IV}Ru^{III}$/ $Ru^{IV}Ru^{III}Ru^{III}$/...$Ru^{III}Ru^{II}Ru^{II}$ redox couples with E^o = 2.16, 1.21, 0.19, -0.98 and -1.4 V. The cyclic voltammetric studies carried out in aqueous solution have shown that at pH>8, the μ-oxo $Ru^{III}Ru^{III}Ru^{II}$ complex undergoes reversible reduction to the μ-oxo $Ru^{III}Ru^{II}Ru^{II}$ complex (E^o = -0.85 V). The reduction of the $Ru^{III}Ru^{III}Ru^{II}$ complex was found to be pH dependent and below pH 4 the reduction proceeds *via* two electrons in a successive way, involving intermediarily a proton dependent step to yield the $Ru^{II}Ru^{II}Ru^{II}$ species without the central oxygen atom. The starting μ-oxo bridged $Ru^{III}Ru^{III}Ru^{II}$ complex can however be regenerated by reversing the potential scan. Support for the lack of the central oxygen was based on the electrochemical behavior of the complex in acetonitrile solutions and comparison with the results reported by Spencer and Wilkinson[7] for the $[Ru_3O(OAc)_6(py)_3]^+$ complex. It is believed that these μ-oxo bridged species are stable above pH 4 but the elimination of the central oxygen atom is favoured below this pH, leading to an $Ru^{III}Ru^{II}Ru^{II}$

intermediate which is further reduced to the $Ru^{II}Ru^{II}Ru^{II}$ complex, at the applied potentials.

The species involved in the electrochemical measurements were characterised by spectroelectrochemical measurements in CH_3CN, and the spectra of the various species are displayed in Figure 3.8.[74] The spectroelectrochemical behavior was found to be reversible except for the μ-oxo $Ru^{III}Ru^{II}Ru^{II}$ and $Ru^{II}Ru^{II}Ru^{II}$ complexes, which could only be detected as transient species. They are believed[74] to react with trace amounts of water to form the corresponding complexes in which the bridging oxygen atom is missing as in the case of the pyridine analogue.[7,71] The electronic transitions of the species were accounted for by the qualitive MO scheme proposed by Cotton and Norman[25] and by Bauman *et al* [8] for the triangular Ru_3O unit (see Figure 3.5)

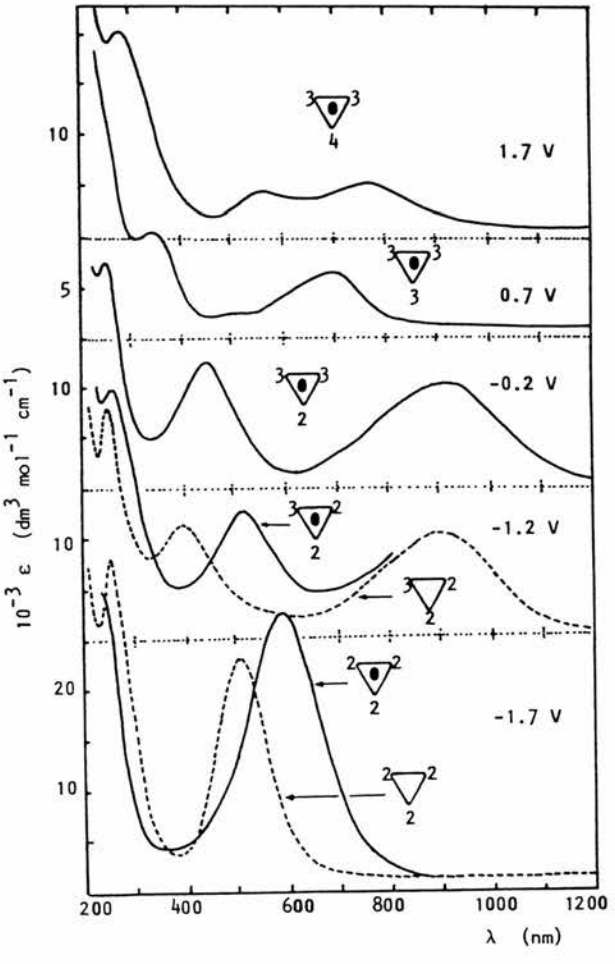

Fig.3.8: Spectroelectrochemical behaviour of $[Ru_3O(OAc)_6(iso)_3]$ in CH_3CN at different potentials (V *vs* SHE), $[NEt_4ClO_4]$ = 0.1 M, 25 °C, μ-oxo species (solid line), loss of the central oxygen (---).

3.1.3.4 Phosphine Derivatives

The green $Ru_3O(OAc)_6(PPh_3)_3$ was originally thought[66] to be a dimer and the formula $Ru_2(OAc)_4(PPh_3)_2$ was proposed. This dimeric compound, yellow in colour was however later synthesised by reacting PPh_3 with $\{Ru_3(OAc)_4Cl\}_n$ in methanol.[75] The trimeric phosphine derivative, $Ru_3O(OAc)_6(PPh_3)_3$, can be prepared by reacting PPh_3 with $Ru_3O(OAc)_6(H_2O)_3^+$ or more rapidly from the reaction between the reduced form of the aqua complex and PPh_3.[7,67] The isostructural propanoate and butanoate complexes are also known.[7] A simplified reaction scheme for the preparation of these phosphine adducts is illustrated below.

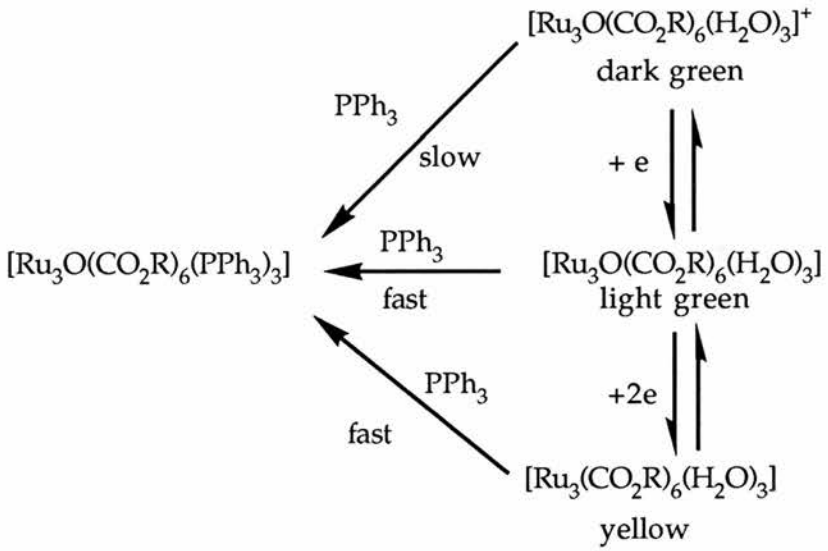

Scheme 3.2

The tris(triphenylphosphine) adduct, $Ru_3O(OAc)_6(PPh_3)_3$, has been firmly established as being Ru(III,III,II), although the X-ray structure[25] indicates that the Ru ions are equivalent. The metal-metal distance is 3.320Å which is large enough to preclude any direct metal-metal interaction. The diamagnetism of the complex indicates that

there must be electron delocalisation *via* the Ru_3O framework. Electronic spectral data for $Ru_3O(O_2CR)_6(PPh_3)_3$ (R = CH_3, C_2H_5 and C_3H_7) are shown in Table 3.1.

Table 3.1: Electronic Spectra of $Ru_3O(O_2CR)_6(PPh_3)_3$ Complexes in $CHCl_3$

Complex (R=)	λ_{max} / nm	ε / $M^{-1}cm^{-1}$	Ref
CH_3	752	4800	25
	400	10000	
	380	11000	
	974	6280	7
	790(sh)	-----	
	410(sh	-----	
	347	11900	
C_2H_5	974	663	7
	790(sh	----	
	410(sh)	-----	
	343	12000	
C_3H_7	974	5060	7
	790(sh	-----	
	410(sh)	-----	
	338	12200	

Solutions of $Ru_3O(OAc)_6(PPh_3)_3$ undergo an irreversible two-electron electrochemical reduction at more negative potential than the pyridine or aqua abducts.[7,75] Attempts to reduce the phosphine adduct in CH_3OH by H_2 at 2 atm in the presence of Adam's catalyst at room temperature failed but the reduction was successful at 40 °C in

ca. 3 h to give a yellow solution.[75] The reduction also occurred in CH_3OH containing HBF_4 in 6-8 h at 1 atm and *ca.* 45 °C.[66] The reduced solutions are extremely air sensitive and unlike the similar yellow solutions obtained when H_2O and pyridine are ligands and which are trimeric species without the central oxygen atom, the yellow phosphine solutions cannot be re-oxidised with molecular oxygen to the oxo-centred complex. The failure of the reduced solutions of $Ru_3O(OAc)_6(PPh_3)_3$ to re-oxidise to the original complex, suggests that breakup of the trinuclear structure has occurred, possibly to $Ru(OAc)_2(PPh_3)(CH_3OH)_n$.[7,75]

3.1.3.5 DMF Derivatives

The kinetics and mechanism of the hydrogenation of $[Ru_3O(OAc)_6(DMF)_3]^+$ has been the subject of a detailed investigation.[76] The tris(DMF) adduct was found to undergo three sequential reduction with molecular hydrogen in DMF at 80 °C and the first stable reduction product is thought to be $[HRu_3O(OAc)_5(DMF)_3]^+$ formed *via* a heterolytic cleavage of H_2 by $[Ru_3O(OAc)_6(DMF)_3]^+$. Unlike the $Ru_2^{III}Ru^{II}$ phosphine adduct this is very easily re-oxidised by oxygen, and also by acids. The second stage of the reduction yielded another air sensitive product which, however, does not re-oxidise to a trimer and a ruthenium (I) dimer has been suggested instead. Decarboxylation of DMF also occurs during the second stage of reduction and / or isolation of the ruthenium (I) species. The dimeric ruthenium (I) species were isolated from the DMF solution as a mixture of $[Ru_2(OAc)_2(CO)_4L_2]$ (L = PPh_3, $SbPh_3$, py, etc.) and $[Ru_2(OAc)_2(HOAc)(CH_3OH)]$. The final products are a mixture of $[Ru(OAc)(CO)_2L_2]$ and $[RuH(CO)_3]_n$.

In separate studies it was shown that these reduced solutions are effective in catalysing the hydrogenation[40,75] and isomerisation[77] of olefins.

3.1.4 Mixed-Metal Ruthenium μ_3-Oxo Carboxylate complexes

The metal complexes $[Ru_2RhO(OAc)_6L_3]^+$ (L = H_2O or py) have been prepared and their mixed metal structures were confirmed by different spectroscopic techniques.[30] The aqua species was prepared by refluxing $RuCl_3.3H_2O$ and $RhCl_3.3H_2O$ with aqueous methanolic acetic acid in the presence of either sodium acetate or silver acetate. The homonuclear rhodium (III,III,III) and ruthenium (III,III,III) species were obtained as well in this preparation and separation was effected using cation-exchange chromatography (Dowex 50W-X2) or preparative ligand chromatography using a JAIGEL - ODS (A-343-10) column. Complete separation of the complexes was achieved using the latter technique but not with the Dowex resin, even after more than 3 weeks. Nevertheless, pure samples of the mixed-metal species were obtained from the Dowex column by collecting the complex in several fractions, the absorption spectra of which were carefully measured in order to find the purity of the complex. The aqua species can be converted to the pyridine complex by refluxing with pyridine. Surprisingly, the corresponding mixed-metal $RuRh_2$ species was not observed by these synthetic routes and its lack of detection may be related to the mechanism of the formation of the trinuclear species.[30]

So far no X-ray crystal structure of this mixed-metal complex has yet been reported but X-ray powder pattern of the pyridine complex is very similar to those of the corresponding homonuclear

ruthenium and rhodium complexes. Conclusive evidence that this species is a true mixed-metal compound was however provided by ^{1}H and ^{13}C NMR spectroscopy.[30] The methyl proton signal of the co-ordinated acetate appears as a sharp singlet for the aqua and the pyridine complexes of Ru_3 and Rh_3, but those for Ru_2Rh split into two peaks in a ratio of 1:2. The splitting of the pyridine signals also provided support for the mixed-metal structure.

The X-ray photoelectron spectra of the mixed-metal complex was also investigated and comparisons of the XPS peak intensities with those of the Rh_3 and Ru_2 complexes confirmed that the ratio of ruthenium to rhodium in the mixed-metal complex is 2:1. The XPS data also indicated that a charge shift does not occur in this mixed-metal species which is different to that observed in the series $[M_3O_2(OAc)_6(H_2O)_3]^{2+}$ (M=Mo_3, W_3, Mo_2W, MoW_2). The absence of any charge shift is believed to be consistent with the much weaker metal-metal direct interaction of these types of trinuclear complexes.[30] The electronic absorption spectra of the mixed-metal complexes have been studied and accounted for by a suitable molecular orbital scheme. Both the aqua and pyridine complexes of the Ru_3Rh exhibit strong absorption bands in the visible region as do the Ru_3 complexes but not the Rh_3 species. However, the strong absorption band of lowest energy appears at a shorter wavelength for the Ru_2Rh complex than for the Ru_3 Complex. These bands have been attributed as before to the intracluster transitions, namely the transition between the metal $d\pi$ orbitals and the μ-oxo $p\pi$ orbital.[30]

The IR spectra of these species are also interesting and the ν_{asym} (CO_2^-) region shows distinct differences for the three different trinuclear cores. Whereas the Ru_3 and Rh_3 aqua complexes show sharp band at 1560 and 1600 cm^{-1}, respectively, that of the Ru_2Rh exhibit

two peaks at 1592 and 1570-^{1}cm-^{1}. The pyridine complexes display similar features.[30]

The Ru_2Rh complex has been studied electrochemically and three reversible one-electron redox waves have been detected in the region from -2 to +2 V *vs* Ag/Ag^+ in CH_3CN. Interestingly, it has two successive oxidation processes at potentials nearly identical with those of the Ru_3 species. It was thus concluded that the rhodium ion in the mixed-metal complex does not play a significant role in the observed redox process.[30]

3.1.4.1 Substitution Studies on the Terminal Ligands

At the commencement of this work, few if any detailed studies on the rates of substitution at the terminal L sites had been reported. A number of qualitative observations had given an indication of relative rates. For example, the much faster rates of replacement of H_2O by Ph_3P in $[Ru_3O(OAc)_6(H_2O)_3]$ in contrast to $[Ru_3O(OAc)_6(H_2O)_3]^+$ being one example[7] although the accompanying redox reaction to give the neutral Ru_3(III,III,III) complex in the latter case makes a detailed assessment difficult. One can nevertheless deduce that substitution of the H_2O's in the Ru_3(III,III,III) complex must be somewhat slower.

Ready displacement of water by pyridine in $[Ru_3O(OAc)_6(H_2O)_3]^+$, on heating, gave an indication that substitution rates are indeed probably quite slow at room temperature.[7] Sasaki *et al* [30] finally reported details of kinetic studies on the rate of substitution of water by CD_3OD on the complexes: $[M_3O(OAc)_6(H_2O)_3]^+$) M = Ru_3, Rh_3, Ru_2Rh) using ^{1}H NMR. They observed changes in the ^{1}H NMR spectrum of the complex with time indicative of a multistep process involving successive replacement of

water by CD_3OD, at the different atoms. Interestingly rate constants (21 °C) determined for the homo Ru_3 and Rh_3 complexes were respectively 5.6 x 10^{-4} s^{-1} and 1 x 10^{-3} s^{-1}; roughly an order of magnitude greater than the rate constants (21 °C) for substitution of water respectively at the Ru and Rh sites in the Ru_2Rh mixed-metal complex; 6 x 10^{-5} s^{-1} (Ru), 1.2 x 10^{-4} s^{-1}(Rh), after allowance for statistical factors. These findings indicate some change in the nature of the metal sites within the mixed-metal cluster, which must be a consequence of an interaction between the two metals. Such presumed subtle effects have still to be understood emphasising the need for more studies in this area. A final point of note is the much faster rates of substitution of water in the late element complexes; $[M_3O(O_2CR)_6(H_2O)_3]^+$ (M = Ru, Rh) *versus* those typically observed for substitution of water in simple mononuclear compounds of these elements.[79]. This is in contrast to the behaviour of the early element 'cluster' complexes $[M_3O_2(O_2CR)_3(H_2O)_3]^{2+}$ (M = Mo, W) which show correspondingly more inert behaviour; presumably due to the steric hindrance at the Mo and W centres. This steric crowding may not be so extensive in the case of the more expanded planar μ_3-O derivatives and as such electronic effects may take over as responsible for the greater lability observed. It was clear that further supportive data was needed in order to verify and understand these factors.

3.2 EXPERIMENTAL

3.2.1 Preparation of Reagents

Manganese (II) triflate was prepared by neutralisation of trifluorumethanesulphonic acid (triflic acid) (Fluorochem) solution with manganese (II) carbonate (May and Baker, reagent grade) followed by recrystallisation two or three times from water. The sodium salt of triflic acid was prepared in a similar manner but using sodium carbonate (BDH, reagent grade) instead. This salt was also recrystallised two or three times from water.

3.2.2 Standardisation of Reagents

Sodium triflate ($NaCF_3SO_3$) solutions were standardised by ion exchange onto Amberlite IR (H) 120 resin (BDH, analytical grade) and the H+ released was titrated with standard sodium hydroxide (Convol, BDH) using phenolphthalein as indicator.

3.2.3 Measurement of pH

The pH of the solutions was measured by using a Radiometer PHM 82 pH meter and a Russell CWR/320/757 glass/Ag/AgCl electrode having a narrow stem. The pH meter was calibrated with solutions at pH 2 and 4 at I = 1.0 M ($NaCF_3SO_3$).

3.2.4 Instrumentation

Ultraviolet and visible spectra were recorded in 1.0-cm quartz cells on a Perkin Elmer Lambda 5 spectrophotometer having auto-cell facilities for kinetic measurements and fitted with electronic thermostatting (± 0.1°C). Infra-red spectra were recorded as KBr discs on a 1710 Perkin Elmer Fourier Transform spectrometer.

3.2.5 Preparation of Complexes

3.2.5.1 Preparation of (μ_3-Oxo) hexakis (μ-acetato)tri-aquatriruthenium(III) acetate, $[Ru_3O(OAc)_6(H_2O)_3]OAc$.

The crude complex was prepared according to the method of Legzdins et al.[66] A solution of $RuCl_3.xH_2O$ (Johnson Matthey, 2g) and sodiun acetat trihydrate (BDH,reagent grade; 4g) in glacial acetic acid (May and Baker, Pronalys; 50 ml) and ethanol (50 ml) was refluxed, whereupon the red-violet colour changed to dark green after 4 hours. The solution was then cooled to -30 °C for approximately 4 hours, and the precipitate of sodium acetate and sodium chloride was removed by filtration. The filtrate was evaporated on a rotary evaporator, dissolved in methanol, filtered, and again evaporated. The complex was still impure at this stage and purification was effected by recrystallisation from methanol-acetone mixture. The UV-visible spectrum of the resulting complex in CH_3OH corresponds fairly well with the published spectrum.[7] The values found are as follows:

$$\lambda_{max} = 686 \text{ nm } (\varepsilon = 1105 \text{ M}^{-1}\text{cm}^{-1})$$

The corresponding literature values are:[7]

$$\lambda_{max} = 686 \text{ nm } (\varepsilon = 1100 \text{ M}^{-1}\text{cm}^{-1})$$

The complex was also characterised by elemental analysis.

	Anal. calcd. for $Ru_3C_{14}H_{27}O_{18}$	
	C	H
	21.40	3.40
Found:	21.17	3.63

3.2.5.2 Preparation of (μ_3-Oxo) hexakis(μ-acetato) tri-aquatriruthenium (III) perchlorate, $[Ru_3O(OAc)_6(H_2O)_3]$-ClO_4.

The perchlorate salt was prepared from the crude acetate salt by employing cation exchange chromatographic techniques.[30] The complex was dissolved in water and to ensure that the complex was in the +1 form the pH was adjusted to approximately pH 2.5 with dilute $HClO_4$. The green complex solution was then passed down the cation-exchange column (Dowex 50W-X2), whereby a greenish solution emerged from the column, while a blue band was retained. The UV-vsible spectrun of thegreen solution not held by the column shows a broad band between 640 - 800 nm and another broad band between 340 - 440 nm. This spectrum differs significantly from that of $[Ru_3O(OAc)_6(H_2O)_3]^+$. The blue ion was eluted with either 2M $HClO_4$ or 2M $NaClO_4$ and the eluate was evaporated to give purple-blue lustrous crystals of the perchlorate salt. The complex was characterised by both UV-visible and IR spectroscopy the spectra of which agrees very well with those reported in the literature.[7,49] The complex was also characterised by elemental analysis, the results of which fitted to the formula $[Ru_3O(OAc)_6(H_2O)_3]ClO_4.HClO_4.H_2O$.

Anal. calcd for $C_{12}H_{27}O_{25}Ru_3Cl_2$

	C	H
	15.24	2.88
Found:	15.20	2.78

Crystals suitable for single crystal X-ray diffraction studies were subsequently obtained (see page 216).

3.2.5.3 Preparation of (μ_3-oxo) hexakis(μ-acetato)tris-isonicotinamide triruthenium (III) hexafluorophosphate, $[Ru_3O(OAc)_6(iso)_3]PF_6$.

0.04 g of the acetate salt was dissolved in the minimum volume of water and an excess of isonicotinamide (0.03 g) was added to the solution. The solution was then heated for ~ 10 minutes and then allowed to cool. During the cooling process solid NH_4PF_6 was added until a blue precipitate started to appear. The solution was cooled further and the blue solid filtered and washed with ether and dried in vacuo. The complex was characterised by its UV-visible spectrum The values found are as follows:

λ_{max} = 700 nm (ε = 6300 $M^{-1}cm^{-1}$)

These values are in close agreement with those reported in the literature.[74] The complex was also characterised by elemental analysis. Anal. calcd for $Ru_3C_{30}H_{26}N_6O_{16}PF_6$

	C	H	N
	30.4	3.10	7.10
Found:	28.11	2.72	6.58

3.2.6 Crystal Data for $[Ru_3O(OAc)_6(H_2O)_3]ClO_4.HClO_4.H_2O$

$C_{12}H_{27}Cl_2O_{25}Ru_3$, mol. wt. 945.42, monoclinic, space group $P2_{1/n}$, a = 11.121(13)Å, b = 15.480(13)Å, c = 17.190(21)Å, β = 91.72(10)°, V = 2959 $Å^3$ (by least-squares refinement on diffractometer

angles for 20 reflections in the range $15° < 2\theta < 28°$ with Mo-K_α radiation, $\lambda = 0.71073Å$), $D_c = 2.123$ g cm^{-3}, Z = 4, red octahedron 0.29 x 0.31 x 0.45 mm, $\mu = 1.76$ mm^{-1}.

3.2.6.1 Data Collection and Processing

The crystal structure data were collected on a Siemens R3m/v diffractometer: ω scan mode with variable scan speed, 1.50 to 14.65 °/min in ω; graphite– monochromatized Mo-Ka radiation; 3056 unique data $2.0 < 2\theta < 50$ °, +h, +k, ±l, 2019 with $F > 6.0\ \sigma$ (F). No significant crystal decay was found. Lorentz and polarization corrections were applied to the data as well as an empirical absorption correction.

3.2.6.2 Structure Analysis and Refinement

The structurewas solved using a Patterson synthesis to the Ru atoms (SHELXTL). Other non-hydrogen atoms were located after successive Fourier synthesis and least-squares refinements. Hydrogen atoms were placed in calculated positions on the cation using a riding model. The Cl and O atoms of the two prechlorate/perchloric acid molecules could be located easily but it was not possible to suggest which of these might be the perchloric acid of crystallisation. One water of crystallisation per asymmetric unit was located. There is evidence from the residual electron density (+3.13 $eÅ^{-3}$ and -1.92 $eÅ^{-3}$ in the final difference map) that there may be more lattice water dissolved throughout the crystals. The crystals themselves showed some evidence of non-crystallinity and possibly twinning in that their reflection profiles were not smooth. It is not possible to say whether this is because of long range lattice disorder or a twinning problem. However, the overall crystal structure of the Ru_3O moieties and the ClO_4 groups can be deduced from the diffraction data obtained, yielding R values of

11.82% and weighted R = 13.36% (weight = $1/[\sigma^2(F) + 0.01485\ F^2]$. In view of the indifferent quality of the data obtainable only the Ru atoms were refined anisotropically. Final data/parameter ratio = 11.0:1. The atomic coordinates with the equivalent isotropic displacement coefficients are shown in the appendix (Table A1) and the anisotropic displacement coefficients are listed in Table A2.

3.2.7 Oxygen-17 NMR Measurements of Water Exchange on $[Ru_3O(OAc)_6(H_2O)_3]^{+}$.

This study was conducted at 25 °C using oxygen 17 isotopic enrichment on 2 cm^3 solutions (0.02 M per Ru_3) at $[H^+]$ = 0.60 M, I = 1.0 M ($NaClO_4$, BDH). Oxygen-17 NMR spectra were recorded up to a total enrichment of 6 atom % following mixing in 10 mm o.d. sample tubes at 40.56 MHz using a Bruker AM-300 spectrometer. Manganese (II) triflate was added prior to mixing with $H_2{}^{17}O$ (Yeda) in order to remove the intense ^{17}O resonance line of bulk water by paramagnetic exchange broadening. Corrections for shifts due to the presence of Mn^{2+} were made assuming a value for ClO_4^- +288 *versus* free water (measured by independent experiments in the absence of Mn^{2+}).at 25 °C The sample was allowed to equilibrate at 25 °C for about 5 minutes before the accumulations were commenced. Conditions were the same as reported in Chapter 2. Spectra were taken at timed intervals and the peak heights were measured and normalised against the height of the non-exchanging ClO_4^- counter ion peak (natural abundance) The peak height is thus reported as the ratio of the height of the exchanging bound H_2O peak to the height of the ClO_4^- peak.

3.2.7.1 Kinetic Analysis

The reaction for an isotopic exchange reaction at an aqua ion can be represented by equation (3.9).

$$M(H_2O)_n^{m+} + nH_2O^* \underset{}{\overset{k_{ex}}{\rightleftharpoons}} M(H_2O^*)_n^{m+} + nH_2O \quad (3.9)$$

The rate constant for exchange of a particular water molecule was obtained by fitting the data (height of H_2O peak / height of ClO_4^- peak *vs* time) to a first-order exponential curve using GraFit.

3.2.7.2 Kinetic Studies of Complexation of Isonicotinamide with $[Ru_3O(OAc)_6(H_2O)]^+$

This reaction was monitored at 360 nm in the presence of excess (>>-fold) isonicotinamide over the complex in order to permit pseudo first-order kinetics, and the data were treated with the assumption that stastical kinetics apply. Each solution was adjusted to an ionic strength of 1.0 M using $NaCF_3SO_3$. For each run the required amounts of $NaCF_3SO_3$ and isonicotinamide were added in a 1-cm quartz cell. The solution wasd then adjusted to the desired pH using dilute triflic acid and / or dilute NaOH as needed. The calculated amount of complex was then added and the solution made up to 3-cm^3 with distilled water. The cuvette was then placed inside the cell holder of the UV-visible spectrophotometer and allowed to fully equilibrate for 15 minutes at the set temperature before absorbance *vs* time readings were commenced. The pH of each solution was measured after the runswere completed and in each case there was close agreement between the starting and final pH (within 0.05 pH unit). The pseudo-first order rate constants, kobs., were computed from the slope of the $\ln(A_\infty - A_t)$ vs time plot by a least -

squares treatment of the data.

3.3 RESULTS AND DISCUSSION

3.3.1 Structure Description and Discussion of $[Ru_3O(OAc)_6(H_2O)_3]ClO_4.HClO_4.H_2O$

The solid compound is characterised by crystallisation of water and $HClO_4$ molecules. This property is due to the preparation of the crystals from 2M $HClO_4$.

The crystal packing is shown in Figure 3.9. It is clear that an extensive network of hydrogen bonds (dotted lines) exists between the coordinated water molecules and the ClO_4^- ions. The bond distances and angles are reported in Table A3 and A4, respectively, in the Appendix.

The Ru_3O core shows a regular geometry (Fig. 3.10). The ion has an equilateral arrangement of ruthenium atoms with a central μ_3-oxygen atom In addition each pair of ruthenium atoms is bridged by two carboxylates and the coordination sphere is completed by a single H_2O molecule coordinated to each metal atom. The crystallographic evidence that it is three Ru(III) atoms is that the Ru-Ru distances, and the Ru-O (central oxygen) distances are equivalent within errors. In view of the large errors on the Ru-O(H_2O) distances, these are also equivalent. These points are clearly indicated by the data in Table A3, (see Appendix). The averaged Ru-Ru bond distance (3.298Å) is very close to those of other μ_3-oxo trinuclear carboxylate species. The structural data for this trinuclear ruthenium species is compared with some other (μ_3-O) bonded trinuclear carboxylates in Table 3.2

In view of the equivalence of the ClO_4^- ions the complex is probably best formulated as $H[Ru_3O(OAc)_6(H_2O)_3](ClO_4)_2.H_2O$ implying a mobile proton. However, there is little chemical doubt that this species is a $Ru(III)_3$ trimer since cyclic voltammetry on the crystals

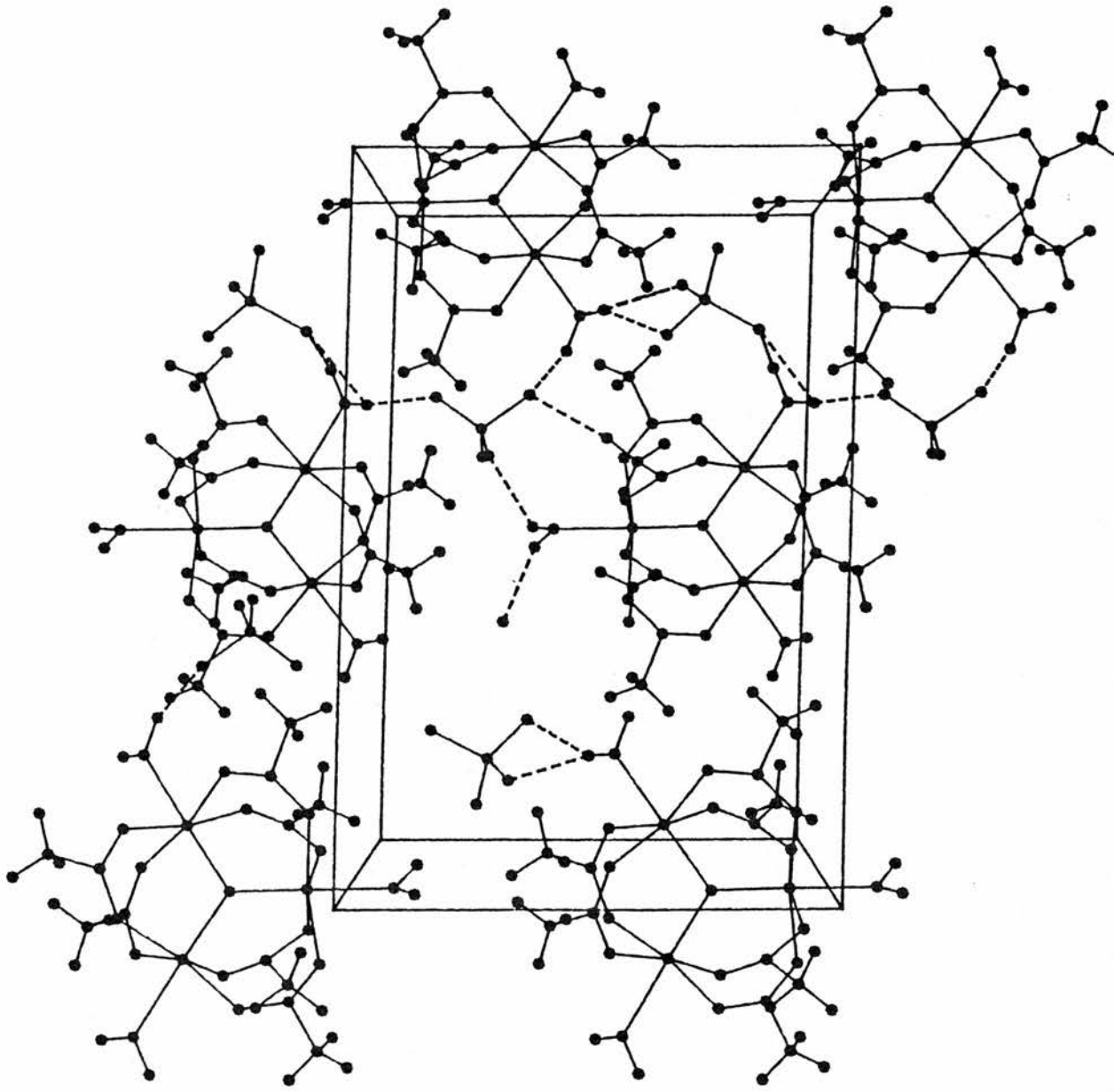

Fig. 3.9: Crystal packing of the $[Ru_3O(OAc)_6(H_2O)_3]^+$ ion. The hydrogen bonds are represented by dotted lines.

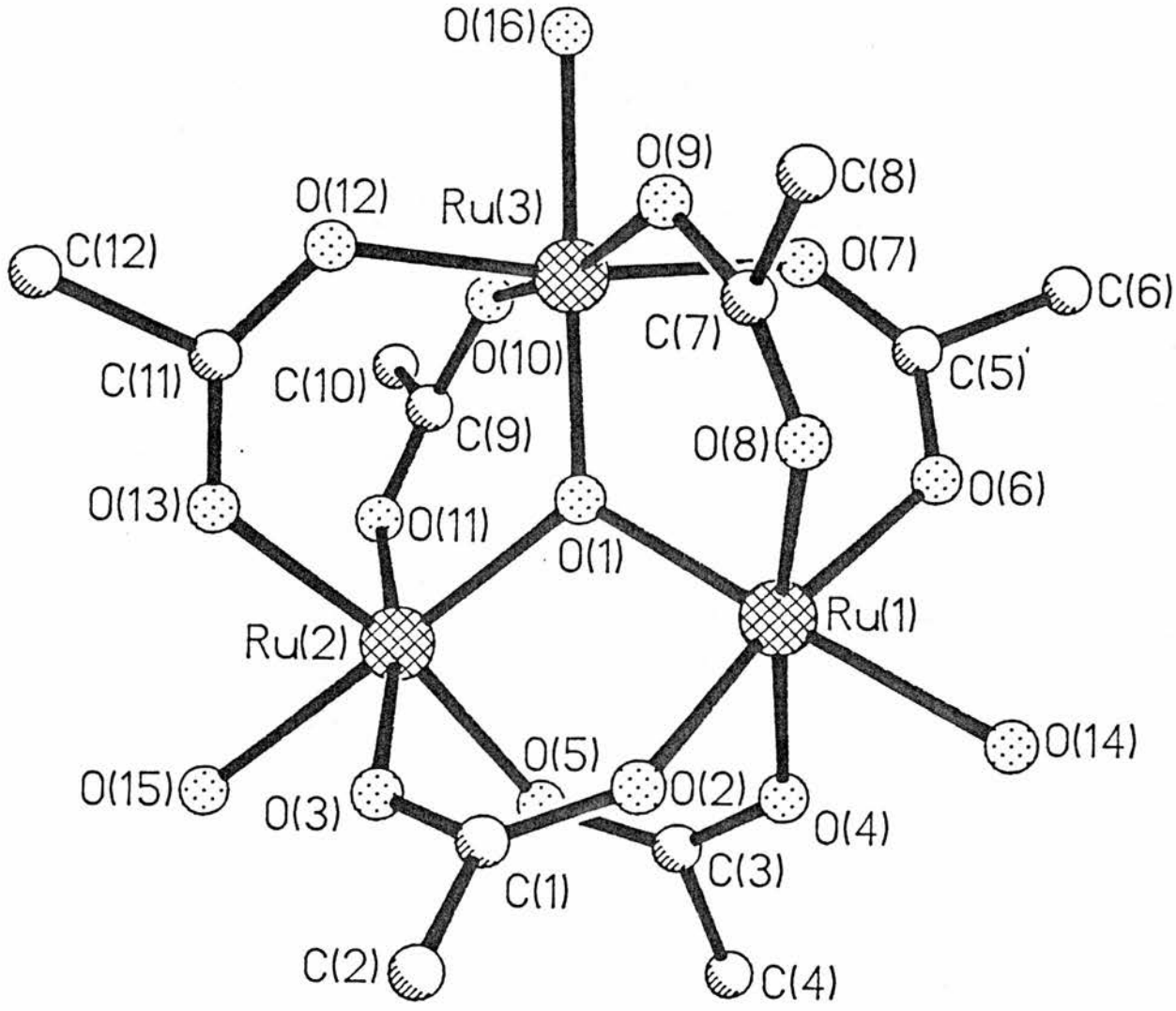

Fig.3.10:View of the trinuclear unit of $[Ru_3O(OAc)_6(H_2O)_3]^+$ indicating the numbering scheme.

Table 3.2: Structural Data for Some Planar (μ_3 - O) Bonded Trinuclear Metal Carboxylat

Compound	Space group	M-(μ_3-O) (Å)	M-O[a] (Å)	M···M (Å)	Ref.
(a) M_3^{III} Complexes					
$[Cr_3O(OAc)_6(H_2O)_3]Cl.6H_2O$	$P2_12_12$	1.89	1.97	3.28	3a
$[Fe_3O(OAc)_6(H_2O)_3]ClO_4$	$P2_1/C$	1.91	2.02	3.29	5
$[V_3O(CH_2ClCO_2)_6(H_2O)_3]ClO_4$	$P2_1/C$	1.93	2.01	3.337	2a
$[Ru_3O(OAc)_6(H_2O)_3]ClO_4.HClO_4.H_2O$	$P2_1/n$	1.91	2.02	3.298	This wor
$[Rh_3O(OAc)_6(H_2O)]ClO_4.2H_2O$	$P2_1/C$	1.923	2.01	3.33	10
(b) $M_2^{III}M^{II}$					
$[Fe_3O(OAc)_6(4\text{-Mepy})_3].C_6H_6$	R32	1.907	2.069	___	23
$[V_3O(OAc)_6(py)_3]$	R32	1.927	2.04	3.337	2b
$[Mn_3O(OAc)_6(py)_3]$	R32	1.941	2.07	3.363	20
$[Ru_3O(OAc)_6(PPh_3)_3]$	P1	1.92	2.06	3.320	25

[a]M-O-Carboxylate, averaged distances

in water show that the $Ru(III)_3$ to Ru(III,III,IV) redox process is an oxidation for the complex. Furthermore the UV-visible spectrum matches that of the $Ru(III)_3$ species which is significantly different from that of the Ru(III,III,IV) (*cf.* spectra for $[Ru_3O(OAc)_6(iso)_3]+$ (iso = isonicotinamide) and its oxidised and reduced forms).[74] The result of the elemental analysis is also in agreement with the crystallographically determined molecular structure.

3.3.2 Water Exchange

A typical plot for a run at 25 °C is shown in Figure 3.11 and the fit to the data gave a rate constant of 1.08×10^{-3} s^{-1}. Interestingly there

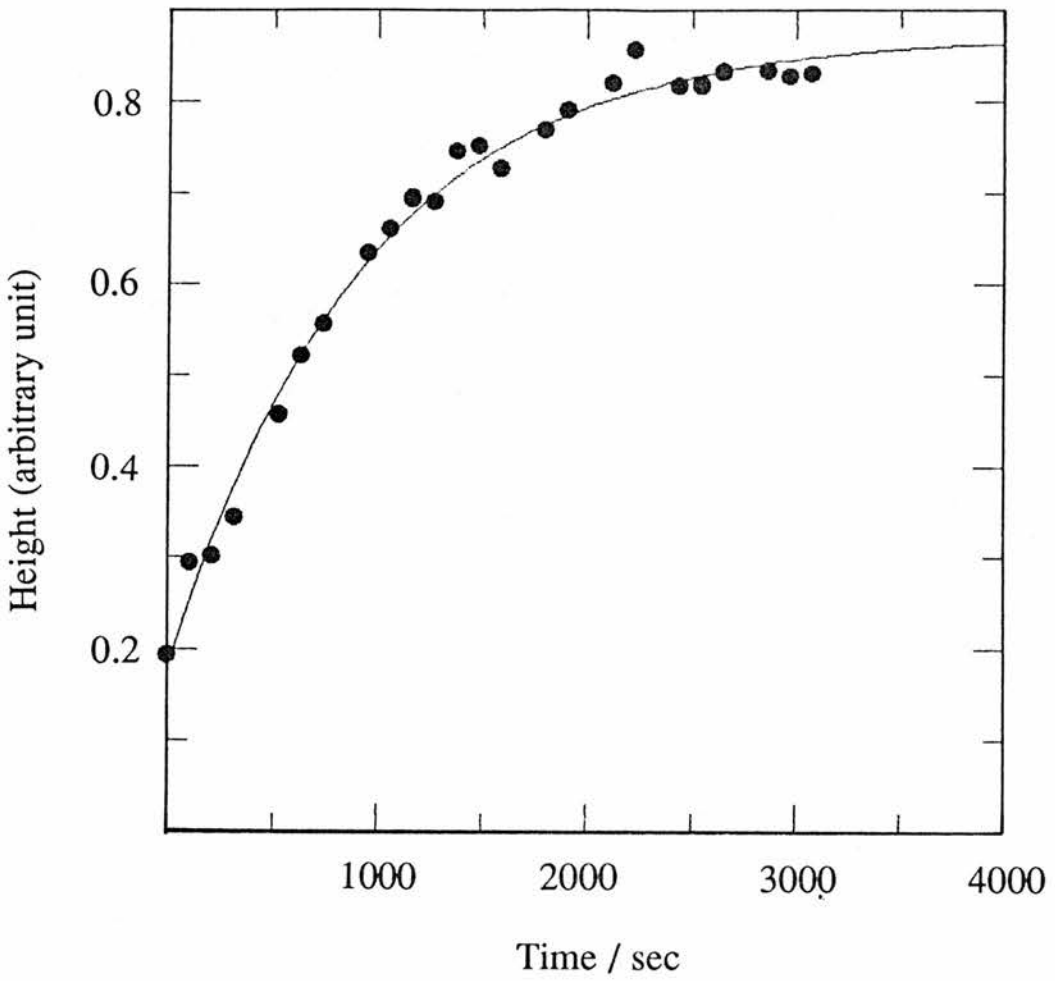

Fig. 3.11: Kinetics of water exchange at $[Ru_3O(OAc)_6(H_2O)_3]^+$ followed by the increase in height (arbitrary unit) of the ^{17}O NMR signal from coordinated water at 25 °C.

was a delay in the onset of the water exchange for up to 30 minutes. This delay appears to be associated with a change in colour of the solution from purple to torquoise-blue, which is now believed to characterise the break up of the hydrogen-bonding network in the trimer (see crystal structure in Fig. 3.9) Attempts were made to follow the associated colour change (seen in the H_2O exchange) spectophotometrically under much more dilute conditions However, the process was found to be completed within a few minutes at room temperature which suggests a $[Ru_3]$ dependence.

3.3.3 Complexation of Isonicotinamide with $[Ru_3O(OAc)_6(H_2O)_3]^+$

3.3.3.1 Product Analysis

The UV-visible spectral changes in the $[Ru_3O(OAc)_6(H_2O)_3]^+$ complex obtained with an excess of isonicotinamide at 50 °C (pH ~3.5) is shown in Fig. 3.12. The figure shows that the reaction proceeds with a gradual increase in absorbance and an initial slight shift in λ_{max} to

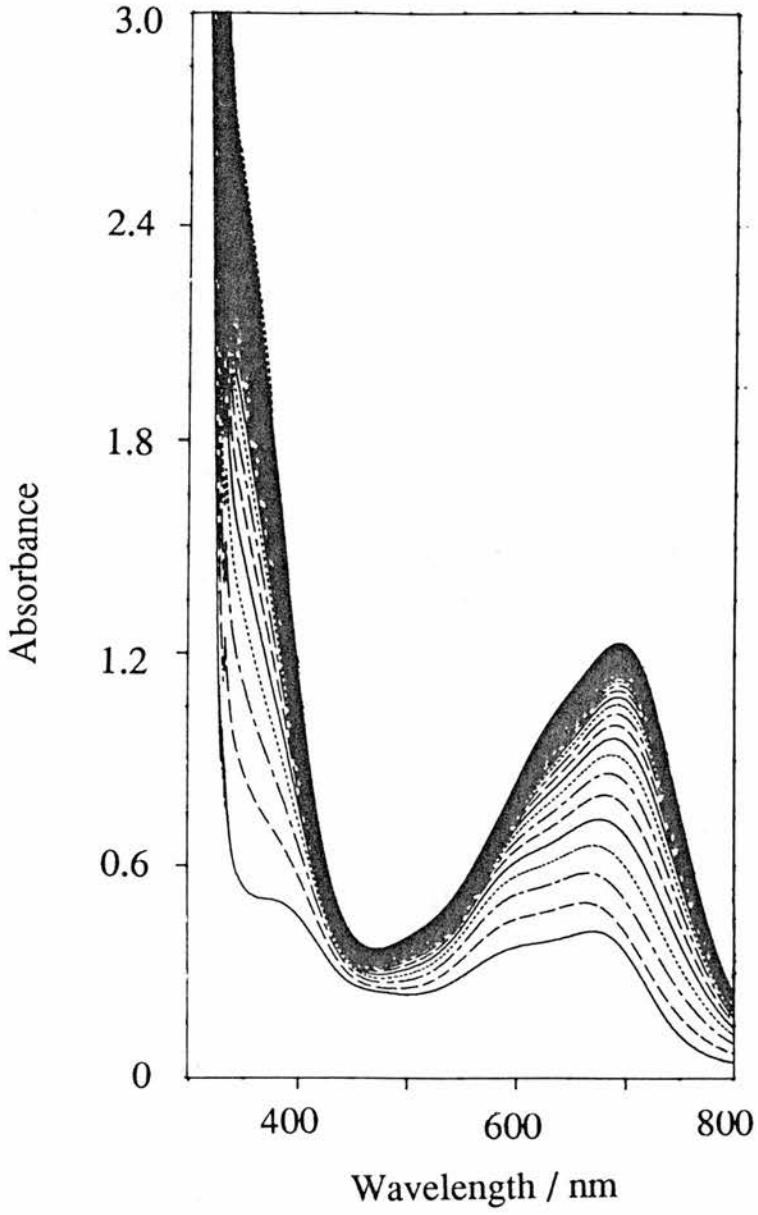

Fig.3.12: Spectral changes during the complexation of $[Ru_3O(OAc)_6(H_2O)_3]^+$ by isonicotinamide (0.30 M), at T = 50 °C, pH ~ 3.2, I = 1.0 M (CF_3SO_3Na); cycle time = 30 minutes.

lower wavelengths which then progressively shifted to higher wavelengths. The final spectrum with a single maximum at 700 nm (ε = 3226 $M^{-1}cm^{-1}$) and a shoulder at ~500 nm is very similar in profile to the tris(isonicotinamide) species, $[Ru_3O(OAc)_6(iso)_3]^+$, but clearly not consistent with its formation[74] (expected maximum at 710 nm ($\varepsilon \sim 6000$ $M^{-1}cm^{-1}$); 700 nm (ε = 6300 $M^{-1}cm^{-1}$; this work). After the kinetic runs were completed and the filled cuvettes allowed to stand fof 1-2 days, a blue solid was found to precipitate within this time. The UV-visible spectrum of this solid showed the presence of free isonicotinamide as an impurity (peak at ~ 260 nm) which was removed by recrystallising the solid from methanol-acetone. Different samples were subsequently analysed by elemental analysis but unfortunately the results were inconsistent and could not be fitted to a definite species. Following the incosistency of the elemental results, it was decided to investigate the solid by positive ion fast atom bombardment (FAB) mass spectrometry (Figure 3.13). An $M^{+\cdot}$ ion at m/e 1041 was clearly obtained for the 102 base peak which is assigned to the fragment $[^{102}Ru_3O(OAc)_6(iso)_3]^+$. The initial fragmentation pattern corresponds to successive loss of one (m/e 919) two (797) and eventually three (675) isonicotinamide ligands. The m/e peak at 738 was assigned as due to the loss of an acetate group. This result could indicate the presence of the tris(isonicotinamide) product, $[Ru_3O(OAc)_6(iso)_3]^+$.

It was concluded that under the conditions of the complexation study, the final product was a mixture of various isonicotinamide containing species with the trisubstituted product isolated as perhaps the least soluble of the species present.

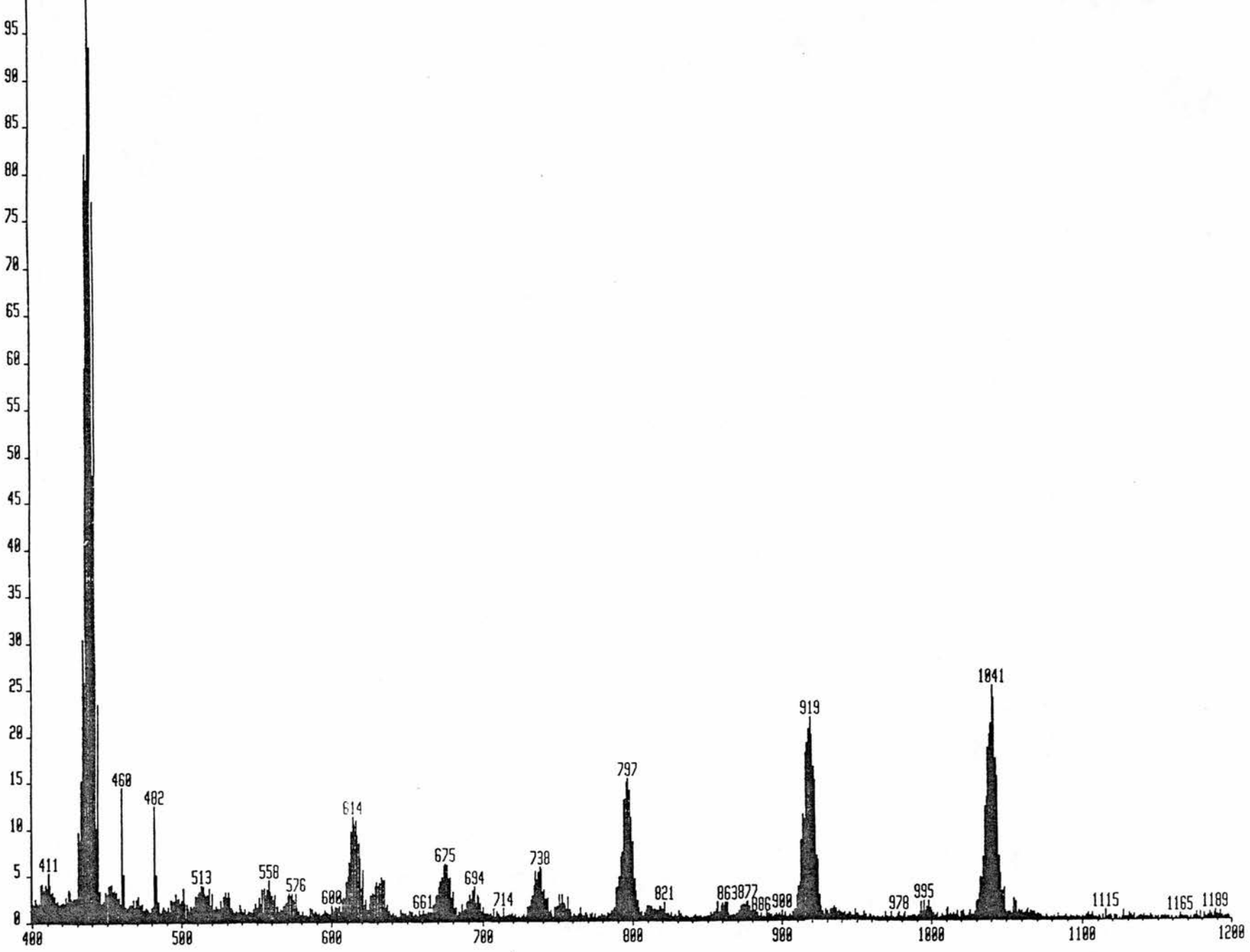

Fig. 3.13: Positive ion FAB MS spectrum of the product isolated from the kinetic runs between $[Ru_2O(OAc)_6(H_2O)_3]^+$ and isonicotinamide.

3.3.4 Kinetics of Isonicotinamide Complexation on $[Ru_3O(OAc)_6(H_2O)_3]^+$

3.3.4.1 Dependence on Total Isonicotinamide Concentration

The dependence of the complexation rate constant on total isonicotinamide concentration was investigated in a series of runs with the [ligand] in excess (>> 10-fold) over the trimer concentration. The total isonicotinamide concentration was varied from 0.10 to 0.50 M. Under these conditions a first-order dependence of $k_{obs.}$ on total isonicotinamide concentration was observed passing through or to the origin. The lack of any appreciable intercept suggests that equilibrium kinetics are not relevant. The values of the pseudo-first-order rate constants ($k_{obs.}$) obtained at 50 °C over the pH range 2.4 - 3.5 are listed in Table 3.3 and plotted against $[isonicotinamide]_T$ as a function of pH in Figure 3.14.

3.3.4.2 Dependence on Hydrogen Ion Concentration

The acid dissociation constant, K_{iso}, (25 °C) for isonicotinamide is 2.4 x 10^{-4} M (pK_a = 3.67).[80] Its pK_a value suggests that in the pH range of study (pH 2.5 - 3.5) appreciable amounts of the free ligand and the protonated form should be present in solution. The total isonicotinamide concentration can thus be represented as shown in equation (3.10):

$$[Isonicotinamide]_T = [Iso] + [IsoH] \qquad (3.10)$$

where $[isonicotinamide]_T$ is the total ligand concentration with [iso] and[isoH] representing the concentrations of free ligand and protonated ligand, respectively. It is also recognised that in this pH range a

Table 3.3: First-Order Rate Constants k_{obs}(50 °C) for the Reaction of $[Ru_3O(OAc)_6(H_2O)_3]^+$ with isonicotinamide, I = 1.0 M ($NaCF_3SO_3$).

pH	$[iso]_T$ /M	$10^5 k_{obs}$ / s^{-1}
2.45	0.10	1.89
	0.20	4.05
	0.30	6.05
	0.40	7.92
	0.50	9.95
2.77	0.10	3.40
	0.20	6.42
	0.30	9.52
	0.40	12.67
	0.50	16.56
3.06	0.10	4.83
	0.20	9.53
	0.30	14.96
	0.40	20.02
	0.50	25.07
3.30	0.10	7.59
	0.20	15.21
	0.40	31.91
	0.50	40.57
3.44	0.05	4.18
	0.10	8.24
	0.20	17.80
	0.25	22.72
	0.30	26.51

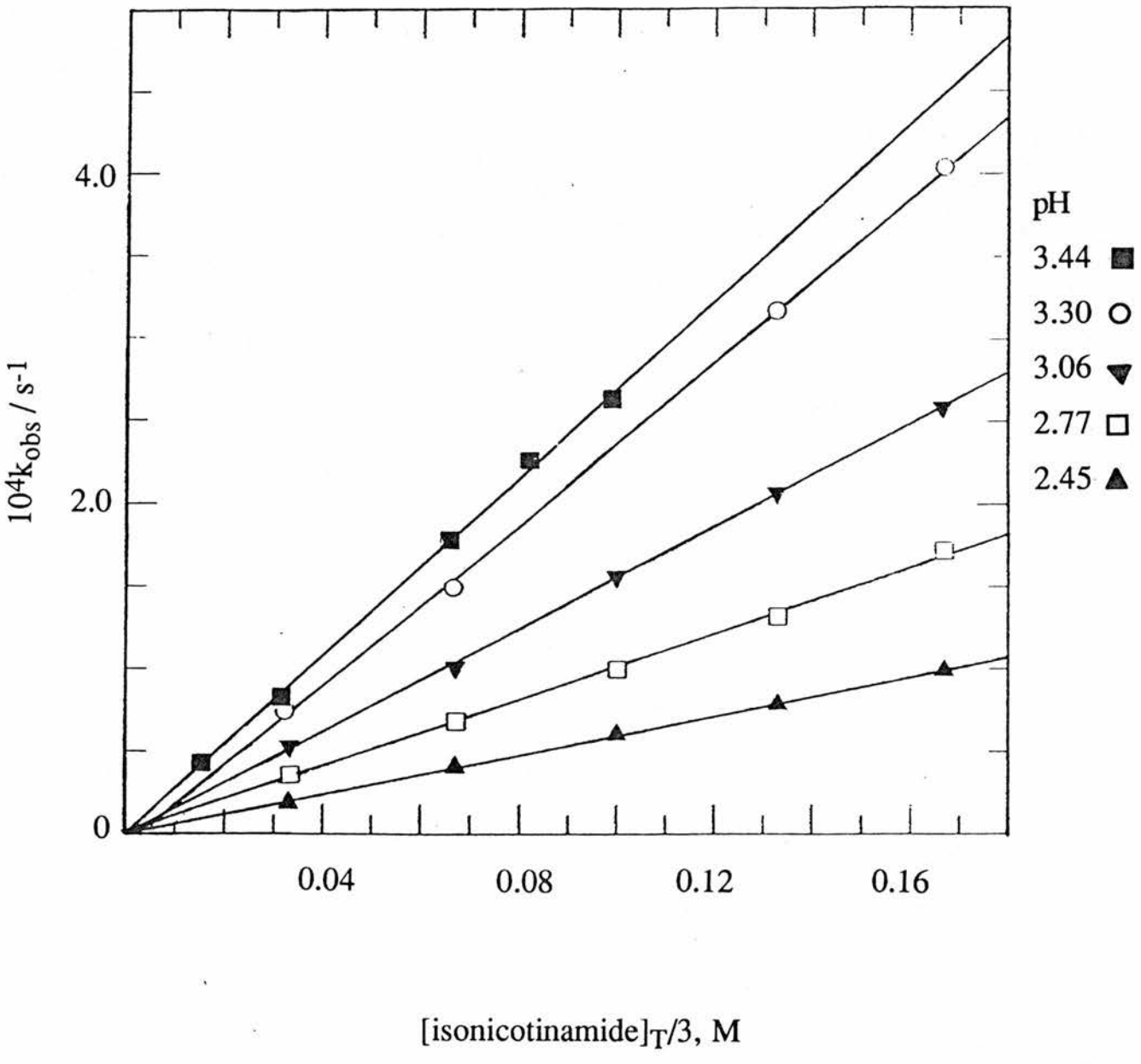

Fig. 3.14: Dependence of first-order rate constants, kobs (50 °C), on [isonicotinamide], for the reaction of $[Ru_3O(OAc)_6(H_2O)_3]^+$ with isonicotinamide at different pHs.

significant amount of the deprotonated form of the Ru_3 complex, $[Ru_3O(OAc)_6(H_2O)(OH)_2]^-$, is likely to be present; the terminal water ligands being weakly acidic and deprotonating reversibly with pK_a ~ 4.35 for the first two protons. The pK_a value for loss of the third proton is > 12 thus only the triaqua species and the dihydroxoaqua species are expected to be in solution at these pH's.[7] The total Ru_3 concentration can then be expressed in terms of the triaqua complex and the dihydroxoaqua species (eqn.3.11):

$$[Ru_3]_T = [Ru_3O(OAc)_6(H_2O)_3]^+ + [Ru_3O(OAc)_6(H_2O)(OH)_2]^- \quad (3.11)$$

The pH of the solutions was thus varied in order to establish what are the reacting species involved in the complexation process. As can be seen from Figure 3.14 the values of k_{obs} increase with increasing pH in the pH range used and it was necessary to try fitting the acid dependence to various rate laws which accounted for the participation or exclusion of the various species. After many varied attempts the observed dependence was successfully fitted to a rate law involving the unprotonated form of isonicotinamide with both forms of the ruthenium trimer. Under pseudo-first-order conditions of the ligand (>> 10-fold excess), the rate law illustrated below (3.12) can be derived (see Appendix for full derivation).

$$k_{obs} = \frac{(k_1/_3K_{ISO}[H^+]^2 + k_2K_MK_{ISO})[ISO]_T}{([H^+]^2 + K_M)([H^+] + K_{ISO})} \quad (3.12)$$

This rate law was derived based on the series of reactions shown in Scheme 3.3. The two parallel reaction pathways are represented by the

$$[Ru_3O(OAc)_6(H_2O)_3]^+ \overset{K_M}{\rightleftharpoons} [Ru_3O(OAc)_6(H_2O)(OH)_2]^- + 2H^+$$

$$ISOH \overset{K_{ISO}}{\rightleftharpoons} ISO + H^+$$

$$[Ru_3O(OAc)_6(H_2O)_3]^+ + ISO \xrightarrow{k_1} Products$$

$$[Ru_3O(OAc)_6(H_2O)(OH)_2]^- + ISO \xrightarrow{k_2} Products$$

Scheme 3.3

second-order rate constants k_1 and k_2 while K_{iso} and K_M are the acid dissociation constants for isonicotinamide and the trimer, respectively. Values of k_1 will carry a statistical factor of 3. Both k_1 and k_2 are probably composite terms involving the ion-pair constants between the ligand and the trimeric species. As can be seen from Figeure 3.14, however, the k_{obs} dependence on isonicotinamide concentration exhibits no curvature up to the highest concentration employed (0.50 M). This is indicating that under these conditions there is little or no ion-pair association between the ligand and the different metal species. The absence of appreciable ion pair association is consistent with the behaviour to be expected at such ionic strengths and for a +1 or -1 species with a neutral ligand. Equation (3.12) can be rearranged into the linear form of equation (3.13):

$$\frac{k_{obs}([H^+]^2 + K_M)([H^+] + K_{ISO})}{[ISO]_T} = k_1/3K_{ISO}[H^+]^2 + k_2K_MK_{ISO} \quad (3.13)$$

This treatment is illustrated in Figure 3.15, where data at three temperatures from Table 3.4 are shown as plots of $k_{obs}([H+]^2 + K_M)([H+] + K_{iso}) / [iso]_T$ *vs* $[H+]^2$. These plots are satisfactorily linear and verifies the derived rate expression. The values of k_1 and k_2 obtained by least-square fitting of the data are listed in Table 3.5 as well as the activation parameters.

Table 3.4: Observed Rate Constants as a Function of pH at Different Temperatures, I = 1.0 M ($NaCF_3SO_3$).

Temp / °C	pH	$[iso]_T$ / M	10^5k_{obs} / s^{-1}
40.0	2.44	0.30	1.59
	2.65	0.30	2.26
	2.87	0.30	3.07
	3.22	0.30	5.43
	3.52	0.30	8.95
45.0	2.42	0.30	3.37
	2.58	0.30	4.12
	2.84	0.30	6.28
	3.30	0.30	12.92
	3.47	0.30	16.36
50.0	2.45	0.30	6.05
	2.77	0.20	6.42
	3.06	0.20	9.53
	3.30	0.20	15.21
	3.44	0.20	17.80

Table 3.5: Kinetic Parameters for the Reaction of Isonicotinamide with $[Ru_3O(OAc)_6(H_2O)_3]^+$ in Aqueous Solution.

Temp / °C	10^3k_1 / $M^{-1}s^{-1}$	10^3k_2 / $M^{-1}s^{-1}$
40.0	5.47	0.71
45.0	12.66	1.44
50.0	22.66	2.44
$\Delta H_1^{\neq} = 116.9 \pm 11.4$ kJ mol^{-1}; $\Delta H_2^{\neq} = 101.2 \pm 7.8$ kJ mol^{-1}		
$\Delta S_1^{\neq} = 85.1 \pm 36.0$ J K^{-1} mol^{-1}; $\Delta S_2^{\neq} = 17.8 \pm 24.6$ J K^{-1} mol^{-1}		

According to Scheme 3.3, the isonicotinamide complexation of the trinuclear oxo-triruthenium ion, $[Ru_3O(OAc)_6(H_2O)_3]+$, proceeds by two parallel pathways involving both the triaqua complex and its doubly deprotonated form, $[Ru_3O(OAc)_6(H_2O)(OH)_2]^-$. Under the conditions of study (pH 2.4 - 3.5) both the free isonicotinamide ligand and its protonated form are expected to be present ($pK_a = 3.67$) but the results seem to suggest that only the free ligand is reactive towards these metal species. Both pathways produce very similar rate constants for substitution of H_2O by the free ligand and the corresponding activation parameters are also very similar indicating that a similar mechanism is relevant for both pathways. A direct comparison of the water exchange rate constant (s^{-1}) with the rate constant ($M^{-1}s^{-1}$) for the isonicotinamide substitution may not be compared directly. However, if it isassumed that the ion-pair constant for the isonicotinmamide substitution process is small, which seems likely from the lack of any detectable curvature in Figure 3.14, then the rate constants may be compared. The extrapolated rate constant ($k_1 = 0.57 \times 10^{-3}$ $M^{-1}s^{-1}$ at 25 °C) for isonicotinamide

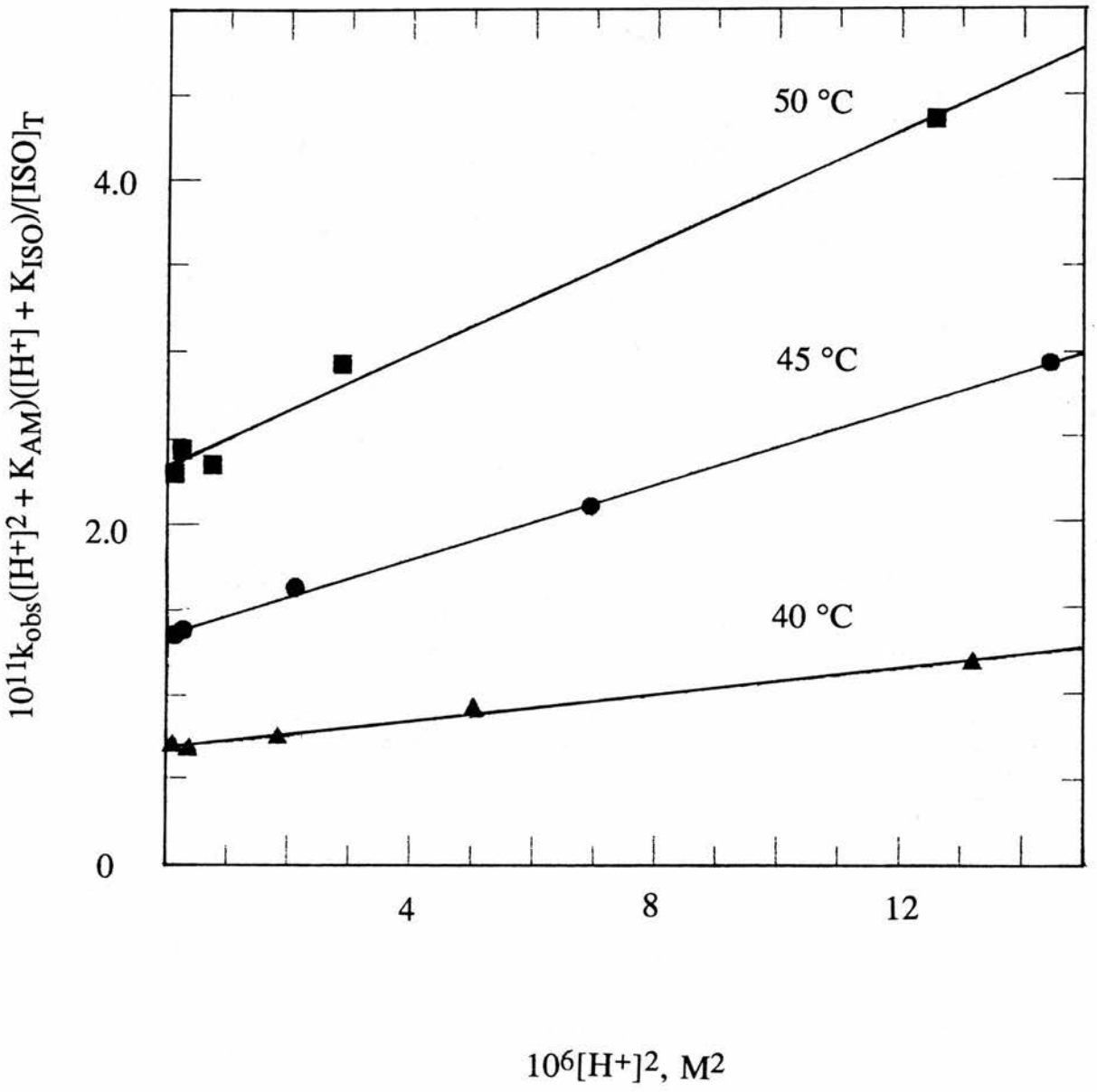

Fig. 3.15: Plot of $k_{obs}([H^+]^2 + K_{AM})([H^+] + K_{ISO})/[ISO]_T$ *vs* $[H^+]^2$ for the reaction of $[Ru_3O(OAc)_6(H_2O)_3]^+$ with ISO at different temperatures, I = 1.0 M ($NaCF_3SO_3$).

substitution is comparable to the water exchange rate constant (1.08 x 10^{-3} s^{-1}) at 25 °C. These values are of similar magnitude to that reported by Sasaki *et al* [30] for the H_2O substitution by CD_3OD in the Ru_3 (0.56 x 10^{-3} s^{-1} at 21 °C) and also in the corresponding Rh_3 and Ru_2Rh species (*vide supra*). Interestingly, these rate constants are several orders of magnitude (10^2 - 10^4 times) faster than the water-exchange reactions of the mononuclear complexes of these metals. These findings are significant and the higher lability of these trinuclear species has been attributed to the existence of a trans labilising effect from the μ_3-oxo group.[81] This is of interest because there seems some evidence of a considrable elongation of the Ru^{III}-OH_2 bonds (2.091Å) in the present complex when compared to those in other Ru(III) aqua species e.g. $[Ru(OH_2)_6]^{3+}$ (Ru-O_{av} = 2.029Å)[82] and this may be responsible for the 10^3 fold increase in substitution rate (25 °C) in the case of $[Ru_3O(OAc)_6(H_2O)_3]^+$. Different trans labilising effects arising from the μ_3-ligand has also been used to explain the different CD_3OD substitution rates between the trimolybdenum species $[Mo_3(\mu_3\text{-}O)_2(\mu\text{-}OAc)_6(H_2O)_3]^{2+}$ and $[Mo_3(\mu_3\text{-}O)(\mu_3\text{-}CCH_3)(\mu\text{-}OAc)_6(H_2O)_3]^{2+}$, with the latter being faster by some 10^5 times.[81] The conclusion was that the μ_3-CCH_3 ligand exerts a larger trans effect than the corresponding μ_3-O cap. This is reflected in the Mo-O(H_2O) distance (2.159 - 2.194Å)[83,84] for the μ_3-CCH_3 complex being somewhat larger than that (2.083 - 2.129Å)[85,86] for the bis(μ_3-oxo) complex. The planar μ_3-nitrido ligand is also believed to introduce a labilising effect in the triiridium complex [87] $[Ir_3N(SO_4)_6(H_2O)_3]^{4-}$ although here the Ir-O(SO_4) distances (2.005 - 2.056Å) and Ir-OH_2 distance (2.059 Å) are not believed to be particularly exceptional.[12] An unusually long Cr-F bond has been recently reported in the complex $[Cr_3O(OAc)_6F_3]^{2-}$ suggestive of a similar trans effect from the planar μ_3-O group in this complex.[88] This

could be a common feature of these planar and bi-capped trinuclear metal species and further kinetic studies of complexation on tghe peripheral sites should be pursued in order to make a general conclusion.

On the basis of the very close correspondence between the water exchange rate constant and those for the isonicotinamide substitution, a dissociative type of mechanism, possibly I_d, seems relevant. Other strong evidence for this type of mechanism is provided by the high $\Delta H^{\neq}$ and positive $\Delta S^{\neq}$ values for this process. Furthermore, in view of the extensive network of hydrogen bonding that exists between the coordinated H_2O ligand and the ClO_4^- ions, an associative type of mechanism seems less likely to occur.

3.4 REFERENCES

1. J. Catterick, P. Thornton, *Adv. Inorg. Chem. Radiochem.* 1977, **20**, 291.
2. (a)T. Glowiak, M. Kubiak, B. Jezowska-Trzebiatowska, *Bull. Acad. Pol., Ser. Sci. Chim.* 1977, **25**, 359.
   (b) F.A. Cotton, M. W. Extine, L. R. Falvello, D. B. Lewis, G. E. Lewis, C. A. Murillo, W. Schwotzer, M. Tomas, J. M. Troup, *Inorg. Chem.* 1986, **25**, 3505.
3. (a) S. C. Chang, G. A. Jeffrey, *Acta. Crystallogr., Sect. B: Struct. Cryst. Chem.* 1970, **B26**, 673;
   (b) B. N. Figgis, G. B. Robertson, *Nature(London)* 1965, **205**, 694; (c) J. T. Wrobleski, C. T. Dziobkowski, D. B. Brown, *Inorg. Chem.* 1981, **20**, 684.
4. L. W. Hessel, C. Romers, *Recl. Trav. Chim. Pays-Bas* 1969, **88**, 545.
5. K. Anzenhofer, J. J. DeBoer, *Recl. Trav. Chim. Pays-Bas* 1969, **88**, 286
6. C. E. Sumner, Jr., G.R. Steinmetz, *J. Am. Chem. Soc.* 1985, **107**, 6124.
7. A. Spencer, G. Wilkinson, *J. Chem. Soc., Dalton Trans.* 1972, 1570.
8. J. A. Baumann, D. J. Salmon, S. T. Wilson, T. J. Meyer, W. E. Hatfield, *Inorg. Chem.* 1978, *17*, 3342.
9. J. B. Bronavski, G. Ya. Mazo, L. M. Dikareva, *Russ, J. Inorg. Chem. (Engl Transl)* 1971, **16**, 1388.
10. T. Glowiak, M. Kubiak T. Szymanska-Buzar, *Acta. Crystallogr., Sect. B: Struct. Crystallogra. Cryst. Chem.* 1977, **B33**, 1732.

11. S. Uemura, A. Spencer, G. Wilkinson, *J. Chem. Soc., Dalton Trans.* 1973, 2565.

12. M. Ciechanowicz, W. P. Griffith, D. C. Pawson, A. C. Skapski, M. J. Cleare, *J. Chem. Soc., Chem. Commun* 1971, 876.

13. A. Müller, R. Jostes, F. A. Cotton, *Angew. Chem. Int. Ed. Eng.*, 1980, **19**, 875.

14. W. P. Griffith, *J. Chem. Soc., A*, 1969, 2270.

15. R. Beckett, R. Cotton, B. F. Hoskins, R. L. Martin, D. G. Vince, *Aust. J. Chem.* 1969, **22**, 2527.

16. Yu. V. Yablokov, B. Ya. Kuyavskaya, A.V. Ablov, A. V. Mosina, M. D. Mazus, *Dokl. Akad. Nauk SSSR* 1981, **256**, 1182; *Dolk. Phys. Chem.*, 1981, *256*, 126.

17. B. S. Tsukerblat, V. M. Norotorfsev, B. E. Kuyavskaya, M. I. Belinskii, A. V. Ablov, A. N. Bazhan, V. T. Kalinnikov, *Pis'ma Zh. Eksp. Teor. Fiz.* 1974, **19**, 525; *JETP Lett.*, 1974, **19**, 277.

18. A. E. Underhill, D. M. Watkins, *J. Chem. Soc, Dalton Trans.* 1977, 5.

19. F. A. Cotton, W. Wang, *Inorg. Chem.* 1982, **21**, 2675.

20. A. R. E. Baikie, M. B. Hursthouse, D. B. New, P. Thornton, *J. Chem. Soc. Chem. Commun* 1978, 62.

21. A. R. E. Baikie, M. B. Hursthouse, L. New, P. Thornton, R.G. White, *J. Chem. Soc., Chem. Commun.* 1980, 684.

22. J. B. Vincent, H. R. Chang, K. Folting, J. C. Huffman, G. Christon, D. N. Hendrickson, *J. Am. Chem. Soc.* 1987, **109**, 5703.

23. S. E. Woehler, R. J. Wittebort, S. M. Oh, D. N. Hendrickson, D. Inness, C. E. Strouse, *J. Am. Chem. Soc.* 1986, **108**, 2938.

24. (a) S. M. Oh, D. N. Hendrickson, K. L. Hassett, R. E. Davis, *J. Am. Chem. Soc.* 1985, **107**, 8009.

(b) S. M. Oh, D. N. Hendrickson, K. L. Hassett, R. E. Davis, *J. Am. Chem. Soc.* 1984, **106**, 7984.

25. F. A. Cotton, J. G. Norman, *Inorg. Chim. Acta*, 1972, **6**, 411.

26. (a) A. B. Blake, A. Yavari, H. Kubiaki, *J. Chem. Soc., Chem, Commun.* 1981, 796;

(b) A. B. Blake, A. Yavari, J. *Chem. Soc., Chem. Commun.* 1982, 1247;

(c) A. B. Blake, A. Yavari, W. E. Hatfield, C. Sethulekshmi, *J. Chem. Soc., Dalton Trans* 1985, 2509.

27. W. Clegg, O. M. Lam, B. P. Straughan, *Inorg. Chim. Acta.* 1984, **90**, L75.

28. W. Clegg, O. M. Lam, B. P. Straughan, *Angew. Chem. Int. Ed. Engl.* 1984, **23**, 434.

29. (a) B.P. Straughan, O. M. Lam, *Inorg. Chim. Acta* 1985, **98**, 7;

(b) B. P. Straughan, O. M. Lam, A. Earnshaw, *J. Chem. Soc., Dalton Trans.* 1987, 97.

30. Y. Sasaki, A. Tokiwa, T. Ito, *J. Am. Chem. Soc.* 1987, **109**, 6341.

31. R. F. Weinland, *Chem. Z.*, 1908, **32**, 812.

32. R. F. Weinland, *Ber. Dtsch. Chem. Ges.*, 1908, **41**, 3236.

33. A. Werner, *Ber. Dtsch. Chem. Ges.* 1908, **41**, 2110.

34. L. A. Welo, *Phys. Rev.* 1928, **32**, 320.

35. L. A. Welo, *Philos. Mag.* 1928, **6**, 481.

36. L. E. Orgel, *Nature (London)*, 1960, **187**, 504

37. D. H. R. Barton, J. Boivin, M. Gastinger, J. Morzycki, R. S. Hay-Motherwell, W. B. Motherwell, N. Ozbalik, K. M. Schwartzentruber, *J. Chem. Soc., Perkin Trans.* 1986,1

38. C. Bilgrien, S. Davis, R. S. Drago, *J. Am. Chem. Soc.* 1987, **109**, 3786.

39. S. Ito, K. Inoue, M. Mastumoto, *J. Am. Chem. Soc.* 1982, **104**, 6450.

40. S. A. Fouda, G. L. Rempel, *Inorg. Chem.* 1979, **18**, 1.

41. R. H. Fish, R. H. Fong, J. B. Vincent, G. Christon, *J. Chem. Soc., Chem. Commun.* 1988, 1504.

42. S. Murata, M. Muira, M. Nomura, *Chem. Lett.* 1988, 361.

43. Y. Sasson, G. L. Rempel, *Tetrahedron Lett.*, 1974, 4133.

44. Y Sasson, G. L. Rempel, *Can. J. Chem.* 1974, **52**, 3825.

45. L. Dubicki, P. Day, *Inorg. Chem.* 1972, **11**, 1868.

46. M. Makles-Grotowska, W. Wojcieshowski, *Bull. Acad. Pol. Sci., Chem.* 1979, **27**, 59.

47. V. M. Norwood, K. M. Morse, *Inorg. Chem.* 1986, **25**, 3690.

48. L. Montri, R. D. Cannon, *Spectrochim Acta* 1985, **41A**, 643.

49. M. K. Johnson, D. B. Powell, R. D. Cannon, *Spectrochim Acta* 1981, **37A**, 995.

50. (a) F. E. Mabbs, D. J. Machin, *Magnetism and Transition Metal Complexes*, Chapman and Hall, London, 1973, Chap. 7; (b) R. L. Martin, *New Pathways in Inorganic Chemistry*, E. A. V. Ebsworth, A. G. Maddock, A. G. Sharpe, Eds., Cambridge Univ. Press, Cambridge, 1968, pp 175-231.

51. D. H. Jones, J. R. Sams, R. C. Thomson, *J. Chem. Phys.* 1984, **81**, 440.

52. C. T. Dziobkowski, J. T. Wrobleski, D. B. Brown, *Inorg. Chem.* 1981, **20**, 671.

53. R. F. Weinland, E. Gussmann, *Ber. Dtsch. Chem. Ges.* 1909, **42**, 3881.

54. R. F. Weinland, H. Holtmeier, *Z. Anorg. Allg. Chem.* 1928, **173**, 49.

55. T. Glowiak, M. Kubiak, T. Szymanska-Buzar, B. Jezowska-Trzebiatowska, *Acta Cryst.* 1977, **B33**, 3106.

56. R. D. Cannon, L. Montri, D. B. Brown, K. M. Marshall, C. M. Elliott, *J. Am. Chem. Soc.*, 1984, **106**, 2591.

57. P. Poganiuch, S. Liu, G. C. Papaefthymiou, S. J. Lippard, *J. Am. Chem. Soc.* 1991, **113**, 4645.

58. P. Nordland, B.-M. Sjöberg, H. Eklund, *Nature*, 1990, **395**, 593.

59. L. Messuk, U. A. Jayasooriya, R. D. Cannon, *J. Am. Chem. Soc.* 1987, **109**, 2009.

60. L. Meesuk, U. A. Jayasooriya, R. D. Cannon, *Spectrochim. Acta*, 1987, **43A**, 687.

61. M. K. Johnson, R. D. Cannon, D. B. Powell, *Spectrochim. Acta*, 1982, **38A**, 307.

62. M. J. Cleare, W. P. Griffith, *J. Chem. Soc. A*, 1970, 1117.

63. D. B. Brown, M. B. Robin, J. D. E. McIntyre, W. F. Peck, *Inorg. Chem.* 1970, **9**, 2315.

64. A. W. Mond, *J. Chem. Soc.* 1930, 1247.

65. T. A. Stephenson, G. Wilkinson, *J. Inorg. Nucl. Chem.* 1966, **28**, 2285.

66. P. Legzdins, R. W. Mitchell, G. L. Rempel, J. D. Ruddick, G. Wilkinson, *J. Chem. Soc. A*, 1970, 3322.

67. F. A. Cotton, J. G. Norman, A. Spencer, G. Wilkinson, *J. Chem. Soc., Chem. Commun.* 1971, 967.

68. F. S. Martin, *J. Chem. Soc.*, 1952, 2682.

69. W. P. Griffith, *J. Chem. Soc. A.* 1969. 2270.

70. M. Mukaida, M. Kusakari, T. Togano, T. Isomae, T. Nomura, T. Ishimori, *Bull. Chem. Soc. Jpn.*, 1975, **48**, 1095.

71. A. Spencer, G. Wilkinson, *J. Chem. Soc., Dalton Trans.* 1974, 786.

72. J. A. Baumann, S. T. Wilson, D. J. Salmon, P. L. Hood, T. J. Meyer, *J. Am. Chem. Soc.*, 1979, **101**, 2916.

73. J. A. Baumann, D. J. Salmon, S. T. Wilson, T. J. Meyer, *Inorg. Chem.* 1979, **18**, 2472.

74. H. E. Toma, C. J. Cunha, *Can. J. Chem.* 1989, **67**, 1632.

75. R. W. Mitchell, A. Spencer, G. Wilkinson, J. *Chem. Soc, Dalton. Trans.* 1973, 846.

76. S.A. Fouda, B.-C.Y. Hui, G. L. Rempel, *Inorg. Chem.* 1978, **17**, 3213.

77. Y. Sasson, A. Zoran, J. Blum, *J. Mol. Catal.*, 1979, **6**, 289.

78. B. Wang. Y. Sasaki, S. Ikari, K. Kumura, T. Ito, *Chem. Lett.*, 1987, 1955.

79. J. O. Edwards, F. Monacelli, G. Ortaggi, *Inorg. Chim. Acta*, 1974, 1147.

80. R. M. Smith, A. E. Martell, *Critical Stability Constants*; Plenum: New York, 1975; Vol. 2, p 198.

81. K. Nakata, A. Nagasawa, N. Soyama, Y. Sasaki, T. Ito. *Inorg. Chem.* 1991, **30**, 1575.

82. B. Bernhard, H.-B. Bürgi, J. Hauser, H. Lehmann, A.Ludi, *Inorg. Chem.* 1982, **21**, 1575.

83. A. Bino, F. A. Cotton, Z. Dori, B. W. S. Kolthammer, *J. Am. Chem. Soc.* 1981, **103**, 5779.

84. A. Bino, F. A. Cotton, Z. Dori, L. Falvello, G. M. Reisner, *Inorg. Chem.* 1982, **21**, 3750.

85. M. Ardon, A. Bino, F. A. Cotton, Z. Dori, M. Kaftory, G. M. Reisner, *Inorg. Chem.* 1982, **21**, 1912.

86. F. A. Cotton, Z. Dori, D. O. Marler, W. Schwotzer, *Inorg. Chem.* 1983, **22**, 3104.

87. E. F. Hills, D. T. Richens, A. G. Sykes, *Inorg. Chem.* 1986, **25,** 3144.

88. R. D. Cannon, *Private Communication.*

CHAPTER 4

4.1 Introduction

Before the turn of the century, saturated hydrocarbons (paraffins) played only a minor role in industrial chemistry. They were mainly used as a source of paraffin wax as well as for heating and lighting oils. Aromatic compounds such as benzene, toluene, phenol and napthalene obtained from destructive distillation of coal were the main source of organic materials used in the preparation of dyestuffs, pharmaceutical products, etc. Calcium carbide-based ethyne was the key starting material for the emerging synthetic organic industry. It was the ever increasing demand for gasoline after the first world war that initiated the study of isomerisation and cracking reactions of petroleum fractions. After the second world war, rapid economic expansion necessitated increasingly abundant and cheap sources for chemical and as a result the industry switched to petroleum-based ethene as the main source of chemical raw material. One of the major difficulties that had to be overcome is the low reactivity of some of the major components of the petroleum. The lower boiling components (up to 250 °C) are primarily straight-chain saturated hydrocarbons or paraffins. The chemical inertness of alkanes is well known and is reflected in one of their old names 'paraffins' (from the Latin *parum affinus*- without affinity). Consequently the lower paraffins were cracked to give olefins (mainly ethene, propene and butene). The straight-chain liquid hydrocarbons also have very low octane numbers, which makes them less desirable as gasoline components. To transform these alkanes into useful components for gasoline and other chemical applications, they have to undergo diverse reactions such as isomerisation, cracking or alkylation. These reactions,which are based on a large scale in industrial processes, necessitate acidic catalysts (at temperature around 100 °C) or

noble metal catalysts (at higher temperature, 240-500 °C) capable of activating the strong covalent C-H or C-C bonds.[1]

The drastic conditions (*i.e.* high temperature, high pressure, strong electrophiles or radicals) usually required for the direct functionalisation of saturated hydrocarbons can result in a mixture of products including polyfunctionalised compounds,[2] and sometimes substances that are damaging to the environment. For example, in the synthesis of adipic acid (one of the starting materials for the manufacture of nylon) from cyclohexane, using nitric acid as oxidant, N_2O is produced as a byproduct as well as N_2, NO and NO_2. With an estimated 2.2 Mt/a of worldwide adipic acid production, up to 1.5 x 10^{10} mol could be released annually.[3]

It is known that nitrous oxide is the major source of stratospheric NO, which catalytically destroys ozone. It is also believed that this gas could contribute to an enhanced greenhouse effect by as much as 10 percent .[4] This is just one example which illustrates the need to develop methods to catalytically oxidise saturated hydrocarbons under mild conditions, and at the same time reduce or eliminate the formation of such hazardous chemicals. This is both an intellectually stimulating and industrially important objective of current relevance.

Many biological systems are able to 'hydroxylate' non-activated carbon-hydrogen bonds and a typical example of such systems are the monooxygenases. Monooxygenases are enzymes catalysing oxidation in coupled processes, which involve C-H bond hydroxylation (or epoxidation of olefins) and simultaneous oxidation of NADH or NADPH according to equation (4.1):

$$RH + O_2 + 2e^- + 2H^+ \longrightarrow ROH + H_2O \quad (4.1)$$

A few monooxygenases able to hydroxylate C-H bonds of alkanes are dependent on non heme iron-proteins. For instance, this is the case for the methane monoxygenase from *methylococcus capsulatus,*[5] as well as for the monooxygenase from *pseudomonas deovorans*, which hydroxylates octane into octan-1-ol.[6] However in most cases, the hydroxylation of unsaturated C-H bonds of alkanes in almost all living organisms such as mammals, microorganisms or plants is catalysed by cytochrome P-450 dependent monoxygenases.[7] These enzymes are involved in many steps of the biosynthesis and biodegradation of endogenous compounds such as steroids, fatty acids or prostaglandins. They also play a central role in the oxidative metabolism of exogenous compounds such as drugs and environmental products allowing their elimination from living organisms.[8-10] The active site of these enzymes comprises an iron porphyrin in which the metal has a thiolate (from a cysteine residue) and a histidine as ligands.[11] The enzyme, and most of its model systems, involves an Fe^{V} oxenoid in a porphyrin structure as the active oxidising species.[7]

While considerable effort has been focused on mimics of cytochrome P-450,[12a-g] few examples have been reported on non-porphyrin complexes.[13a-d] The interest in non-porphyrin complexes as C-H activation catalysts coincides with the recent reports on methane monooxygenase enzymes[5,14a,b] which have in the resting state at the hydroxylation site a μ-oxo Fe_2^{III} group, which has been characterised.[15,17]

The metallo-non-porphyrin C-H activation catalysts that have been reported are predominantly mononuclear metal complexes,[18a-d] while only a few studies were directed towards metal clusters.[13b,c,19] Also the cheap and ready source of oxygen as oxidant is by passed in many instances and alternatives such as iodobenzene, hydroperoxides,

hypochlorites, etc. are frequently used. In a series of studies conducted by Barton *et al* [13b,20] it has been demonstrated that the iron complex $[Fe^{II}Fe_2^{III}O(OAc)_6(py)_{3.5}]$ possesses catalytic activity towards the monoxygenation of certain cyclic hydrocarbons. Their system, called the Gif IV system (see below) was found to selectively oxidise the cyclic hydrocarbons to cyclic ketones in isolated yields superior to those reported for other comparable model systems. It consisits of oxygen (oxidant), acetic acid (or other suitable acid as H^+ source), pyridine (solvent) and iron powder (source of electrons). Early systems also employed sodium sulphide (Gif I) or hydrogen sulphide (Gif II) which could form an iron-sulphur bond as in cp 450.[21,22] It was shown that the H_2S is not a reductant in the system and that formation of an Fe-S bond is not essential to the oxidation process; it served only to catalyse the dissolution of the iron powder by a surface effect.[20] Without the sulphide the system was called Gif III.[13b] Later the Gif IV system was formulated being similar to Gif III but having the trinuclear iron carboxylate catalyst with suspended zinc dust as the source of electrons and again oxygen as the oxidant.[20] Barton and coworkers[23] subsequently developed the Gif-Orsay(Go) electrochemical system in which the zinc dust was replaced by a mercury cathode. This system was found to possess a coulombic yield for cyclohexanone generation of up to 50%. More recently, three more systems have been developed: GoAggI, GoAggII and GoAggIII.* The GoAggI consists of pyridine-acetic acid with stoichiometric Fe(II) and KO_2 under argon.[24] The GoAggII system differs in that the oxidant is now H_2O_2 and the catalyst

*These systems peculiar names are geographical with Gif (or G) being derived from Gif-sur-Yvette, O is for Orsay and Agg is for 'Aggieland,' the places where these systems were developed.[25]

is $FeCl_3$ or simple Fe(III) salts.[24] The final one, GoAggIII, uses Fe(III) salts with H_2O_2 in the presence of picolinic acid or other special ligands.[26] The picolinic acid was found to have a marked effect on the rate of oxdation (50-fold) and at the same time maintaining the Gif selectivity for oxidation at secondary C-H bonds.

The Gif system has been used for the selective oxidation of natural products with steroids being among the first to be studied.[27] These studies have shown that the GifIV system can oxidise the cholestane derivatives with the formation of the industrially important side-chain degradation product, the 20-ketone as the major isolated product. This method has allowed , for example, the conversion of cholestenone(**1**) to progesterone (**2**) in one step.[28]

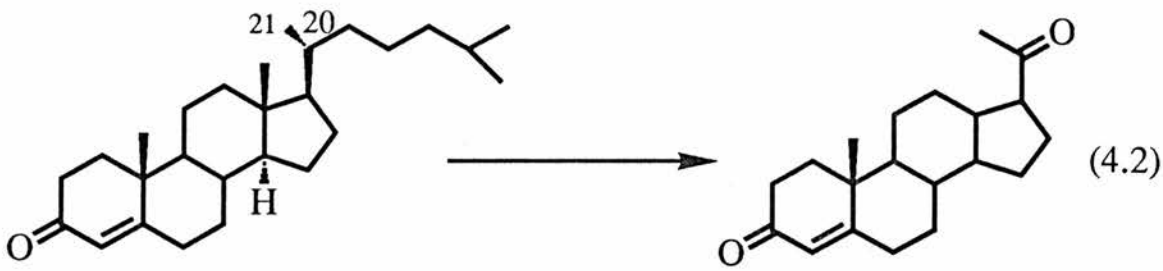

(4.2)

(1) (2)

A mechanism has been proposed for this degradation.[28,29]

There are certain features of the Gif systems that are worthwhile highlighting: (i) they oxidise secondary C-H bonds to mainly ketones, without alcohols being intermediates; (ii) the oxidation of alkanes are not suppressed to any significant degree by the presence of excess of alcohols or any other more easily oxidisable species;[30] (iii) cyclic olefins are not epoxidised, but rather give rise to conjugated ketones.[31] The non-oxidation of sulfur compounds, or of primary and secondary alcohols, is believed to indicate the non-participation of hydroxyl radical;[24] (iv) the selectivity order for C-H bonds is sec > tert ≥

primary. This is different from what is observed for cytochrome P-450 and most of its model systems (selectivity: tert.> sec.> primary) which also epoxidise olefins, and oxidises sulphides to sulphoxides;[24] (v) seconday alkyl radicals are not intermediates in the activation process; the reaction proceeds smoothly even in the presence of different radical trapping reagents with the formation of functionalised hydrocarbons.[32]

To explain these observations Barton *et al* [33] have proposed a mechanism. To begin with they suggest that $Fe^{II} + O_2^-$ is produced in the Gif III, Gif IV and Go systems. These species are already present in GoAggI to start with. In GoAggII and GoAggIII, Fe(III) plus H_2O_2 produces the same iron species. This formalism (Scheme 4.1) is the same as that used in arguments about the mechanism of P-450 oxidation.

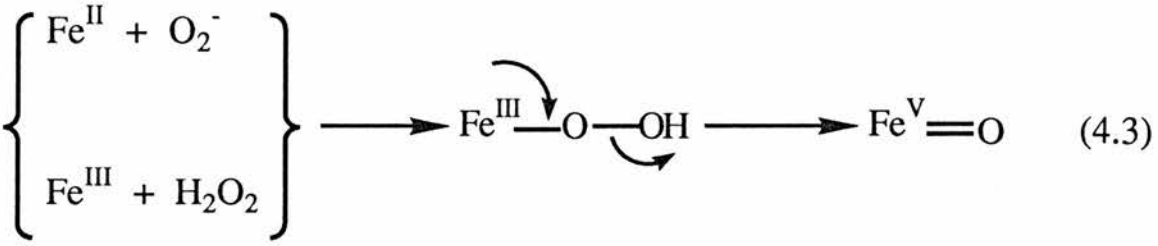

(4.3)

Scheme 4.1

Barton and his group[26] have claimed identification of two intermediates, A and B, in the selective oxidation of saturated hydrocarbons to ketone by the Gif type systems. A is an Fe^V species with an iron-carbon σ-bond; B was formulated as an Fe^{III} alkoxide species. They have also indentified cyclohexyl hydroperoxide as an intermediate during the oxidation of [1-^{13}C] cyclohexane under GoAggII conditions.[33] This intermediate was transformed quantitatively into cyclohexane and the reaction followed by ^{13}C NMR. These and other observations have allowed Barton *et al* [33] to propose a reaction

scheme to explain these Gif-type systems (scheme 4.2)

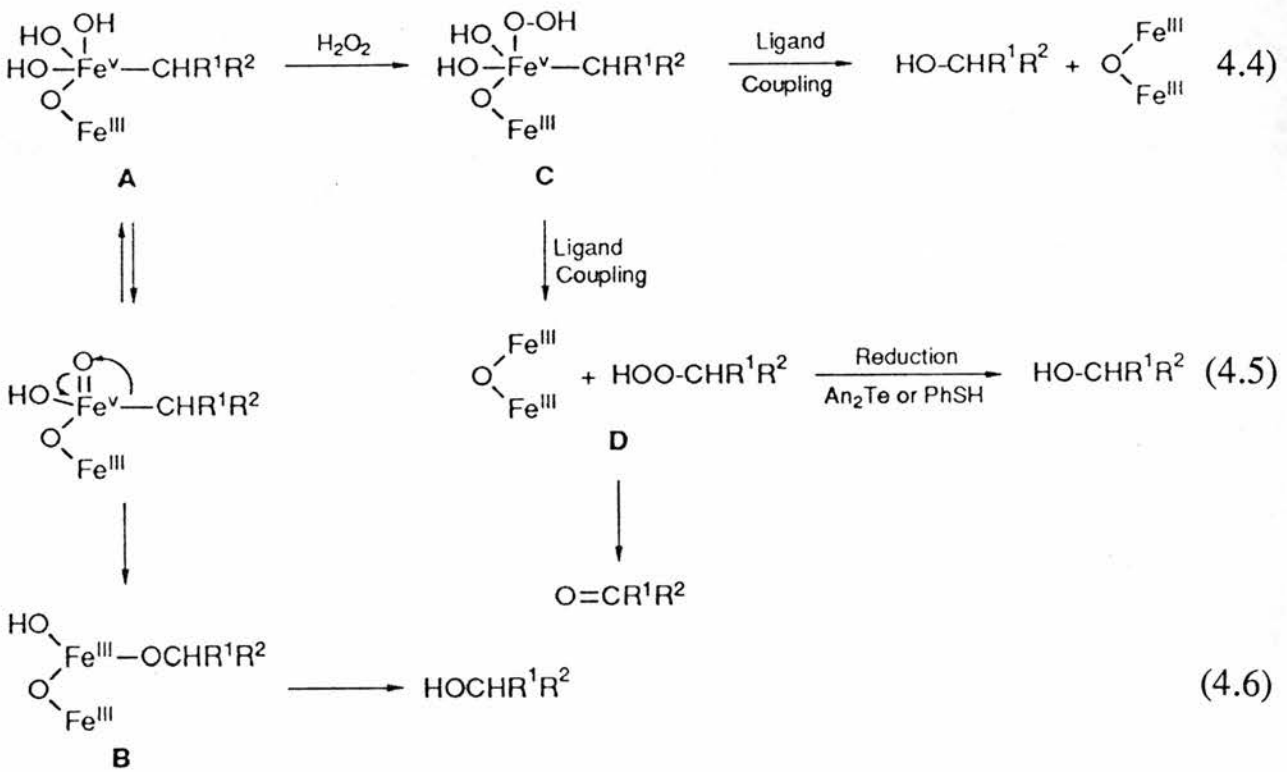

Scheme 4.2

(ligands are omitted or written as OH for clarity)

It is believed that the main route is *via* intermediate C. The hydroperoxide group may be delivered to the Fe^{V} by first reacting with the Fe^{III}. It is thought that the resting state of 2 Fe^{III} and the hydroperoxide D arise *via* ligand coupling of carbon and the hydroperoxide. This process normally produces ketone but the reducing agents dianisyl telluride (An_2Te, An = p-$MeOC_6H_4$) or benzenethiol convert D to the alcohol. Another route to the alcohol is believed to

occur through ligand coupling carbon and OH in C. There is also another, but minor, route to alcohol which involves B. Efforts are still being made in order to identify A by various physical methods and the question is now posed as to whether methyl monooxygenase, which always produces alcohols, does so *via* B,C,or D.[33]

Geletti *et al* [34] have made the suggestion that the oxidant in Gif system is the radical cation formally derived from pyridine-*N*-oxide (equation 4.7).

$$HO_2^{\cdot} \quad + \quad Py^{+}H \longrightarrow Py^{+}O^{\cdot} \quad + \quad H_2O \qquad (4.7)$$

However, Barton *et al* [24] have argued against such a proposal based on the evidence provided by the reagent diphenyldiselenide. In these studies they found that the Gif system also phenylselenates saturated hydrocarbons, using iron powder as reductant with diphenyldiselenide and oxygen as reactants. They thus dismissed the radical mechanism in favour of the iron-carbon bond since they could not conceive that the pyridine-*N*-oxide radical or any other oxygen radical would attack a saturated hydrocarbon faster than it would attack diphenyldiselenide, which is a very easily oxidised compound. Also the mechanism proposed by Geletti *et al* [34] fails to explain the formation of secondary phenylselenides.[24]

Knight and Perkins[35] have however recently reported that the oxygen atom of cyclodecanone, formed by the oxidation of cyclodecane using the GoAggII system ($FeCl_3$-H_2O in pyridine-acetic acid) is largely derived from molecular oxygen. This result in conjuction with radical-trapping experiments, supports a free-radical mechanism for the oxidation of this and presumably the other cyclic hydrocarbons.

A clear controversy thus exists with regard to the interpretation

of the mechanism of action of the Gif-type catalytic systems as to whether free radical processes are involved.

Barton had also reported investigations into Gif IV systems based on other trinuclear carboxylate catalysts :$[M_2^{III}M'^{II}O(OAc)_6(H_2O)_3]$ (M = Fe, M' = Ni, Zn, Co; M = M' = Mn and Ru).[20] Interestingly the Mn analogue showed no activity whereas the Ru species appeared to show comparable activity to that of the Fe complex during the few experiments that were carried out. Early indications were that more alcohol and less ketone were produced using the trinuclear ruthenium carboxylate complex as catalyst for cyclohexane oxidation. Given the knowledge of the much slower ligand substitution rates it was thus felt intriguing to perform some further experiments in the 'Ru-GifIV' system to see if these findings by Barton and coworkers could be substantiated. In particular the generation of reactive labile intermediates A-C as in Barton's mechanism (Scheme 4.2) would seem more unlikely in the case of the more inert Ru species. Furthermore as highlighted in chapter 3 the trinuclear ruthenium carboxylate show a rich redox chemistry offering the possibility of multiple electron transfer steps.[36] Also because of the periodic relationship between ruthenium and iron, these species might represent good models for $Fe^{V}=O$ species, thought to play an important role in the chemistry of the cytochrome P-450 porphyrin model and also the Gif IV system. Very recently it was shown that a $Ru^{V}=O$ pecies $[Ru^{V}L(O)]^{2+}$ {HL=[2-hydroxy-2-(2-pyridyl)-ethyl]bis[2-(2-pyridyl)ethyl]amine} was an active oxidant towards various hydrocarbons.[37] With saturated alkanes containing a tertiary C-H bond the Ru complex was found to be a selective oxidant; only tertiary alcohols and no secondary or primary alcohol was detected. In the case of cyclohexane, cyclohexanone was found to be the only product. Interestingly there was no evidence of a

radical being formed. It was suggested that a charge-transfer from the C-H bond to the Ru=O oxidant was likely to be responsible for the oxidation of the hydrocarbons.

For these studies we intend to use air(oxygen) as the primary oxidant. Though there are many reports in the literature describing trinuclear ruthenium carboxylates as catalyst,[38] it was only recently that oxygen was used as an oxidant for these systems.[39,40] The results of preliminary studies conducted with different ruthenium carboxylates as catalysts in comparison with $[Fe_3O(OAc)_6(py)_{3.5}]$ under Gif IV conditions are thus reported herein.

4.2 Experimental

4.2.1 Spectrometry

Ultraviolet and visible spectra were recorded on a Perkin Elmer Lambda 5 recording spectrophotometer using 1.0-cm quartz cells. Mass spectra were recorded using a Finnigan MAT INCOS 50 instrument in conjunction with a Hewlett Packard 5890 gas chromatograph.

4.2.2 Gas Chromatograph

For analytical g.l.c. measurements a Pye Unicam 4500 gas chromatograph with a 20% FFAP on 80/100 chromosorb coulmn was used according to the following conditions:
For the oxidation of cyclohexane: column temperature 150 °C, detector and injector temperature 250 °C. The hydrocarbon (10 mmol; May and

Baker, HPLC grade), pyridine (28 ml, Fisons), glacial acetic acid (2.3 ml; May and Baker, Pronalys AR), distilled water (1.85 ml), catalyst (10^{-6} mol) and zinc powder (1.31 g (20 mmol; BDH) were placed in a 100 ml conical flask and stirred with the flask open to the air. The crude reaction mixture was analysed directly by g.l.c. and the amounts of oxidised products: cyclohexanol and cyclohexanone, were calculated by standard addition of known amounts of these compounds. Peak intergration was performed using a Spectra Physics SP4290 digital integrator.

4.2.3 Preparation of tris(pyridine) hexa -μ-acetato-μ_3-oxo-triruthenium(III) perchlorate[41]: $[Ru_3O(OAc)_6(py)_3]ClO_4$

This complex was prepared from crude oxotriruthenium(III) acetate, the preparation of which is described in Chapter 3. To 0.50 g of the crude acetate complex in methanol (5 ml) was added pyridine (2 ml). The solution was heated for 5 minutes on a steam bath, after which the colour changed from dark green to dark blue. The solution was then cooled to room temperautre and sodium perchlorate monohydrate (0.125 g, Aldrich) in methanol (2 ml) was added. A blue precipitate was formed and dried in *vacuo* over silica gel. Yield = 0.32 g. The solid was characterised by its UV-visible spectrum which was in agreement with that published in the literautre.[36] The following values were found:

$$\lambda_{max}\ (CH_2Cl_2) = 692\ nm\ (\varepsilon = 5790\ M^{-1}cm^{-1})$$

The corresponding literature values are as follows:[36]

$$\lambda_{max}\ (CH_2Cl_2) = 692\ nm\ (\varepsilon = 5800\ M^{-1}cm^{-1})$$

The complex was also characterised by elemental analysis.

Anal. calculated for $Ru_3C_{27}H_{33}O_{17}N_3Cl$

	C	H	N
	32.0	3.29	4.10
Found:	31.9	2.96	4.11

4.2.4 Preparation of tris(pyridine) hexa -μ-acetato-μ_3-oxo-triruthenium(III, III, II) : $[Ru_3O(OAc)_6(py)_3]$.[36]

0.25 g of $[Ru_3O(OAc)_6(py)_3]ClO_4$ in 5 ml of pyridine was cooled to 0 °C in an ice bath and hydrazine (Aldrich 65% in H_2O) was added dropwise with stirring until a green solid became visible as a suspension. The mixture was stirred for 15 minutes and 1-2 additional drops of hydrazine were added. The green complex was obtained by filtration and then washed with water, methanol and finally with plenty of ether. The solid was dried in *vacuo* over silica gel. Yield = 0.15 g. The purity of the complex was checked by UV-visible spectrophotometry and by elemental analysis. The following values were obtained which are in satisfactory agreement with the literature values:[36]

λ_{max} (CH_2Cl_2) = 895 nm (ε = 6710 $M^{-1}cm^{-1}$)
= 390 nm (ε =11750 $M^{-1}cm^{-1}$)
= 238 nm (ε = 22400 $M^{-1}cm^{-1}$)

The corresponding literature values are as follows;[36]

λ_{max} (CH_2Cl_2) = 895 nm (ε = 6700 $M^{-1}cm^{-1}$)
= 390 nm (ε =11700 $M^{-1}cm^{-1}$)
= 238 nm (ε = 22380 $M^{-1}cm^{-1}$)

Anal. Calculated for $Ru_3C_{27}H_{33}N_3O_{13}$

	C	H	N
	35.61	3.65	4.61
Found:	35.90	3.46	4.63

4.2.5 Preparation of bis(pyridine) carbonyl hexa-μ-acetato-μ_3-oxo-triruthenium (III) : $[Ru_3O(OAc)_6(CO)(py)_2]$.[36]

The dark blue solid was prepared in a similar manner to that described in the literature except that toluene was used in the place of benzene. 0.8 g of $[Ru_3O(OAc)_6(py)_3]$ was added to a nitrogen saturated solution of toluene (60 ml) and methanol (20 ml). The reaction mixture was refluxed under a gently flow of CO for 5 hours. The resulting blue solution was cooled to produce a dark blue precipitate which was collected by filtration. The complex was then washed with ether and dried in the air. Yield = 0.40 g. The purity of the complex was checked by its UV-visible spectrum which corresponds very well with that reported.[36]

λ_{max} = 585 nm (ε = 4560 $M^{-1}cm^{-1}$)

= 345 nm (ε = 6550 $M^{-1}cm^{-1}$)

The corresponding published values are as follows;[36]

$\lambda_{max}(CH_2Cl_2)$ = 585 nm (ε = 4590 $M^{-1}cm^{-1}$)

= 345 nm (ε = 6750 $M^{-1}cm^{-1}$)

The compelx was also characterised by elemental analysis

Anal. calculated for $Ru_3C_{23}H_{28}N_2O_{14}$

	C	H	N
	32.13	3.28	3.26
Found:	34.41	3.30	3.25

4.2.6 Preparation of μ_3-oxo-triaquahexakis(acetato)-iron(II) diiron(III); $Fe^{II}Fe_2^{III}O(OAc)_6(H_2O)_3$.[42]

60 g (0.30 mol) of $FeCl_2.4H_2O$ (BDH, reagent grade) were dissolved in 200 ml of water in a 2-litre round bottom flask. To this solution was added a suspension of 111.4 g (0.63 mol) of $Ca(CH_3CO_2)_2.H_2O$ (BDH, reagent grade) in 178 ml of H_2O and 378 ml(6.3 mol) of concentrated acetic acid (May and Baker, Pronalys AR). The mixture was then heated at 70 °C for ~ 6 hours. After this the mixture was cooled to room temperature and the black crystalline solid collected by filtration. This was washed twice with 50 ml of 0.08 M acetic acid and dried under high vacuum. Yield = 42 g. The complex was stored in a sealed round botttom flask under nitrogen. Elemental analysis was used to check the purity of the solid.

Anal. calculated for $C_{12}Fe_3H_{24}O_{16}$

	C	H
	24.35	4.09
Found:	23.47	4.19

4.2.7 Prepartion of μ_3-oxotris(pyridine)hexakis(acetato)-iron(II) diiron(III)hemipyridine:$[Fe^{II}Fe_2^{III}O(OAc)_6(py)_3]\cdot(py)_{0.5}$.[43]

8.5 g of $Fe^{II}Fe_2^{III}O(OAc)_6(H_2O)_3]$ was added to 50 ml of pyridine saturated with nitrogen.The mixture was kept stirring for ~ 20 minutes, after which the black crystalline solid was collected by filtration and dried under high vacuum. Yield = 5.10 g. The complex

was kept in a sealed flask under nitrogen and was characterised by elemental analysis.

Anal. calculated for $Fe_3C_{29.5}H_{35.5}N_{3.5}O_{13}$

	C	H	N
	43.49	4.39	6.02
Found:	44.76	4.23	6.47

4.2.8 Preparation of bis(μ-acetato)(μ-oxo)bis(tris(pyridine) ruthenium (III)) ion: $[Ru_2O(OAc)_2(py)_6]^{2+}$.[44]

0.5 g of $RuCl_3$.nH2O (Johnson Matthey) was refluxed in an acetic acid-water-ethanol (20 ml each) mixture at 70 °C for 10 minutes. 10 ml of pyridine were then added to the mixture which was refluxed for another 30 minutes. The complex was isolated by adding saturated $NaClO_4$ solution to the mixture during the cooling process. Yield = 0.30 g. The dimer was characterised by its UV-visible spectrum which compares very well with that reported.[44]

$$\lambda_{max}\ (CH_3CN) = 581\ nm\ (\varepsilon = 9410\ M^{-1}cm^{-1})$$

The corresponding published values are as follows:

$$\lambda_{max}\ (CH_3CN) = 581\ nm\ (\varepsilon = 9400\ M^{-1}cm^{-1})$$

4.3 Results and Discussion

The catalytic properties of three ruthenium species (**2**) - (**4**) were compared with that of the iron trimer(**1**). Cyclohexane was chosen as

$[Fe_3O(OAc)_6(py)_3](py)_{0.5}$ (**1**)

$[Ru_3O(OAc)_6(py)_3]^+$ (**2**)

$[Ru_3O(OAc)_6(py)_2CO]$ (**3**)

$[Ru_2O(OAc)_2(py)_6]^{2+}$ (**4**)

initial substrate because of its simple structure and that its oxidation products are readily identified. All reactions were monitored by g.l.c. and the products of the reactions were confirmed by using g.l.c. and g.c.m.s. A representative g.l.c. plot using catalyst (**1**) is shown in Figure 4.1.

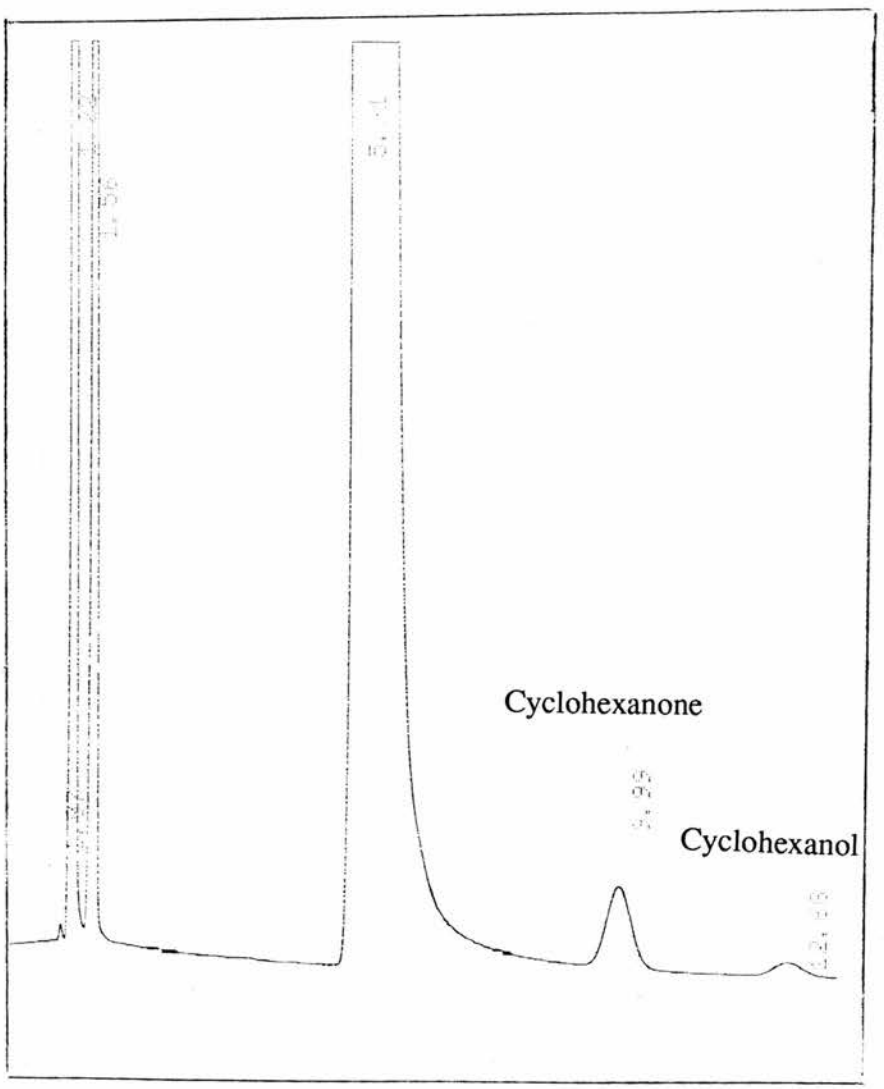

Figure 4.1: A representative g.l.c. plot of a catalytic run using $[Fe_3O(OAc)_6(py)_{3.5}]$ as catalyst.

The results for the reaction of cyclohexane after 5 1/2 hours and 24 hours are presented in Table 4.1. The results clearly show the high activity of the trinuclear complexes (**1**) and (**2**) and in particular the high activity of the iron complex (turnover no.~1000 after 24 hours). Separate studies [20] have shown that virtually all of the zinc is consumed in the first 8 hours of reaction. The studies show that the ruthenium system shows no further reaction beyond the first 5 hours but that the

Table 4.1: Percentage Yield and Distribution of Products Formed From the Oxidation of Cyclohexane After Various Times at Room Temperature (~20 °C).

Catalyst(10^{-6} mol)	Yield (%)		Total(oxidised products, m mol)	Turnover*
	Cyclohexanone	Cyclohexanol		
(**1**) 1.60	8.70	1.30	1.00	628[a]
	14.10	1.89	1.590	998[b]
(**2**) 1.39	1.35	3.61	0.496	357[a]
	1.69	3.20	0.490	352[b]
(**3**) 1.74		0.27	0.027	15[a]
		0.91	0.091	55[b]
(**4**) 1.20		0.94	0.094	78[a]
		1.54	0.154	130[b]

* Turnover = moles of oxidised products /mol of catalyst

a- after 5.5 hours, b- after 24 hours

iron system carries on functioning probably until all the zinc is used up. An interesting finding in these studies is that with the use of the iron trimer (**1**) as catalyst , the major product is the ketone, as found by Barton *et al* [20] whereas the use of the ruthenium trimer (**2**) resulted in the alcohol as the major product. The results also show that catalysts (**3**) and (**4**) gave predominantly the alcohol as the final product with trace amounts of the ketone. Apart from giving poorer yields, as is evident from Table 4.1, the turnover numbers for these catalysts are very low in comparison to complexes (**1**) and (**2**). Further independent studies[45] conducted in our laboratory have shown that with the iron trimer (**1**) as catalyst, adipic acid and possibly other carboxylic acids are formed after 3-4 days. The adipic acid can be extracted in ~ 90% yield with ethyl acetate and its identity confirmed by elemental analysis, NMR, melting point, IR, and GCMS. This is a significant finding and is probably the first time that cyclohexane has been catalytically oxidised to adipic acid using oxygen under mild conditions.

The ruthenium carboxylate species are known to possess somewhat higher solution stability than that of the iron species and this may be in part responsible for the lower activity. It may be that the trinuclear species are precursors to the active catalyst involving reduction of one or more of the metal centres with retention of the μ_3-oxo framework, formation of a dimeric or monomeric species, or even complete degradation of the trimer. Alternatively the redox properties of the iron trimer though not as extensive as the ruthenium analogues may contain the appropriate potentials which when coupled with the higher lability gives rise to the activity. These options will be tested in due course. It is conceivable that the greater yields of alcohol product in the Ru-Gif IV system could be due to the greater retention of reducing equivalents by the Ru_3 complex.

In view of the limited results it is not as yet possible to assign a definitive mechanism for these oxidations. However, it is possible that the oxidations may involve the formation of a hydrocarbon radical, hydrogen atom abstraction, reaction of the radical with O_2 to form a hydroperoxide, and subsequent Haber-Weiss decomposition of the hydroperoxide. A similar mechanism was recently proposed[40] to account for the air oxidation of alkanes by $[Ru_3O(pfb)_6(Et_2O)_3]$ (pfb = $CF_3CF_2CF_2CO_2^-$). Whether this mechanism is relevant for both iron and ruthenium species remains to be clarified. The presence of cyclohexyl hydroperoxide as an intermediate was recently detected by Barton *et al* [33] during the oxidation of cyclohexane under GoAggII conditions. This intermediate may also be present in our system. Its presence might explain why the ketone /alcohol ratio is different for catalysts (**1**) and (**2**); with possibly two different pathways competing for the intermediate cyclohexyl hydroperoxide.

The poor reactivity shown by the complexes; $[Ru_3O(OAc)_6(py)_2(CO)]$ and $[Ru_2O(OAc)_2(py)_6]$ was a disappointment but could be due to a lack of comparable redox chemistry of lower valence states. The dinuclear complex was viewed as a close ruthenium model for the active site of methane monooxygenase.

Much remains to be understood and detailed mechanistic studies will be further pursued in an effort to get a better understanding of these oxidation processes. With regard to future objectives there are a number of important goals relating to the oxygenation of alkanes and the reactivity of the metal species that need to be addressed experimentally. One such goal is to develop catalysts for the oxidation of alkanes that are not only stable toward high turnover but more reactive and selective. It would be also an advantage if catalyst could be developed that can utilise dioxygen (air) exclusively, as the oxidant in

non-radical-chain alkane oxidation reactions. Another important goal is to design thermal alkane oxygenation catalysts that exhibit high selectivities for desired products at high substrate conversions.

4.4 References

1. F. Asinger, *Paraffins, Chemistry and Technology*, Pergamon Press, New York, 1965.
2. B. P. Leddy, M. A. McKervey, P. McSweeney, *Tetrahedron Lett.*, 1980, **21**, 2261; (b) Z. Cohen, E. Keinan, Y.Mazur, T. H. Varkong, *J. Org. Chem.*, 1975, **40**, 2141; (c) J. Buddrus, H. Plettenberg, *Angew. Chem., Int. Edn. Engl.*, 1976, **15**, 436.
3. *Science*, 1991, **251**, 932.
4. *Chemistry and Industry*, 1991, **6**, 187.
5. D. J. Leak, H. Dalton, *Biocatalysts* 1987, **1**, 23.
6. R. T. Ruettinger, G. R. Griffith, M. J. Coon, *Arch. Biochem. Biophys.* 1977, **183**, 528.
7. P. R. Ortiz de Montellano., ed., *Cytochrome P-450, Structure, Mechanism and Biochemsitry*, Plenum Press, New York and London, 1986.
8. L. S. Alexander, M. M. Goff, *J. Chem. Educ.*, 1982, **59**, 179.
9. F. P. Guengerich, T. L. McDonald, *Acc. Chem. Res.*, 1984,**17**, 9.
10. D. E. Williams, S. E. Hale, R.T. Okita, B. S. Silermasters, *J. Biol. Chem.*, 1984, **259**, 14600.
11. R. E. White, M. J. Coon, *Ann. Rev. Biochem.*, 1980, **49**, 315.
12. (a) J. T. Groves, T. E. Nemo, R. S. Myers, *J. Am. Chem. Soc.*, 1979, **101**, 1032; (b) C. L. Hill, B. C. Schardt, *J. Am. Chem. Soc.*, 1980, **102**, 6375; (c) M. Fontacave, D. Mansuy, *Tetrahedron*, 1984, **21**, 4297; (d) B. R. Cook, T. J. Reinert, K. S. Suslick, *J. Am. Chem. Soc.*, 1986, **108**, 7281; (e) J. Smegal,

C. L. Hill, *ibid.*, 1983, **105**, 3515; (f) M. J. Nappa, C. A. Tolman, *Inorg. Chem.*, 1985, **24**, 4711; (g) B. DePoorter, M. Ricci., B. Meunier, *Tetrahedron Lett.*, 1985, **26**, 4459.

13. (a) H. Mimoun, I. Seree De Roch, *Tetrahedron*, 1975, **31**, 777; (b) D. H. R. Barton, M. J. Gastiger, W. B. Motherwell, *J. Chem. Soc., Chem. Commun.*, 1983, 731; (c) R. H. Fish, R. H. Fong, J. B. Vincent, G. Christou, *J. Chem. Soc., Chem. Commun.*, 1988, 1504; (d) S. J. Lippard, *Angew. Chem. Int. Ed. Engl.* 1988, **27**, 344.

14. (a) I. J. Higgins, D. J. Best, R. J. Hammond, *Nature*, 1980, **286**, 561; (b) H. Dalton, *Adv. Appl. Microbiol.*, 1980, **26**, 71.

15. M. P. Woodland, D. S. Patil, R. Cammack, H. Dalton. *Biochim. Biophys. Acta*, 1986, **873**, 237.

16. B. G. Fox, K. K. Surerus, E. Muenck, J. D. Lipscomb, *J. Biol. Chem.*, 1988, **263**, 10553.

17. A. Ericson, B. Hedman, K. O. Hodgson, J. Green, H. Dalton, J. G. Bentsen, R. H. Beer, S. J. Lippard, *J. Am .Chem. Soc.*, 1988, **110**, 2330

18. (a) M. Farji, C. L. Hill. *J. Chem. Soc., Chem. Commun.*, 1987, 1487; (b) J. D. Koola, J. K. Kochi, *Inorg. Chem.*, 1987, **26**, 908; (c) K. Srinivasan, P. Michaud, J. K. Kochi., *J. Am. Chem. Soc.*, 1986, **108**, 2309; (d) L. Saussine, E. Brazil, A. Robine, H. Mimoun, J. Fisher, R. Weiss, *ibid*, 1985, **107**, 3534.

19. S. Ito, K. Inoue, M. Mastumoto, *J. Am. Chem. Soc.*, 1982, **104**, 6450.

20. D. H. R. Barton, J. Boivin, M. Gastiger, J. Morzycki, R. S. Hay-Motherwell, W. B. Motherwell, N. Ozbalik, K. M. Schwartzentruber, *J. Chem. Soc. Perkin Trans*, I, 1986, 947.

21. D. H. R. Barton, M. J. Gastiger, W. B. Motherwell, *J. Chem.*

Soc., Chem. Commun., 1983, 41.

22. D. H. R. Barton, R. S. Hay-Motherwell, W. B. Motherwell, *Tetrahedron Lett.*, 1983, **24**, 1979.
23. G. Belavoine, D. H. R. Barton, J. Boivin, A. Gref, N. Ozbalik, H. Riviére, *Tetrahedron Lett.* 1986, **27**, 2849.
24. D. H. R. Barton, F. Halley, N. Ozbalik, E. Young, G. Balavoine, A. Gref, J. Boivin, *New. J. Chem.* ,1989, **13**, 177.
25. D. H. R. Barton, E. Csuhai, D. Doller, N. Ozbalik, G. Balavoine, *Proc. Natl. Acad. Sci. USA*, 1990, **87**, 3401.
26. E. About-Jaudet, D. H. R. Barton, E. Csuhai , N. Ozbalik, *Tetrahedron Letters*, 1990, **31**, 1657.
27. D. H. R. Barton, A. K. Göktürk, J. W. Morzycki, W. B. Motherwell, *J. Chem. Soc., Perkin Trans* I,1985, 583.
28. D. H. R. Barton, J. Boivin, D. Crich, C. H. Hill. *J. Chem. Soc. Perkin Trans* I, 1986, 1805.
29. D. H. R. Barton, A. K. Göktürk, K. Jankowski, *J. Chem. Soc., Perkin Trans* I, 1985, 2109.
30. D. H. R. Barton, E. Csuhai, N. Ozbalik, *Tetrahderon*, 1990, **46**, 3743.
31. D. H. R. Barton, K. W. Lee, W. Mehl, N. Ozbalik, L. Zhang, *Tetrahedron*, 1990, **46**, 3753.
32. D. H. R. Barton, E. Csuhai, D. Doller, Y. V. Geletti, Tetrahed-*ron*, 1991, **47**, 6561.
33. D. H. R. Barton, E. Csuhai, D. Doller, G. Balavoine, *J. Chem. Soc., Chem. Commun.*, 1990, 1787.
34. Y. V. Geletti, V. V. Lavrushko, G. V. Lubimova, *J. Chem. Soc., Chem. Commun.*, 1988, 936.
35. C. Knight, M. J. Perkins, *J. Chem. Soc., Chem. Commun.* 1991, 925.

36. J. A. Baumann, D. J. Salmon, S. T. Wilson, T. J. Meyer, W. E. Hatfield, *Inorg. Chem.* 1978, **17**, 3342.

37. C.-M. Che, C. Ho, T.-C. Lau, *J. Chem. Soc., Dalton. Trans*, 1991, 1259.

38. See S. Davis, R. S. Drago, *Inorg. Chem.* 1988, **27**, 4759 and refs. cited therein.

39. C. Bilgrien, S. Davis, R. S. Drago, *J. Am. Chem. Soc.*, 1987, **109**, 3786.

40. S. Davis, R. S. Drago, *J. Chem. Soc.Chem. Commun.*, 1990, 250.

41. A. Spencer, G. Wilkinson, *J. Chem. Soc., Dalton. Trans* 1972, 1570.

42. C.T. Dziobkowski, J. T. Wrobleski, D. B. Drown, *Inorg. Chem.*, 1981, **20**, 679.

43. C.T. Dziobkowski, J. T. Wrobleski, D. B. Brown, *Inorg. Chem.*, 1981, **20**, 671.

44. Y. Sasaki, M. Suzuki, A.Tokiwa, M.Ebihara, T. Yamaguchi, C. Kabuto, T.Ito, *J. Am. Chem. Soc.*, 1988, **110**, 6251.

45. L. Khan, D. T. Richens, *Unpublished results.*

APPENDICES

Appendix 1

Estimation of final absorbance values (A_∞) using the Swinbourne Method.

When doing kinetic studies using conventional UV-visible spectrophotometry, it is sometimes difficult to measure the final absorbance values due to drifting absorbance readings. Different methods have been devised to estimate both the rate constant and the final absorbance reading.[1,2] One of these is the method of Kezdy and Swinbourne[3] which is described below.

The course of a reaction may be followed by measuring the absorbance which varies with time according to equation (1).

$$A_\infty - A_t = (A_\infty - A_0) \exp(-kt) \qquad (1)$$

where A_0 and A_∞ are the initial and final absorbance readings, respectively and k is the rate constant for a simple first-order reaction. If readings A_1, A_2, ...A_n are made at times t_1, t_2, ...t_n, and a second series A'_1, A'_2, ...A'_n is made at the corresponding times $t_1 + d_t$, $t_2 + d_t$, ...$t_n + d_t$ (where dt is constant) then

$$A_\infty - A_n = (A_\infty - A_0) \exp(-kt_n) \qquad (2)$$

and

$$A_\infty - A'_n = (A_\infty - A_0) \exp(-k(t_n + dt) \qquad (3)$$

---

[1]Guggenheim, *Phil. Mag.*, 1926, **2**, 538.

[2]Hartley, *Biometrika*, 1948, **35**, 32.

[3]E. S. Swinbourne, *J. Chem. Soc.*, 1960, 2371.

Dividing (2) by (3) and rearranging gives,

$$A_n = A_\infty(1 - \exp(kdt)) + A_n\exp(kdt) \qquad (4)$$

A plot of A_n *vs* A'_n should give a straight line and the logarithm of the slope of this line is therefore an estimate of the rate constant k. Furthermore at $t = \infty$, $A_n = A'_n = A_\infty$; hence A_∞ is the point on the line when both A_n and A'_n are equal. The graph may also be used for easy extrapolation to A values outside the range of the recorded data. In order to obtain reliable estimates of k and A_∞, the data should normally be recorded over a period of time greater than the half-life ($t_{1/2}$) and preferably greater than 2 $t_{1/2}$ (this will depend on the accuracy of the recorded values. The dt value should be of the order of 0.5 $t_{1/2}$ to $t_{1/2}$.

Appendix 2

Derivation of rate law for the $[Mo_3O_2(OAc)_6(H_2O)_3]^{2+}$ / SCN^- anation reaction. (Mo_3 complex hereafter abbreviated as Mo-OH_2)

The observed rate law was found to be of the form:

$$k_{obs} = \frac{k_i K_{IP}[NCS^-][H^+]}{(1 + K_{IP}[NCS^-])([H^+] + K_{AM})} \qquad (5)$$

and is derived from scheme 2.1 (see page 90) as follows:

$$\text{Rate} = k_1[Mo_3\text{-}OH_2, NCS^-] \qquad (6)$$

From eqn. (2.2) in scheme 2.1 the amount of the ion-pair species can be written as follows :

$$[Mo_3\text{-}OH_2, NCS^-] = \frac{K_{IP}[Mo_3\text{-}H_2O][NCS^-]}{1 + K_{IP}[NCS^-]} \qquad (7)$$

Substituting eqn. (7) into eqn. (6) gives eqn. (8)

$$\text{Rate} = \frac{k_1 K_{IP}[Mo_3\text{-}OH_2][NCS^-]}{1 + K_{IP}[NCS^-]} \qquad (8)$$

From eqn. (2.1) in scheme 2.1 eqn. (9) is obtained as

$$K_{AM} = \frac{[Mo_3\text{-}OH^-][H^+]}{[Mo_3\text{-}OH_2]} \qquad (9)$$

Rearranging eqn. (9) gives

$$[Mo_3\text{-}OH_2] = \frac{[Mo_3\text{-}OH][H^+]}{K_{AM}} \qquad (10)$$

Thus expression $[Mo_3]_T = [Mo_3\text{-}OH_2] + [Mo_3\text{-}OH]$ can be written as

$$[Mo_3]_T = \frac{[Mo_3\text{-}OH_2]([H^+] + K_{AM})}{[H^+]} \qquad (11)$$

and therefore

$$[Mo_3\text{-}OH_2] = \frac{[H^+][Mo_3]_T}{[H^+] + K_{AM}} \qquad (12)$$

Substituting eqn.(12) into eqn. (8) gives

$$\text{Rate} = \frac{k_1 K_{IP}[Mo_3]_T[NCS^-][H^+]}{(1 + K_{IP}[NCS^-])([H^+] + K_{AM})} \qquad (13)$$

Also

$$\text{Rate} = k_{obs}[Mo_3]_T \qquad (14)$$

Hence equation (5).

APPENDIX 3

Derivation of the rate law for the $[Mo_3O_2(OAc)_6(H_2O)_3]^{2+}$ oxalate anation

The proposed rate law is of the form:

$$k_f = \frac{k_1[H^+]^2 + k_2K_2[H^+]}{([H^+] + K_A)([H^+] + K_2)} \qquad (15)$$

and is derived from scheme 2.2 (see page 94) as follows:

$$\text{rate} = k_1[Mo_3\text{-}OH_2][HC_2O_4^-] + k_2[Mo_3\text{-}OH_2][C_2O_4^{2-}] \qquad (16)$$

Substituting equations (2.3) and (2.4) from page 94 into equation (16) gives

$$\text{rate} = \frac{(k_1[Mo_3][H^+] + k_2[Mo_3]K_2)[Ox]_T}{([H^+] + K_2)([H^+] + K_A)} \qquad (17)$$

Also

$$\text{rate} = k_{obs}[Mo_3]_T \qquad (18)$$

From equation 2.5 (scheme 2.2) the $[Mo_3]$ can be expressed in terms of total complex as demonstrated in Appendix 2 . Thus

$$\text{rate} = \frac{(k_1[H^+]^2 + k_2K_2[H^+])[Mo_3]_T}{([H^+] + K_2)([H^+] + K_A)} \qquad (19)$$

The relationship between equations (18) and (19) gives the proposed rate law with k_f representing $k_{obs}/[Ox]_T$.

APPENDIX 4

The derivation of the rate law for complexation of isonicotinamide with $[Ru_3O(OAc)_6(H_2O)_3]^{2+}$.

The observed rate law was found to be of the form:

$$k_{obs} = \frac{(k_1K_{ISO}[H^+]^2 + k_2K_{AM}K_{ISO})[ISO]_T}{([H^+]^2 + K_{AM})([H^+] + K_{ISO})} \qquad (20)$$

and is derived from scheme 3.1 (page 150) as follows:

$$\text{rate} = k_1[Ru_3\text{-}OH_2][ISO] + k_2[Ru_3\text{-}OH][ISO] \qquad (21)$$

Also

$$\text{rate} = k_{obs}[Ru_3]_T \qquad (22)$$

where

$$[Ru_3]_T = [Ru_3\text{-}OH_2] + [Ru_3\text{-}OH] \qquad (23)$$

With the use of equation (3.1) (see scheme 3.1) and equation (23) [Ru-OH_2] and [Ru-OH] can be expressed in terms of $[Ru_3]_T$. Thus equation (21) becomes

$$\text{rate} = \frac{k_1[H^+]^2[ISO] + k_2K_{AM}[ISO][Ru_3]_T}{([H^+]^2 + K_{AM})} \qquad (24)$$

Similarly with the use of equation (3.2) (see scheme 3.1) and equation (25) then [ISO] can be expressed in terms of $[ISO]_T$.

$$[ISO]_T = [ISO] + [ISOH] \qquad (25)$$

It follows then that

$$[ISO] = \frac{K_{ISO}[ISO]_T}{[H^+] + K_{ISO}} \qquad (26)$$

Substituting equation (26) for [ISO] into equation (24) gives

$$\text{rate} = \frac{(k_1K_{ISO}[H^+]^2 + k_2K_{AM}K_{ISO})[Ru_3]_T[ISO]_T}{([H^+]^2 + K_{AM})([H^+] + K_{ISO})} \qquad (27)$$

The relationship between equations (22) and (27) then gives the derived rate expression.

Appendix 5: Structural information for $[Ru_3O(OAc)_6(OH_2)_3]^+$

Table A1 . Atomic coordinates ($x10^4$) and equivalent isotropic displacement coefficients ($Å^2 x10^3$)

	x	y	z	U(eq)
Ru(1)	1667(3)	2920(1)	5900(1)	20(1)
Ru(2)	1559(3)	2051(1)	4148(1)	22(2)
Ru(3)	4177(4)	2527(2)	4989(1)	22(2)
O(1)	2560(36)	2516(11)	5020(9)	19(4)
O(2)	430(24)	3620(12)	5266(9)	26(5)
O(3)	402(28)	3030(15)	4109(12)	46(6)
C(1)	53(37)	3588(18)	4595(14)	26(7)
C(2)	-825(40)	4198(21)	4338(16)	40(8)
O(4)	485(29)	1947(15)	5948(12)	47(6)
O(5)	452(25)	1328(12)	4804(10)	28(5)
C(3)	131(36)	1410(17)	5453(14)	23(6)
C(4)	-803(42)	736(23)	5709(18)	48(9)
O(6)	2771(29)	2332(13)	6669(10)	34(5)
O(7)	4412(31)	2083(17)	6074(14)	57(7)
C(5)	3774(47)	2037(21)	6612(17)	37(8)
C(6)	4342(38)	1628(22)	7366(16)	40(8)
O(8)	2690(29)	4018(15)	5979(12)	45(6)
O(9)	4371(28)	3748(15)	5407(12)	44(6)
C(7)	3594(47)	4257(24)	5749(19)	49(9)
C(8)	4158(41)	5134(22)	5960(17)	45(9)
O(10)	4298(31)	1325(17)	4570(14)	59(7)
O(11)	2654(32)	1010(15)	4004(12)	45(6)
C(9)	3555(48)	845(22)	4248(18)	39(8)
C(10)	4085(47)	-57(25)	4032(20)	64(12)
O(12)	4244(28)	3013(14)	3905(12)	39(6)
O(13)	2431(30)	2708(14)	3349(11)	39(6)
C(11)	3446(47)	3026(21)	3387(17)	37(8)
C(12)	3895(42)	3516(23)	2635(17)	48(10)
O(14)	755(24)	3388(13)	6887(10)	34(5)
O(15)	506(24)	1546(12)	3194(10)	30(5)
O(16)	5982(38)	2519(16)	4978(12)	59(8)
Cl(1)	7619(15)	4166(8)	6482(7)	75(3)
O(17)	6557(36)	4314(23)	6983(17)	97(11)
O(18)	7538(50)	4938(34)	6040(28)	180(19)
O(19)	8660(62)	3994(38)	6965(32)	185(23)
O(20)	7476(49)	3436(34)	6091(27)	156(18)
Cl(2)	2242(17)	-294(10)	6658(7)	95(4)
O(21)	2481(35)	191(22)	5958(17)	102(10)
O(22)	3476(35)	-526(22)	7084(17)	93(10)
O(23)	1753(54)	-1015(33)	6395(26)	153(19)
O(24)	1406(50)	184(34)	7193(26)	162(18)
O(25)	-2921(42)	2585(24)	3562(20)	112(13)

* Equivalent isotropic U defined as one third of the trace of the orthogonalized U_{ij} tensor

Table A2 . Anisotropic displacement coefficients ($A^2 x 10^3$)

	U_{11}	U_{22}	U_{33}	U_{12}	U_{13}	U_{23}
Ru(1)	19(4)	22(1)	19(1)	-5(1)	-1(1)	-3(1
Ru(2)	29(4)	21(1)	17(1)	0(1)	-2(1)	-3(1
Ru(3)	9(7)	27(1)	29(1)	-4(2)	-2(1)	-3(1

The anisotropic displacement exponent takes the form:

$-2\pi^2(h^2a^{*2}U_{11} + \ldots + 2hka^*b^*U_{12})$

Table A3. Bond lengths (A)

Ru(1)-Ru(2)	3.299	(5)	Ru(1)-Ru(3)	3.299	(6)
Ru(1)-O(1)	1.939	(25)	Ru(1)-O(2)	2.041	(22)
Ru(1)-O(4)	2.004	(28)	Ru(1)-O(6)	1.998	(25)
Ru(1)-O(8)	2.046	(26)	Ru(1)-O(14)	2.130	(21)
Ru(2)-Ru(3)	3.295	(6)	Ru(2)-O(1)	1.976	(25)
Ru(2)-O(3)	1.988	(27)	Ru(2)-O(5)	2.032	(22)
Ru(2)-O(11)	2.040	(28)	Ru(2)-O(13)	1.985	(24)
Ru(2)-O(15)	2.134	(20)	Ru(3)-O(1)	1.801	(40)
Ru(3)-O(7)	1.998	(24)	Ru(3)-O(9)	2.032	(23)
Ru(3)-O(10)	2.000	(26)	Ru(3)-O(12)	2.012	(20)
Ru(3)-O(16)	2.008	(43)	O(2)-C(1)	1.216	(32)
O(3)-C(1)	1.271	(36)	C(1)-C(2)	1.419	(51)
O(4)-C(3)	1.245	(35)	O(5)-C(3)	1.188	(32)
C(3)-C(4)	1.545	(53)	O(6)-C(5)	1.212	(59)
O(7)-C(5)	1.185	(50)	C(5)-C(6)	1.559	(46)
O(8)-C(7)	1.152	(58)	O(9)-C(7)	1.321	(52)
C(7)-C(8)	1.534	(54)	O(10)-C(9)	1.231	(53)
O(11)-C(9)	1.104	(60)	C(9)-C(10)	1.564	(55)
O(12)-C(11)	1.239	(49)	O(13)-C(11)	1.232	(59)
C(11)-C(12)	1.591	(47)	Cl(1)-O(17)	1.500	(40)
Cl(1)-O(18)	1.417	(52)	Cl(1)-O(19)	1.430	(64)
Cl(1)-O(20)	1.321	(53)	Cl(2)-O(21)	1.450	(34)
Cl(2)-O(22)	1.577	(41)	Cl(2)-O(23)	1.315	(55)
Cl(2)-O(24)	1.519	(54)			

Table A4 . Bond angles (°)

Ru(2)-Ru(1)-Ru(3)	59.9(1)	Ru(2)-Ru(1)-O(1)	32.9(10)
Ru(3)-Ru(1)-O(1)	27.0(10)	Ru(2)-Ru(1)-O(2)	73.9(5)
Ru(3)-Ru(1)-O(2)	114.3(6)	O(1)-Ru(1)-O(2)	96.2(10)
Ru(2)-Ru(1)-O(4)	74.0(6)	Ru(3)-Ru(1)-O(4)	116.5(8)
O(1)-Ru(1)-O(4)	98.1(11)	O(2)-Ru(1)-O(4)	89.4(10)
Ru(2)-Ru(1)-O(6)	115.0(6)	Ru(3)-Ru(1)-O(6)	73.6(8)
O(1)-Ru(1)-O(6)	92.9(11)	O(2)-Ru(1)-O(6)	170.8(8)
O(4)-Ru(1)-O(6)	91.2(11)	Ru(2)-Ru(1)-O(8)	113.8(6)
Ru(3)-Ru(1)-O(8)	73.0(8)	O(1)-Ru(1)-O(8)	91.3(11)
O(2)-Ru(1)-O(8)	87.7(10)	O(4)-Ru(1)-O(8)	170.3(11)
O(6)-Ru(1)-O(8)	90.3(10)	Ru(2)-Ru(1)-O(14)	149.5(7)
Ru(3)-Ru(1)-O(14)	150.6(7)	O(1)-Ru(1)-O(14)	177.6(12)
O(2)-Ru(1)-O(14)	85.2(8)	O(4)-Ru(1)-O(14)	83.9(9)
O(6)-Ru(1)-O(14)	85.7(9)	O(8)-Ru(1)-O(14)	86.7(9)
Ru(1)-Ru(2)-Ru(3)	60.0(1)	Ru(1)-Ru(2)-O(1)	32.2(10)
Ru(3)-Ru(2)-O(1)	27.8(10)	Ru(1)-Ru(2)-O(3)	74.1(6)
Ru(3)-Ru(2)-O(3)	114.0(8)	O(1)-Ru(2)-O(3)	95.6(11)
Ru(1)-Ru(2)-O(5)	73.9(5)	Ru(3)-Ru(2)-O(5)	114.9(6)
O(1)-Ru(2)-O(5)	96.7(9)	O(3)-Ru(2)-O(5)	92.1(10)
Ru(1)-Ru(2)-O(11)	115.3(6)	Ru(3)-Ru(2)-O(11)	73.0(8)
O(1)-Ru(2)-O(11)	93.2(11)	O(3)-Ru(2)-O(11)	170.6(9)
O(5)-Ru(2)-O(11)	90.3(10)	Ru(1)-Ru(2)-O(13)	114.7(6)
Ru(3)-Ru(2)-O(13)	75.3(8)	O(1)-Ru(2)-O(13)	93.6(10)
O(3)-Ru(2)-O(13)	85.1(11)	O(5)-Ru(2)-O(13)	169.5(10)
O(11)-Ru(2)-O(13)	90.9(11)	Ru(1)-Ru(2)-O(15)	148.8(7)
Ru(3)-Ru(2)-O(15)	151.2(7)	O(1)-Ru(2)-O(15)	179.0(13)
O(3)-Ru(2)-O(15)	85.0(9)	O(5)-Ru(2)-O(15)	84.1(8)
O(11)-Ru(2)-O(15)	86.2(10)	O(13)-Ru(2)-O(15)	85.6(9)
Ru(1)-Ru(3)-Ru(2)	60.0(1)	Ru(1)-Ru(3)-O(1)	29.2(5)
Ru(2)-Ru(3)-O(1)	30.8(5)	Ru(1)-Ru(3)-O(7)	73.1(10)
Ru(2)-Ru(3)-O(7)	115.0(10)	O(1)-Ru(3)-O(7)	94.1(11)
Ru(1)-Ru(3)-O(9)	75.1(9)	Ru(2)-Ru(3)-O(9)	116.5(9)
O(1)-Ru(3)-O(9)	95.4(10)	O(7)-Ru(3)-O(9)	88.8(9)
Ru(1)-Ru(3)-O(10)	114.2(10)	Ru(2)-Ru(3)-O(10)	72.7(10)
O(1)-Ru(3)-O(10)	94.6(11)	O(7)-Ru(3)-O(10)	90.5(10)
O(9)-Ru(3)-O(10)	170.0(14)	Ru(1)-Ru(3)-O(12)	115.2(9)
Ru(2)-Ru(3)-O(12)	74.6(9)	O(1)-Ru(3)-O(12)	95.5(10)
O(7)-Ru(3)-O(12)	170.2(13)	O(9)-Ru(3)-O(12)	88.5(8)
O(10)-Ru(3)-O(12)	90.5(9)	Ru(1)-Ru(3)-O(16)	150.0(6)
Ru(2)-Ru(3)-O(16)	149.9(6)	O(1)-Ru(3)-O(16)	178.5(8)
O(7)-Ru(3)-O(16)	84.5(12)	O(9)-Ru(3)-O(16)	85.0(11)
O(10)-Ru(3)-O(16)	85.0(12)	O(12)-Ru(3)-O(16)	85.9(11)
Ru(1)-O(1)-Ru(2)	114.8(20)	Ru(1)-O(1)-Ru(3)	123.8(13)
Ru(2)-O(1)-Ru(3)	121.4(12)	Ru(1)-O(2)-C(1)	133.8(21)
Ru(2)-O(3)-C(1)	135.0(21)	O(2)-C(1)-O(3)	123.2(32)
O(2)-C(1)-C(2)	118.9(26)	O(3)-C(1)-C(2)	117.9(25)
Ru(1)-O(4)-C(3)	131.9(22)	Ru(2)-O(5)-C(3)	131.8(21)
O(4)-C(3)-O(5)	128.0(33)	O(4)-C(3)-C(4)	117.2(25)
O(5)-C(3)-C(4)	114.8(25)	Ru(1)-O(6)-C(5)	131.8(20)
Ru(3)-O(7)-C(5)	133.2(31)	O(6)-C(5)-O(7)	128.0(33)
O(6)-C(5)-C(6)	115.9(30)	O(7)-C(5)-C(6)	115.9(41)
Ru(1)-O(8)-C(7)	137.1(25)	Ru(3)-O(9)-C(7)	130.4(27)
O(8)-C(7)-O(9)	123.4(35)	O(8)-C(7)-C(8)	124.0(36)
O(9)-C(7)-C(8)	111.3(39)	Ru(3)-O(10)-C(9)	132.2(31)
Ru(2)-O(11)-C(9)	132.4(24)	O(10)-C(9)-O(11)	128.3(36)
O(10)-C(9)-C(10)	113.1(42)	O(11)-C(9)-C(10)	117.4(35)
Ru(3)-O(12)-C(11)	128.8(27)	Ru(2)-O(13)-C(11)	129.3(20)
O(12)-C(11)-O(13)	131.8(30)	O(12)-C(11)-C(12)	110.9(38)
O(13)-C(11)-C(12)	117.2(31)	O(17)-Cl(1)-O(18)	98.1(27)
O(17)-Cl(1)-O(19)	109.4(29)	O(18)-Cl(1)-O(19)	120.4(34)

O(17)-Cl(1)-O(20)	109.8(29)	O(18)-Cl(1)-O(20)	116.3(29)
O(19)-Cl(1)-O(20)	102.7(33)	O(21)-Cl(2)-O(22)	108.9(23)
O(21)-Cl(2)-O(23)	103.7(25)	O(22)-Cl(2)-O(23)	108.2(29)
O(21)-Cl(2)-O(24)	112.4(26)	O(22)-Cl(2)-O(24)	111.7(23)
O(23)-Cl(2)-O(24)	111.5(34)		